Posters 1

Monday, August 9
12:00 – 13:40

P1-1	Signal processing
P1-2	MEG: Spontaneous activity
P1-3	MEG: Memory and cognition
P1-4	DC Phenomena
P1-5	Magnetic particles and magnetic fields from other organs and non-human sources

Topographic classification of EEG patterns in Huntington's disease

Bellotti R.[1,2], De Carlo F.[2], Massafra R.[2], de Tommaso M.[1,3], Sciruicchio V.[3]

[1] TIRES, Center of Innovative Technologies for Signal Detection and Processing, Bari, Italy
[2] Dipartimento di Fisica, Università di Bari, and Istituto Nazionale di Fisica Nucleare, Sezione di Bari, Italy
[3] Dipartimento di Scienze Neurologiche e Psichiatriche, Policlinico di Bari, Italy

ABSTRACT

The aim of this study is to perform a topographic classification of electroencephalographic (EEG) patterns in subjects affected by the Huntington's disease (HD). The *alpha* activity is a discriminating feature for HD, as its amplitude reduction turns out to be a clear mark of the illness. When used as input variable to a supervised neural network, a good classification of pathological patterns and control ones is achieved with high values of sensitivity and specificity. It should be useful to get more insights into the local discriminating capabilities of the *alpha* rhythm by implementing a neural network approach to classify EEG patterns extracted from groups of channels corresponding to specific regions of the scalp. ROC curve analysis enables to label each region with the value of the area under the curve, thus providing a local significance for HD classification. A reduction of the area when processing regions of the scalp, with respect to the whole, suggests that all channels provide significant contribution to HD pattern discrimination. These results can be interpreted as an effect of an abnormal subcortical modulation of the *alpha* rhythm, due to the dysfunctional action of the thalamus on the cortical activities. In a further study, morphometric features of thalamus and basal ganglia, evaluated by MRI, will be matched with the electrophysiological findings.

KEY WORDS: Huntington's disease; electroencephalography; supervised neural networks.

INTRODUCTION

The Huntington's disease (HD) is an autosomal dominant neurodegenerative illness. Its genetic origin relies in the mutation of the HD gene, named IT15, consisting in the expansion of the cytosine-adenine-guanine (CAG) tri-nucleotide repeat in the first exon of the gene: typical numbers of repeats are 9-35 in healthy subjects, while it grows up to 250 in pathological subjects. Clinical manifestations show in a progressive deterioration of the functional capabilities, leading to disorders of movements, cognition and behavior. Though the DNA test allows the individuation of the genetic mutation, yet it fails in predicting the illness severity [Squitieri et al., 2001], nor it gives information about the onset modality [Paulsen et al., 2001]. From this point of view, the electroencephalography may get insights into the evolution of the disease.

The most widely observed EEG abnormality for HD consists in the amplitude reduction of the *alpha* activity [Bylsma et al., 1994]. In [de Tommaso et al., 2003], this mark emerges out in a clear and natural way as a consequence of a neural network (NN) analysis of the EEG patterns recorded over the whole scalp. Neural networks allow the classification of EEG signals through a non linear mapping from the original n-dimensional space, where n is the number of recording channels, onto a one-dimensional space where the neural output distribution should enable to separate pathological patterns from control ones. NN performance, measured in terms of the area under ROC curve, increases for *alpha* rhythm with respect to *beta*, *delta* and *theta* frequencies.

In this work, we extend the previous study by focusing on a topographic classification of the EEG patterns. To this purpose, a NN approach was implemented to investigate the local significance of the *alpha* activity for HD discrimination.

METHODS

We selected 15 HD patients (8 women, 7 men) and as many control subjects (9 women, 6 men). HD was diagnosed from hyper-kinetics movements, family history and DNA test. EEG were recorded, with Micromed apparatus and System 98 software, at 19 channels positioned on FP1, FP2, F7, F3, FZ, F4, F8, T3, C3, CZ, C4, T4, T5, P3, PZ, P4, T6, O1 and O2 derivations, according to the 10-20 system, with a common average reference. Signals were filtered at 1-70 Hz and sample at 256 Hz rate in 0.5 second epochs. A number of 20 epochs, 5 second long and free of artifacts, was selected for computing the *alpha* power.

In order to study the local significance of the *alpha* activity, we chose six partially overlapping regions of the scalp: this procedure is believed to provide more realistic results than for the case of a disjoined (besides rather arbitrary) partition of the channels. The selected regions are: frontal (FP1, FP2, F7, F3, FZ, F4, F8), back (T5, P3, PZ, P4, T6, O1, O2), fronto-central (F3, FZ, F4, C3, CZ, C4), parieto-central (P3, PZ, P4, C3, CZ, C4), left (F7, F3, T3, C3, T5, P3) and right (F4, F8, C4, T4, P4, T6). A supervised two-layered feed-forward neural network was implemented for each of the above mentioned region: the size of the input layer was determined by the number of the channels belonging to the area under investigation, while the hidden layer size was tuned to maximize the network performance. A gradient descent learning rule ($\eta=0.01$) with momentum term ($\alpha=0.1$) was adopted to train the network. The ROC curve [Swets, 1988] is particularly suitable when testing a binary hypothesis, as the area under the curve provides a measure of the discriminating capability. The curve is obtained by plotting the sensitivity (fraction of pathological patterns correctly diagnosed) against the specificity (fraction of control patterns correctly identified). Random decision results in a line along the diagonal with an area under the curve $a = 0.5$, while maximum value is $a = 1$, for perfectly separated distributions. Data were analyzed with the software package Matlab.

RESULTS

Fig.1 shows the ROC curves obtained for the above mentioned regions together with the value of the area. For comparative purpose, the curve of the classification with all channels is reported too. The discriminating capabilities of the scalp regions clearly decrease with respect to the whole scalp processing, thus suggesting that all channels provide significant contribution to HD pattern classification. To confirm this guess, the neural analysis was repeated for groups of $n = 7,10,13,16$ randomly selected channels, not corresponding to specific regions: the relating curves are reported in fig.2, together with the case $n = 19$. The statistical errors for the areas, computed as in [Hanley et al., 1982], were approximately 0.02 or less for all cases.

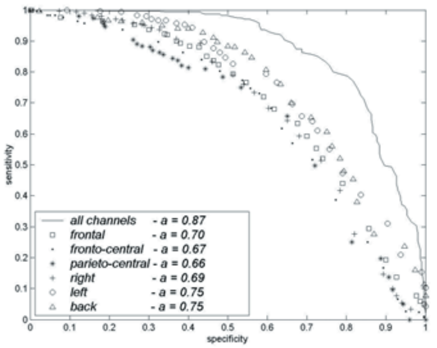

Figure 1. ROC curve for scalp regions.

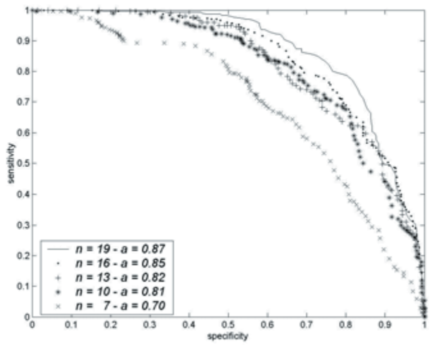

Figure 2. ROC curve for random channels.

DISCUSSION

We found significant reduction of the area under the curve when processing groups of channels with respect to the whole scalp. Moreover, for no values of sensitivity and specificity, the local analysis improves the global one. The significance reduction when classifying local areas can be explained with the lack of significant information carried by the other channels. To confirm this guess, a number of *n* channels were randomly chosen for classification and the results showed a lowering of the area under the curve at decreasing *n*; for *n* = 7, the performance was about the same as for the processing of the local regions.

This result can be interpreted as an effect of an abnormal subcortical modulation of the *alpha* rhythm, due to the dysfunctional action of the thalamus on the cortical activities. In a further development of the study, the morphometric features of the thalamus and basal ganglia, evaluated by MRI, will be matched with the electrophysiological findings.

REFERENCES

Bylsma FW, Peyser CE, Folstein SE, Folstein MF, Ross C, Brandt J, EEG power spectra in Huntington's disease: clinical and neuropsychological correlates. Neuropsychologia 1994; 32 (2): 137-150.

de Tommaso M, De Carlo F, Difruscolo O, Massafra R, Sciruicchio V, Bellotti R, Detection of subclinical brain electrical activity changes in Huntington’s disease using artificial neural networks. Clin. Neur. 2003; 114: 1237-45.

Hanley JA, McNeil BJ, The Meaning and Use of the Area under a Receiver Operating Characteristic (ROC) Curve. Radiology 1982; 143: 29-36.

Paulsen JS, Zaho H, Stout JC, Brinkman RR, Guttman M, Ross CA, Como P, Manning C, Hayden MR, Shoulson I, Clinical markers of early disease in persons near onset of Huntington's disease. Neurology 2001; 57: 658-62.

Squitieri F, Cannella M, Giallonardo P, Maglione V, Mariotti C, Hayden MR, Onset and pre-onset studies to define the Huntington's disease natural history. Brain Res. Bull. 2001; 56 (3-4): 233-8.

Swets JA, Measuring the accuracy of diagnostic systems. Science 1988; 240: 1285-93.

Detection of Power Changes Between Conditions using Split-Half Resampling of Synthetic Aperture Magnetometry Data

Wilkin Chau, Anthony T. Herdman, Terence W. Picton

The Rotman Research Institute of Baycrest Centre, University of Toronto, Toronto, Canada

ABSTRACT

Synthetic Aperture Magnetometry (SAM) measures changes in task-related power using pseudo-t values which are affected by changes in both signal and noise. Detecting significant signal power changes between two separate experimental conditions should not be done directly due to possible fluctuation in the noise as well as the response. This study proposes a method to estimate the noise within a single condition, which is then used to test the null hypothesis of no difference between the conditions. The noise estimation is based on a split-half resampling technique. For each resampling, the data of a given condition is divided into two halves. The difference of the pseudo-t volumes between the pair of the datasets is calculated. After multiple resamplings, the confidence limits of the differences within this single condition are computed for a given p-value so that one can test the null hypotheses that the second condition is within the same distribution as the first. The limits are calculated using a bootstrap technique to correct for any bias in the estimated threshold. Power changes between the two conditions are considered significantly different if the difference of the pseudo-t value is larger than expected within conditions. To demonstrate the effectiveness of the technique, the proposed method was applied to MEG responses to two distinct visual stimuli recorded from a single subject. Major differences of brain activity between the two conditions were found in the occipital region. These results were validated using four pairs of split-half datasets, generated from either the odd or even trials in each condition. The method of split-half resampling should therefore be useful for localizing significant differences in brain activity between conditions within individual subjects.

KEY WORDS: Synthetic Aperture Magnetometry, Split-Half Resampling, Bootstrap, Nonparametric Statistic.

INTRODUCTION

Synthetic Aperture Magnetometry (SAM), developed based on the concept of beamformer technique, is a useful tool to analyze MEG data, especially for complex tasks that involve activity in multiple different brain regions. For a given location in the brain, SAM first derives a spatial filter to suppress the interference of unwanted signals from other locations [Robinson and Vrba, 1998]. The source power at that location is then estimated from the filtered signals. The task-related power change is represented by a pseudo-t value, which is a measurement of the power difference between the active and control conditions normalized by the power of the noise. Due to temporal fluctuation of both response and noise, the obtained pseudo-t value for a given condition can vary. To make the pseudo-t values as stable as possible, the active and control conditions should be close together in time. When the two experimental tasks are separated by more than 1 second, the pseudo-t value may not accurately reflect the signal power change between the tasks when one task serves as an active condition and the other as a control condition. Any difference could just as easily reflect changes in the background noise levels. To compare the brain activity between the two conditions, the pseudo-t SAM volume of each condition, calculated relative to an adjacent baseline period, should be computed separately, and statistical analysis performed based on the difference of the pseudo-t values between the conditions. In this study, we propose a statistical procedure to detect the difference of the brain activity between two experimental conditions. By assuming that the pseudo-t values within a volume are independent, the variation of the pseudo-t value within a single condition is estimated. Confidence limits can then be used to identify the brain regions with significant difference in activity between two conditions.

METHODS

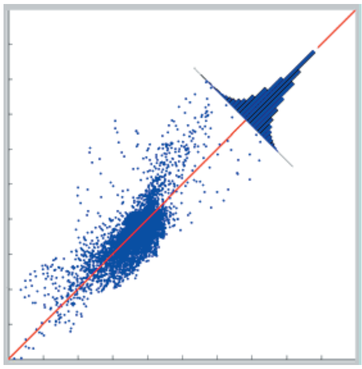

Figure 1. Distribution of pseudo-t values of two conditions

The proposed analysis method is based on the idea that if the difference of pseudo-t values between the two conditions is significant larger than the variation of the pseudo-t values within each condition then it is highly probable that the difference is due to the difference of brain responses for the two conditions. Each pseudo-t value can be broken down into two components, one for the stable response (S) and the other for the variant component (E) that due to either signal fluctuations or noise. For the proposed method to work, the variant component has to be extracted from the pseudo-t value. By just knowing the pseudo-t value, it is not possible to separate the components. However, one can obtain the difference of E from the multiple measurements. Let T_1 and T_2 be the pseudo-t values of the same condition obtained from the two measurements. Their absolute difference is $\Delta T_{12} = | T_1 - T_2 | = | (S_1 + E_1) - (S_2 + E_2) |$. Since S_1 is equal to S_2 by definition, $\Delta T_{12} = | E_1 - E_2 |$. With multiple measurements, one can estimate the distribution of the ΔT within the condition. Now consider the absolute difference of the pseudo-t values between the two conditions, A and B: $\Delta T^{AB} = | T^A - T^B | = | (S^A + E^A) - (S^B + E^B) | = | (S^A - S^B) - (E^A - E^B) |$. We can then test a null hypothesis that the brain responses are identical in both conditions, by considering the two data sets as separated measurements of the same condition. In this case, ΔT^{AB} should have the same distribution as the ΔT within the condition. On the other hand, if the value of ΔT^{AB} is significant different from the ΔT values, the brain responds differently for the two conditions.

Since we have no model of the distribution of ΔT within a condition, we used a nonparametric method to estimate the confidence limits. To avoid the high experimental cost of repeated measurements, a split-half resampling technique was used to estimate the distribution of ΔT values. For each experimental condition, the dataset is divided into two halves, each containing half of the trials. The pseudo-t values for each brain location from the split-half datasets are obtained. Their differences are used to estimate the expected range of the ΔT values for a given p value. The process can be visualized using the scatter plot of the pseudo-t values of the two half datasets. Due to the signal fluctuation, the pseudo-t values form a cloud of values along the diagonal. The deviation between a point and the line represents the difference between two pseudo-t values from the same brain location. Geometrically, this is the projection of the point to the line orthogonal to the 45^{O} line (Figure 1). Based on the distribution of the absolute values of the projected points, a critical value of the ΔT can be determined for any given p value. For example, the point at the upper 5th percentile of the distribution defines the critical point for $p = 0.05$. Any values below this confidence limit are within the expected range of the ΔT values for the condition.

The above procedure determines the expected range of ΔT values from a pair of the split-half datasets; however, the critical value may change when the dataset is divided differently. Ideally, the ΔT distribution should be estimated based on all the split-half datasets. With total of N trials, there are ${}_N C_{N/2}$ different ways to split the dataset. It is usually not feasible to use each pair of the possible split-half datasets to estimate the distribution. Instead a subset of split-half datasets are used to determine the critical value. The mean of the critical values from the split-half resamplings is then used for the significant test. With only small number of samples, the estimated critical value may be biased. A bootstrap technique[Efron, 1993] can adjust for this bias. Once the critical value for the confidence limit is defined, one can test whether a brain location response differs significantly in a second experimental condition.

RESULTS

To demonstrate the effectiveness of the technique, the proposed method was applied to MEG responses to two distinct visual stimuli recorded from a single subject. The data was obtained from two experimental conditions in a visual attention task. The two conditions, referred as Complex and Easy, have different stimulus sets. A total of 64 different stimuli, different in shape, color and shading-orientation, occurred in the Complex condition, and 4 stimuli, different shapes with white color and no shading, in the Easy condition. The subject identified specific target stimuli within each condition. MEG recordings were taken between 400 ms before and 700 ms after the onset of each test stimulus. For each trial, the subject responded by pressing a button on his right side if the test stimuli matched the target and on his left side if not. Only the mismatch trials with correct response are analyzed in this study. The total number of trials for each condition is 328. Five pseudo-t volumes of each condition are generated using the band-pass filters of 4-8Hz, 8-16Hz, 16-30Hz, 30-60Hz, and 60-100Hz, the time interval 50-350ms after stimulus onset for the active window, and 0-300ms before stimulus onset for the control window.

To estimate the normal range of the pseudo-t value difference within a single condition using the proposed method, 100 pairs of the split-half datasets are randomly sampled from the original dataset to obtain the critical value for each pair for the p value of 0.01. The bias of the mean critical value is then estimated by performing 1000 bootstraps on the values. The bias corrected critical value is compared against with the pseudo-t value differences between the Easy and Complex conditions.

The responses (Figure 2) show their main activity in the occipital areas. Among the five frequency bands, relatively large response differences are found in occipital region at the frequency bands of 4-8Hz and 16-30Hz. Compared to the Easy condition, Complex condition has larger pseudo-t values at 4-8Hz band (white areas), but a smaller values at 16-30Hz band (black areas). Inspecting the pseudo-t values of each condition in the region, both conditions show event related synchronization at 4-8Hz and desynchronization at 16-30Hz. The responses may be due to the visual stimuli alone or the target matching process.

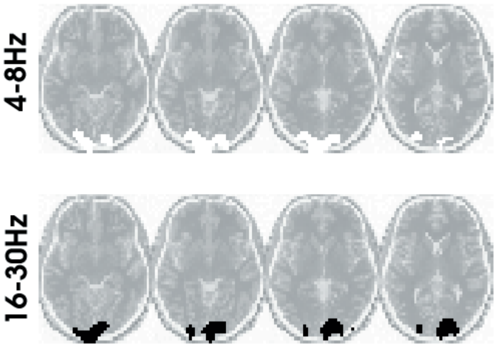

Figure 2. Regions with different power changes between the Complex and Easy Conditions

DISCUSSIONS

This novel statistical analysis method can detect the power change between the two experimental conditions based on the pseudo-t values for each condition. The method estimates the confidence limits for the difference in the pseudo-t value using the split-half resampling technique, with bootstrap bias correction. Brain region with difference of pseudo-t value significantly larger than the expected range are classified as having different response for the two conditions.

The proposed method can localize the significant brain activity within individual subjects. It is particularly useful for the studies for which only a few subjects are available. However, several issues have to be addressed to improve the performance of the method. Traditionally the split-half resampling technique is used for reliability testing [Cronbach, 1951] to detect the consistency of measurement. Strother et al.[2002] used it to derive the prediction and reproducibility metrics for cross-validation. In our method, split-half resampling is used to estimate the expected range of the pseudo-t value deviation. The major drawback for all applications of the split-half technique derives from reducing the sample size by half. Since only half of the trials are used to estimate the expected range, there would be more noise in the variant component of the pseudo-t value. Consequently, the critical value for the significant test is higher (more conservative) than it should be. In addition, there are some situations in which the region with different response for the two conditions is not detected. The pseudo-t value difference between the conditions, ΔT^{AB}, can be small even for the region that responds differently for the two conditions. This happens when the difference of the stable component, $(S^A - S^B)$, and the variant component, $(E^A - E^B)$, are similar.

Results were validated using four pairs of split-half datasets, generated from either the odd or even trials in each condition. Some extra spurious regions were found in each of the four results; however, the regions identified with the original dataset are the common detected regions to all the split-half results. The spurious regions of the split-half results are caused by the reduction of the data. Further study is needed to determine the number of trials required to obtain reliable results. The proposed method is the first statistical analysis technique designed to handle the problem of instability of the pseudo-t values for comparing power changes between conditions. Since this technique also provides a way to analyze differences between conditions in single subjects, it will be useful for studies with only a few subjects.

REFERENCES

Robinson S.E., Vrba, J. Functional neuroimaging by synthetic aperture magnetometry (SAM). In: Yoshimoto T, Kotani M, Kuriki S, Karibe H, Nakasato N, editors. Recent Advances in Biomagnetism. Sendai: Tohuku University Press; 1998. p. 302–305.

Efron, B., Tibshiran, R. An Introduction to the Bootstrap. Chapman and Hall, London, 1993.

Cronbach, L. J. Coefficient alpha and the internal structure of tests. Psychometrika, 1951, 16, 297-334.

Strother, S.C., Anderson, J., et al. The Quantitative Evaluation of Functional Neuroimaging Experiments: The NPAIRS Data Analysis Framework., NeuroImage, 2002, 4:747-771.

Noise Reduction in MEG Data Recorded by a New 500-Channel MEG Vectorgradiometer System

[1]DeMelis, M., [1]DeCesaris, I., [2]DiPietroPaolo, D., [1]Müller, H.-P., [3]Nolte, G., and [1]Erné, S. N.

[1]Division for Biosignals and Imaging Technologies, ZIBMT, University of Ulm, Germany
[2]Advanced Technologies Biomagnetics, Pescara, Italy
[3]NINDS/NIH, Bethesda, USA

ABSTRACT

By performing blind source separation, it is possible to extract noise components in MEG data. In this study, singular value decomposition (SVD) and independent component analysis (ICA) were applied as techniques to reduce noise and to eliminate artefacts in MEG data recorded by a new 500-channel MEG vectorgradiometer system, ARGOS 500.

KEY WORDS

Magnetoencephalography, vectorgradiometer, noise reduction, singular value decomposition

INTRODUCTION

During the last few years, a number of new methodologies have been developed for noise reduction or for the enhancement of important features in biomedical signal analysis. Among other methods, the most important ones proved to be SVD and ICA. By performing blind source separation, it is possible to extract noise components in MEG data [Hyvärinen, 2002]. Singular value decomposition (SVD) and independent component analysis (ICA) have already shown to work as tools for noise reduction and artefact elimination in MCG data [Müller, 2004, DiPietroPaolo, 2004]. In this study, SVD and ICA were applied as techniques to reduce noise and to eliminate artefacts in MEG data recorded by a new 500-channel MEG vectorgradiometer system, ARGOS 500.

METHODS

The MEG recording was performed using a new, 500-channel SQUID vectorgradiometer helmet system, Argos500 (Atb, Pescara, Italy). A volunteer was performing a motor task paradigm (finger ticks). Sampling rate was 1025 Hz. Recording time was 5 minutes. Triggering of the finger ticks was performed by a myogram.

SVD is a technique used to solve sets of linear algebraic equations. A matrix A can be rewritten as a product of a matrix U, a diagonal matrix W, whose elements are either positive or zero (singular values) and the transpose of the Eigenvector matrix V.

$$A = U W V^T \tag{1}$$

Zeroing noise-related components in the matrix U and reconstructing

$$A' = U' W V^T , \tag{2}$$

A' is noise reduced. The disadvantage of this method is in the geometry of the base space. It is desirable to represent it, not in an orthogonal base, but rather in a base of independent components. This is performed by ICA

ICA was initially proposed to solve the problem of blind source separation, for a source signal, after a linear mixture. The input mixture data matrix is whitened before the ICA process, and the whitened data are assumed to be a mixture of independent components. The independent components are latent variables, meaning that they can be measured indirectly. In addition, the mixing matrix is unknown. The basic principle in ICA is that the components are statistically independent. By calculating the mixing matrix with the assumption that the components have maximum statistical independence and by zeroing noise components in the unmixed data, leads to the elimination of noise from the original data.

ICA was applied in the following way: ICA assumes the measured signal $\vec{x}(t)$ to be a linear mixture of unknown source signals $\vec{s}(t)$ with unknown weights A.

$$\vec{x}(t) = A\ \vec{s}(t) \tag{3}$$

The sources are mutually statistically independent*:* their joint probability density function is factorable as the product of their single probability density functions. Before performing ICA, the input data must be centred and whitened [Hyvärinen, 2002].

$$\vec{y}(t) = M\ \vec{x}(t) \tag{4}$$

The ICA algorithms solve

$$\vec{s} = W\ \vec{y} \tag{5}$$

for the unmixing matrix W. After calculating the unmixed data $\vec{s}$, the task is then to properly identify the components representing the artefacts and disturbances from those containing brain related information.

Using appropriate rules, the measured noise signals can be reconstructed by:

$$\vec{n} = \left(W\ M\right)^{-1} Z\ \left(W\ M\right)\ \vec{x} \tag{6}$$

where $Z = diag(z_i)$ with z_i equal to 1 if the respective component should be eliminated, and 0 otherwise.

The measured brain related signals $\vec{x}_r$ can be reconstructed by subtracting the reconstructed noise signals.

$$\vec{x}_r = \vec{x} - \vec{n} \tag{7}$$

RESULTS

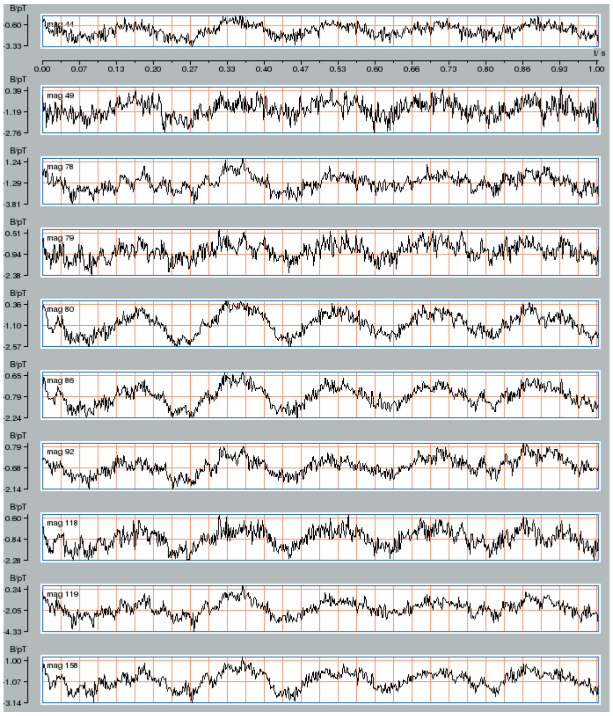

Figure 1. MEG measurement with the 500-channel system, 10 channels are displayed.

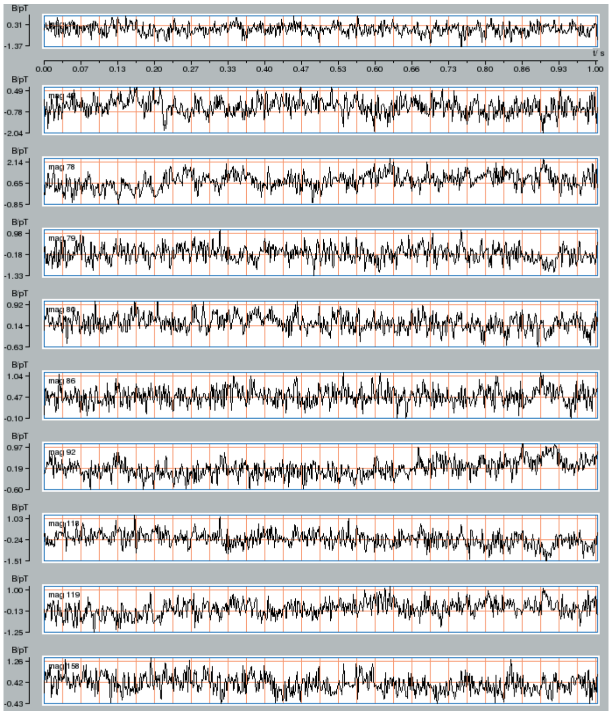

Figure 2. MEG measurement with the 500-channel system, 10 channels after SVD data cleaning are displayed.

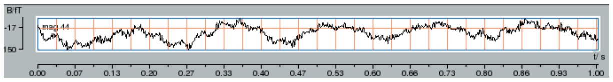

Figure 3. SVD: Unmixed channel to be eliminated.

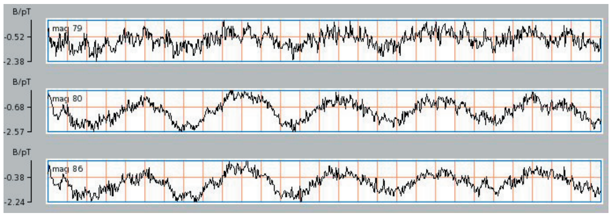

Figure 4. ICA: Unmixed channels to be eliminated.

For the data sets presented here, SVD is able to separate the disturbances in such a way that only one unmixed channel has to be eliminated, whereas the ICA algorithms used here show disturbances in more than one unmixed channel. The appropriate method required for separating the noise has to be determined in the future when more MEG data sets become available.

DISCUSSION

It has been shown, that with SVD it is possible to extract noise components from noisy MEG data. Up until now, ICA had been unsuccessful. The remaining task is to identify noise and heart beat components from the unmixed data. Then, SVD and ICA will emerge as promising methods to eliminate noise and artefacts from standard MEG data sets.

REFERENCES

DeMelis M, Müller H-P, Pasquarelli A, Erné SN. Magnetocardiographic Signal Analysis. Proceedings of BIOMAG 2002, 2002, Jena, Germany, p. 987-989.

DiPietroPaolo, D., Müller, H-P, Nolte, G, DeCesaris, I, Erné, SN. Noise Reduction in MCG data by Singular Value Decomposition and Independent Component Analysis, this conference.

Hyvärinen A, Oja E. Independent Component Analysis: Algorithms and Applications. Neural Netw. 2000, 13: 411-430.

Müller, H-P, Nolte, G, DeCesaris, I, Pasquarelli, A, Erné, SN. Noise Reduction of Magnetocardiographic Data: Exercise with Ergometer, this conference.

Noise Reduction in MCG Data by Singular Value Decomposition and Independent Component Analysis

[1]DiPietroPaolo, D., [2]Müller, H.-P., [3]Nolte, G., [2]DeCesaris, I., and [2]Erné, S. N.

[1]Advanced Technologies Biomagnetics, Pescara, Italy
[2]Division for Biosignals and Imaging Technologies, ZIBMT, University of Ulm, Germany
[3]NINDS/NIH, Bethesda, USA

ABSTRACT

Blind source separation is used for noise reduction in MCG data in which the noise components are detected and removed. In this study, singular value decomposition (SVD) and independent component analysis (ICA) were applied to reduce the noise in MCG data, thereby showing SVD and ICA to be promising methods in eliminating noise and artefacts from standard MCG data sets.

KEY WORDS

Magnetocardiography, noise reduction, independent component analysis, singular value decomposition

INTRODUCTION

During the last few years, a number of new methodologies have been developed for noise reduction or for the enhancement of important features in biomedical signal analysis. Among other methods, the most important ones proved to be SVD and ICA. ICA has already been successfully used for reduction of small disturbances in MCG rest measurements [Steinhoff, 2003, Müller, 2004]. Using ICA and SVD in the implementation of the Open Magnetic and Electric Graphic Analysis (OMEGA) environment [DeMelis, 2003], as shown in this work, highly noisy MCG data can be cleaned with sufficient quality.

METHODS

The MCG recording was carried out on a 55-channel planar SQUID magnetometer system, Argos55 (Atb, Pescara, Italy) [Erné, 1998]. For this standardised MCG recording a map of 55 magnetic channels, three orthogonal HRECG leads and a breathing channel are used. The MCG signals are sampled at 8.2 kHz, digitally filtered and decimated to a final sampling frequency of 1 kHz and a bandwidth between DC and 250 Hz.

SVD is a technique used to solve sets of linear algebraic equations. A matrix A can be rewritten as a product of a matrix U, a diagonal matrix W, having elements which are either positive or zero (singular values) and the transpose of the Eigenvector matrix V.

$$A = U W V^T \tag{1}$$

Zeroing noise-related components in the matrix U and reconstructing

$$A' = U' W V^T , \tag{2}$$

A' is noise reduced. The disadvantage of this method is in the geometry of the base space, as it is desirable to represent it, not in an orthogonal base, but rather in a base of independent components. This is performed by ICA.

ICA was initially proposed to solve the problem of blind source separation, for a source signal, after a linear mixture. The input mixture data matrix is whitened before the ICA process, and the whitened data are assumed to be a mixture of independent components. The independent components are latent variables, which mean they can be measured indirectly. In addition, the mixing matrix is unknown. The basic principle in ICA is that the components are statistically independent. Calculating the mixing matrix with the assumption that the components have maximum statistical independence and zeroing the noise components in the unmixed data will lead to a reduction of noise in the original data.

We experimentally observed that it is possible to separate the 55 channels into 2 groups (28 and 27 channels, homogeneously distributed over the sensor area) in a suitable way. This division of the data into 2 subgroups results in the dramatic improvement in the operational speed of the algorithm as the computation time of the following algorithm is mainly dependent on the number of sensors. Thus, two unmixing matrices were calculated and the reconstruction of the signals was performed independently for the two groups of sensors.

ICA was applied in the following way: ICA assumes the measured signal $\vec{x}(t)$ to be a linear mixture of unknown source signals $\vec{s}(t)$ with unknown weights A.

$$\vec{x}(t) = A\ \vec{s}(t) \tag{3}$$

The sources are mutually statistically independent**:** their joint probability density function is factorable as the product of their single probability density functions. Before performing ICA, the input data must be centred and whitened [Hyvärinen, 2002].

$$\vec{y}(t) = M\ \vec{x}(t) \tag{4}$$

The fast ICA algorithm [Hyvärinen, 2002] solves

$$\vec{s} = W\ \vec{y} \tag{5}$$

for the unmixing matrix W. After calculating the unmixed data $\vec{s}$, the task was then to properly identify the components representing the artefacts and disturbances from those containing the heart information. Basically, there are 2 approaches: 1) positively identifying the heart signals and 2) positively identifying the disturbances. The positive identification of heart related components was performed by taking advantage of the simultaneous recorded HRECG data and the derived trigger points list. Averaging the time-series using HRECG trigger points provided a drastic improvement of the signal-to-noise ratio. A comparison (via cross-correlation) of the averaged odd and even beats demonstrated to be an excellent indicator for heart activity related to the unmixed channels. Vice versa, an important heuristic finding was that unmixed channels were associated with artefacts and disturbances when the maximum of the power spectrum was above a certain threshold. Using these two rules, the measured noise signals were then reconstructed by:

$$\vec{n} = \left(W\ M\right)^{-1} Z\ \left(W\ M\right)\ \vec{x} \qquad (6)$$

where $Z = diag(z_i)$ with z_i is 1 if the respective component should be eliminated, and 0 otherwise.

The measured heart signals $\vec{x}_r$ were then reconstructed by subtracting the reconstructed noise signals.

$$\vec{x}_r = \vec{x} - \vec{n} \qquad (7)$$

RESULTS

Figure 1 shows an example for data cleaning of standard MCG data by SVD. Due to the high signal-to-noise ratio of the recording system, the cleaning effect, judged by visual inspection, is very low. Therefore, in Figure 2, the result of cleaning by SVD in data with a lower signal-to-noise ratio is shown. The noisy data was artificially produced by placing a radio near the recording sensor. In Figure 3, the data cleaning by ICA of the same data set is shown. Note that there are some problems with the reconstruction of the T-wave.

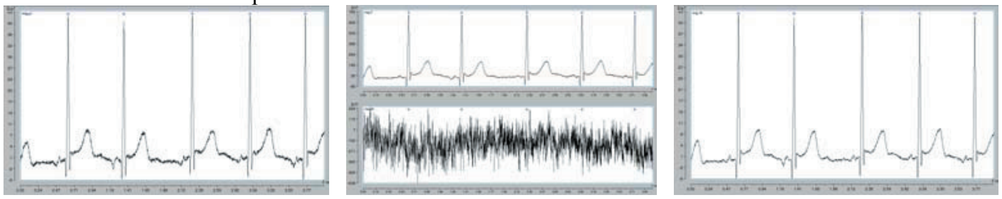

(a) (b) (c)

Figure 1. Example for cleaning MCG data with SVD: **(a)** measured channel with maximum QRS-amplitude. **(b)** unmixed signals: upper row: heart beat related, lower row: noise related. **(c)** cleaned channels (compare (a)).

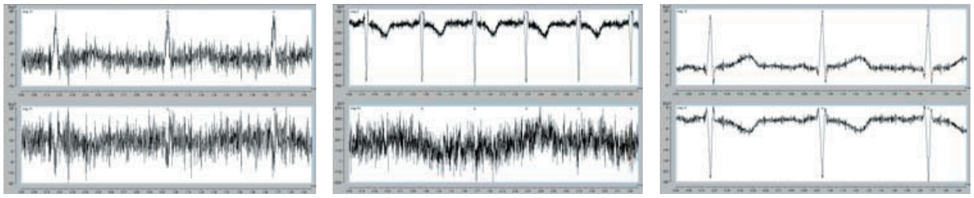

(a) (b) (c)

Figure 2. Example for cleaning MCG data with SVD: **(a)** measured channel with maximum and minimum QRS-amplitude. **(b)** unmixed signals: upper row: heart beat related, lower row: noise related. **(c)** cleaned channels (compare (a)).

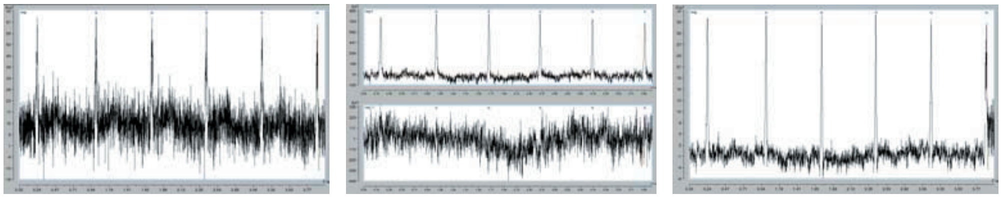

(a) (b) (c)

Figure 3. Example for cleaning MCG data with ICA: **(a)** measured channel with maximum QRS-amplitude. **(b)** unmixed signals: upper row: heart beat related, lower row: noise related. **(c)** cleaned channels (compare (a)).

DISCUSSION

As shown, both SVD and ICA are able to extract the noise components from noisy MCG data. The only remaining task is to automatically identify the noise and heart beat components from the unmixed data, thus making SVD and ICA promising methods in the elimination of noise and artefacts from standard MCG data sets.

REFERENCES

DeMelis M, Müller H-P, Pasquarelli A, Erné SN. Magnetocardiographic Signal Analysis. Proceedings of BIOMAG 2002, 2002, Jena, Germany, p. 987-989.

Erné SN, Pasquarelli A, Kammrath H, Della Penna S, Torquati K, Pizzella V, Rossi R, Granata C, Russo M. Argos 55 - The New MCG System in Ulm. Proceedings of BIOMAG98, 1998, Sendai, Japan.

Hyvärinen A, Oja E. Independent Component Analysis: Algorithms and Applications. Neural Netw. 2000, 13: 411-430.

Steinhoff U, Mäntynen V, Kürsten R, Nenonen J. Independent Component Analysis for the Suppression of Different Noise in Magnetocardiographic Data. Biomed. Technik 2003, 48 suppl. 1: p. 170-171.

Müller, H-P, Nolte, G, DeCesaris, I, Pasquarelli, A, Erné, SN. Noise Reduction of Magnetocardiographic Data: Exercise with Ergometer, this conference.

Rejection of stimulus-related MEG artifacts using independent component analysis

Iwaki, S.[1),2)], Yamamoto, C.[3)], Tonoike, M.[2)], Yamamoto, T.[3)]

[1)] NMR Center, Massachusetts General Hospital, Charlestown, MA, USA, [2)] National Institute of Advanced Industrial Science and Technology, Osaka, Japan, [3)] Graduate School of Human Sciences, Osaka University, Osaka, Japan

ABSTRACT

Electro-gustatory (EG) stimuli have been used to investigate the gustatory information processing in the human brain with precise temporal and spatial accuracy. But this technique was not widely applicable to magnetoencephalographic measurements due to the difficulty in eliminating huge stimulus-related artifact. In this study, we used independent component decomposition of the measured signal to reject the stimulus-related artifact from other brain activities based on information maximization (infomax) approach. Infomax ICA was applied to raw MEG data measured by 122 magnetometer channels producing 122 temporally independent components, and the trials for each component were averaged separately. Each independent component was visually inspected and the components obviously representing the EG stimulus-related artifacts were excluded from remixing and the signal projection onto the original MEG signal space to reconstruct the artifact-free MEG signals. Results showed that large EG stimulus-related artifacts were clearly removed from MEG waveforms. We were also able to separate blink related components and magnetocardiographic components as well as the components representing alpha-band (8-13 Hz) spontaneous brain activity.

KEY WORDS

Electro-gustatory stimuli, MEG, independent component analysis, information maximization, artifact rejection

INTRODUCTION

Neuromagnetic recording (MEG: magnetoencephalography) is one of the most promising techniques to investigate the human gustatory function with high temporal and spatial accuracy, though, it requires millisecond accuracy to synchronize each stimulus delivery for signal averaging. In this study, we used electro-gustatory (EG) stimuli, in which weak anodal currents (< 50 mA) were applied to subjects' anterior tongue tip, to ensure precise control of stimulus location and timing [Frank, 1991]. These currents predominantly stimulate the gustatory system, while higher currents increasingly stimulate somatosensory systems [Barry, 2001]. Only few studies were reported using EG stimuli for MEG and EEG (electroencephalography) measurements, largely due to the difficulty in eliminating large EG stimulus-related artifacts in the MEG/EEG data.

Here, we introduce independent component analysis (ICA) to differentiate stimulus-related artifacts from EG MEG signals.

METHODS

Stimulus and Data Acquisition: Ag/AgCl electrodes connected to the electrogustometer (Rion TR-05) by twisted-pair copper wires were used to deliver EG stimuli to the subjects sitting inside of the MEG shielded room. An anode was placed on the right lateral margin of tongue 20 mm apart from tongue tip; the cathode was placed on the inferior surface of tongue. The EG stimuli were 200 ms square electric current pulses with the intensity of 25-64 mA, which was chosen for each subject to be consistently detectable, yet below that causing mild tingling, generated by the electrogustometer. MEG signals were measured with a whole-cortex-type MEG system (Neuromag-122) [Hamalainen, 1993]. The stimulus-related epochs of 1500 ms, including a 200 ms pre-stimulus baseline, were recorded more than 40 trials with a pass-band of 0.03 - 100 Hz and a sampling rate of 400 Hz.

Signal Processing: We adopted the ICA [Common, 1994] technique to differentiate the EG stimulus-related artifact from other signals corresponding to brain activities. ICA was originally proposed to solve the blind source separation problem, in which the statistically independent source signals $s = [s1(t), \ldots, sN(t)]$ are reconstructed from their linear mixture $x = As$. The important assumption used in ICA is that the time courses of the original source signals are as statistically independent as possible [Jung, 2001]. The algorithms to find out a linear 'unmixing' matrix W to recover the original sources as $u = Wx$ were proposed recently, most of which is performed using unsupervised learning algorithms. In this study, we used 'information maximization (infomax)' algorithm [Makeig, 1997] to calculate unmixing matrix W, which minimizes the mutual information among the output independent components by maximizing the joint entropy of the output of simple neural network. Infomax ICA was applied to all 40 trials measured by 122 magnetometer channels producing 122 temporally independent components, and the trials for each component were averaged separately. Each independent component was visually inspected and the components obviously representing the EG stimulus-related artifacts were excluded from remixing and the signal projection onto the original MEG signal space to reconstruct the artifact-free MEG signals.

RESULTS

As shown in Fig. 1, large stimulus-related artifacts were observed between 0 and 200 ms after the EG stimulus onset.

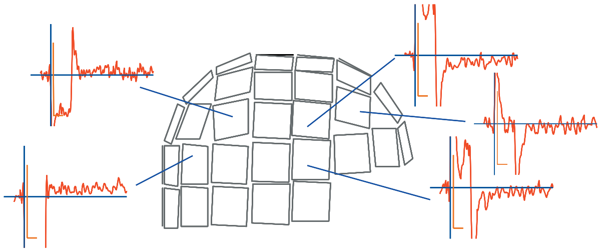

Fig. 1 Measured MEG signals with large stimulus- related artefacts during EG experiment.

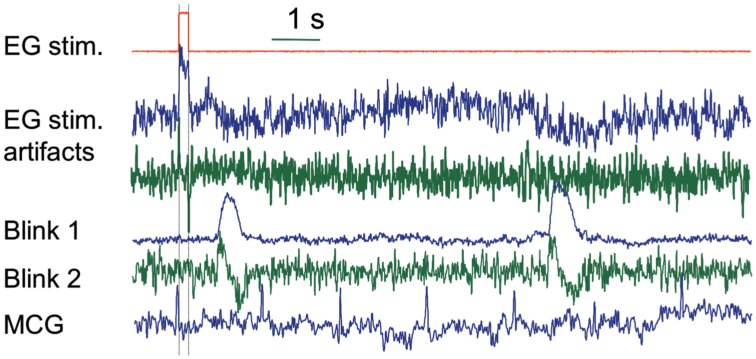

Fig. 2 Examples of the raw waveforms decomposed using Infomax ICA.

Example of the decomposed independent components are shown in Fig. 2, and the averaged waveforms of predominant components and their field distributions, which are projected onto the original MEG signal space, are shown in Fig. 3. In this example, components (a) and (b) in Fig. 3 were rejected as the EG stimulus-related artifacts. Results of the ICA-based artifact rejection are shown in Fig. 4. Large stimulus-related artifacts as shown in Fig. 1 were clearly removed from MEG waveforms.

We were also able to separate blink related components and magnetocardiographic components as well as the components representing alpha-band (8-13 Hz) spontaneous brain activity (Fig. 2).

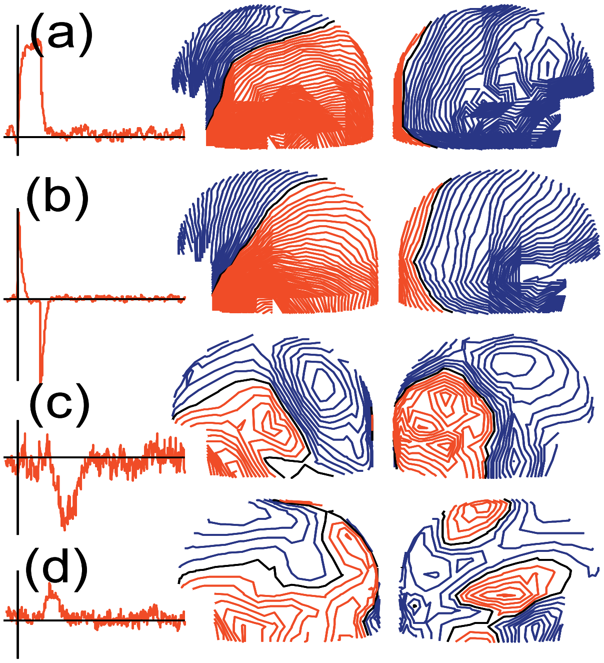

Fig. 3 Examples of the averaged waveforms of decomposed components and their spatial distribution projected to the sensor space..

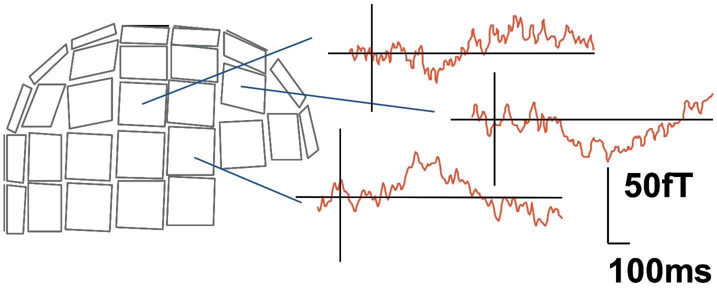

Fig. 4 Averaged MEG signals after artefact rejection.

DISCUSSION

The ICA derives a set of spatial filters that decompose MEG signals into a weighted sum of temporally independent components with fixed spatial distributions [Makeig, 1997]. Unlike principal component analysis (PCA) that requires the spatial orthogonality of each component, ICA does not impose any condition on the spatial filters, which makes it possible to detect concurrent brain activity arising from any spatially overlapping source distributions. One limitation of the method used here is that the artifact rejection requires visual inspection of the independent components. In our application of ICA to EG stimulus-related artifact removal, the major artifactual components were distinct as shown in Figures 2 and 3, which suggests the possibility to develop automatic procedure to detect and remove these components from contaminated MEG signals.

ACKNOWLEDGEMENTS

The authors would like to thank M. Yamaguchi in National Institute of Advanced Industrial Science and Technology for his assistance to acquire MEG signals evoked by electro-gustatory stimuli. This study was supported in part by the research grant from Japan Society for the Promotion of Science.

REFERENCES

Frank, M.E., Smith, D.V., Electrogustometry: a simple way to test taste. in Smell and Taste in Health and Disease. T.V. Getchell et al. Eds. New York: Raven Press, pp.503-514, 1991.

Barry, M.A., Gatenby, J.C., Zeiger, J.D., Gore, J.C., Hemispheric dominance of cortical activity evoked by focal electrogustatory stimuli. Chem. Senses. 2001; 26: 471-482.

Hamalainen M, Hari R, Ilmoniemi RJ, Knuutila J, Lounasmaa OV, Magnetoencephalography - theory, instrumentation, and application to noninvasive studies of the working human brain. Rev. Mod. Phys. 1993; 65: 413-497.

Comon, P., Independent component analysis, a new concept? Signal Process. 1994; 36: 287-314.

Jung, T-P., Makeig, S., McKeown, M.J., Bell, A.J., Lee, T-W., Sejnowski, T.J., Imaging brain dynamics using independent component analysis. Proc IEEE. 2001; 89: 1107-1122.

Makeig, S., Jung, T-P., Bell, A.J., Ghahremani, D., Sejnowski, T.J. , Blind separation of event-related brain responses into independent components. Proc. Natl. Acad. Sci. 1997; 94: 10979-10984.

Magnetic Noise Rejection Method using Independent Component Analysis for the Magnetocardiogram –magnetic noise by the wire for the operation-

K. Kobayashi[1], K. Yamazaki[2], Y. Uchikawa[2], T. Simizu[3], K. Nakai[4], K. Kawazoe[4], H. Izumoto[4], and M. Yoshizawa[1]

[1]Iwate University, Japan, [2]Tokyo Denki University, Japan
[3]Iwate Industrial Promotion Center, Japan, [4]Iwate Medical University, Japan

ABSTRACT

In magnetocardiogram (MCG) measurements, the magnetic noise from the wire used to suture the sternum after heart surgery becomes a problem. As one method of noise rejection, independent component analysis is effective.

In this study, MCG measurements were carried out under the conditions that the wire was attached to a normal subject and that the wire was not attached. Signal processing by independent component analysis [Kobayashi, 2004] was carried out in order to reduce the effect of magnetic noise from the wire. From the comparison of the waveforms after this signal processing and the waveforms where the wire was not attached, it was apparent that the magnetic noise from the wire was reduced.

From this result, it is clear that independent component analysis is effective for the removal of the magnetic noise from the wire.

KEY WORDS

Magnetocardiogram, independent component analysis, wire noise, signal processing

INTRODUCTION

Recently, the clinical application of magnetocardiograms (MCGs) has been widely studied, and analysis of the conduction process and evaluation of ischemic heart disease have been carried out. However, postoperative diagnosis using a MCG becomes difficult in the patient who has a wire fixed in the sternum by the thoracotomy operation, since the magnetic noise from the wire is very big.

As a signal analysis technique, independent component analysis is a useful method for separating the independent signals from overlapping signals.

We carried out MCG measurements under the conditions that a wire was attached to a normal subject and that a wire was not attached. The signal processing by independent component analysis was carried out in order to reduce the effect of the magnetic noise from the wire. We compared the waveforms after this signal processing and the waveforms where the wire was not attached.

METHODS

The MCGs were measured at 64 points at 2.5cm intervals on the chest wall of a normal subject. To simulate of the magnetic noise from the wire in a postoperative, the wire (SUS304) for the operation was placed on the chest wall (3cm under the episternum) of a normal subject. This wire was equipped with a strap and was fixed by tape to allow simple detachment. First, the MCG measurements were carried out with the wire attached. Next, the strap was pulled, the wire removed, and MCGs were measured without moving the subject. These measurements differ only in the effect of the wire. This method allows the comparison of the waveforms with the wire attached and those without the wire. The magnetic field data was processed with a 50Hz notch filter and 0.1Hz - 90Hz band pass filter, and the data was separated into seven components by principal component analysis (PCA). The reason as seven components was experientially decided, considering the noise level. Independent component analysis was done for these data, and it was separated to seven independent components. For each component, a Fourier transformation was carried out and the ratio (LF/HF) of the signal under 0.6Hz (LF) and over 0.6Hz (HF) was calculated. The component over LF/HF = 0.1 was deleted as an effect of the wire. Finally, the waveforms were reconstituted from the component of the remainder. Then, the MCG waveforms were averaged 40 times in the R wave synchronization of the ECG.

RESULTS

Fig.1 shows the averaged MCG waveforms with the wire attached. The effect of magnetic noise from the wire appears at a T wave, and it is clear that noise rejection is difficult using the averaging method only. Fig.2 shows the waveforms separated into seven components by independent component analysis. Since the wire vibrates due to respiration, the magnetic noise appears in the 1st, 6th, and 7th components. Also, low frequency environmental magnetic noise appears 4th component. Fig.3 shows the reconstructed MCG waveforms that removed the 1st, 4th, 6th, and 7th components. The effect of the wire which has appeared the T wave can be reduced. For comparison, Fig.4 shows the averaged MCG waveforms without the wire. The waveforms of Fig.3 and Fig.4 resemble each other well, and it is clear that the effect of the wire can be reduced.

Fig.5 shows the isofield contour maps of each T wave (600ms). In the isofield contour map such as the one on the left, the effect of the wire appears mainly in the

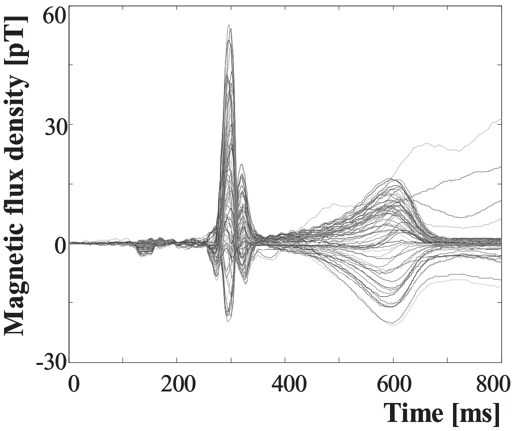

Figure 1. The averaged MCG waveforms with the wire attached to a normal subject.

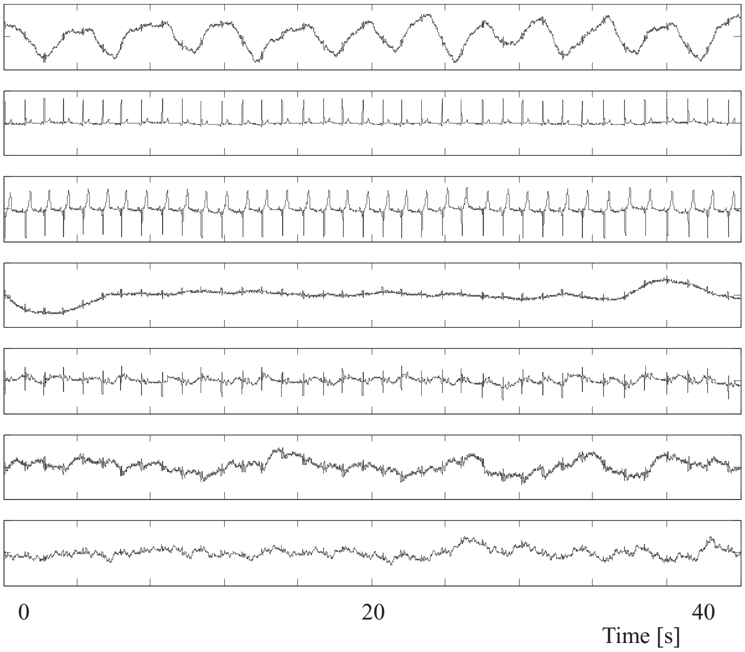

Figure 2. The waveforms separated into seven components by independent component analysis.

upper part, but there is also a small effect in the center map, and the two maps on the right resemble each other well. It is clear that the signal processing using independent component analysis is effective.

CONCLUSION

Signal processing by independent component analysis was carried out in order to reduce the effect of magnetic noise from the used to suture the sternum after heart surgery. It was shown that independent component analysis was effective for the removal of the magnetic noise from the wire.

ACKNOWLEDGEMENTS

This work was supported by the joint research project of Regional Entities for the Advancement of Technological Excellence in Iwate Prefecture, on "Advanced Applications of Magnetic Fields".

REFERENCES

K. Kobayashi, Y. Uchikawa, et al: 2004. Visualization of the current density distribution for MCG with WPW syndrome patients using independent component analysis, IEEE Trans. Magnetics, Vol.40 (in press).

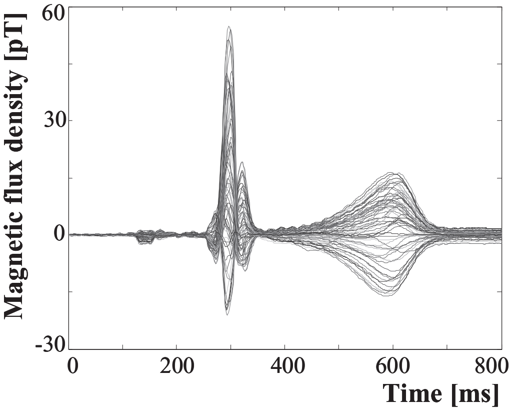

Figure 3. The reconstructed MCG waveforms that removed the 1st, 4th, 6th, 7th components.

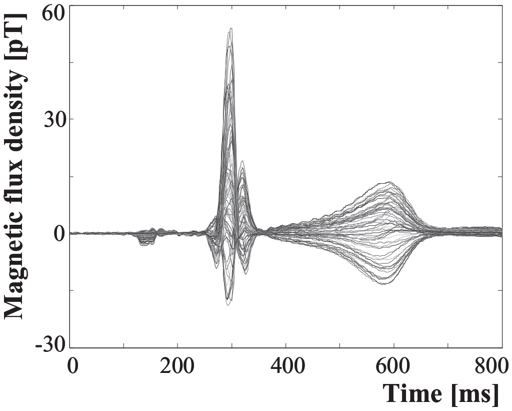

Figure 4. The averaged MCG waveforms without the wire.

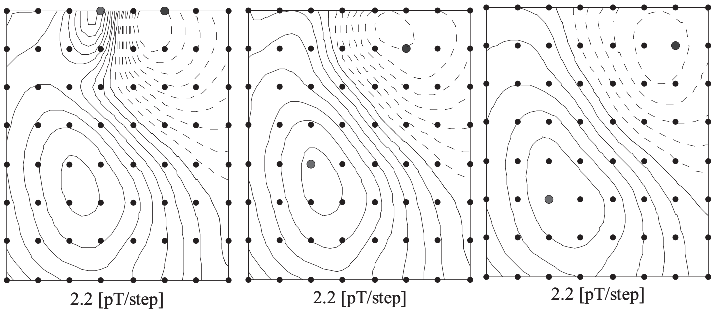

Figure 5. The isofield contour maps of each T wave (600ms). The left map shows the results with the wire attached. The center map shows the reconstructed MCG. The right map shows the results without the wire.

P1-1

Elimination of Brain Noise from MEG Data using ICA with Robust Pre-Whitening Technique

Yoshio Konno (1), Jianting Cao (2,3), Tsunehiro Takeda (4), Hiroshi Endo (5), Mamoru Tanaka (1), and Takayuki Arai (1)

(1) Sophia University, Japan. (2) Saitama Institute of Technology, Japan. (3) RIKEN, Japan.
(4) Tokyo University, Japan. (5) National Institute of Bioscience and Human-Technology, Japan.

ABSTRACT

In this paper, single-trial and averaged multiple-trials data are analysed applying proposed robust pre-whitening technique with independent component analysis (ICA), in order to study the performance of source decomposition in each case. To evaluate the performance of source decomposition, we use a synthesized MEG data set. The main advantage of our data set is that dipole location of evoked responses and its dynamics are known in advance, which facilitates the evaluation of the decomposed components. Moreover, some existing ICA algorithms such as JADE, Fast-ICA, and Natural gradient-based ICA with robust pre-whitening technique are used to eliminate brain noise. Our results show the performance of source decomposition applying proposed approach and the effectiveness of JADE algorithm for our MEG data analysis.

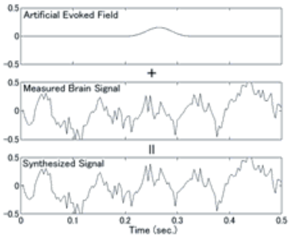

Figure 1. An example for data synthesizing.

KEY WORDS: Magnetoencephalography (MEG), robust pre-whitening technique, independent component analysis (ICA), JADE algorithm, fast-ICA, and natural gradient-based ICA, source localization.

INTRODUCTION

When detecting an MEG signal applying ICA, spontaneous and environmental noises may seriously affect recorded data because the magnetic field of brain signals is weak. The most widely used technique for reducing noises is to take averages across many stimulation trials. However, by taking averages, important information such as the trial-by-trial variation will be lost, making it advantageous to decrease the number of averages across data trials. The disadvantage of having fewer averages is that because SNR is very poor, the decomposition of a low-power source signal from recorded data is still influenced by noise. In this paper, we deal with both single-trial and averaged multiple-trials data, in order to study the accuracy of source decomposition in each case.

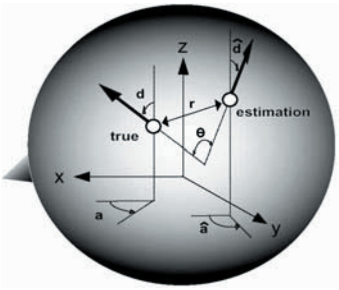

Figure 2. Distance and angle between true and estimated evoked fields.

MEG DATA SET

In this study, we use a synthesized MEG data set, which includes an artificial evoked field and real measured data (recorded by Omega-64). The behavior of our data set is similar to auditory evoked fields (AEFs). The sampling rate was 250 Hz with duration of 40 sec. and our data set was segmented into 80 trials. The source signals in this data set include evoked field response as well as the electrical power interference and the alpha-wave component involved in the real measured MEG data. The evoked field signal was artificially evoked from 0.2 to 0.3 sec. with a peak at 0.25 sec. (see Fig. 1). Dipole location, direction vector, and dipole moment of evoked field are set at [x, y, z]=[10, 10, 60] mm, [az, dec]=[50, 103] deg., and Q=40 (nAm), where a head model presupposes a sphere with a radius of 75 mm.

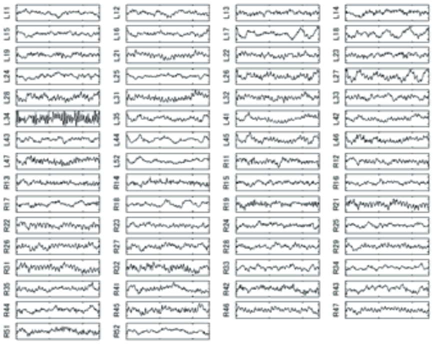

Figure 3. Averaged of 10 trials. The horizontal and vertical axes express time (0 - 0.5 sec.) and amplitude (-0.3 to 0.3 pT), respectively.

SIMULATION AND EVALUATION METHODS

In order to decompose brain sources, we apply the JADE [1], Fast-ICA [2], and natural gradient-based algorithm [3]. Moreover, we introduce our robust pre-whitening technique [4] for pre-processing. This technique is very capable of reducing the power of additive noises. A similar noise reduction approach that applies factor analysis to the decomposition of MEG data has been reported. Both this method and ours take additive noises into account, but with our robust pre-whitening technique, the distribution of additive noises is not restricted. Therefore, our technique is more robust and effective for data with non-Gaussian noises such as the outlier. In order to investigate the performance of source decomposition, we focus on: 1) the accuracy of source estimation, and 2) the power of decomposed components. In this study, we take averages across different numbers of trials from 1 to 50 trials, and in each averaging process, we use 30 moving samples.

To investigate the accuracy of source estimation, we apply dipole estimation to averaged observation and the decomposed evoked signal focusing on evoked response. Since dipole location and direction vector of evoked field were known in advance, the estimation error of evoked field can be obtained, comparing the true and estimated ones. We used the standard spatio-temporal dipole fitting routine, MEG v3.3a (CTF System Inc., Canada), to find the dipole. The distance between true and estimated source locations and the angle between true and estimated direction vectors, used for evaluation of source decomposition, are obtained as (see Fig. 2),

$$r = \left\{(x-\hat{x})^2 + (y-\hat{y})^2 + (z-\hat{z})^2\right\}^{1/2},\ \theta = \cos^{-1}\left\{\sin d \sin \hat{d} \cos(a-\hat{a}) + \cos d \cos \hat{d}\right\}. \quad (1)$$

In order to investigate the power of decomposed components, we take averages of the power of decomposed evoked field signal, electrical power interference, and alpha-wave component, in each number of averages.

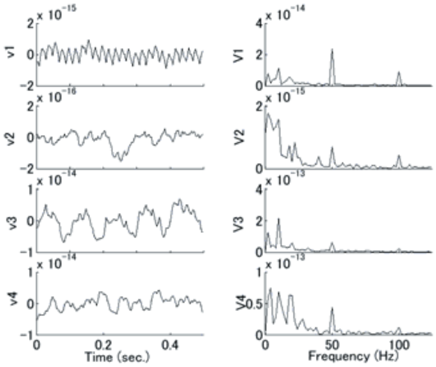

Figure 4. Result of source decomposition and its frequency contents.

RESULTS

We first demonstrate the results of the source decomposition and localization, using the JADE algorithm, to the averaged 10 trials data as shown in Fig. 3. The results v(t) and the power spectra V(f) are shown in Fig. 4. Applying automatic classifying approach [5] to these decomposed components, v1, v2 and v3 in Fig. 4 are regarded as electrical power interference, evoked field response, and alpha-wave component, respectively. The estimated maps derived by averaged data and decomposed evoked response are shown in Fig. 5. Note that the evoked response appears on the left-front area of the brain. The estimated evoked field and the estimation error are shown in Tab. 1. Comparing the results of the JADE and taking averages, we conclude that estimated evoked field becomes more accurate by applying proposed approach.

Here, we demonstrate the performance of JADE, Fast-ICA, and natural gradient-based algorithm with robust pre-whitening technique. The accuracy of source estimation, the estimation error of evoked field calculated by Eq. (1), is shown in Fig. 6. Given these results, regardless of the analysis, the larger the number of averages, the lower estimation error becomes. Comparing the results of averaged data with decomposed evoked field, regardless of the number of averages, evoked field signal is accurately decomposed by applying any ICA algorithm. This means that estimated evoked fields derived by proposed approach are more accurate than those of taking averages and the number of average can be reduced by applying proposed approach.

The relationship between the power of each decomposed component and the number of averages is shown in Fig. 7. As for the power of electrical power interference and alpha-wave component, the larger the number of averages, the lower the power of these components become. This means that these components are influenced by taking averages. In contrast, the power of evoked response is not influenced by taking averages. The results of JADE algorithm especially appear to be stable against the number of averages. This means that JADE algorithm is very efficient for our data analysis. But, as for single-trial data analysis, the power of evoked field becomes very large, because of the influence of additive noise.

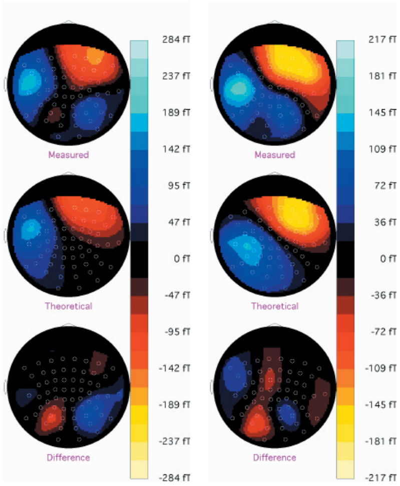

Figure 5. Estimated map focusing on evoked field: (left) averaged data, and (right) decomposed evoked field.

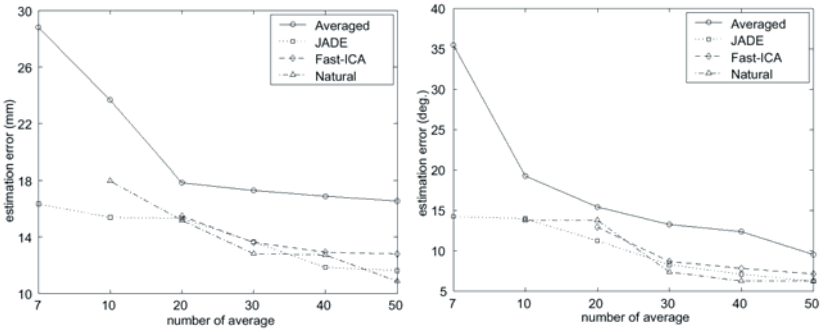

Figure 6. Estimation error applying JADE, Fast-ICA, and natural gradient-based algorithm: (left) dipole location, and (right) direction vector.

CONCLUSIONS

In this paper, the performances of source decomposition applying ICA with robust pre-whitening technique for single-trial and averaged MEG data are investigated. Besides, some existing ICA algorithms are used to eliminate brain noise from MEG data. Our results show the relationship between the accuracy of source decomposition and the number of averages, and applying our ICA approach, the number of average can be reduced. These results strictly confirmed the effectiveness of developed analysis methods.

REFERENCES

[1] J. F. Cardoso and A. Souloumiac, "Jacobi angles for simultaneous diagonalization," SIAM J. Mat. Anal. Appl., Vol. 17, No. 1, pp. 145-151, 1996.
[2] A. Hyvaerinen and E. Oja, "A fast fixed-point algorithm for independent component analysis," Neural Computation, Vol. 9, No. 7, pp. 1483-1492, 1997.
[3] S. Amari, A. Cichocki, H. H. Yang, "A new learning algorithm for blind signal separation," Advances in Newral Information Processing System 8, MIT Press, pp. 757-763, 1996.
[4] J. Cao, N. Murata, S. Amari, A. Cichocki and T. Takeda, "A robust approach to independent component analysis of signals with high-level noise measurements," IEEE Trans. on Neural Networks, Vol. 14, No. 3, pp. 631-645, June 2003.
[5] Y. Konno, J. Cao, T. Arai and T. Takeda, "Visualization of Brain Activities of Single-Trial and Averaged Multiple-Trials MEG Data," IEICE Trans. on Fundamentals, Vol. E86-A, No. 9, pp. 2294-2302, Sep 2003.
[6] S. Makeig, A. J. Bell, T. -P. Jung and T. J. Sejnowski, "Independent component analysis of electroencephalographic data," Advances in Neural Information Processing System 8, MIT press, pp.145-151, 1996.

Table 1. Estimated map and estimation error.

	Dipole location (mm)				Direction vector (dec.)		
	x	y	z	r	az	dec	theta
True value	10.0	10.0	60.0	-	50.0	103.0	-
Before ICA	16.4	14.7	37.7	23.7	40.7	120.3	19.3
After ICA	-2.1	0.6	61.5	15.4	48.2	89.1	14.0

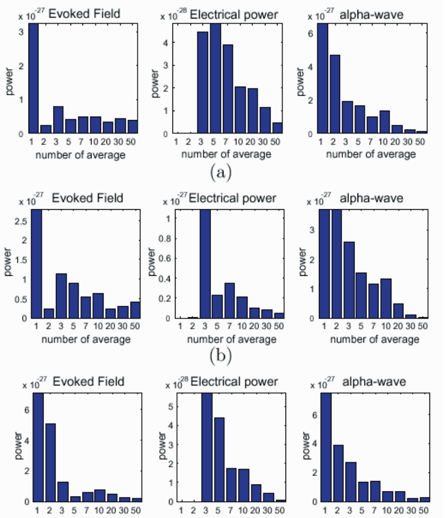

Figure 7. Power of decomposed components : (a) JADE, (b) Fast-ICA, and (c) natural gradient-based algorithm.

Automatic Artifact Component Removal Using a Neural Network in MCG Signal

D.H. Lee* and C.B. Ahn

Department of Electrical Engineering, Kwangwoon University, *ConverTech Co., Seoul, Korea

ABSTRACT

An algorithm combining a neural network and a principal component analysis (PCA) is proposed to remove a pulse-type artifact which often occurs in the 61 channel MCG system installed at Samsung Medical Center in Seoul, Korea. In the proposed work, the acquired signal is first decomposed into components by the PCA, and the components corresponding to the artifact are identified and removed by the neural network. The neural network is an essential component in the automation procedure. Unlike existing artifact rejection algorithms, the proposed algorithm is on a component-by-component basis, and the restored signal is used for further processing once the artifact components are successfully removed. Seven parameters are extracted from each time-domain component and are used as the input to the neural network. They are maximum, minimum, peak-to-peak value, variance, mean, skewness, and quatorsis. In the experiments with volunteers, 97% of the decisions made by the neural network are identical to those by the human experts. Using the proposed technique, the artifact was successfully removed from the MCG signal.

KEY WORDS

Magnetocardiography, Artifact, Principal Component Analysis, Neural Network

INTRODUCTION

Biomagnetic signal carries important information related to organ functions. Since the intensity of the biomagnetic field is so weak that it is often suppressed by external environmental noise. In our 61 channel MCG system installed at Samsung Medical Center in Seoul, Korea, a pulse-type artifact is often observed in some channels related to the operations of other machines near the MCG system. Since the occurrence of the artifact is random, and the duration of the artifact is about 50-100 milliseconds with a broad range of frequencies, it was difficult to remove it by conventional filtering techniques or time-domain analysis. In order to remove the artifact, an algorithm combining a neural network and a principal component analysis (PCA) is proposed.

METHODS

Principal component analysis (PCA) has been known as an effective technique to remove a correlated noise. For instance, it has been successfully applied to the improvement of SNR in the evoked neuromagnetic field by eliminating correlated spontaneous field. In this paper, the technique is applied to the removal of pulse-type artifact in the 61 channel MCG system installed at Samsung Medical Center. The noise is supposed to be correlated in character due to operations of other machines near by the MCG system. With a pulse-type shape with a relative long duration (50~100ms), it's not easy to remove it by simply applying filtering or time domain analysis.

The MCG signal is decomposed into components by the PCA method, and some dominant components are identified as either signal component or noise component. Dominant components are chosen based on the PC score, the relative magnitude of the component with the eigenvalues. Figure 1 shows some dominant components of the acquired MCG signal. As seen in Fig.1, the component in the lower left corner is identified as a noise component. Although the identification of the noise component is not a difficult procedure, it is important to implement it in an automatic manner for a practical application. For this purpose, a neural network is combined for an automatic identification as shown in Fig.2. Seven parameters (maximum, minimum, peak-to-peak value, variance, average, skewness, and kurtosis) are used as the input to the neural network. Once the noise components are removed, the signal components are reconstructed to make a restored signal for further processing.

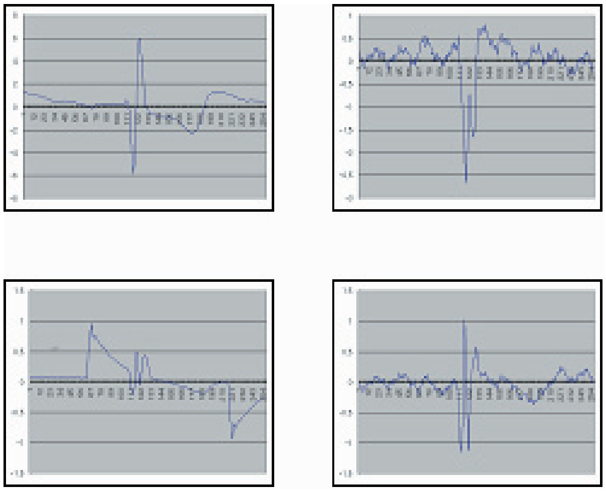

Fig.1 Dominant components of the measured MCG signal

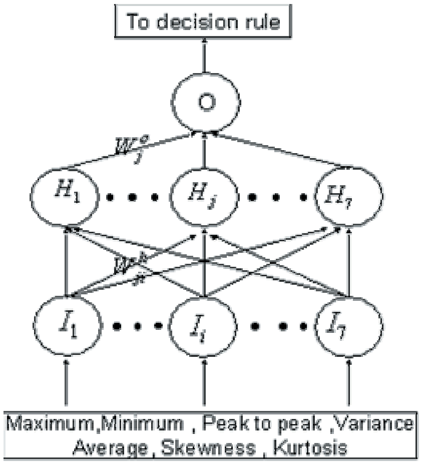
To decision rule
O
W_j^o
H_1
H_j
H_7
W_{ji}^h
I_1
I_i
I_7
Maximum,Minimum , Peak to peak ,Variance
Average, Skewness , Kurtosis

Fig.2 Architecture of the neural network used for the automatic identification of the noise component

RESULTS

Experiments for the artifact removal are carried out for five volunteers. For each volunteer, 100 epochs of MCG signal are acquired. For the training of the network, a supervised learning is applied with an error back propagation algorithm. Ninety seven percent of identical decisions are obtained from the neural network compared to human experts after completion of the training. Figure 3 shows the signal waveforms before and after processing with the proposed method. As seen in Fig.3, the pulse-type noise can be completely removed by the proposed method.

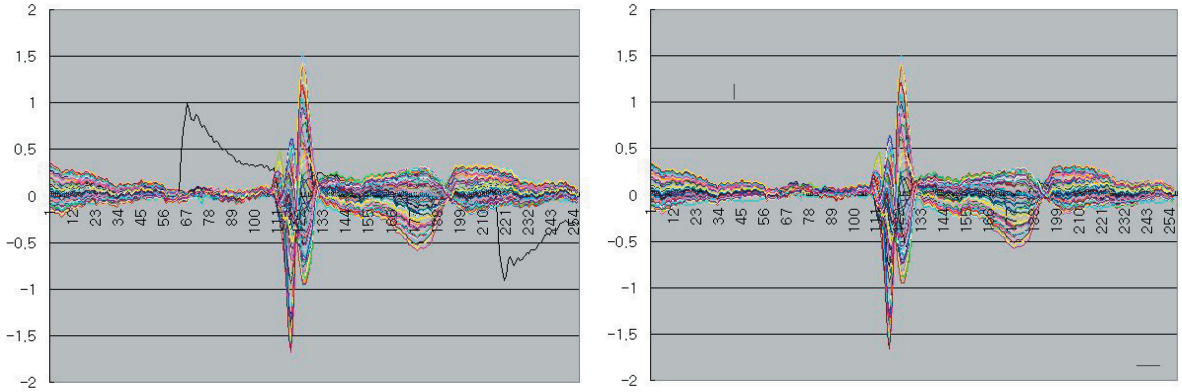

Fig.3 Multichannel MCG signal before (left) and after (right) processing with the proposed method.

DISCUSSION

Unlike previous artifact removal methods mainly based on the entire waveform of the signal, the proposed technique is applied to the component after the principal component analysis, which appears more advantageous over previous methods in the characterization of the noise. Instead of rejection of the contaminated signal, the proposed algorithm restores the signal, which may be an important feature when signal averaging is limited, e.g., single event experiment or measurement of evoked field with some organs easily adopted to stimuli.

ACKNOWLEDGEMENTS

This research is supported in part by the Ministry of Commerce, Industry, and Energy of Korea

P1-1

MEG Latency Difference Measurement for Priming Experiments

Matani, A.[1)2)], Hayakawa, T.[2)3)], Munetsuna, S.[4)2)], and Fujimaki, N.[2)4)]
1) University of Tokyo, Japan, 2) National Institute of Information and Communication Technology, Japan,
3) Teikyo University, Japan, 4) Kyushu Institute of Technology, Japan

ABSTRACT

Analysis of magnetoencephalography (MEG) latency difference for priming experiments not in motor readiness level but in cognition level may be useful for identification of the brain system. The MEG latency difference is, however, difficult to measure, especially if stimulus onset asynchrony (SOA) is short. We applied a spatio-temporal MEG pattern analyzing method, which is a similarity level measure of MEG data, to a visual word repetition priming experiment. The stimuli of the experiment consisted of mask (duration: 700 ms) – prime (70 ms) – target (1000 ms). There exist four kinds of experiments depending on the combination of the primes (related/pseudo-characters) and targets (in-category/out-of-category). Subjects were asked to press yes or no button according to in-category/out-of-category of the target. The similarity levels between MEG data of related/out-of-category and a) MEG data of related/in-category, b) MEG data of pseudo-character/in-category, and c) MEG data of pseudo-character/out-of-category were calculated. The order of peak appearance in the similarity levels of a), b) and c) was the same order of the averaged reaction-times.

KEY WORDS

similarity measure, adaptive filter, stimulus onset asynchrony (SOA), repetition priming, word categorization, magnetoencephalography (MEG)

INTRODUCTION

Reaction time (RT) measurements are often used for priming experiments. In priming experiments for language processing, one often see that RTs for the semantically same target words and for the same instructed task are different depending on previously presented prime words. A graphical presentation of stimulus onset asynchrony (SOA) between primes and targets versus RT is useful for investigating language processing. Brain imaging is occasionally performed simultaneously with the RT measurements. Electroencephalography (EEG) or magnetoencephalography (MEG), both of which have essentially high temporal resolution, is often employed as a brain imaging modality. EEG/MEG activity, whichever by a prime or by a target, can be typically observed for several hundred seconds. If SOA is, thus, shorter than several hundred seconds, then EEG/MEG activities generated by a prime and a target are overlapped. Inconvenience of EEG/MEG analysis arises out of the overlap but the interest of SOA versus RT is independent of the inconvenience. In fact, one sometimes sets SOA a couple of hundred seconds or shorter in language priming studies [Levelt 1998]. Even for such short SOA, if one seeks the difference of EEG/MEG activity in motor readiness level directly relevant to RT [Dehaene, 1998], then the inconvenience does not probably occur because the motor readiness EEG/MEG activity appears last. One may, however, be rather interested in cognition level, and the inconvenience remains accordingly.

As already mentioned above, a merit of EEG/MEG is their high temporal resolution. Their spatial resolution, coexisting with the ill-posed inverse problem, is not sufficiently high. This is nature characteristics of EEG/MEG. In this paper, we propose usage of an adaptive spatial filter for solely utilizing the temporal merit and for avoiding the above inconvenience.

METHODS

A visual word repetition priming experiment was performed. The mask (five '#'s), a prime (five pseudo-characters or five Japanese *hiragana* characters), and a target (five Japanese *katakana* characters) were sequentially replaced at the same area of the visual word presentation screen. The duration of the presentation of the mask, a prime, and a target were 700, 70, and 1000 ms, respectively, and hence SOA was set 70 ms accordingly. The pseudo-characters were generated by deforming *katakana* characters [Fujimaki, 1999]. In case of choosing a word written in *hiragana* for a prime, the same word but in *katakana* for the paired target was used. A subject was given notice of a semantic category and was asked to respond whether the target word in each epoch belonged to the semantic category by pressing yes or no button. Thus, there exist four groups of the epochs depending on the combination of the primes and targets, i.e., prime (*hiragana* or pseudo-character) x target (in-category or out-of-category). In the combinations, the neural processing relevant to the *hiragana*/out-of-category epochs may contain not the category bias but repetition of the primes and targets. RTs and MEG (with whole-head, 148ch, BTi) during the tasks were measured.

First, the MEG data were selectively averaged in each of the four groups. Second, the averaged MEG data were transformed to the half-inverse space [Matani, 2003], which is virtual space lying between signal source and MEG data spaces. The half-inverse transform is described as $\mathbf{x}'[n]=\mathbf{U}\mathbf{S}^{-1}\mathbf{U}^{\mathrm{T}}\mathbf{x}[n]$, where $\mathbf{x}[n]$ is MEG vector time series and $\mathbf{U}$ and $\mathbf{S}$ are derived from the eigenvalue decomposition regarding the leadfield matrix of the measurement, $\mathbf{L}\mathbf{L}^{\mathrm{T}}=\mathbf{U}\mathbf{S}\mathbf{U}^{\mathrm{T}}$. In the half-inverse space, the scaling is equal to the signal source space and the spatial information can correspond to only the MEG data space. Thus, the half-inverse transformed vector time series, $\mathbf{x}'[n]$, has normalized sensitivity for anywhere in the signal source space except the kernel of $\mathbf{L}$. Third, the similarity between pairs of the groups of MEG data were evaluated with the virtual beamformer [Masuda, 2001]. The virtual beamformer can derive scalar time series from a half-inverse transformed MEG data A, $\mathbf{x}'_{\mathrm{A}}[n]$, similar to another half-inverse transformed MEG data B, $\mathbf{x}'_{\mathrm{B}}[n]$, as $s_{\mathrm{A|B}}[n]=\mathbf{x}'_{\mathrm{A}}[n]^{\mathrm{T}}\mathbf{x}'_{\mathrm{A}}[n]/(\mathbf{x}'_{\mathrm{A}}[n]^{\mathrm{T}}\mathbf{V}'_{\mathrm{BS}}\mathbf{V}'^{\mathrm{T}}_{\mathrm{BS}}\mathbf{x}'_{\mathrm{A}}[n])$, where $\mathbf{V}'_{\mathrm{BS}}$ consists of the eigenvectors corresponding to the small half of eigenvalues of the variance-covariance matrix of $\mathbf{x}'_{\mathrm{B}}[n]$. Although MEG data A can maintain its spatio-temporal structure in the virtual beamformer output, $s_{\mathrm{A|B}}[n]$, MEG data B, which is called the virtual beamformer target, can do its spatial structure only.

We applied the virtual beamformer to the MEG data of the visual word repetition priming experiment. The *hiragana*/out-of-category averaged MEG data for the duration of 200-600 ms (from the target onset) was used for the virtual beamformer target.

RESULTS

Table 1 shows the typical performance of the visual word repetition priming experiment. The percentages of correct answer are around 90%. Comparing RTs, group #1 < group #2 < group #3 ≈ group #4 is observed, and hence a typical repetition priming effect can be seen in between groups #1 and #2 ($p<0.005$).

Figure 1 shows the MEG data and the virtual beamformer outputs. The first two rows describe the iso-contour maps from MEG of the groups #1 and #2 (hereafter, MEG #1, MEG #2), respectively, at the specified latencies. The iso-contour maps are top view (nose up) in the azimuthal equidistant chart manner, the black and grey lines indicate positive and negative magnetic field iso-contours, respectively, and their division is 50 fT. The third row shows the time course stack of MEG #1. The time origin is set to the onset of the target. MEG #2-#4 revealed the same characteristics, i.e., MEG responses from the primes and the targets were hardly recognized separately and their activities lasted until long latency with their spatial pattern unchanged so much for the duration of long latency. The bottom figure presents the virtual beamformer outputs. In the virtual beamformer outputs, the solid, dashed, alternate long and short dashed lines indicate the measures from MEG #1, #2, and #4, respectively, similar to MEG #3. Note that the value along vertical axis does not have absolute meaning. Some peaks can be seen around the duration of 300-400 ms. In this duration, the first peak of MEG #1, #2, and #3 are located at 312, 347, and 380 ms, respectively, and then this order is coincident with the order of RTs listed in Table 1. The specified latencies for describing the iso-contour maps are determined by the first peak from MEG #1, by the second peak from MEG #1 and also the first peak from MEG #2, and by the second peak from MEG #2. In spite of the similarity among the six iso-contour maps, MEG #1 is similar to MEG #3 at 312 and 347 ms whereas MEG #2 347 and 420 ms.

Table 1. Performance of the visual word repetition priming experiment.

group id #	prime	target	RT (SD) [ms]	correct answer [%]
1	*katakana*	in-category	662 (117)	89
2	pseudo-character	in-category	738 (172)	95
3	*katakana*	out-of-category	788 (189)	92
4	pseudo-character	out-of-category	781 (164)	94

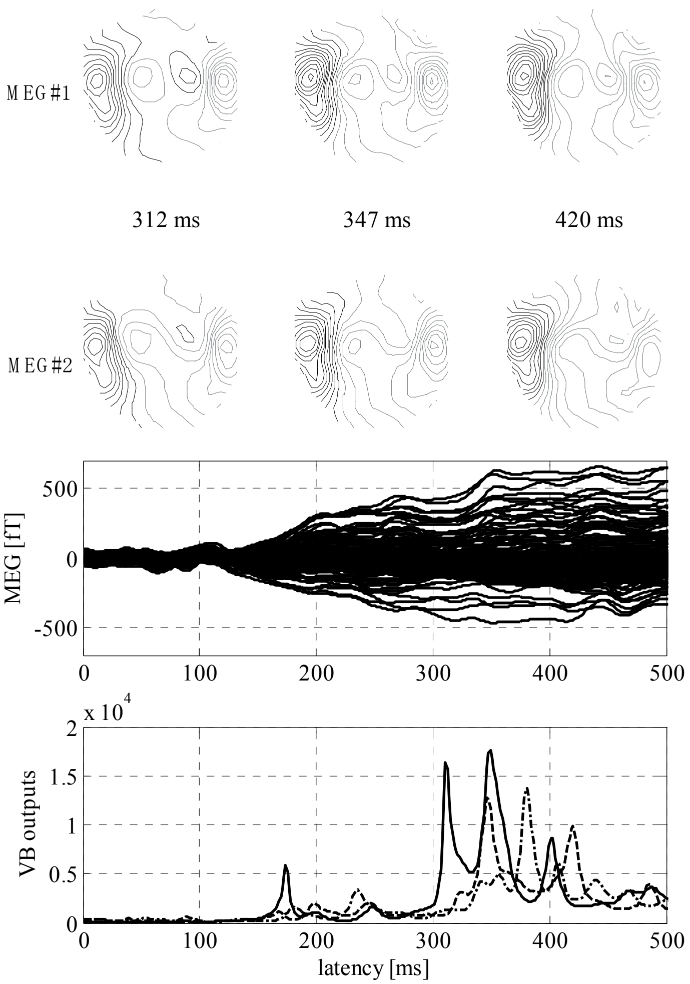

Figure 1. MEG data and the virtual beamformer outputs.

DISCUSSION

In an application of the virtual beamformer, the interpretation of the virtual beamformer target is important and is often difficult. The virtual beamformer target here, or MEG #3, contains 'repetition', and thereby may correspond to 'coincidence' semantically. There exists 'coincidence' not only in the pairs of the primes and targets but also in the combination of the categories and the primes or targets. The virtual beamformer target also contains 'decision of out-of-category'. 'Decision of out-of-category' perhaps means 'negative coincidence'.

Because RTs are around 650-800 ms, MEG activity during 300-400 ms contains cognition neural process and no motor neural process. Although the virtual beamformer output is a matter of argument with coexistence of the above interpretation, it can derive similarity information from MEG/EEG data which are difficult to analyze with conventional methods: e.g. subtraction, signal source localization, and etc. One can often find such EEG/MEG data for higher-order neural processes. The virtual beamformer in the half-inverse space is at least useful for latency difference measurement even in cognition level.

ACKNOWLEDGEMENTS

This work partially supported by a Grant-in-Aid from the Ministry of Education, Culture, Sports, Science and Technology (No. 16300083).

REFERENCES

Dehaene S, Nccache L, Le Clec'H G, Koechlin E, Nueller M, Dehane-Lambertz G, et al. Imaging unconscious semantic priming. Nature 1998;395:597-600.

Fujimaki N, Miyauchi S, Pütz B, Sasaki Y, Takino R, Sakai K, et al. Functional magnetic resonance imaging of neural activity related to orthographic, phonological, and lexico-semantic judgments of visually presented characters and words. Human Brain Mapping 1999;8:44-59.

Levelt WJM. Spoken word production: A theory of lexical access. Proceedings of the National Academy of Science of the United States of America 1998;98:13464-71.

Masuda Y, Naganawa M, Matani A, Chihara K. PCA analysis of ITD auditory evoked field. In: Nenone J, Ilmoniemi RJ, Katila T, editors. Biomag2000. Proceedings of the 12th International Conference on Biomagnetism; 2000 Aug 13-17; Espoo, Finland. Helsinki Univ. of Technology;2001. p.97-8.

Matani A, Masuda Y, Okubo H, Chihara K. Hierarchical clustering and filtering in half-inverse space for MEG and/or EEG hypothesis-free analysis. IEEE Trans. on Signal Processing 2003;51:350-61.

Noise Reduction in Stress MCG Data by Independent Component Analysis

[1]Müller, H.-P., [1]DeCesaris, I., [1]DeMelis, M., [2]Nolte, G., and [1]Erné, S. N.

[1]Division for Biosignals and Imaging Technologies, ZIBMT, University of Ulm, Germany
[2]NINDS/NIH, Bethesda, USA

ABSTRACT

It has already been shown that there are substantial changes in the magnetocardiogram (MCG) when comparing the repolarisation at rest to that of during stress. To avoid the pharmacological stress on patients, a common complaint associated with other measurement techniques, a non-magnetic ergometer for stress testing during MCG measurements has been developed and constructed. During the stress testing, a 55-channel stress MCG (SMCG) is recorded, which, after acquisition, requires denoising to eliminate the artefacts related to mechanical works. The separation of the signals from the noise is thus performed by an independent component analysis (ICA). Hereby, it is possible to analyse SMCG data which have been recorded during ergometer testing.

KEY WORDS

Magnetocardiography, stress testing, noise reduction, independent component analysis

INTRODUCTION

In addition to the emerging stress Cardiac Magnetic Resonance Imaging (CMR), exercise testing techniques such as stress ECG, stress Echocardiography and stress Radionuclide Cardiac Imaging have been used in clinical practice for many years as diagnostic tools for the detection of ischemic pathologies. Magnetocardiography is gaining interest and acceptance as clinical diagnostic tool because it is intrinsically non-invasive with excellent temporal resolution. SMCG is an exploitation of the biomagnetic method, as it is, in principle, compatible with both pharmacological and exercise induced stress. Since substantial changes in the magnetocardiogram have already been shown by the comparison of repolarisation at rest to that of during stress [Brockmeier, 1997], SMCG can contribute to the diagnostic assessment provided that sufficient noise reduction techniques are applied.

A newly developed ergometer [Pasquarelli, 2002], designed to fit the demands for clinical application in regards to exercise SMCG, was used. The main scope of this work is to apply ICA to the recorded exercise SMCG data in order to reduce the effects of disturbances caused by the patient movement performing the exercise. ICA has already been successfully used for magnetoencephalography [Hyvärinen, 2002] and for the reduction of small disturbances in MCG rest measurements [Steinhoff, 2003]. In this work it is shown that ICA, used in the implementation of the Open Magnetic and Electric Graphic Analysis (OMEGA) environment [DeMelis, 2003], is able to denoise exercise SMCG data to a satisfactory quality (signal-to-noise-ratio >> 1).

METHODS

The MCG/SMCG recording was carried out on a 55-channel planar SQUID magnetometer system, Argos55 (Atb, Pescara, Italy) [Erné, 1998]. A standardised set up, consisting of a map of 55 magnetic channels, three orthogonal HRECG leads and a breathing channel were used for the SMCG recording. The MCG signals were sampled at 8.2 kHz, digitally filtered and decimated to a final sampling frequency of 1 kHz and a bandwidth between DC and 250 Hz.

The ergometer was built exclusively from non-magnetic materials. The gears are nylon and their shafts are brass. The frame, pedals, flywheel and mounting brackets are aluminium. In addition, the pedals' linings are made out of PVC and the adjustable weight consists of a telescopic aluminium lever. Magnetic recordings performed without a load have shown no significant artefacts or noise introduced by the ergometer.

The standard stress testing protocol starts with a 1-5 minutes rest measurement. This is followed by a warming-up stage of several minutes which progressively reaches a steady exercise stage. The initial workload is incremented every 30 seconds so that the heart activity gradually increases to a target endpoint at 85% of age-predicted maximal heart beat rate

$$f = 0.85\ (220 - age/\,years)\ beats/\min \cdot \tag{1}$$

This is followed by a second exercise acquisition, lasting several minutes, depending on the fitness of the subject. The exercise is then discontinued and a third recording is started. Since abnormal heart wall motion normalises rapidly after discontinuing the exercise, stress specific information must be acquired within 30 seconds to 1 minute following exercise.

The data acquired during the exercise measurement had unexpected disturbances (Figure 1). Apparently, the forces applied to operate the ergometer under typical workloads produced movements and vibrations which were in someway transferred to the bed, and then may have reached the structure of the magnetically shielded room and perhaps the dewar gantry, leading to the generation of artefacts. Straight forward filtering was not successful in eliminating the artefacts and disturbances. However, due to the fact that the artefacts and disturbances show a spatio-temporal distribution different from the heart signal, ICA was applied to the data in order to extract the cardiac signals.

To denoise the data, different ICA approaches were tested. Generally, the main problem that prevented effective use of the cleaned data was the swapping of channels in which the spatial mapping properties were lost. We experimentally observed that separating the 55 channels into 2 groups (28 and 27 channels, homogeneously distributed over the sensor area) in a suitable way eliminated the swapping of channels. Furthermore, this division of the data into 2 subgroups provides, as a side-effect, dramatically improved operational speed of the algorithm. This is because the computation time of the following algorithm mainly depends on the number of sensors. Thus, two unmixing matrices were calculated and the reconstruction of the signals was performed independently for the two groups of sensors.

ICA was applied in the following way: ICA assumes the measured signal $\vec{x}(t)$ to be a linear mixture of unknown source signals $\vec{s}(t)$ with unknown weights A.

$$\vec{x}(t) = A\ \vec{s}(t) \tag{2}$$

The sources are mutually statistically independent*:* their joint probability density function is factorable as the product of their single probability density functions. Before performing ICA, the input data have to be centred and whitened [Hyvärinen, 2002].

$$\vec{y}(t) = M\ \vec{x}(t) \tag{3}$$

The fast ICA algorithm [Hyvärinen, 2002] solves

$$\vec{s} = W\ \vec{y} \tag{4}$$

for the unmixing matrix W.

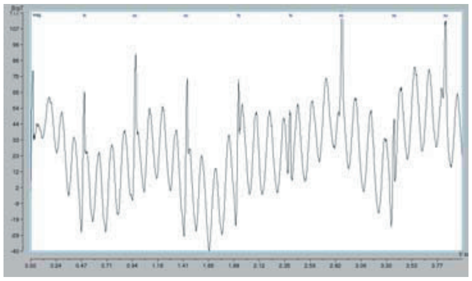

Figure 1. Example for recorded SMCG data: Channel with maximum QRS-amplitude.

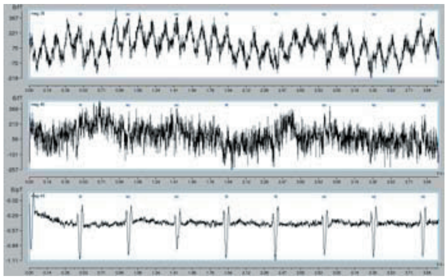

Figure 2. Example for unmixed SMCG data: Channel with ergometer noise, channel with background noise, channel with heart beat signal.

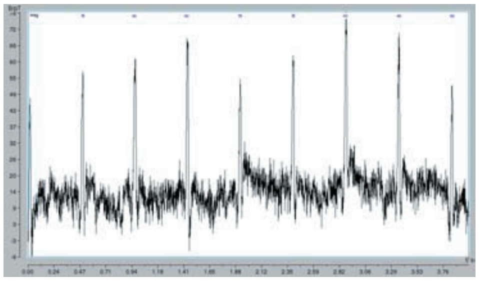

Figure 3. Example for cleaned SMCG data: Channel with maximum QRS-amplitude (compare Figure 1).

After calculating the unmixed data $\vec{s}$ (Figure 2), the task was to properly identify the components representing the artefacts and disturbances from those containing the heart information. Basically, there are 2 approaches: 1) positively identifying the heart signals and 2) positively identifying the disturbances. The positive identification of heart related components was performed by taking advantage of the simultaneously recorded HRECG data and the derived trigger points list. Averaging the time-series using HRECG trigger points provided a drastic improvement of the signal-to-noise ratio. A comparison (via cross-correlation) of the averaged odd and even beats demonstrated to be an excellent indicator for heart activity related to the unmixed channels. Vice versa, an important heuristic finding was that unmixed channels, where the maximum of the power spectrum was above a certain threshold*,* could be associated to artefacts and disturbances.

Using these two rules, the measured noise signals were then reconstructed by:

$$\vec{n} = \left(W\ M\right)^{-1} Z\ \left(W\ M\right)\ \vec{x} \tag{5}$$

where $Z = diag(z_i)$ with z_i is 1 if the respective component should be eliminated, and 0 otherwise.

The measured heart signals $\vec{x}_r$ could then be reconstructed by subtracting the reconstructed noise signals.

$$\vec{x}_r = \vec{x} - \vec{n} \tag{6}$$

RESULTS

Figure 3 shows the channel with maximum R-peak after ICA data cleaning. The main disturbances have been eliminated but high frequency muscular noise components remain.

DISCUSSION

As already shown in previous works [Brockmeier, 1997], MCG exercise testing is a promising new tool to detect obstructive coronary atherosclerotic heart disease. MCG recordings during ergometer treatment usually contain noise resulting from the treatment. Thus, previous studies used pharmacological stress or MCG recordings that started immediately after the treatment. In this work it has been shown that, using ICA,, it has become possible to perform SMCG recordings during ergometer treatment.

REFERENCES

Brockmeier K, Schmitz L, Bobadilla Chavez J, Burghoff M, Koch H, Zimmermann R, Trahms L. Magnetocardiography and 32-Lead Potential Mapping: Repolarisation in Normal Subjects During Pharmacologically Induced Stress. J. Cardiovasc. Elektrophysiol. 1997, 8: 615-626.

DeMelis M, Müller H-P, Pasquarelli A, Erné SN. Magnetocardiographic Signal Analysis. Proceedings of BIOMAG 2002, 2002, Jena, Germany, p. 987-989.

Erné SN, Pasquarelli A, Kammrath H, Della Penna S, Torquati K, Pizzella V, Rossi R, Granata C, Russo M. Argos 55 - The New MCG System in Ulm. Proceedings of BIOMAG98, 1998, Sendai, Japan.

Hyvärinen A, Oja E. Independent Component Analysis: Algorithms and Applications. Neural Netw. 2000, 13: 411-430.

Pasquarelli A, Schless BG, Müller H-P, Hombach V, Erné SN. A Non-Magnetic Ergometer for MCG Stress Testing. Proceedings of BIOMAG 2002, 2002, Jena, Germany, p. 949-951

Steinhoff U, Mäntynen V, Kürsten R, Nenonen J. Independent Component Analysis for the Suppression of Different Noise in Magnetocardiographic Data. Biomed. Technik 2003, 48 suppl. 1: p. 170-171.

P1-1

Removal of the Baseline Drift in Magnetocardiogram Using the Morphological Filter

Mun, K. W., Lee, Y. H., Kim, K., Kwon, H. and Kim, J. M.

Biomagnetism Research Center, Korea Research Institute of Standards and Science, Daejeon, Korea

ABSTRACT

Low frequency noise or baseline drift in magnetocardiogram (MCG) is removed using the morphological filter. Usually MCG signals are contaminated by subjects' movements and external noise sources, for example, car or subway. Since the shielding performance of the shielded room is not good enough in the low frequency range, these noises cause baseline drift in MCG. Several methods have been used to remove the baseline drift, for example, high-pass filtering, wavelet transform, cubic-spline method. Among them, the cubic-spline method is the most commonly used method. However, the performance of this method depends on the accuracy of detection of the isoelectic points (eg. PR-segments). The morphological operators have been used as a baseline correction algorithm for electrocardiogram (ECG). The existing algorithm uses two sets of sequence elements to extract baseline. However, the T-wave which is critical to the diagnosis is often distorted in this method. To overcome this problem, we used 3 sets of sequence elements instead of 2 sets. And the relation between RR-interval and the length of sequence element is proposed. The improved algorithm is tested using real MCG signals and the result is compared with that of existing algorithm. It showed better performance when it is compared with the existing algorithm, especially in the aspect of T-wave distortion. And the proposed relation between RR-interval and the length of sequence elements was useful within our test results.

KEY WORDS: magnetocardiogram (MCG), baseline drift, morphological filter, sequence element.

INTRODUCTION

Magnetocardiogram (MCG) is the method measuring the weak magnetic field (order of 10^{-11} T) induced by the bioelectric current of the heart. MCG is easily contaminated by various resources. Movement and respiration of a subject and low frequency noises are the main resources to the baseline drift in MCG. And the baseline drift degrades MCG signal and affects post-processing. So, baseline correction is prerequisite for MCG analysis.

Currently, several methods are used in the correction of the baseline drift in electrocardiogram (ECG) and MCG. Wavelet transform is a promising technique to ECG signal processing. In wavelet transform, a number of coefficients at different scales are obtained by decomposing signal into transform domain. By selecting suitable scales and disregarding the coefficients below predefined threshold, additive noise and baseline drift can be separated from the ECG signal component. However, it has a disadvantage: the scales and thresholds for the non-stationary baseline and noise suppression cannot be selected adaptively [Sun, 2002]. Cubic-spline method is a widely used method in baseline correction [Meyer, 1977] [Takala, 2002]. This method requires the following conditions; accurate ECG complex detection, accurate ECG complex classification, sophisticated arrhythmia detection, accurate PR-segment and/or TP-segment detection [Jeffrey, 1988]. And most of all, the accurate determination of the isoelectric region is important. However, there exist some situations to make difficult to find the reliable isoelectric region; premature complexes, AV dissociation, arterial and ventricular tachycardia, Wolff-Parkinson-White (WPW) syndrome.

The morphological filtering method applied to the baseline correction in ECG has been published in the several papers. The combination of opening and closing operator eliminates the baseline drift effectively [Chu, 1989]. And this method does not require the conditions of cubic-spline method mentioned above. However, it often distorts the original signal, especially the T-wave. For the successful application, this problem should be solved. In this paper, we simply introduce the morphological operator and the existing morphological filters applied to ECG. And then we present the newly designed morphological filter. The performance of the morphological filter is tested using real MCG signals and compared with existing algorithm.

METHODS

MORPHOLOGICAL OPERATORS

In this paper, we will give the simple description on the morphological operators. Please refer to the references for further information [Chu, 1989] [Sun, 2002] [Maragos, 1987]. The fundamental operators of morphological methods are dilation and erosion. Dilation expands the given signal and erosion shrinks. Using the combination of dilation and erosion, another set of operators is created; opening and closing. Opening is defined as erosion followed by dilation. Closing is defined as dilation followed by erosion. The opening operator(◦) suppresses the peaks and closing operator(•) suppresses the pits.

MORPHOLOGICAL FILTER

The performance of the morphological filter depends on the design of the sequence element. A sequence element is characterized by its width and height. The width of the sequence element is determined by the duration of the given signal and the sampling rate. Experientially, the width is more influential than the height. If particular part of the given signal is to be removed, the sequence element with longer duration should be used.

The basic morphological filter was proposed by Chu [Chu, 1989]. The algorithm is composed of two steps; the impulsive noise suppression and the baseline correction. Because we are only concerned with the baseline correction, we will only mention the baseline correction. The baseline correction is performed by estimating the baseline drift and subtracting it from the signal. Two sets of sequence elements are used. Denoting the short sequence element E_1 and the long sequence element E_2, the estimation of baseline drift is performed according to the following expression. B denotes the extracted baseline drift of a given signal. $B=(S \bullet E_1 \circ E_2 + S \circ E_1 \bullet E_2)/2$ where S is the input signal with the baseline drift. Then, the final output is expressed as $S_1=S-B$, where S_1 is final output signal. Chu's method is applied in our multi-channel MCG system experimentally. The result is shown in Fig. 1. The baseline drift seems to be removed. However, a close examination reveals that part of the T-wave as well as the baseline drift is removed. This phenomenon results from the fact that the lengths of the sequence elements are not sufficient to remove T-wave. On the other hand, sequence element with excessive length generates rough baseline extraction.

So, we designed the 3 sets of sequence element instead of 2 sets in baseline correction. For computational efficiency, we used the zero-valued sequence elements [Sun, 2003]. The length of each sequence elements is determined by the RR-interval. The relation between the RR-interval and the length of the sequence element is given as following.

$$L_1= (\text{RR-interval}) \times (\text{sampling frequency}) \times 0.16,\ L_2= L_1\times 2,\ L_3= L_1\times 3$$

Though this formula is applied for the limited number of the subjects, it showed good a result. In the future, however, we will test this formula for the larger number of the subjects. The relation between RR-interval and the length of sequence element is described [Sun, 2003]. Sun used Bazett's formula for neonatal ECG. However, it is difficult to apply the Bazett's formula to all ages. Denoting the sequence elements N_1, N_2, N_3 with the lengths of L_1, L_2, L_3, we designed the procedure as follows.

$$Y_1=(S\bullet N_1\circ N_1 + S\circ N_1\circ\bullet N_1)/2,\ Y_2=(Y_1\bullet N_2\circ N_2 + Y_1\circ N_2\circ\bullet N_2)/2,\ Y_3=(Y_2\bullet N_3\circ N_3 + Y_2\circ N_3\circ\bullet N_3)/2,\ S_{out}=S-Y_3$$

where S is the input signal, S_{out} is the signal with corrected baseline and Y_1, Y_2, Y_3 are the extracted baseline in each step. The morphological operations, opening-closing and closing-opening, have the effect of removing peaks and valleys. The disadvantage of the zero-valued sequence elements is that the baseline is extracted like step-function, i.e. discontinuity happens in the baseline. To solve this problem, we smoothed the signal by unweighted sliding-average smooth; it simply replaces each point in the signal with the average of m adjacent points, where m is a positive integer called the smooth width.

RESULTS

The morphological filter is applied to the real MCG signal of our multi-channel MCG system. The data shown in Fig. 1 is used again to compare the newly designed algorithm with the existing one. And the calculating time for the given data set (sampling rate: 500 Hz, measurement time: 30 s, number of channel: 64) is less than 5 s by using the personal computer of Pentium-Ⅳ 2.4 GHz.

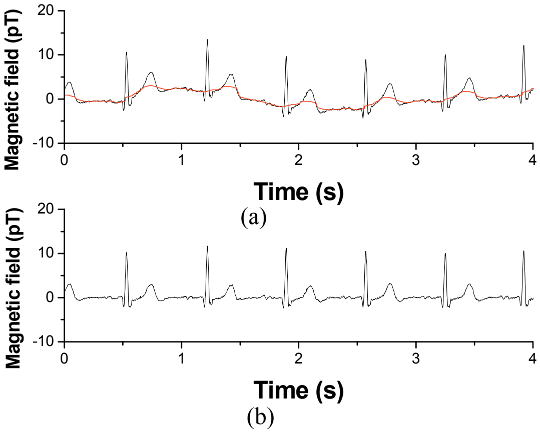

(a)

(b)

Figure 1. The result of the Chu's method. (a) The black line is the MCG signal before baseline correction. The red line is extracted baseline. (b) The MCG signal after baseline correction. The baseline seems to be corrected. However, T-wave as well as the drift of baseline is removed.

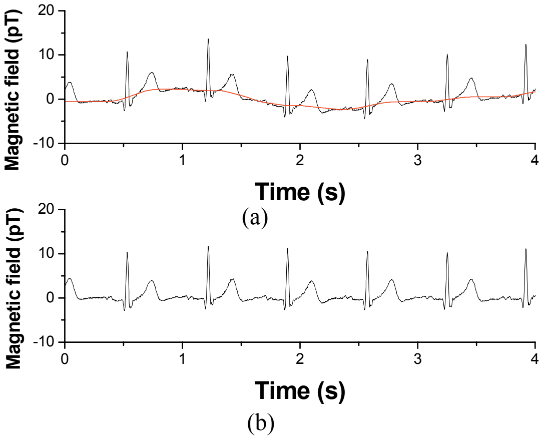

(a)

(b)

Figure 2. The result of the newly proposed method. (a) The black line is the MCG signal before baseline correction. The red line is extracted baseline. (b) The MCG signal after baseline correction. The baseline seems to be corrected. The baseline drift is removed safely.

DISCUSSION

In this paper, we designed morphological operators for the multi-channel MCG system. Using the zero-valued sequence elements and smoothing method, we succeeded in the extraction of baseline drift while minimizing the signal distortion. And we proposed the relation between RR-interval and the length of sequence element. In the future, we will test the relation for the larger number of patients and verify the relation.

REFERENCES

Chu CHH, Delp EJ. Impulsive noise suppression and background normalization of electrocardiogram signals using morphological operators. IEEE Trans Biomed Eng 1989;36:262-273.

Jeffery N, Froning JN, Olson MD, Froelicher VF. Problems and limitations of ECG baseline estimation and removal using a cubic spline technique during exercise ECG testing: recommendations for proper implementation. J Electrocardiol 1988;21 Suppl:S149-57

Maragos P, Schafer RW. Morphological filters-part□: their set-theoretic analysis and relations to linear shift-invariant. IEEE Trans Acous Speech, Sign Proc 1987;ASSP-35;1153-1169.

Meyer CR, Keiser HN. Electrocardiogram baseline noise estimation and removal using cubic splines and state-space computation. Comput Biomed Res 1977;10:459-470.

Sun P, Wu QH, Weindling AM, Finkelstein A, Ibrahim K. An improved morphological approach to background normalization of ECG signals. IEEE Trans Biomed Eng 2003; 50(1):117-121.

Sun Y, Chan KL, Krishnan SM, ECG signal conditioning by morphological filtering. Comp Biol Med 2002;32: 465-479.

Takala P, Hänninen H, Montonen J, Korhonen P, Mäkijävi M, Neonen J, Oikarinen L, Toivonen L, Katila T. Heart rate adjustment of magnetic field map rotation in detection of myocardial ischemia in exercise magnetocardiography. Basic Res Cardiol 2002;97:88-96.

A Grid Computing Infrastructure for MEG Data Analysis

Nakagawa, S.[1], Kosaka, T.[2], Date, S.[2], Shimojo, S.[3], and Tonoike, M.[1]

[1]Institute for Human Science and Biomedical Engineering (HSBE),
National Institute of Advanced Industrial Science and Technology (AIST), Japan
[2] Graduate School of Information Science and Technology, Osaka University, Japan
[3] Cybermedia Center, Osaka University, Japan

ABSTRACT

Magnetoencephalography (MEG) is widely used for studying brain functions, but clinical applications of MEG have been less prevalent. One reason is that only clinicians who have highly specialized knowledge can use MEG diagnostically, and as such these clinicians are found at only a few major hospitals. Another reason is that MEG data analysis is very complicated, and deals with a large amount of data, and thus requires high-performance computing. These problems can be solved only by the collaboration of human and computing resources distributed in multiple facilities. A new computing infrastructure for brain scientists and clinicians in distant locations was therefore developed by the Grid technology, which provides virtual computing environments composed of geographically distributed computers and experimental devices. A prototype system connecting an MEG system at the AIST in Japan, a Grid environment composed of PC clusters at Osaka University in Japan and Nanyang Technological University in Singapore, and user terminals in Baltimore was developed. MEG data measured at the AIST were transferred in real-time through a 1-GB/s network to the PC clusters for processing by a wavelet cross-correlation method, and then monitored in Balimore. The current system is the basic model for remote-access to MEG equipment and high-speed processing of MEG data.

KEY WORDS

Grid computing, remote experiment, parallel computation, MEG

INTRODUCTION

Magnetoencephalography (MEG), a widely accepted method for studying brain functions, is completely noninvasive and provides a high degree of temporal resolution. Clinical applications of MEG, however, are comparatively rare. One of the problems is that only clinicians with highly-specialized knowledge can use MEG diagnostically, and such clinicians are found at only a few major hospitals. Another is that MEG data analysis, such as source estimation, is very complicated and deals with a large amount of data, and few research facilities or hospitals have the computing resources needed for this kind of data analysis. These problems lead to a need for the collaboration of geographically distributed researchers and clinicians sharing access to MEG systems and computing resources all over the world.

In this study, a prototype of an infrastructure enabling geographically distributed researchers to collaborate and share access to the MEG devices and computing resources needed for remote cooperative experiments and high-performance analyses of brain functional data was developed using Grid computing technology [Foster, 2004], which provides a large-scale but low-cost computing infrastructure by aggregating resources distributed in multiple facilities.

METHODS

1. Grid computing

Grid computing is a method for developing a computing infrastructure by aggregating resources distributed in multiple facilities. This method has been studied since the latter half of 1990s. Its original aim was to acquire a large amount of computing power by aggregating a large number of computers distributed on the Internet. Since this scheme does not require a facility to provide a supercomputer or a large-scale computer cluster, it can reduce the cost of high-performance computing substantially.

Grid computing requires middleware to federate heterogeneous computing resources and make it possible to use them as one integrated computing resource. The Globus Toolkit [The Globus Alliance, 2004] is one example of such middleware and it is widely utilized because of its pioneering contribution to scientific communities. Currently, a wide range of research projects are investigating the use of the Globus Toolkit and its applications in scientific computing.

One application of Grid computing is large-scale parallel computing. Multiple computing resources in a Grid environment can generate synergy to accelerate complex data analyses. Becasuse communication delays between the resources are problematic, a Grid is most suited for computation that does not require frequent communication or synchronization of the activities of the resources. This kind of computation is common in the studies of brain function, and Grid computing can be expected to be a useful tool for the processing of MEG data.

2. Application of Grid computing to MEG data analysis

MEG data were measured by a whole-head neuromagnetometer (Neuromag-122$^{\mathrm{TM}}$, 122ch, 400 Hz A/D sampling, 32-bit quantized) in

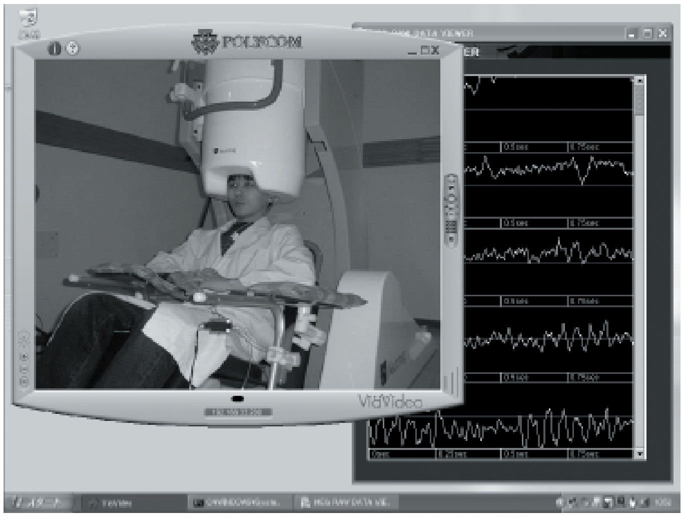

Figure 1. A Screen shot of the user interface in a remote site. The user interface visualizes a subject and MEG data.

a magnetically shielded room at Kansai Center of AIST in Ikeda, Japan. The applicability of Grid computing to the analysis of brain function was evaluated by using it for wavelet cross-correlation analyses [Mizuno-Matsumoto, 2002] and Independent Component Analysis (ICA) [Kaishima, 2002] [Hyvarinen, 2001], both of which require relatively large amounts of computation. The analysis methods were parallelized because the processing of the data in one MEG channel is independent of the processing of the data in any other channels. These methods were implemented into an experimental Grid environment composed of two PC clusters at the Cybermedia Center of Osaka University in Suita, Japan, and one PC cluster at Nanyang Technological University in Singapore. The Grid environment consisted of 60 PCs, and was developed by utilizing the Globus Toolkit. During measurements, MEG data were transferred via a 1-GB/s network in real-time from the MEG system to the Grid environment. In addition, a real-time video transfer system was developed to monitor the MEG activity at the MEG facility. Figure 1 shows a screen shot of these systems.

3. Experiment connecting four sites

The experiment was conducted by connecting geographically distributed resources in four sites: an MEG device in the AIST, PC clusters in Osaka University and Nanyang Technological University, and user terminals (windows PCs) in the Baltimore Convention Center in the United States. Figure 2 illustrates the structure of the experimental system.

RESULTS AND DISCUSSION

MEG measurement, real-time data transfer, data analysis, and visualization of the results were carried out successfully by the developed system.

The experiment demonstrated in this study revealed the potential of Grid computing for MEG by allowing large-scale analyses through a collaboration of people at data acquisition sites and analysis sites. It is also significant that the experiment has drawn a roadmap for remote experiments involving geographically distributed researchers. These results have been accomplished by designing and implementing an experimental environment using Grid computing technologies, which enable us to build a large-scale but low-cost computing infrastructure from pre-existing resources.

The experiment is a first step toward a collaborative environment for MEG data analysis. We still need to improve the performance of various analysis methods by Grid computing and we also must develop a database system for sharing information, such as setting the parameters of analysis programs.

ACKNOWLEDGEMENTS

This study was supported by the IT-program of the Ministry of Education, Culture, Sports, Science and Technology of Japan (MEXT). This product includes software developed by and/or derived from the Globus project (http://www.globus.org).

REFERENCES

Foster I, Kesselman C. The Grid 2: Blueprint for a New Computing Infrastructure. 2nd ed. San Francisco (CA): Morgan Kaufmann Publishers; 2004.

Hyvarinen A, Oja E, and Karhunen J. Independent Component Analysis. New York: John Wiley & Sons; 2001.

Kaishima T, Mizuno-Matsumoto Y, Date S, Shimojo S. The experience and practice of developing a brain functional analysis system using ICA on a Grid environment. Proceedings of the 7th Asian Computing Science Conference (ASIAN'02); 2002 Dec 4-6; Hanoi, Vietnam. London: Springer-Verlag; 2002. p. 98-109.

Mizuno-Matsumoto Y, Tamura S, Sato Y, Zoroofi RA, Date S, Tabuchi Y, Shinosaki K, Ukai S, Ishii R, Inoue K, Tatsumi H, Kadobayashi Y, Shimojo S, Takeda M, Miyahara H. Propagation of epileptiform discharges using wavelet-cross correlation analysis in MEG. Medical Imaging Technology. 2002; 18(1):61-70.

The Globus Alliance. Available at: http://www.globus.org. Accessed May 26, 2004.

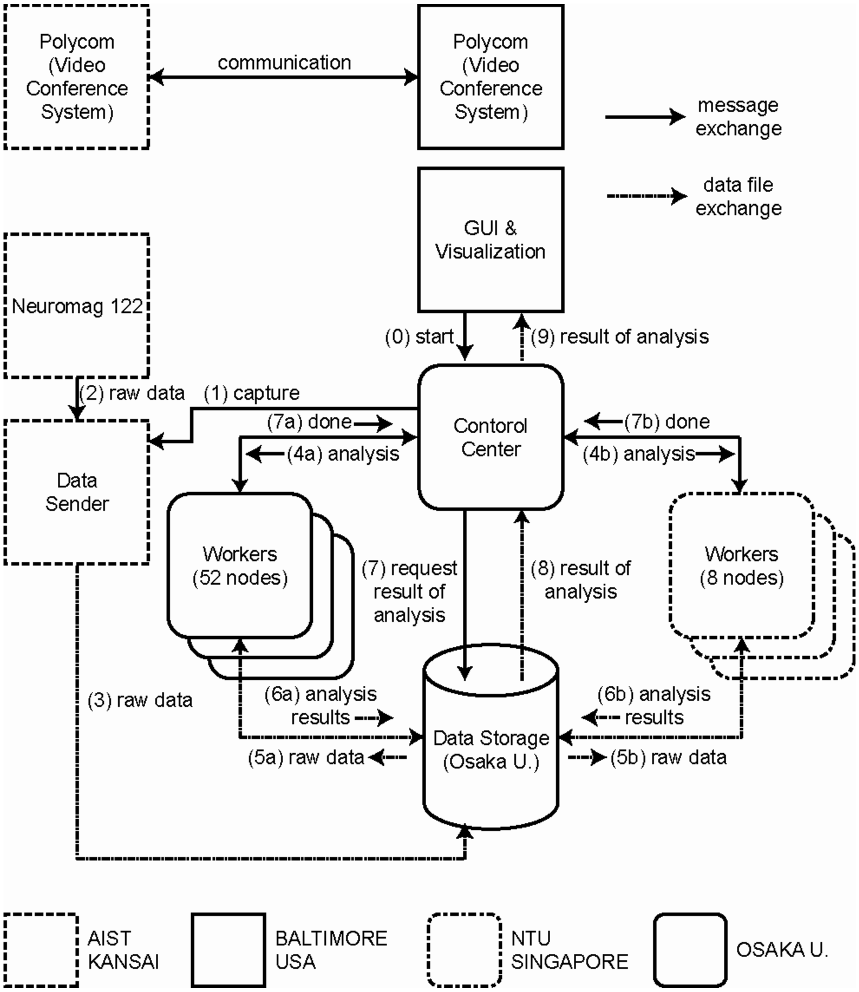

Figure 2. The structure of our prototype system. This system aggregates resources in geographically-distributed four sites: a neuromagnetometer in AIST Kansai, Japan, the user terminal at Baltimore, USA, and PC clusters in Osaka University, Japan and NTU, Singapore.

The Use of Non-parametric Statistics for Signal Subspace Detection in MEG/EEG

A. Ossadtchi[1,], M.E. Pflieger[1]

[1] Source Signal Imaging, San Diego, 92102, USA

ABSTRACT

Signal subspace detection plays an important role in many source localization and spatial filtering algorithms used for analysis of MEG and EEG evoked response data. Singular value (SV) spectrum analysis followed by visual threshold detection remains a primary technique for signal subspace detection in the presence of spatially colored noise. An alternative approach based on task-onset Mutual Information (MI) was proposed in [Ossadtchi, 2000]. However, both of the methods require visual examination of the intermediate results before a set of signal subspace components can be identified. Here we present a generalized objective approach based on non-parametric statistical theory [Edgington, 1995] for the detection of components with a statistically significant amount of task-related signal. Non-parametric randomization tests yield a *p*-value corresponding to the null-hypothesis H_0 of no task-related signal present in a component. Our permutation scheme applies a randomization procedure to the original task onset signal to yield a null-hypothesis distribution for a chosen measure of task-relatedness (for instance, singular values or mutual information). A component is determined to belong to the signal subspace if the corresponding *p*-value is below a pre-specified threshold.

KEY WORDS

Signal Subspace, Detection, Non-Parametric Statistics, Mutual Information, Singular Value Decomposition, Task-Bound, Task-Related.

INTRODUCTION

Spatial decompositions, (e.g., PCA, VARIMAX, PROMAX, ICA), may be used for data exploration in order to identify the signal subspace and denoise the data obtained from ERP/F experiments. Exploratory analysis using these decompositions attempts to differentiate between measurement space components which are related to a task performed by a subject during an ERP/F experiment and those which can be explained by the sources whose activity is not bound to the task. The task-related components span the signal subspace (SS). In the model-based approach, the SS components are then interpreted using electromagnetic model in order to obtain location, orientation and activation waveform of the neuronal sources responsible for the task. Identifying SS components is typically subjective and difficult to automate task. In [Ossadtchi, 2000] we proposed to use a Mutual Information (MI) measure in order to select task-related components obtained from ICA of ERP/F data. However, visual analysis of the MI spectrum is still required. In this paper we present an objective method based on the theory of non-parametric statistics for the detection of components with a statistically significant amount of task-related signal. The proposed method can be used with any kind of spatial decomposition and any kind of task-relatedness measure. We demonstrate the use of the proposed approach by applying it to the selection of task related PCA components of realistically simulated MEG ERF data. We also demonstrate the use of the proposed method for automatic eye artifact rejection.

METHODS

We will describe our method in a general setting, emphasizing the fact that it can be used with any spatial decomposition and any meaningful measure of task-relatedness. Assume that as a result of an ERP/F experiment we have a digital record of length T_R samples where

- $\mathbf{s}^T$ - is $1 \times T_R$ binary vector obtained as a digitized version of the stimulus onset signal (1 – task onset instance, 0 - otherwise),
- $\mathbf{X}$ - is $N_C \times T_R$ data matrix, where N_C is the number of channels and T_R is the number of time slices in the record.

Suppose that, using a spatial-temporal decomposition, we can represent data matrix $\mathbf{X}$ as a linear combination of the outer products, i.e., $\mathbf{X} = \sum_{i=1}^{N_c} \mathbf{u}_i \mathbf{v}_i^T$, where $\mathbf{u}_i$ are $N_C \times 1$ component spatial topography vectors, $\mathbf{v}_i$ are $1 \times T_R$ component activation waveforms. Each *i*-th component has an associated measure of task relatedness $\rho_i = F(\mathbf{v}_i, \mathbf{s})$. Our goal now is to develop a procedure that will allow us to select the components that carry a statistically significant amount of the task-related signal. In order to do that we will develop a test for the null-hypothesis H_0 that a component does not bear any task related signal. In order to test H_0 for the *i*-th component we obtain probability distribution $p_{H_0}(\rho_i)$ of the task-relatedness measure ρ_i under H_0 using a non-parametric randomization approach [Edgington, 1995]. We assume that the functional used to compute task relatedness measure depends (directly or indirectly) on the stimulus onset indicator signal $\boldsymbol{s}^T$. In order to obtain $p_{H_0}(\rho_i)$ we perform N_r randomizations of the binary stimulus onset signal to obtain randomized signal $\boldsymbol{s}^{*T}$. To randomize $\boldsymbol{s}^T$, we start from all the zero signal and assign value of “1” to the $N_e = \sum_{i=1}^{T} s_i$ randomly selected time instances. The idea is that if the *i*-th component does not bear a task related signal than $\rho_i = F(\mathbf{v}_i, \mathbf{s}_i)$ will come from the same distribution as $\rho_i^* = F(\mathbf{v}_i, \mathbf{s}^*)$, computed using the randomized stimulus onset signal. Then, *p*-value for the hypothesis is computed as a ratio of the number of times ρ_i^* exceeds the observed value ρ_i for the total number of randomizations.

The task-relatedness measure of a component is a scalar that depends on the amount of task-related signal present in the component. The SV spectrum of the ERP/F data averaged on the basis of stimulus onset signal **s** can serve as an example of task relatedness measure, since the singular value is equal to a square root of the power of the averaged component, and averaging tends to boost signals that “go along” with the stimulus onset signal. This task relatedness measure depends indirectly on **s**. However, SV-based measures may be biased by strong spatially coherent artifacts present in the data. Another example of task-relatedness measure is MI, which is computed using a deterministic expansion of binary stimulus onset signal as described in [Ossadtchi, 2000]. This measure is robust against the spatially coherent artifacts in the data but takes longer to compute. The technique proposed in this paper can use either of these two measures.

RESULTS

In order to evaluate the performance of our method, we simulated data obtained from the median nerve stimulation ERF experiment. We have placed two dipoles in the somatosensory area and oriented them according to the typical results obtained from median nerve stimulation study.

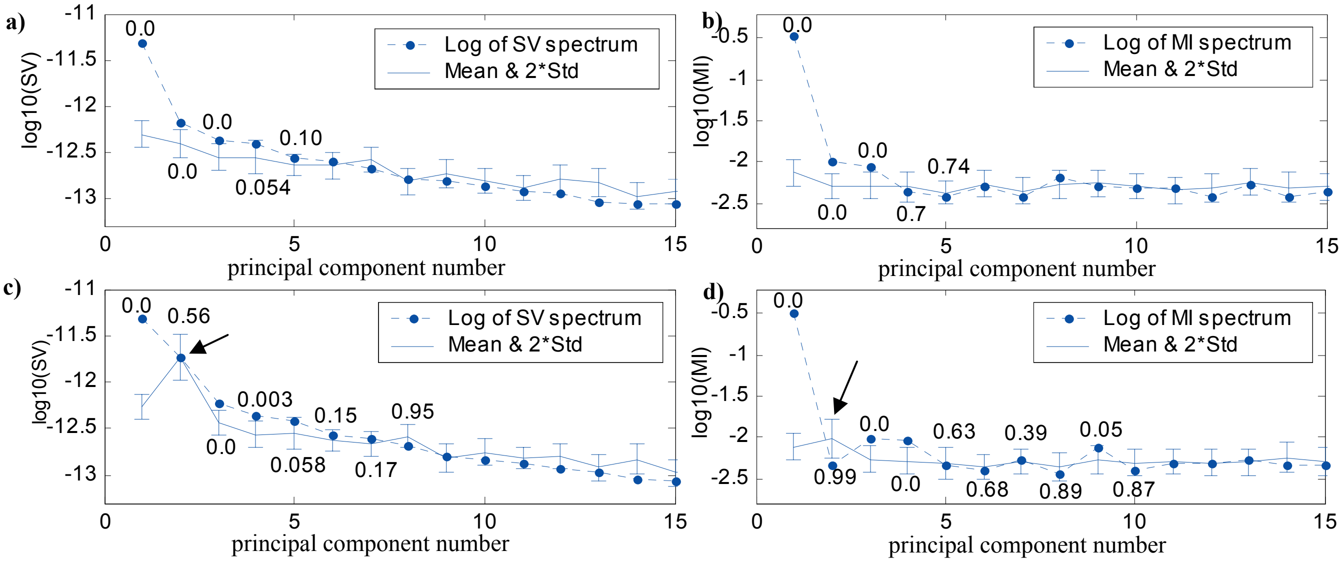

Fig.1 Results of realistic simulations. a) non-parametric analysis of the SV spectrum of the averaged ERF data; b) non-parametric analysis of the MI spectrum corresponding to the singular components in a); c), d) Same as a),b) correspondingly but for the dataset with eye-blink artefact. Artifact components is pointed by arrow. In all plots dashed curve corresponds to the SV or MI spectrum of the SVD of the data. Solid error-bar plot illustrates $p_{H0}(\rho_i)$ by showing the mean and +/- 2 standard deviations of the non-parametrically obtained distribution. Numbers above and below the error-bars correspond to the non-parametrically computed *p*-values. For the sake of clarity we have shown only first 15 components.

The dipoles were driven with biphasic harmonic time series modulated by a Gaussian kernel with correlation coefficient 0.76. Simulated dipolar activity was added to the spontaneous interictal activity recorded from a subject with focal epilepsy at rest. For the first experiment we have generated 200 repetitions of the task, and performed SVD of the averaged data. Then the described randomization procedure was applied to principal components generated by projecting un-averaged data onto a set of left singular vectors found by SVD. Fig. 1a shows that selecting significance threshold of 0.01 the first 3 components are sufficient for capturing SS. Indeed, subspace correlation [Golub, 1984] between the estimated subspace and the true signal subspace increases dramatically from $[0.999\ 0.927]^T$ to $[0.999\ 0.9785]^T$ when the third component is added and only slightly $[0.999\ 0.9793]^T$ if we were to add the fourth component. A similar conclusion may be obtained based on the analysis of the MI spectrum of the singular components, as shown in Fig 1.b. Note that due to spatially colored noise present in the data in order to capture two-dimensional SS we have to include three singular components. In the second set of experiments we added eye artifact to our simulated data and used only 100 repetitions to increase effect of the artifact in the averaged data. Eye artifact manifests itself in the second singular component (subspace correlation > 0.99). Based on the high singular value, see Fig. 1.c, the second component can be erroneously taken as a part of signal subspace estimate. However, by applying the described randomization procedure, the second component has $p = 0.56$, and thus does not get included in the signal subspace estimate. Instead, as it follows from the results in Fig 1.c the SS estimate is comprised of the 1st, 3rd and 4th components resulting in a $[1.0000,\ 0.8813]^T$ subspace correlation vector. A similar decision can be made by analysis of the MI spectrum Fig 1.d.

DISCUSSION

We described an objective method for identifying components bearing a statistically significant amount of task-related signal. The procedure allows for automatic processing of the ERP/F data and can be used with any kind of spatial decomposition. The approach handles easily the situation when strong spatially coherent artifacts contaminate the data. The method can be useful for routine analysis of the ERP/F as well as for automatic processing of large number of datasets, e.g., in the bootstrap model-based analysis of the ERP/F data to establish confidence intervals for electromagnetic model parameters.

ACKNOWLEDGMENT

This work was supported by NIMH g R44 MH 64343. Dr. W. Sutherling kindly provided the MEG data used to construct the simulations.

REFERENCES

A. Ossadtchi, S. Baillet & R.M. Leahy, "Mutual Information - Criterion for Selecting ICA-Produced Components, MI2CA", Proceedings of BIOMAG2000, 12th International Conference on Biomagnetism, August 13-17 2000, Helsinki, Finland.

E.S. Edgington, "Randomization Tests" 3rd Revision edition, Marcel Dekker, 1995.

G.H. Golub, and C. F. V. Loan, Matrix Computations, ch. Computer Applications. Baltimore, MD: Johns Hopkins Univ. Press, 1984.

Spatiotemporal noise covariance model for MEG/EEG data source analysis

S. M. Plis, J. S. George, S. C. Jun, J. Paré-Blagoev, D. M. Ranken, D. M. Schmidt, C. C. Wood

Biological & Quantum Physics Group, MS-D454, Los Alamos National Laboratory, Los Alamos, New Mexico, USA

ABSTRACT

A new method for approximating spatio-temporal noise covariance for the use in MEG/EEG source analysis is proposed. This new approach builds on one introduced previously [Huizenga, 2002] but improves the old result in several important ways. Our method uses Kronecker formulation and thus possesses the very useful feature of fast inverse calculation. The method does not need estimation of the full covariance in order to compute an approximation, which provides for reliable estimates of the model using a smaller data set. It does not suffer from convergence problems due to numerical difficulties, and. notably, it captures more information about the noise which will lead to better analysis results.

KEY WORDS: MEG, EEG, Spatiotemporal Analysis, Noise Modelling, Inverse Problem.

INTRODUCTION

Statistical properties of MEG/EEG noise are needed to accurately identify the signal. For example in many probabilistic formulations of the inverse problem for averaged evoked response data the likelihood function (1) is used [Schmidt, 1999].

$$L \propto e^{-\frac{1}{2}\sum_{k,t}^{M} b_{k,t} COV^{-1}_{k,t',k',t} b_{k,t}} \quad (1)$$

Commonly, covariance is taken to be diagonal where there is ample evidence that the background averaged data is correlated within space and time. This can affect the results of inverse calculations: biasing both the mean or most likely results as well as the error or uncertainty in the result. In principle, if a normal distribution is assumed, the full covariance matrix of the averaged data can be estimated in the following way. MEG/EEG is measured in M trials, on L sensors and in T time samples. If we assume that source parameters are fixed over trials, then noise and data can be averaged. Let $\mathbf{E}_\mathrm{m}$ be the L by T single trial noise matrix at trial m. Conventionally, full averaged noise covariance matrix is defined by

$$\boldsymbol{COV}=\frac{1}{M(M-1)}\sum_{m=1}^{M}(vec(\boldsymbol{E}_m)-vec(\bar{\boldsymbol{E}}_m))(vec(\boldsymbol{E}_m)-vec(\bar{\boldsymbol{E}}_m))^T\text{ , }\bar{\boldsymbol{E}}=\frac{1}{M}\sum_{m=1}^{M}\bar{\boldsymbol{E}}_m \quad (2)$$

where $vec(\boldsymbol{E})$ is all the columns of $\boldsymbol{E}$ stacked in a vector.

Since this noise covariance matrix is extremely large, it is almost impossible to handle in a likelihood formulation. For example, for 100 time samples and 122 channels, 12200(12200+1)/2=74426100 variables should be determined. Experimental data is rarely available for that number of parameters. Inverting a matrix of that size is hard for any interesting N, not even considering memory consumption. A close approximation of full covariance is needed. It should be estimable from limited data and it must be possible to calculate its inverse.

METHODS

DIAGONAL APPROXIMATION: It is common when solving the inverse problem, to model covariance as a diagonal or even just as an identity. Here we adopted the following simple model which could be used for comparisons. Full spatiotemporal covariance is assumed to be $\boldsymbol{COV} \approx \boldsymbol{T} \otimes \boldsymbol{S}$. In this formulation T is the temporal covariance which is taken to be identity and S is the diagonal spatial covariance with elements of the main diagonal being sensor variances. This model is very simple yet still generates noise with variance levels consistent with those of noise generated by more complex models described below.

KRONECKER PRODUCT APPROXIMATION: A single pair model was proposed by Huizenga et. al. [Huizenga, 2002]. It is a Kronecker product of a temporal covariance matrix $\boldsymbol{T}$ and a spatial covariance matrix $\boldsymbol{S}$ [Huizenga, 2002][De Munck, 2002] shown in (3). To reduce the number of free parameters in the model both spatial and temporal covariances are parameterized. This idea allows us to manipulate noise covariances using an approximated model whose inversion is easily calculated using the following identity:

$$\boldsymbol{COV} \approx \boldsymbol{T} \otimes \boldsymbol{S} = \begin{bmatrix} t_{11}\boldsymbol{S} & t_{12}\boldsymbol{S} & \cdots & t_{1T}\boldsymbol{S} \\ t_{21}\boldsymbol{S} & t_{22}\boldsymbol{S} & \cdots & t_{2T}\boldsymbol{S} \\ \vdots & \vdots & \ddots & \vdots \\ t_{T1}\boldsymbol{S} & t_{T2}\boldsymbol{S} & \cdots & t_{TT}\boldsymbol{S} \end{bmatrix} \quad (3)$$

$$(\boldsymbol{T} \otimes \boldsymbol{S})^{-1} = \boldsymbol{T}^{-1} \otimes \boldsymbol{S}^{-1}$$

However, the Huizenga model was found unsuitable for our dataset due to numerical instabilities attributable to the form of parameterization. Here we introduce a new model in which model both spatial and temporal covariances are unparameterized leading to several benefits. Importantly it is not prone to numerical instability. Data solutions in our experiment were always invertible. The increased number of free parameters allows the proposed model to capture more information about the noise than Huizenga's. Finally, our model represents an improvement in that analytical calculations of the derivative of the Maximum Likelihood formulation of the cost function become possible. Thus, solutions can be obtained quickly with iterative algorithms.

SUM OF SERIES OF KRONECKER PRODUCTS APPROXIMATION: We propose an alternative estimation of noise covariance as a series of Kronecker products of temporal and spatial covariance matrices as in (4). Our approximation is based on the orthogonal spatial components of the data obtainable through singular value decomposition (SVD). The orthogonality feature makes it easy to invert this approximation (5).

$$\boldsymbol{COV} \approx \sum_{l=1}^{L} \boldsymbol{T}^l \otimes \boldsymbol{S}^l \text{ (4)}, \qquad \boldsymbol{COV}^{-1} \approx \sum_{l=1}^{L} (\boldsymbol{T}^l)^{-1} \otimes \boldsymbol{S}^l \text{ (5)}$$

USEFUL PROPERTIES: Our multipair model has fewer free parameters than full spatiotemporal covariance estimate (1) and has more expressive power than one Kronecker product models. An additional important and favorable feature distinguishing this model is that it does not require full spatiotemporal covariance and can be estimated directly from the data. At the same time, inversion remains computationally manageable and only constant times slower than inversion of (3).

COMPARISON OF COVARIANCE MODELS

We compared 3 models described above using the empirical background data collected from a 38 year old male on a Neuromag 122. Median nerve stimulation at the motor twitch threshold was applied using a block design of 30s on, 30s off for a total of 10 blocks for each of 8 runs, with left and right side stimulation alternating across runs, randomized ISIs between .25 and .75s. The data from this experiment was filtered with a median filter for 1 Hz lowpass effects. This signal was subtracted from the original data in order to get 1 HZ hipass filtering. A median filter was chosen as hipass filtering was introducing substantial distortions to the signal in the averaged data. 60Hz noise and harmonics were handled by removal of peaks in the spectrum and then interpolating between adjacent spectrum points.

COMPARING MODEL COVARIANCES TO FULL COVARIANCE: Figure 1 shows plots of spatiotemporal covariance approximation models with the full covariance. All figures show a scatterplot of each model overlaid on top of the full covariance line. In cases where approximation is very close to the full covariance, the scatterplot should map closely onto the full covariance line. As the figures suggest, multipair spatio-temporal covariance most closely resembles the structure of the full spatiotemporal.

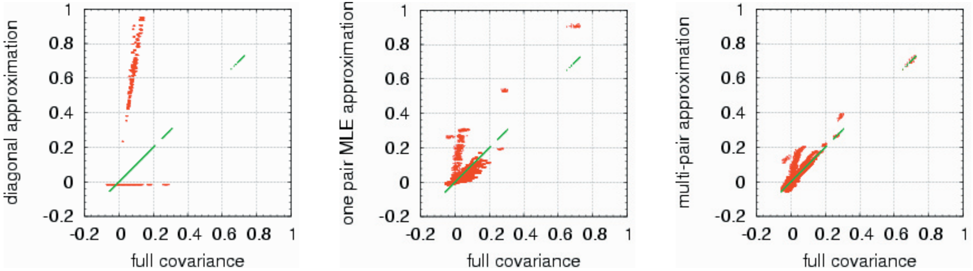

(a) **(b)** **(c)**

Figure 1: (a) diagonal approximation; (b) Kroneker product MLE approximation; (c) multipair approximation

SAMPLING THE LIKELIHOOD:

To compare the models' performance against each other and against a known ideal performance case, we examined the solution dipole positions when the models were applied to simulated data. Simulated data was constructed with 3 dipoles acting in the region of 35 ms. Dipole positions are (0,0,30), (-30,0,30) and (-30,30,30); corresponding orientations: (1,0,0), ($1/\sqrt{2}, -1/\sqrt{2}$,0) and (0,1,0); corresponding strengths: 50, 20 and $20/\sqrt{2}$ nAm. To these simulated dipoles, we added noise extracted from prestimulus regions of right side stimulation collection data collection runs. Signal to noise ratio of the simulated data is described by reduced χ^2 (figure 2). It was calculated as $(\sum_k b_k^2(t)/\sigma_k^2(t))/N$, where $b_k(t)$ is simulated data, $\sigma_k^2(t)$ - sensor variances and N is number of sensors.

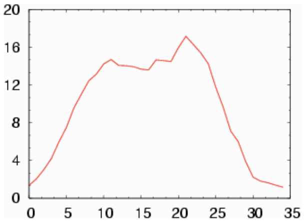

Figure 2: Reduced χ^2

Maximum likelihood results cannot provide the comprehensive information needed for comparison of the effect of different covariance models. Instead, it is more instructive to examine the behavior of the distribution of the likelihood when using different covariances. To obtain this sampling, we used Monte Carlo Markov Chain (MCMC) sampling [Gelman,1995]. The code used for sampling was developed in our group for the Bayesian inference dipole analysis [Jun,2004][Schmidt, 1999]. Likelihoods of the distances between true locations of dipoles and those obtained using different covariance models are plotted in Figure 3. This shows that multipair approximation gives consistently better results for this data although its distribution is wider than that of the diagonal approximation. This fact could be explained if we calculate the variances of likelihood function for each of those models accounting for the fact that some part of noise is not described by the model. In this case, diagonal approximation is consistently sharper, then goes multipair and the widest among all is the one pair approximation. This means that sharpness here is the result of not accounting for part of the noise.

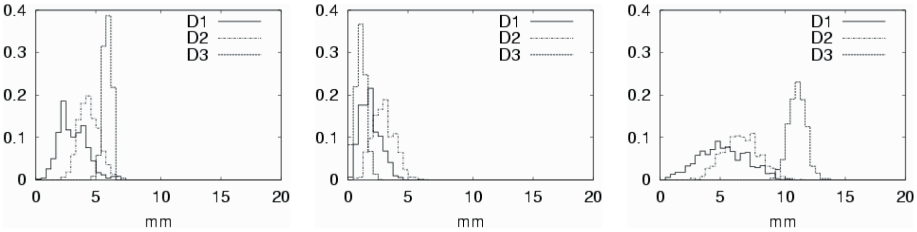

(0,0,30) (30,30,30) (-30,0,30)

Figure 3: Likelihoods of the distances between true locations of dipoles and those obtained using different covariance models. D1 - multipair, D2 - one pair MLE, D3 - diagonal.

CONCLUSIONS AND FUTURE WORK

A key feature of multipair model, making it useful for the analysis of MEG/EEG data, is that it captures more information about noise due to increased degrees of freedom (Fig. 1). It is straightforward to estimate: full covariance for estimation is not required, thus a comparatively small number of data samples is needed. Desirable properties of previous approximations are preserved: inversion is easy to calculate, space requirements are low, and number of free parameters is small. Further improvements are under development with a new model that uses independent, not orthogonal components. Preliminary results show its potential strengths for modeling full spatiotemporal covariance.

AKNOWLEDGEMENTS: This work was supported by NIH grant 2 R01 EB000310-05.

REFERENCES

De Munck J.C. et al. Estimating stationary dipoles from MEG/EEG data contaminated with spatially and temporally correlated background noise. IEEE Trans Biomed. Engin. 2002;50:15651572.

Gelman A. et al. Bayesian Data Analysis. London: Chapman & Hall; 1995.

Huizenga H.M. et al. Spatiotemporal EEG/MEG source analysis based on a parametric noise covariance model. IEEE Trans Biomed. Engin. 2002;50:533539.

Jun S.C. et al. Dipole analysis on spatiotemporal MEG signals using bayesian inference. Brain Topography. 2004;16:186.

Schmidt D.M. et al. Bayesian inference applied to the electromagnetic inverse problem. Human Brain Mapping. 1999;7:195212.

QRS-Fragmentation Detected by Filtering with Binomial Non-Recursive Filters

[1]Schless, B.G., [2]DiPietroPaolo, D., [3]Müller, H.-P., [3]Pasquarelli, A., [3]DeMelis, M., [3]Erné, S.N.

[1]Department of Cardiology, University of Ulm, Germany
[2]Advanced Technologies Biomagnetics, Pescara, Italy
[3]Division for Biosignals and Imaging Technologies, ZIBMT, University of Ulm, Germany

ABSTRACT

High-frequency components in signals, correlating to ventricular depolarisation, are thought to be an indicator of the patient's risk of suffering from cardiac diseases [Cain, 1987]. In this study the structure of such components was investigated.

55-channel magnetocardiography (MCG) recording were obtained from about 50 subjects, subdivided into 4 categories: normal volunteers, patients with coronary heart disease (CHD), patients with myocardial infarction (MI) and patients with ventricular tachycardia (VT). Following the rules of [Endt, 1998], a band-pass (37Hz-90Hz) binomial filter was first applied to each channel of signal-averaged (SA) MCG.. Next, two values, the number of extrema M and a QRS fragmentation S-score, calculated from the filtered signals, were used as parameters. The results of previous studies [Müller, 1999] were confirmed. In fact, the QRS fragmentation S-score and the number of extrema M showed significant differences between normal subjects, CHD-, MI- patients.

KEY WORDS

Magnetocardiography, binomial non-recursive filter, QRS-fragmentation

INTRODUCTION

For visualizing and quantifying high-frequency components, recursive Butterworth, high-pass filters are often used. However, this type of filter generates a "ringing" in the time domain, so that it is hard to find the actual QRS length. For this reason, in this work, a non-recursive filter (FIR filter), that provides a linear phase response and circumvents the problem of filter ringing, has been used.

Using high order, non-recursive filters may yield problems similar to that of the Butterworth filter. On the other hand, high-order coefficients cause a spreading of the filter's response in the time domain. To solve this conflict, binomial filters of a higher order [Link, 1994], which have the property that their coefficients decrease rapidly with an increased order, were taken into account [Endt, 1998].

The aim of this analysis is to confirm previous studies showing that fragmented depolarisation can be detected, not only at the terminal part of QRS complex, but throughout the depolarisation of the ventricle and then to differentiate patients with CHD, MI, VT, and healthy subjects.

METHODS

The measurements were carried out on a 55-channel planar SQUID magnetometer system, Argos55 (Atb, Pescara, Italy) [Erné, 1998]. The MCG sensor system operates inside a magnetically shielded room. The MCG signals were sampled at 8.2 kHz, digitally filtered and decimated to a final sampling frequency of 1 kHz and a bandwidth between DC and 250 Hz.

The duration of the MCG recordings were at least 300s. To check the reproducibility of the results, two measurements were obtained for all patients and healthy volunteers.

About 50 subjects were selected from our database. Selection criteria was set to provide the optimum group compositions, taking into consideration the following: 1. classification of MI (Posterior Wall Infarction -PWI, Anterior Wall Infarction -AWI), 2. accompanying diagnosis, 3. measurement quality.

None of the 16 healthy volunteers (mean age 41.3 ± 10.8 years) had a history or symptoms of heart disease.

16 patients (mean age 66.8 ± 8.6 years) had a history of CHD, but without a history of previous MI.

15 patients (mean age 63.0 ± 8.4 years) had a history of previous MI, 7 with PWI and 8 with AWI.

4 patients (mean age 56.5 ± 21.0 years) had a history of documented ventricular tachycardia (VT).

A binomial non-recursive band-pass filter was applied to each channel of the SAMCG. The band-pass filter was performed in 2 steps: first a binomial high-pass filter of the 90th order corresponding to 37 Hz was applied [Brockmeier, 1994] [Link, 1992], followed by a binomial low pass filter with a cut-off frequency of 90 Hz [Müller, 1999].

Given a low-pass filter with N coefficients, it is known that an high pass filter can be defined as its supplement to an all-pass filter:

$$B_f(t) = B(t) - \sum_{k=-N}^{K=N} c(k)B(t-k) \tag{1}$$

where N is chosen according to $m \approx 9.824 / \theta_c^2$, $N = m/2$,

$B(t)$ is the input signal, $c(k)$ the filter coefficients and $B_f(t)$ the output sequence.

In order to quantify the fragmentation of these band-pass filtered signals, the number of extrema M on the normalized signal for each SAMCG channel was counted. Then the following algorithm was used to obtain the fragmentation score S.

$$S = M\left(\left|y(t_1)\right| + \left|y(t_M)\right| + \sum_{k=2}^{K=M} \left|y(t_k) - y(t_k - 1)\right| \right) \tag{2}$$

S is a dimensionless number representing the fragmentation of the QRS complex.

RESULTS

The analysis shows that volunteers and CHD-patients have a rather regular pattern in the QRS interval, corresponding to a low number of extrema and a low fragmentation value S (Figs 1,2), whereas, the MI- and VT- patients have a larger number of deflexions and a higher fragmentation score S (Figs. 3,4).

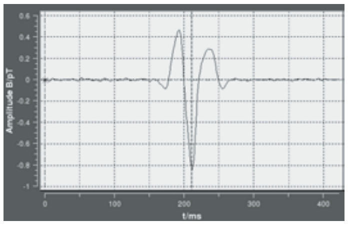

Figure 1. Averaged, filtered MCG of a normal subject.

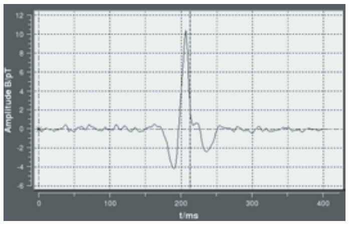

Figure 2. Averaged, filtered MCG of a CHD patient.

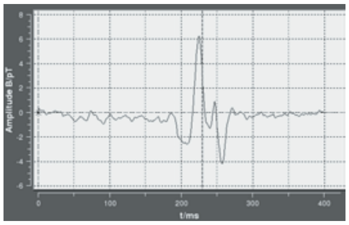

Figure 3. Averaged, filtered MCG of a MI patient.

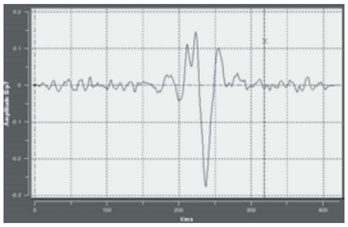

Figure 4. Averaged, filtered MCG of a VT patient.

The QRS fragmentation score, S and the number of extrema M yield the results shown in Table 1. The results of the t-test using the same parameters are listed in Table 2. Up until now, only a few VT-patients, without a defibrillator, participated in this study. Thus, this group was not considered in the in the t-test. In Fig. 5 a graphical display of the results is shown.

	Avg.(S)	Std(S)	Avg.(M)	Std(M)
Normals	25.88	8.52	6.34	1.28
CHD	26.94	8.47	6.16	1.09
MI	34.29	8.35	7.33	1.28
VT	37.16	--	7.60	--

Table 1 Average (avg) and standard deviation (std) of fragmentation-score S and of the number of extrema M for the various groups.

	CHD (S)	MI (S)	CHD (M)	MI (M)
Normals	0.729	0.010	0.679	0.033
CHD		0.021		0.008

Table 2. p-value ($p<0.05$) of the fragmentation-score S and of the number of extrema M (corresponding to Tab. 1) evaluated by a two-sided Student's t-test.

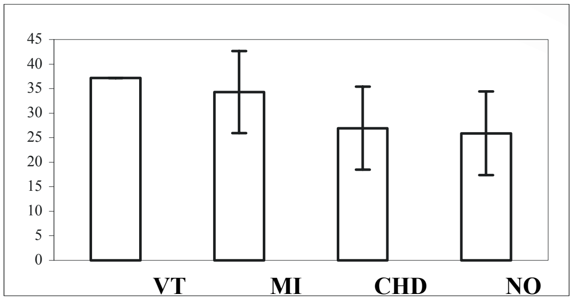

Figure 5. Mean values (blocks) and standard deviations (lines) of QRS fragmentation S-score for the various groups

DISCUSSION

This study is a revision of previous studies and suggests that irregular fragmentation of the filtered QRS complex does provide a means to identify conduction disturbances in patients with malignant arrhythmia. In the future, it would be useful to repeat the study with an increased number of subjects, especially for the group concerning the VT- patients.

REFERENCES

Brockmeier K, Schimdt S, Kreiseler D, Trahms L, Schimtz L, Oeff M, Hahlbohm HD. Fragmented ventricular depolarisation detectable in the QRS complex of the magnetocardiogram after filtering with binomial non-recusive filters. In: Computer in Cardiology 1994. Los Alamitos: IEEE Computer Society Press, 1994, p. 685-687.

Cain ME, Ambos H-D, Lindsay BD. Fast Fourier transform analysis of the signal averaged electrocardiogram in the management of patients with or prone to ventricular tachycardia or fibrillation. In: Cardiac Arrhythmia: Where to Go from Here? Eds. Brugada P and Wellems HJJ (Futura Publishing Company, Mount Kisko, NY), 1987, p. 311-328.

Erné SN, Pasquarelli A, Kammrath H, Della Penna S, Torquati K, Pizzella V, Rossi R, Granata C, Russo M. Argos 55 - The New MCG System in Ulm. Proceedings of BIOMAG98, 1998, Sendai, Japan.

Link A, Trahms L. Highpass filters for detecting late potentials. In: Computers in Cardiology 1992. Los Alamitos: IEEE Computer Society Press, 1992: p. 159-62.

Link A, Trahms L, Zimmermann R, Oeff M. Complex binomial bandpass filters for analysis phase and envelope of high frequency components in cardiac signals. In: Computer in Cardiology 1994. Los Alamitos: IEEE Computer Society Press, 1994, p. 617-629.

Endt P, Hahlbohm HD, Kreiseler D, Oeff M, Steinhoff U, Trahms L. Fragmentation of bandpass-filtered QRS-complex of patients prone to malignant arrhytmia. Medical & Biological Engineering & Computing, 1998, 36; p. 723-728.

Müller H-P, Gödde P, Czerki K, Oeff M, Agrawal R, Endt P, Kruse W, Steinhoff U, Trahms L. Magnetocardiographic analysis of the two dimensional distribution of intra-QRS fractionated activation. Physics in Medicine and Biology, 1999, 44; p. 105-120.

Magnetocardiographic Study of Heart Repolarisation Disturbances

[1]Schless B.G., [2]Zhu R., [2]DeMelis M., [2]Müller, H.-P., [2]Pasquarelli A., [3]DiPietroPaolo D., and [2]Erné, S. N.

[1]Departement of Cardiology, University of Ulm, Germany
[2]Division for Biosignals and Imaging Technologies, ZIBMT, University of Ulm, Germany
[3]Advanced Technologies Biomagnetics, Pescara, Italy

ABSTRACT

A promising method, based on the current vector map (CVM) obtained from magnetocardiography analysis, was recently proposed [Tsukada, 2000, Miyashita, 2003] in order to investigate cardiac repolarisation inhomogeneities. This study is aimed at evaluating, quantitatively, the differences between normal subjects and patients affected by myocardial infarction in terms of current vector diagrams (CVD), which are the temporal evolution of the CVM.

KEY WORDS

Magnetocardiography, current vector map, myocardial infarction.

INTRODUCTION

Myocardial infarction and ischemia cause changes in the electrophysiological properties of the myocardium. Conduction properties of the muscle cells change inhomogenously in the ischemic areas resulting in the dispersion of the activation wavefront. Ischemic and infarcted regions have different electromagnetic properties that can be detected as depolarisation and repolarisation abnormalities in the ST-segment. Such deviations can be visualised in terms of CVD, showing the differences between the current flow in normal subjects and in patients with previous myocardial infarction (MI).

METHODS

The measurements were carried out on a 55-channel planar SQUID magnetometer system, Argos55 (Atb, Pescara, Italy) [Erné, 1998]. The MCG sensor system operates inside a magnetically shielded room. The MCG signals were sampled at 8.2 kHz, digitally filtered at 250 Hz and decimated to a final sampling frequency of 1 kHz and a bandwidth between DC and 250 Hz. The duration of the MCG recordings was at least 300s. To check the reproducibility of the results, two measurements were obtained for all patients and healthy volunteers. The data analysis was performed using the OMEGA software [DeMelis 2002].

MCG recordings were obtained from 68 normal subjects with no history or symptoms of heart disease and 39 MI patients. The current vector can be defined as

$$\vec{C} = \frac{\vartheta B}{\vartheta y}\vec{i} - \frac{\vartheta B}{\vartheta x}\vec{j} \qquad (1)$$

This vector was calculated for all sensors in each time point to evaluate the current flow over the whole ST segment.

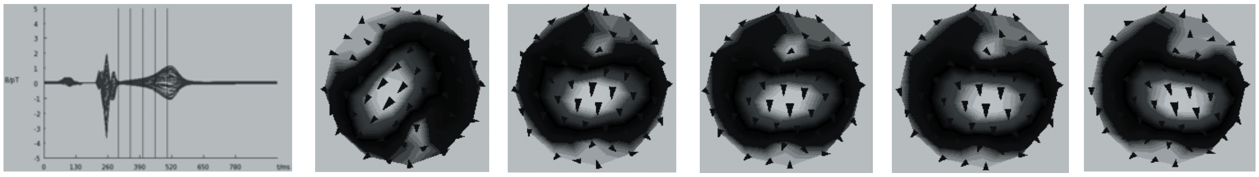

Figure 1. Current vector maps in 5 time points of the ST segment in a normal subject.

The current vector maps show similar patterns for normal subjects. They are generally oriented in one direction, and their amplitudes have a uniform distribution over the whole chest. In MI patients, the current vectors usually show a less regular distribution of the current flow due to deviations of the ST segment and/or alterations of the T-wave.

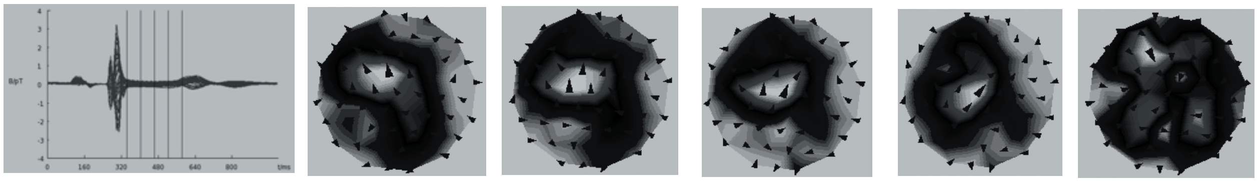

Figure 2. Current vector maps of 5 time points of the ST segment in a MI patient.

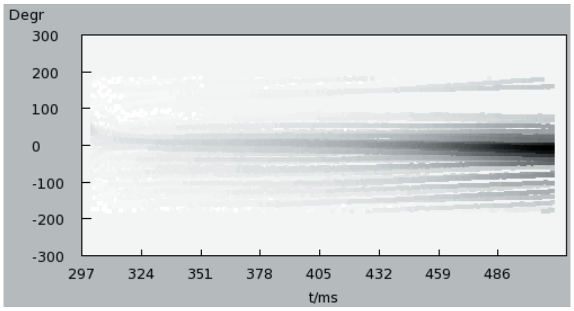

Figure 3. CVD of a normal subject.

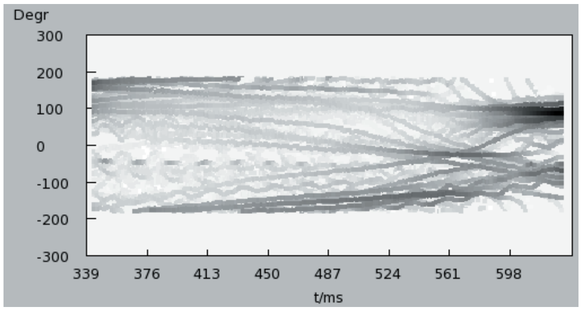

Figure 4. CVD of an MI patient.

In Figs. 3 and 4, the temporal evolutions of the orientation for all current vectors are shown. Each curve corresponds to a different channel, and the greyscale is proportional to the amplitude of the vectors. Normal patients with homogeneous repolarisation have CVDs in which the orientation of the current vectors changes slowly in the ST segment. Generally, MI patients have a less regular distribution, and also higher values for the vector amplitudes.

To evaluate quantitatively the differences between normals and MI patients, a parameterisation is performed for each channel: The parameter is a weighted variability that takes into account the orientation and the amplitude of the current vectors calculated over the whole ST segment:

$$f_j^{ST} = \sqrt{\frac{\sum_{i=1}^{L} A(i,j)\vartheta(i,j)^2}{L * \sum_{i=1}^{L} A(i,j)}} \qquad (2)$$

where $j \in [1, N_S]$ is the channel index, N_S is the number of sensors of the system, L is the ST segment length, A(i,j) is the demeaned amplitude of the current vector for a given time instant i, and channel j and $\partial(i,j)$ are the demeaned orientation of the current vector.

RESULTS

In MI patients, depolarisation and repolarisation disturbances result in less regular patterns in the CVDs and thus in higher values for the parameter, whereas normal subjects show a more uniform distribution of the current vectors and thus lower values.

	Avg. (f^{ST})	Std. (f^{ST})
Normals	2.13	1.19
MI	2.91	1.22

Table 1. Avaraged values and standard deviations of the estimated variabilities for the different groups.

DISCUSSION

The CVMs obtained by the magnetocardiogram (Figs. 1,2) can be used to investigate heart disturbances in the repolarisation phase. CVDs (Figs. 3,4) provide an even better evaluation of the inhomogeneities of cardiac activity. Irregular patterns of the current vectors can be parameterised.

REFERENCES

Tsukada, K., Miyashita, T., Kandori, A., Mitsui, T., Terada, Y., Sato, M., Shiono, J., Horigome, H., Yamada, S., Yamaguchi, I.. An iso-integral mapping technique using magnetocardiogram and its possible use for diagnosis of ischemic heart disease. Int J Card Imaging 16, pp 55-66, 2000.

Miyashita, T., Kandori, A., Ogata, K., Tsukada, K., On, K., Horigome, H., Watanabe, S., Miyauchi, T., Yamaguchi, I. Evaluating Inhomogeneity of Myocardial Activity of Ischemic Heart Disease by Using MCG. Proceedings of NFSI 2003, Chieti, Italy.

Erné SN, Pasquarelli A, Kammrath H, Della Penna S, Torquati K, Pizzella V, Rossi R, Granata C, Russo M. Argos 55 - The New MCG System in Ulm. Proceedings of BIOMAG98, 1998, Sendai, Japan.

DeMelis M, Müller H-P, Pasquarelli A, Erné SN. Magnetocardiographic Signal Analysis. Proceedings of BIOMAG 2002, 2002, Jena, Germany, pp. 987-989.

Spatial-Temporal Analysis of Nonstationary fMEG Data

P. Soni[a], Y. Chan[a,1], H. Preissl[b,c], H. Eswaran[c], J. D. Wilson[a], P. Murphy[c], C. L. Lowery[c]
[a]Univ. of Arkansas at Little Rock, Little Rock, USA; [b]MEG Center, Univ. of Tübingen, Germany;
[c]Univ. of Arkansas for Medical Sciences, Little Rock AR, USA

ABSTRACT

Non-invasive technique such as Magneto-encephalography (MEG), initially pioneered to study human brain signals, has found many other applications in medicine. SARA (SQUID[2] Array for Reproductive Assessment) is a unique scanning noninvasive device developed at the University of Arkansas for Medical Sciences (UAMS) that can detect fetal brain and other activities. The fetal magneto-encephalography (fMEG) signals collected often has many bio-magnetic signals mixed in. Examples include the movement of fetus or muscle contraction of the mother. As a result, the recorded signals may show unexpected patterns, other than the target signal of interest. These "*interventions*" makes it difficult for a physician to assess the exact fetal condition, including its response to various stimuli. We propose using *intervention analysis* and *spatial-temporal autoregressive moving average* (STARMA) modeling to address the problem. STARMA is a statistical method that examines the relationship between the current observations as a linear combination of past observations as well as observations at neighboring sites. Through intervention analysis, the change in pattern due to "interfering" signals can be well accounted for. The end product generated from this model is a "*template*" time series, or a typical signal from the target of interest. It will assist physicians in monitoring the actual signal generated by fetal brain and other organs of interest.

KEY WORDS

Fetal magneto encephalography (fMEG), spatial-temporal analysis, nonstationarity, nonhomogeniety, intervention analysis

INTRODUCTION

A time series of fetal MEG observations can sometimes be affected by unknown movement of fetus, commonly called interventions. Interventions can convert an otherwise stationary series to non-stationary series. Intervention analysis is a classical method of dealing with external events that affect a time series or a process [8]. A standard procedure to detect an "intervention" is "template matching", where the correlation between the template and a non-stationary series is computed. The correlation will indicate whether there is an intervention. By this template matching method, we can assess whether an intervention has occurred. However, a scientific method to obtain such a template has yet to be found.

As described by Pfeifer and Deutsch [6], a family of space-time models called STARMA can be synthesized for modeling a wide variety of space-time processes. These models are characterized by autoregressive and moving-average terms lagged both in space and time. As Giaocomini and Granger point out, STARMA can be derived through a (nontrivial) transformation of the Vector Autoregressive Moving Average model. the transformation is in fact a restriction related to the neighborhood structure as revealed by a set of weight matrices. Kamarianakis [4] has researched on three alternate modeling techniques that apply to multiple time-series data corresponding to different spatial locations. Built upon on STARMA, Greene [3] removes an intervention using an exogenously derived template. Instead of a template, Wright [8] models interventions with a transfer function. Similar approach can be carried out in SARA. Correspondingly, an intervention is modeled with a transfer function added to STARMA, where an intervention may be a movement of the fetus.

METHODS

The process of modeling the intervention and producing the "template" series can be broadly divided in two blocks. The first block accounts for the "intervention" using intervention analysis, while the second block applies STARMA. The data, used in this research, consisting of 10000 points, is from a 37-week fetus. The sampling rate is 312.5 Hz. Applying a viewing filter of 0.5 to 10 Hz, known maternal interventions are removed using CTF Data Editor.

Intervention Analysis

As mentioned, A transfer function is used to model the effect of an intervention. For example, a bivariate transfer-function model can be represented in general form as

$$Y_t = d(B)X_t + v_t \qquad \text{Equation 1}$$

where X_t is the input time series, $d(B)$ is the transfer function, Y_t is the output time series of interest, and v_t is the combined effects of all other factors influencing Y_t. An inspection of the signal suggests that fetal breathing is present. Observing the frequency spectrum, the signal is very

---

[1] Correspondent can be reached at Department of Systems Engineering, University of Arkansas at Little Rock, 2801 South University, Little Rock, AR 72204-1099, Tel. 501-569-8926; Fax 501-569-8698; E-mail: yxchan@ualr.edu

[2] Superconducting Quantum Interference Device

sinusoidal at about 0.8-1Hz. Correspondingly, The transfer function for this problem is assumed to be sinusoidal making the intervention complex. It will be calibrated by calculating the magnetic-field intensity at every sensor, where the magnetic field intensity is calculated using Maxwell's Laws of electromagnetism.

Spatial Temporal analysis

The STARMA model is given by the equation

$$Z_t = \sum_{k=1}^{p} \sum_{l=0}^{\lambda_k} \varphi_{kl} L^{(l)} Z_{t-k} - \sum_{k=1}^{q} \sum_{l=0}^{m_k} \theta_{kl} L^{(l)} a_{t-k} + a_t \qquad \text{Equation 2}$$

where Z_t is the time series, a_t is the residual series, and φ_{kt} and θ_{kt} are calibration constants. L works as the backshift operator on the spatial component. Hence, $L^{(l)}Z_t$ is the calculations performed on Z_t's lth-order neighbor. λ_k is the spatial order of the kth autoregressive term and m_k is the spatial order of the kth moving-average term.

Realization of a STARMA model starts with an extensive visualization of data and its statistical parameters such as autocorrelation, partial autocorrelation from different perspectives. The data is checked for non-stationarity and non-homogeneity in time and space dimension respectively. After "sanitization" of data, i.e., after the data has been made stationary and homogeneous, the temporal and spatial autocorrelation decides the order of the STARMA model. STARMA parameters are then estimated and a tentative model is formed. Model is passed through various diagnostic checks to determine whether this model represents the data exactly. If not the whole process is repeated again and another tentative model is tested.

One of the important parameter is assigning the spatial weights to each order of neighbor. Weights are assigned to each sensor to reflect its contribution toward the target sensor under consideration. The end result is a re-write of Eqn 1 as

$$\beta_t \bullet \bullet d(B)\alpha_t \bullet \bullet \frac{\varphi_z(B)}{\theta_z(B)}\upsilon_t \bullet \bullet d(B)\,\alpha_t \bullet \bullet \varepsilon_t, \qquad \text{Equation 3}$$

where. β_t is the estimated output from the prewhitened input-series α_t , $\bullet_z(B)$ is the autoregressive operator, $\theta_z(B)$ is the moving-average operator, and ε_t is the transformed noise-series Once a model is formed and series is estimated a standard procedure to detect an "intervention" is "template matching", where the correlation between the template and a non-stationary series is computed. The correlation will indicate whether there is an intervention.

RESULTS

Preliminary work has been done on data sanitization. It included the check for stationarity and homogeneity. Out of data collected from 151 SARA channels, one of the sensors that showed high breathing activity is chosen to start the procedure. Channel MLI1 was selected as target sensor. Its first-order, second-order and third-order neighbors are defined with respect to distance from the target sensor as shown in Fig 1.

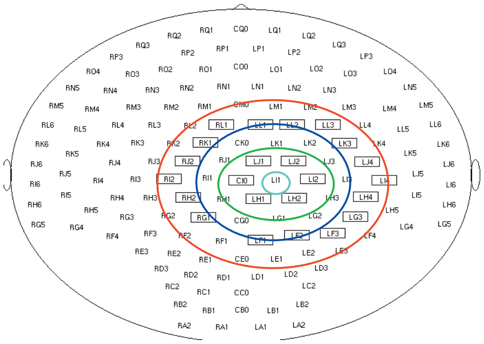

Fig.1 Target Sensor and Neighbors

Stationarity in time dimension A time-series is analyzed for stationary and periodicity. Many time series display periodicity, which is characterized by a cyclic movement in the data that usually repeats itself. A cyclic pattern in an autocorrelation plot confirms periodicity .If the data contains periodicity, the cycles can be removed by taking a difference equal to the number of periods in the cycle τ, i.e., $z(t) = z(t) - z(t - \tau)$. Here in the line spectrum the cycle length is approximately 350. A stationary process has the property that the mean, variance and autocorrelation structure do not change over time. These two characteristics are checked by two different techniques: line spectra and autocorrelation plots. Autocorrelation analysis is to ensure that the data is stationary, which means that the joint distribution of any sequence of observations $z(t+1)$, $z(t+2)$, ..., $z(t+n)$ does not depend on t. The autocorrelation measures the relationship or how much interdependence exists between neighboring points in a time series. A plot of the autocorrelations of the original data (against time-lag n) reveals periodicity in the data, as shown in Fig.2a. After removing the cycles and second-order differencing, the data appeared stationary as shown in Fig 2b.

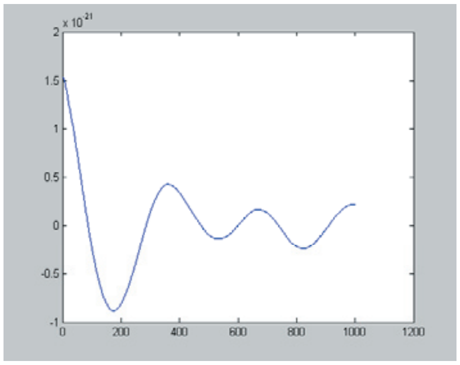

Fig.2a Autocorrelation of Raw Series

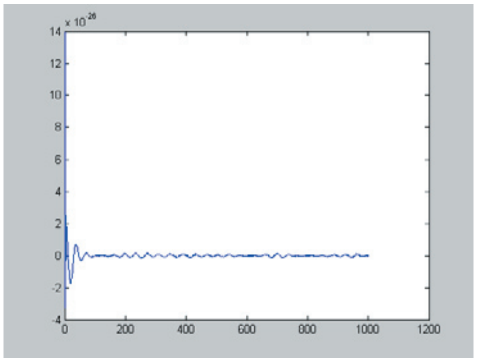

Fig.2b Auto correlation of second-order differenced series

Homogeneity in Space Dimension When n observations are made on a variable that is spatially dependent, the amount of information carried by the sample is less then amount of information that will be carried if data is independent. To remove this spatial dependency, differencing in space dimension needs to be done .This is accomplished by subtracting the zeroth order neighbor that is the target sensor series from the weighted consolidated first-order and second-order neighbor series. Fig 3 shows spatial correlation, as a result of difference between zeroth and first-order neighbors. It can be seen that homogeneity is achieved, by constant spatial correlation.

CONCLUSION

For an accurate analysis of fMEG data, we outlined a procedure to discern if any intervention—such as movement, breathing or heartbeat—has occurred in recorded signals. Frequency spectrum of the filtered fMEG signals from a 37-week fetus shows a high peak at around 1 Hz, which matches the observed fetal breathing pattern in the raw data. Armed with this observation, we hypothesized that the data had interventions caused by fetal breathing. Preliminary steps have been shown in this paper to remove these interventions temporally and spatially.

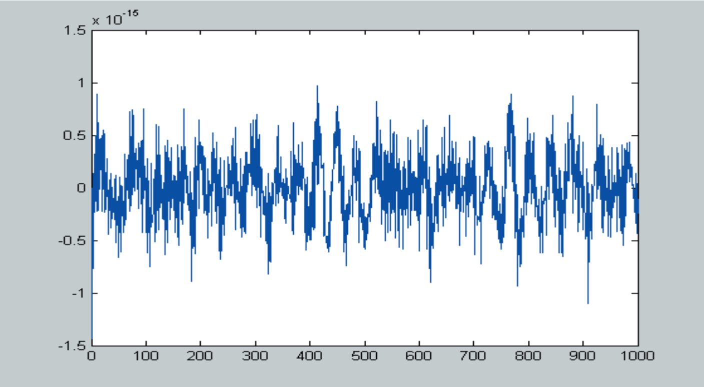

Fig.4 Spatially differenced data

A useful STARMA model to be identified is contingent upon removing interventions from the signal. The resulting series will be a signature series that will closely resemble a target signal when nonstationary activities are absent. Such a signatory series will be used as a template for comparison with other recorded fMEG signals in the future. Through its correlation with a subject signal, this template can be used to account for any interventions in the subject series. When there are different types of fetal or maternal activities interfering with the subject signals, it is hypothesized that this modeling procedure will be able to identify them. For accurate hypothesis testing and easy interpretation of the biomagnetic signals by physicians, a 3D visualization tool is proposed to supplement our current modeling procedure.

ACKNOWLEDGEMENT

The authors gratefully acknowledge the contributions of C. Bayrak, Q. Campbell, R. Draganova, M. Holst, J. Norton, X. Wu and other SARA researchers toward this research. Obviously, the authors alone are responsible for the content of this paper. This work is supported the National Institutes of Health grant 1R01NS36277-03, USA.

REFERENCES

[1] Box, George EP, Tiao GC. Time Series Analysis. *Journal of the American Statistical Association*, 70: 70–79, March 1975
[2] Lowery CL. “Assessment and Analysis of Temporal-Spatial Biomagnetic Fields of the Fetus”. Proposal submitted to the National Institute of Health, University of Arkansas Medical Sciences, Little Rock AR, 2002.
[3] Greene**,** KA. “Causal Univariate Spatial Temporal Autoregressive Moving Average Modeling Of Target Region Information To Generate Tasking Of A Worldwide Sensor System.” Master of Science Thesis, Department of Operational Sciences, Air Force Institute of Technology. May 1992.
[4] Kamarianakis, Y. “Spatial-time series modeling: A review of the proposed methodologies*.”* Discussion Paper, Regional Analysis Division REAL 03-T-19, May 2003
[5] Habib, MK. “A modern approach to time series analysis.” Department of Applied Science and Engineering Statistics, George Mason University. Summer 2000.
[6] Pfeifer, PE; Deutsch, SJ. “A three-stage iterative procedure for space-time modeling.” *Technometrics* 22(1) (1980): 35–47.
[7] Box, GEP; Jenkins, GM. *Time Series Analysis: Forecasting and Control* (Revised edition). San Francisco: Holden-Day, Inc. 1997.
[8] Wright, SA. “Spatial-Temporal Time Series: Pollution Pattern Recognition under Irregular Intervention.” Master of Science Thesis, Department of Operational Sciences, Air Force Institute of Technology, Wright-Patterson AFB, Ohio 1995.

MEG Recordings of DC Fields Using the Signal Space Separation Method (SSS)

Taulu, S., Simola, J., and Kajola, M.

Elekta Neuromag Oy, Helsinki, Finland

ABSTRACT

Stationary SQUID sensors record time-varying magnetic fields only. Any DC sources, such as magnetic impurities on the scalp or physiological DC currents, are invisible in conventional MEG with stationary sources and sensors. However, movement of the subject relative to the measurement device transforms the DC fields into time-varying MEG signals, which are either signals of interest from biomagnetic sources, or movement artifacts when caused by magnetic residue on the head. These signals can be demodulated to DC by tracking the head movement and by using this recorded information to decompose the signals into a device-independent source model. To do this we have used the signal space separation method (SSS) along with a continuous head position monitoring system. From time variations of the recorded signal, a linear equation is obtained relating the averaged MEG signal variation, the DC-source in the head, and the varying external interference. In this way an unbiased estimate is obtained for the DC source as it is automatically separated from external interference. The method was tested by feeding DC current in an artificial current dipole on a phantom head and by continuously moving and rotating this phantom randomly with a motion amplitude of several centimeters. After the SSS based movement demodulation and reconstruction of the signal from inside of the helmet, the location of the DC current dipole in the phantom could be determined with an accuracy of 2 mm. It is concluded that the method enables localization of DC sources with MEG using voluntary head movements.

KEY WORDS

Magnetoencephalography, DC measurements, DC currents, head position monitoring, movement artifacts, signal space separation

INTRODUCTION

DC phenomena are of interest in several physiological and patophysiological conditions, e.g. in stroke and migraine, and MEG provides advantages over other modalities in DC measurements [Mackert, 1999]. The basic problem in DC-MEG recordings is the insensitivity of SQUID sensors to static fields. However, movement of the subject with respect to the measurement device modulates the DC fields into time-varying MEG signals. Because of the high environmental interference level at the lowest frequencies, a relatively high modulation frequency is preferred in these measurements.

In previous studies the movement of the head has been produced by mechanical instrumentation, such as a moving bed [Mackert, 1999] or by using air cushions between the head and the sensor array [Weiskopf, 2001]. The mechanical modulation has been used to transform DC signals to AC with a carefully controlled movement having a predefined frequency and amplitude. The required additional instrumentation reduces clinical utility of the DC application.

In contrast to using special instrumentation for mechanical modulation, we propose a method based on voluntary and unrestricted head movements for recording of the DC fields of the brain. In this method, we use the continuous head position monitoring system described in [Uutela, 2001] and then, according to the movement information, reconstruct the brain signals in the head coordinate system using the signal space separation method (SSS) which also suppresses external interference. In this method the AC signals produced by the DC currents are demodulated and appear as static fields in the reconstructed signals which are free of external interference signals.

The removal of the artifacts caused by magnetic contamination attached to a moving subject has been reported before [Taulu, 2004a]. In this paper we present a method for reconstruction of the true DC field based on voluntary head movements, and the verification of this method by a phantom experiment.

METHODS

The signal space separation method describes the signal vector $\boldsymbol{\phi}$ of a multichannel measurement device with a linear model including separate subspaces $\mathbf{S}_{\mathrm{in}}$ and $\mathbf{S}_{\mathrm{out}}$ for the biomagnetic signals and external interference signals, respectively:

$$\boldsymbol{\phi} = \begin{bmatrix} \mathbf{S}_{\mathrm{in}} & \mathbf{S}_{\mathrm{out}} \end{bmatrix} \begin{bmatrix} \mathbf{x}_{\mathrm{in}} \\ \mathbf{x}_{\mathrm{out}} \end{bmatrix} \tag{1}$$

where $\mathbf{x}_{\mathrm{in}}$ and $\mathbf{x}_{\mathrm{out}}$ are vectors containing the amplitudes of harmonic basis functions corresponding to the columns of $\mathbf{S}_{\mathrm{in}}$ and $\mathbf{S}_{\mathrm{out}}$, respectively. This novel separation method [Taulu, 2004b] is based on classical electromagnetic theory.

The zero level of the MEG signals is set by subtracting the initial DC level from the signals and therefore only the dynamic parts of $\mathbf{x}_{\mathrm{in}}$ and $\mathbf{x}_{\mathrm{out}}$ contribute to the measured data. However, if the signal difference $\Delta\boldsymbol{\phi}(t_i) = \boldsymbol{\phi}(t_{i+1}) - \boldsymbol{\phi}(t_i)$ between times t_i and t_{i+1} is associated with a change in the head position, we get from Eq. (1)

$$\Delta\boldsymbol{\phi}(t_i) = \Delta\boldsymbol{\phi}_{\mathrm{in}}^{\mathrm{d}}(t_i) + \Delta\mathbf{S}_{\mathrm{in}}(t_i)\mathbf{x}_{\mathrm{DC}} + \mathbf{S}_{\mathrm{out}}\Delta\mathbf{x}_{\mathrm{out}}(t_i) \tag{2}$$

where $\Delta\boldsymbol{\phi}_{\mathrm{in}}^{\mathrm{d}}(t_i) = \mathbf{S}_{\mathrm{in}}(t_{i+1})\mathbf{x}_{\mathrm{in}}(t_{i+1}) - \mathbf{S}_{\mathrm{in}}(t_i)\mathbf{x}_{\mathrm{in}}(t_i)$ is the signal change due to the dynamic brain signals, $\Delta\mathbf{S}_{\mathrm{in}}(t_i) = \mathbf{S}_{\mathrm{in}}(t_{i+1}) - \mathbf{S}_{\mathrm{in}}(t_i)$ is the change in the biomagnetic subspace caused by the head movement, $\mathbf{x}_{\mathrm{DC}}$ contains the harmonic amplitudes of the biomagnetic DC currents, and $\Delta\mathbf{x}_{\mathrm{out}}(t_i) = \mathbf{x}_{\mathrm{out}}(t_{i+1}) - \mathbf{x}_{\mathrm{out}}(t_i)$. Because the head movements and dynamic brain signals are statistically independent, the expectation value of the signal changes due to Eq. (2) is

$$\mathrm{E}(\Delta\boldsymbol{\phi}) = \mathrm{E}(\Delta\mathbf{S}_{\mathrm{in}})\left[\mathbf{x}_{\mathrm{DC}} + \mathrm{E}(\mathbf{x}_{\mathrm{in}})\right] + \mathbf{S}_{\mathrm{out}}\mathrm{E}(\Delta\mathbf{x}_{\mathrm{out}}) = \begin{bmatrix} \mathrm{E}(\Delta\mathbf{S}_{\mathrm{in}}) & \mathbf{S}_{\mathrm{out}} \end{bmatrix} \begin{bmatrix} \mathbf{x}_{\mathrm{DC}} + \mathrm{E}(\mathbf{x}_{\mathrm{in}}) \\ \mathrm{E}(\Delta\mathbf{x}_{\mathrm{out}}) \end{bmatrix} = \mathbf{Y}\mathbf{d}\,. \tag{3}$$

Eq. (3) models the contribution of the brain signals and the external interference, and therefore the estimate for the DC component is not distorted by the interference. The least squares solution for $\mathbf{d}$ is

$$\hat{\mathbf{d}} = \mathbf{Y}^{\dagger} \mathrm{E}(\Delta\boldsymbol{\phi}) , \tag{4}$$

where $\mathbf{Y}^{\dagger}$ is the pseudoinverse of $\mathbf{Y}$.

The estimate $\hat{\mathbf{d}}$ contains the estimate $\hat{\mathbf{x}}_{\mathrm{DC}} + \mathrm{E}(\hat{\mathbf{x}}_{\mathrm{in}})$. However, the dynamic brain signals are generally uncorrelated with the averaged signal differences leading to $\mathrm{E}(\mathbf{x}_{\mathrm{in}}) \approx \mathbf{0}$. Consequently, we get an estimate for the true DC component produced by the brain and the DC field can be reconstructed as

$$\hat{\boldsymbol{\phi}}_{\mathrm{DC}} = \mathbf{S}_{\mathrm{in},0}\, \hat{\mathbf{x}}_{\mathrm{DC}} , \tag{5}$$

where $\mathbf{S}_{\mathrm{in},\,0}$ is the basis for the biomagnetic signals corresponding to the chosen reference head position.

RESULTS

To verify the method, we recorded MEG signals from a continuously moving phantom head with an artificial current dipole activated with DC current. The measurement was carried out using the 306-channel Elekta Neuromag® device in the genuine DC mode. Continuous head position monitoring was used to determine the head positions every 167 milliseconds, the DC component was estimated and the reconstructed signal was calculated according to Eqs. (4) and (5), respectively. The reconstructed signal vector was calculated by aligning the coordinate systems of the head and device and the current dipole was fitted to the reconstructed data by using a single dipole fit.

The DC component was estimated from the first 2.5 seconds of raw data providing 15 averages and including head movements of about 2 cm. To get an idea of the movement induced signals, the left side of figure 1 shows the magnetometer waveforms from the first 24 seconds of raw data. The external interference has been suppressed from these signals by SSS and thus the waveforms are produced solely by movement modulation of the DC signal. The amplitude of the removed external interference signals was roughly of the same order as the amplitude of the DC signals shown.

The right side of figure 1 shows the field distribution of the reconstructed DC field. The field is clearly dipolar and a single dipole fit gives a localization accuracy of 2 mm as compared to the known geometry of the phantom.

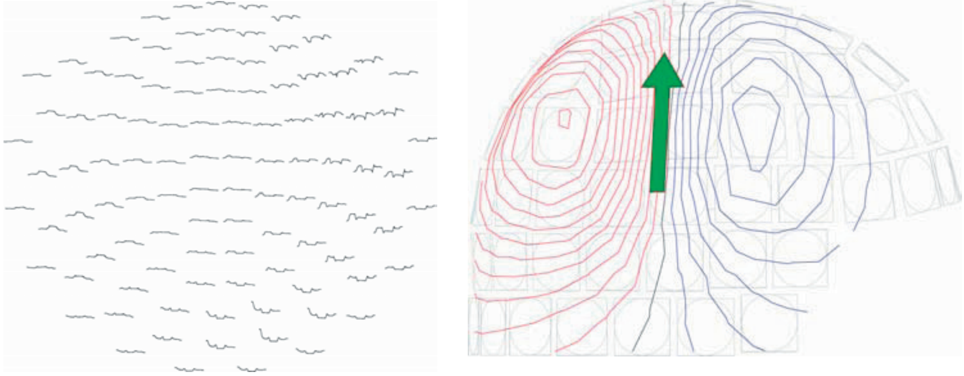

Figure 1.

Left: waveforms of the magnetometer channels caused by moving a phantom with DC dipole in the helmet. The peak-to-peak scale is 0.12 nT. Right: the reconstructed field distribution from the DC dipole. The contour step of the figure is 10000 fT.

DISCUSSION

The proposed method of using SSS based movement compensation and external interference suppression allows measurements of DC fields using voluntary and unrestricted head movements. The method is simple and robust. The recording is done as easily as any MEG measurement without any extra instrumentation. A good signal-to-noise ratio is obtained because the relatively high external interference typical for low frequencies is automatically suppressed by the SSS algorithm.

With this technique the movement artifacts produced by magnetic impurities can be removed also. This comes about by a simple baseline correction done after the SSS based movement correction. This boosts the clinical application of MEG for patients having post-operational magnetic residue or components in their head.

The method is particularly apt for magnetoencephalographic recordings where voluntary movement of the head inside the helmet is easy. In the magnetocardiographic application the method can be used as well if a continuous torso position indicator system is available. In this case some kind of mechanical device for moving the torso would be necessary to make the measurement reasonably comfortable for the subject and to avoid strong muscle artefacts.

REFERENCES

Mackert B-M, Wuebbeler G, Burghoff M, Marx P, Trahms L, Curio G, Non-invasive long-term recordings of cortical 'direct current' (DC-) activity in humans using magnetoencephalography, Neurosci. Lett. 1999; 273: 159-162.

Taulu S, Simola J, Kajola M, Clinical applications of the signal space separation method. ISBET2004. Proceedings of the 15th Congress of the International Society for Brain Electromagnetic Topography; 2004 Apr 11-14; Tokyo, Japan. Amsterdam: Elsevier; 2004(a).

Taulu S, Kajola M, Simola J, Suppression of Interference and Artifacts by the Signal Space Separation Method, Brain Topography 2004(b); 16, in press.

Uutela K, Taulu S, Hämäläinen M, Detecting and correcting for head movements in neuromagnetic measurements, NeuroImage 2001; 14: 1424-1431.

Weiskopf N, Braun C, Mathiak K, MEG-recordings of DC fields using a 151-channel whole-head device, In: Nenonen J, Ilmoniemi R, Katila T, editors. Biomag2000. Proceedings of the 12th International Conference on Biomagnetism; 2000 Aug 13-17; Espoo, Finland. Helsinki University of Technology; 2001. p. 500-3.

Software Magnetic Shield by Signal Space Separation (SSS)

Taulu, S., Simola, J., Kajola, M., Nenonen, J.

Elekta Neuromag Oy, Helsinki, Finland

ABSTRACT

Conventional interference reduction in biomagnetism includes e.g. magnetically shielded rooms, gradiometers, reference channels and software methods like the Signal Space Projection (SSP). The hardware methods are not very effective in compensation for interference from sources inside the room near the MEG device. SSP or other adaptive methods based on statistics can compensate for any reasonably low dimensional interference pattern but they require updating the disturbance subspace for new nearby sources of strong interference. Therefore, extreme magnetic hygiene is required in traditional MEG measurements. Stimulators producing magnetic fields are prohibited and persons inside the shielded room are carefully demagnetized and asked to avoid moving during the measurement. SSS relaxes these requirements thus improving clinical applicability of MEG. The method allows the use of conventional medical equipment and moderately magnetic assisting personnel inside the room. Because SSS is entirely based on the physics of the magnetic fields and the geometry of the sensor configuration, the ultimate achievable shielding factor is roughly inversely proportional to the calibration accuracy of the sensors. An accuracy well below 1% regarding the sensitivity, balance, and cross talk is required for SSS to perform properly.

KEY WORDS

Biomagnetism, multichannel measurements, interference suppression

INTRODUCTION

The basic problem of biomagnetic measurements is the weakness of the interesting signals as compared to the external interference signals. Therefore, magnetoencephalography (MEG) and magnetocardiography (MCG) measurements practically always require some kind of compensation for the interference arising from environmental or subject-related sources.

Commonly used hardware based compensation methods include magnetically shielded rooms and gradiometer pick-up coils. The shielded room does not shield against interference sources located inside the room. Also the gradiometers are insensitive to spatially homogeneous fields only, which limits the shielding performance against sources near-by. Further interference suppression can be obtained using software compensation, such as the Signal Space Projection method (SSP) [Uusitalo, 1997] or extrapolation based on reference channels [Vrba, 2001], but these methods always require information about the statistics or spatial complexity of the fields.

Because of these limitations of the traditional interference suppression methods, extreme magnetic hygiene is required in biomagnetic measurements. This severely limits the clinical applicability of MEG and MCG as obtaining reliable data requires that stimulators and other electric equipment are non-magnetic and that the subject and the personnel operating inside the shielded room are carefully demagnetized. In addition, the personnel in the room are not allowed to move and the subject must stay still during the measurement.

The Signal Space Separation method (SSS) [Taulu, 2004] relaxes these requirements and therefore considerably facilitates MEG and MCG measurements. Using minimal assumptions, SSS separates the signals arising from inside of the sensor array from signals arising from outside of the array. However, as the method is based only on the physics and geometry of the fields and the sensor array, it is sensitive to the accuracy of the calibration of the measurement device, in contrast to SSP, for example. In order to suppress the interference caused by nearby sources, a high dimensional SSS basis must be used, which increases the noise sensitivity of the basis. Therefore, accurate calibration and proper sensor configuration is necessary for optimal operation of SSS. On the other hand, related to its sensitivity to calibration, SSS can be used as a precise calibration method: deviations of the measured signals from the SSS model are due to calibration errors and can be used for correcting the calibration parameters.

This paper demonstrates the software shielding effect provided by SSS and the effect of the calibration accuracy on the achievable shielding factor. It will also be shown how the dimension of the SSS basis affects the software shielding.

METHODS

The SSS method is based on the idea that with modern multichannel devices sampling the magnetic field in hundreds of distinct locations, any signal vector of magnetic origin can be expressed with a fundamental linear model having a smaller number of basis vectors than number of channels. In addition, based on classical electromagnetic theory, the SSS basis can be divided into two separate subspaces: one for the signals arising from inside of the sensor array and the other for the external interference signals. Thus, any multichannel signal vector can be uniquely decomposed into the SSS basis, and the external interference can be elegantly suppressed by reconstructing the biomagnetic signals from the estimated components of the internal basis only.

In practice, the SSS basis can be constructed using expansions of e.g. spherical harmonic functions with increasing content of spatial fine detail, one expansion diverging at the origin and another diverging at infinity. The former expansion describes the biomagnetic signals, having their sources inside the helmet, and its extent is determined by the order L_{in} chosen for this expansion, whereas the latter expansion contains the interference signals from external sources and has an extent defined by the order L_{out}. The origin of the expansions can be set anywhere inside of the biomagnetic volume conductor and an L_{in} high enough to include the details of even the most superficial sources must be used. Similarly, a high enough L_{out} has to be chosen to explain the signals of even the closest external interference sources, such as the heart of a newborn baby, for example. The dimension of the entire SSS basis is given by $n = (L_{\text{in}} + 1)^2 + (L_{\text{out}} + 1)^2 - 2$.

Increasing the dimension n refines the reconstruction but also increases the sensitivity of the SSS reconstruction to calibration errors. On the other hand, this sensitivity is also affected by the geometry of the sensor array. This is described by the ratio of the largest and smallest singular values of the SSS basis matrix, also called the condition number, k. The reconstruction error due to measurement errors and perturbations of the SSS basis matrix is proportional to k when numerical regularization is not used.

The achievable level of software shielding is studied by simulating a source moving continuously from the interior to the exterior of the sensor array. The corresponding signal vector is decomposed in the SSS basis without numerical regularization and the signal corresponding to the internal sources is reconstructed. The shielding factor is defined as the ratio of the norms of the actual signal vector and the reconstructed signal vector. Ideally, this factor would be 1 when $r_{\text{source}} < r_{\min}$ and infinite when $r_{\text{source}} > r_{\max}$. Here r_{source} is the distance of the source from the origin and $r_{\min}$ and $r_{\max}$ are the distances from the origin of the closest and most distant sensor, respectively.

The accuracy of the SSS reconstruction is not sensitive to the number of sources nor to the spatial behavior of the current source at a specific distance. Consequently, it is enough to simulate a single source, e.g. a magnetic dipole.

RESULTS

Figure 1 shows the shielding factor of the SSS reconstruction with three different calibration accuracies for the case $L_{\text{in}} = 8$, $L_{\text{out}} = 4$. For simplicity, random calibration errors were only produced for the scalar calibration coefficients of all channels and to the balance of the gradiometer channels. The sensor array used in the simulation was the 306-channel Elekta Neuromag® MEG device including 204 planar gradiometers and 102 magnetometers. The imbalance signal was modeled as the signal of a point magnetometer located at the center between the gradiometer loops and with a normal in the plane of the gradiometer. The source was a magnetic dipole with dipole moment pointing to direction [1 1 1] moving along the negative z-axis of the device coordinate system from 0 to -3 m and the center of the harmonic expansions was at the origin of the device coordinate system. In this case, $r_{\min} = 0.1063$ m and $r_{\max} = 0.1457$ m. It is seen that when using SSS, a "software shielding wall" starts to develop when r_{source} exceeds $r_{\min}$. When the interference source moves further away through this wall, the shielding factor grows monotonously toward an asymptotic value limited by the calibration accuracy. A calibration accuracy of 0.1% gives an asymptotic shielding factor of over 150 while this factor with calibration accuracy of 1% is about 15 only.

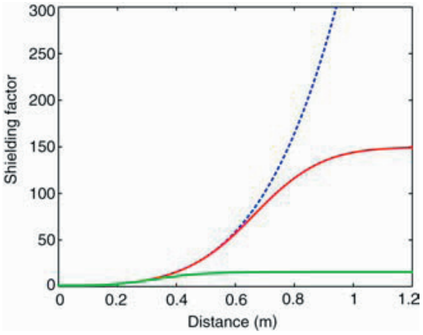

Figure 1. The SSS shielding factor as a function of distance of the source from the origin with three calibration accuracies: upper (dashed) curve: perfect accuracy, middle curve: accuracy of 0.1 %, and the lowermost curve: accuracy of 1 %.

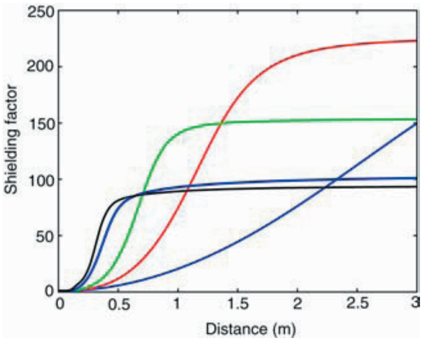

Figure 2 demonstrates how the width of the software shielding wall is affected by the value of L_{out} when $L_{\text{in}} = 8$ and the calibration accuracy is 0.1 %. The asymptotic value of the shielding factor is higher for lower values of L_{out} but a thinner shielding wall is achieved by increasing L_{out}. The latter is desirable for interference sources located very close to the sensor array. From Fig. 2 one can actually determine which value of L_{out} is optimal for an interference source at a given distance. For example, in the range $0.7 \text{ m} < r_{\text{source}} < 1.3$ m, $L_{\text{out}} = 4$ would be optimal.

Figure 2. The SSS shielding factor as a function of distance of the source from the origin with five different values of L_{out} with $L_{\text{in}} = 8$. The L_{out} values for curves from left to right are 6, 5, 4, 3, and 2.

The effect of the SSS-operation on the noise depends crucially on the geometry of the sensor array as described by the condition number of the SSS basis. In the worst case the increase of noise is proportional to the condition number k. These numbers for three different whole head MEG devices, 306 channel (Elekta Neuromag® triple sensors), 275 channel (5 cm base axial gradiometers), and 248 channel (magnetometers) relate to each other as 1:1.26:1.37, when $L_{\text{in}} = 8$, $L_{\text{out}} = 4$ are used. For these parameter values there is on the average no increase in the noise for the 306 channel system. The better condition number of the 306 channel device stems from the intrinsic differentiation between near-by and far-away sources achieved by the triple sensor comprising of both short base-length gradiometers and magnetometers. The lower condition numbers also explains the high bit/sample rate of the Elekta Neuromag®, as reported in [Nenonen, 2004].

The asymptotic shielding factors also depend on the condition number because the reconstruction error is proportional to k.

DISCUSSION

The software magnetic shielding provided by the SSS-method contributes to clinical applicability of MEG. Normal working practices and stimulators of a neurological clinic can be applied without extra attention and training of the personnel regarding sources of magnetic interference. A high precision multichannel MEG device calibrated to a relative accuracy of about 0.1 % or better is a necessary prerequisite for efficient magnetic shielding based on SSS.

REFERENCES

Nenonen J, Kajola M, Simola J, Ahonen A, Total Information of Multichannel MEG Sensor Arrays. This volume.

Taulu S, Kajola M, Simola J, Suppression of Interference and Artifacts by the Signal Space Separation Method, Brain Topography 2004; 16: in press.

Uusitalo MA, Ilmoniemi RJ, Signal-space projection method for separating MEG or EEG into components, Med. Biol. Eng. Comput. 1997; 32: 35-42.

Vrba J, Robinson SE, Signal Processing in Magnetoencephalography, Methods 2001; 25: 249-271.

Model selection in spatio-temporal electromagnetic source analysis

Lourens J. Waldorp[1], Hilde M. Huizenga[1], Arye Nehorai[2], Raoul P.P.P. Grasman[1], and Peter C.M. Molenaar[1]

1: Department of Psychology, University of Amsterdam, The Netherlands
2: Department of Electrical and Computing Engineering, University of Illinois at Chicago, USA

ABSTRACT

Estimating the source parameters from spatio-temporal electro- or magneto-encephalogram (EEG or MEG), requires an estimate of the number of sources. Several methods (model selection procedures, MSPs) to determine the number of sources in EEG and MEG have previously been investigated for instantaneous data. These methods are extended to a spatio-temporal analysis. It is seen that the residual variance (RV) tends to overestimate the number of sources. The Akaike information criterion (AIC) and the Wald test on amplitudes (WA) and the Wald test on locations (WL) have the highest probabilities of selecting the correct number of sources.

KEY WORDS

Equivalent current dipole, goodness-of-fit, fitness measure, inverse problem, human brain data, testing source parameters.

INTRODUCTION

When using relatively few sources (dipoles) to describe the measured electro- or megneto-encphalogram (EEG or MEG), an estimate of the number of sources is required [de Munck, 1990]. Model selection procedures (MSPs) give such an estimate. An example of an MSP is the well-known residual variance (RV). Previously, the RV was compared to several alternatives in [Waldorp et al., 2002] for instantaneous data. The RV appeared to over-fit, that is, it selected too many sources. Alternatives like the Wald test on source amplitudes or locations (WA and WL), or the Akaike and Bayesian information criterion (AIC and BIC) were seen to be better. Not only did they have high probabilities of selecting the correct number of sources, but they were also reasonably robust against colored noise (i.e. correlations and unequal variances on sensor noise).

Here, these methods are extended to spatio-temporal data. In a simulation the RV, AIC, BIC, WA, and WL are compared as a function of distance between two modeled sources. To realistically generate sensor noise, it is simulated as colored. As it is difficult to obtain an estimate of the noise covariance matrix in spatio-temporal data [Huizenga et al., 2002], [de Munck et al., 2002], a parametric bootstrap procedure was used for the noise covariance matrix in the simulations [Waldorp et al., 2004].

METHODS

The MEG data from m sensors and t samples are collected for each independent trial $j = 1, \dots, n$ in the $m \times t$ matrix $\mathbf{Y}_j = (\mathbf{y}_{1j}, \dots, \mathbf{y}_{tj})$, with $\mathbf{y}_{ij} = (y_{1ij}, \dots, y_{mij})'$. Denote the average over trials by $\bar{\mathbf{Y}} = \frac{1}{n}\sum_{j=1}^{n} \mathbf{Y}_j$. It is assumed that both the location and orientation of the d dipolar sources are fixed over time (samples), and only the amplitudes are allowed to vary over samples [de Munck, 1990], [Huizenga et al., 2002]. The model for the averaged data is then $\bar{\mathbf{Y}} = \mathbf{GA} + \mathbf{E}$. The $m \times d$ matrix $\mathbf{G}$ contains the sensor gains of d sources with unit amplitudes. The matrix $\mathbf{G}$ depends on the location and orientation parameters of the dipolar sources. The $d \times t$ matrix $\mathbf{A}$ contains the time varying amplitudes of d sources, and the $m \times t$ matrix $\mathbf{E}$ is the residual. The residual consists of pure error (e.g., spontaneous EEG or MEG) and modeling error (e.g., due to an incorrect number of sources). The number of parameters in MEG for d sources and t samples is $p = 5d + td$, and the parameters are collected in the vector $\boldsymbol{\theta}$. The pure error is colored (i.e. correlated and heteroscedastic), and the covariance is assumed to be structured as $\frac{1}{n}(\boldsymbol{\Upsilon} \otimes \boldsymbol{\Sigma})$, where $\boldsymbol{\Upsilon}$ is the temporal correlation and $\boldsymbol{\Sigma}$ the spatial covariance matrix, and $\otimes$ denotes the Kronecker product [Huizenga et al., 2002] (see [Waldorp et al., 2004] for more details). The source parameters are estimated by (estimated) generalized least squares (GLS). Assume that an estimate of the covariance parameters is available (see e.g. [Waldorp et al., 2001]), and denote the ensuing temporal and spatial matrices respectively by $\mathbf{U} = \boldsymbol{\Upsilon}(\hat{\beta})$ and $s^2\mathbf{V} = \mathbf{S} = \boldsymbol{\Sigma}(\hat{\boldsymbol{\omega}})$, with s^2 the average of the diagonal of $\mathbf{S}$ [Waldorp et al., 2002]. A GLS estimate $\hat{\boldsymbol{\theta}}$ minimizes $\tilde{r}^2(\boldsymbol{\theta}) = \mathrm{tr}[\mathbf{V}^{-1}(\bar{\mathbf{Y}} - \mathbf{GA})\mathbf{U}^{-1}(\bar{\mathbf{Y}} - \mathbf{GA})']$, where $\mathrm{tr}[\cdot]$ denotes the trace. At the minimum $\tilde{s}^2(\hat{\boldsymbol{\theta}}) = \tilde{r}^2(\hat{\boldsymbol{\theta}})/(mt - p)$ is an estimate of the residual variance.

Model selection procedures. The RV compares the squared residuals to the squared data for all sensors and samples simultaneously. The RV decreases as a function of the number of parameters, and will therefore over-fit easily. The RV is defined as

$$\mathrm{RV} = 100\mathrm{tr}[\mathbf{V}^{-1}(\bar{\mathbf{Y}} - \mathbf{GA})\mathbf{U}^{-1}(\bar{\mathbf{Y}} - \mathbf{GA})'](\mathrm{tr}[\mathbf{V}^{-1}\bar{\mathbf{Y}}\mathbf{U}^{-1}\bar{\mathbf{Y}}])^{-1}. \tag{1}$$

A model is said to fit if the RV is below 5%, say [Scherg, 1992].

The AIC penalizes the log-likelihood function for additional parameters (i.c. source parameters) that are required to describe the data [Akaike, 1973]. In doing so, the number of sources should be limited since additional sources will at one point hardly decrease the log-likelihood function but increase the penalty. The AIC is defined as

$$\mathrm{AIC} = nmt\ln(\pi n^{-1}s^2) + n^{-1}s^{-2}\mathrm{tr}[\mathbf{V}^{-1}(\bar{\mathbf{Y}} - \mathbf{GA})\mathbf{U}^{-1}(\bar{\mathbf{Y}} - \mathbf{GA})'] + 2p, \tag{2}$$

where the log-likelihood function has been multiplied by -2. The model with the smallest AIC value is selected.

The BIC penalizes the log-likelihood function for additional parameters more severely than the AIC [Chow, 1981]. Consequently the BIC is more conservative than the AIC and should lead to less over-fitting. The BIC is defined as the AIC only with the penalty $2p$ replaced by $p\ln(mt)$, where $\ln(\cdot)$ denotes the natural logarithm. The model with the smallest BIC value is selected.

The Wald test gives the opportunity to test a hypothesis on a specific subset of the parameters [Huizenga et al., 2002]. Let $\mathbf{r}$ be a q vector function of the source parameters (i.c. amplitudes or locations), $\mathbf{r}_h$ the q vector of hypothesized value of $\mathbf{r}$, $\mathbf{R}$ the $q \times k$ Jacobian matrix of $\mathbf{r}$ with respect to k source parameters, and $\mathbf{C}$ the $k \times k$ covariance matrix of a subset of source parameters (amplitudes or locations). Then the Wald test is defined as

$$\mathrm{W} = \tfrac{1}{q}(\mathbf{r} - \mathbf{r}_h)'(\mathbf{RC}^{-1}\mathbf{R}')^{-1}(\mathbf{r} - \mathbf{r}_h). \tag{3}$$

If the hypotheses are correct then W is approximately distributed as $F(q, mt - p)$ and is tested at significance level α. In the WA test a source is included if the following is true: the multivariate test is significant, the semi-univariate tests are significant for all sources, and the univariate tests are significant at least at one sample for all sources [Waldorp et al., 2004]. In the WL test a source is included if the following is true: the multivariate test is significant, and the semi-univariate tests are significant for all sources.

Simulation. Similar to the simulations in [Waldorp et al., 2002], MEG data are generated by two sources with increasing distance. The signal on 61 sensors is generated by two dipoles inside a unit sphere. Both sources are in the midcoronal plane (crossing both ears and the vertex) with a varying angle $5^\circ - 20^\circ$, with steps of 5°, between the location vectors. Both sources are at eccentricity 0.80 in the unit sphere. The orientation of both dipoles is toward the nose and completely tangential. The amplitude functions for both dipoles for 50 samples are constructed from two positively censored sinus waves. The absolute temporal correlation between the sources is 0.31. Normally distributed colored pure error is added to the signal at each sensor for 300 trials. The pure error standard deviation for the mean (over trials) is set at 10% of the maximal signal (without error) from the 61 sensors and 50 samples when the angle between the dipoles is 12.5°. A total of 300 simulations is generated. The pure error covariance matrices $\mathbf{U}$ and $\mathbf{V}$ are obtained from a parametric bootstrap procedure (see [Waldorp et al., 2004] for details).

RESULTS

To evaluate the MSPs three types of decision are considered: correct (two sources), under-fit (one source), and over-fit (three sources). A desirable pattern is then that when the sources are close the decision of one source has high probability and when they are more distant, the decision of two sources has high probability. In Fig. 1 the probabilities of the decisions of the MSPs are shown. The RV tends to over-fit. The BIC is seen to under-fit. The WL shows the best overall performance. The AIC and WA showed good performance in the sense that the probability of selecting one source was high when the true sources were close, and the probability of selecting two sources was high when the true sources were more distant.

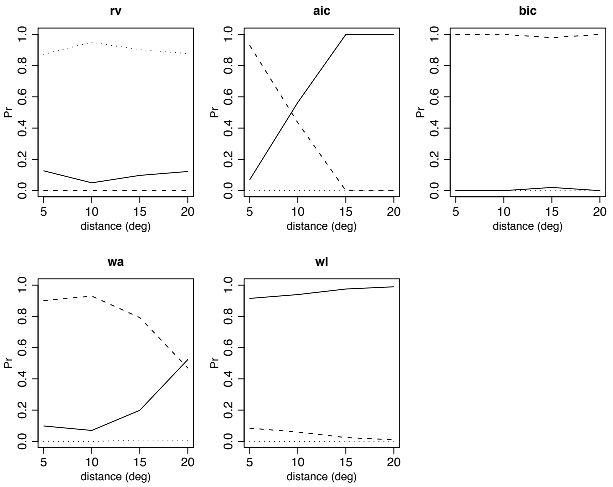

Figure 1: The probabilities of correct and incorrect decisions as a function of the distance between the two true sources (in degrees). Solid line: correct (two sources), dashed line: under-fit (one source), dotted line: over-fit (three sources).

DISCUSSION

It could be argued that the over-fitting of the RV was caused by using a threshold value which was too low. However, there is no clear procedure how to set the threshold in the RV, and more importantly, how this threshold depends on the data (see [Waldorp et al., 2002]). The RV as defined in this paper shows the results of using a commonly used threshold.

The BIC tended to under-fit due to the large penalty in spatio-temporal analysis and the estimation of the spatio-temporal pure error covariance matrix [Waldorp et al., 2004].

The better performance of the WL in spatio-temporal analysis than in instantaneous analysis can be explained by the higher precision of the location parameters due to the additional information from the samples (see [Huizenga et al., 2002]). Accordingly, the null hypothesis that the locations were the same was more easily rejected when two sources were tested.

ACKNOWLEDGEMENTS

The Netherlands Organization for Scientific Research (NWO) is gratefully acknowledged for funding this project. This research was conducted while L.J. Waldorp (527-25-013), R.P.P.P. Grasman (527-25-014) were supported by a grant of the NWO foundation for Behavioral and Educational Sciences of this organization awarded to H.M. Huizenga, P.C.M. Molenaar, J.C. de Munck, and J.L. Kenemans. The research has also been made possible by a KNAW fellowship to H.M. Huizenga.

REFERENCES

Akaike, H. (1973). Information and an extension of the maximum likelihood principle. In B. Petrov & F. Csáki (Eds.), *Proceedings of the second international symposium on information theory. Supplement to problems of control and information theory* (pp. 267–281). Budapest: Akademiai Kiado.

Chow, G. (1981). A comparison of information and posterior probability criteria for model selection. *Journal of Econometrics*, *16*, 21–33.

de Munck, J.C. (1990). The estimation of time varying dipoles on the basis of evoked potentials. *Electroencephalography and Clinical Neurophysiology*, *77*, 156–160.

de Munck, J.C., Huizenga, H.M., Waldorp, L.J., & Heethaar, R. (2002). Estimating stationary dipoles from MEG/EEG data contaminated with spatially and temporally correlated background noise. *IEEE Transactions on Signal Processing*, *50*, 1565–1572.

Huizenga, H.M., Heslenfeld, D., & Molenaar, P.C.M. (2002). Optimal measurement conditions for spatiotemporal EEG/MEG source analysis. *Psychometrika*, *67*, 299–313.

Huizenga, H.M., de Munck, J.C., Waldorp, L.J., & Grasman, R.P.P.P. (2002). Spatiotemporal EEG/MEG source analysis based on a parametric noise covariance model. *IEEE Transactions on Biomedical Engineering*, *49*, 533–539.

Scherg, M. (1992). Functional imaging and localization of electromagnetic brain activity. *Brain Topography*, *5*, 103–111.

Waldorp, L.J., Huizenga, H.M., Dolan, C.V., & Molenaar, P.C.M. (2001). Estimated generalized least squares electromagnetic source analysis based on a parametric noise covariance model. *IEEE Transactions on Biomedical Engineering*, *48*, 737–741.

Waldorp, L.J., Huizenga, H.M., Grasman, R.P.P.P., Böcker, K.B.E., de Munck, J.C., & Molenaar, P.C.M. (2002). Model selection in electromagnetic source analysis with an application to VEFs. *IEEE Transactions on Biomedical Engineering*, *49*, 1121–1129.

Waldorp, L.J., Huizenga, H.M., Nehorai, A., Grasman, R.P.P.P., & Molenaar, P.C.M. (2004). Model selection in spatio-temporal electromagnetic source analysis. *IEEE Transactions on Biomedical Engineering* in revision.

Time-Frequency and Coherence Analysis of fMEG Signals

X. Wu[a], Y. Chan[a,1], H. Preissl[b,c], H. Eswaran[c], J. D. Wilson[a], P. Murphy[c], C. L. Lowery[c]
[a]Univ. of Arkansas at Little Rock, Little Rock, USA; [b]MEG Center, Univ. of Tübingen, Germany;
[c]Univ. of Arkansas for Medical Sciences, Little Rock AR, USA

ABSTRACT

Fetal magnetoencephalographic (fMEG) measurements are performed with interference from the fetal and maternal magneto-cardiogram (MCG). Fetal movement, fetal breathing, fetal eye blinks or eye rollings and maternal muscle-contraction may generate detectable signals. These factors make the fMEG signals nonstationary, and can be called "interventions." "*Interventions*" can be manifested space and/or time. By examining temporal relationship of the multi-channel records, we are able to find the spatial signature of the "*interventions.*" The aim of this study is to examine nonstationarity in single channel and nonhomogeniety in multiple channels of the fMEG data. The preliminary results reported here may be used in further studies, leading toward intervention identification, and ultimately fetal state determination.

KEY WORDS

Fetal magnetoencephalography (fMEG), time-frequency analysis, coherence, nonstationarity, nonhomogeniety

INTRODUCTION

Fetal MEG is a passive and non-invasive technique of studying fetal brain and heart activity for the diagnoses of fetal normal and abnormal development [1]. The fMEG recordings are often nonstationary signals due to the interference of MCG, muscle contraction and fetus movement [5]. By doing time-frequency analysis, whether, when there is an "*intervention*" and which kind of "intervention" can be uncovered. In addition, checking nonhomogeniety in multiple channels can discover spatial "interventions," such as the position change of fetus or uterus. We apply the multiple-window (MW) time-frequency analysis (TFA) to fMEG signals, to extract the nonstationarity caused by MCG interventions. Then we construct a multiple-window time-frequency coherence-function to study the relationship between fMEG signals in different channels, with the ultimate goal of determining the spatial location of the MCG interventions.

METHODS

Time-frequency analysis reveals the temporal characteristics of a signal by its spectral components in the frequency domain. In this way, important features of the signal can be observed and analyzed in order to understand or model the physiological system. The conventional time-frequency methods include the spectrogram wavelet transform (WT), the Wigner–Ville distribution (WVD), and the reduced interference distribution (RID).

To estimate time-frequency distribution for a random process (particularly a nonstationary series), we must consider the bias/variance dilemma. Recently, several researchers have extended Thomson's multiple-window method (MWM) [3] to random nonstationary signals, resulting in a low bias and time-varying spectral estimator.

Thomson's Multiple Window Method

The periodogram is the classical spectral estimator for stationary signals. While it is asymptotically unbiased, it suffers from high variance. For short, time-limited signals, Thomson suggested using a bank of optimal bandpass filters (windows), instead of rectangular windows (as in the periodogram method). These filters compute several periodograms of the entire signal and then averaging the resulting periodograms to construct a spectral estimate. To obtain a low bias and low variance estimate, the windows must be orthogonal (to minimize variance) and optimally concentrated in frequency (to minimize bias). The optimal windows satisfying these requirements for signals with finite length are Slepian sequences or discrete prolate spheroidal sequences [4].

The procedure to compute the spectral estimate of $x(n), (n = 0, 1, \dots, N-1)$ using Thomson's MWM consists of the following steps:

(1) Specify N and W, where N is the number of data points, and W is a half bandwidth. The size of W is dependent upon the desired time-bandwidth NW (or frequency resolution).

(2) Choose optimal windows (or segmentation of the time series into k = 1, 2, 3, … , K) to compute the eigenvalues λ_k and γ_n^k . Here, the first $K = 2NW$ terms with the largest eigenvalues are needed. Let us take the first four Slepian sequences for the case of N = 512 and $NW = 4$. The Slepian sequences are the eigenvectors of the Toeplitz eigenvalue equation

$$\sum_{m=0}^{N-1} \frac{\sin 2\pi W(n-m)}{\pi(n-m)} \gamma_m^{(k)}(N,W) = \lambda(N,W)\, \gamma_n^k(N,W) \qquad (1)$$

where N is the length of the eigenvectors (or data), and W defines a small, local frequency band centered on frequency f, with frequencies $f' : |f - f'| \le W$. Figure 1 shows the first four Slepian sequences.

(3) Apply γ_k to the entire series of N data points $x(n)$ and take the discrete Fourier transform

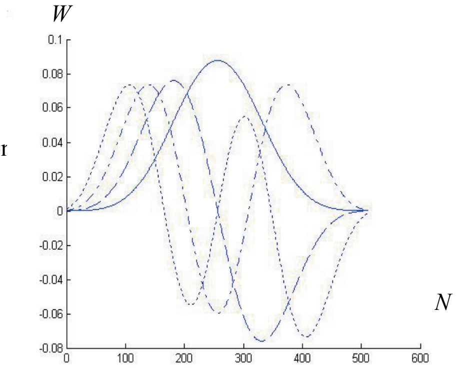

Figure 1: Slepian sequences
(Zero-order: solid line; first order: dashed line; second order: dash-dotted line; third order: dotted line)

---

[1] Correspondent can be reached at Department of Systems Engineering, University of Arkansas at Little Rock, 2801 South University, Little Rock, AR 72204-1099, Tel. 501-569-8926; Fax 501-569-8698; E-mail: yxchan@ualr.edu

$$x_k(f)=\sum_{n=0}^{N-1} x(n)\,\gamma_n^k\, e^{-j2\pi fn} \qquad k=1,2,\ldots,K \tag{2}$$

where $x_k(f)$ is called the *k*th eigencoefficient and $\left|x_k(f)\right|^2$ the *k*th eigenspectrum.

(4) Average the *K* eigenspectra so obtained to get an estimate of the spectrum

$$\hat{S}(f)=\frac{1}{K}\sum_{k=0}^{K-1}\frac{1}{\lambda_k}\left|x_k(f)\right|^2 \tag{3}$$

Since the first few eigenvalues are very close to one, Eqn (3) can be simplified to

$$\hat{S}(f)=\frac{1}{K}\sum_{k=0}^{K-1}\left|x_k(f)\right|^2 \tag{4}$$

Coherence

The coherence function essentially gives a measure of the *similarity* between signals and is related to the cross-correlation function. More specifically, coherence is a measure of the linear dependence of one signal on another. The ordinary squared-coherence function between two wide-sense stationary random processes *x* and *y* is defined as:

$$\gamma_{xy}^2(\Omega):=\frac{\left|S_{xy}(\Omega)\right|^2}{S_{xx}(\Omega)\,S_{yy}(\Omega)} \tag{5}$$

It follows immediately from the properties of the PSD that the coherence function satisfies

$$0\le\gamma_{xy}^2(\Omega)\le 1 \tag{6}$$

Coherence can be obtained from one realization of the multi-channel data using Thomson's MWM. Given two time series $x(n)$ and $y(n),(n=0,1,\ldots,N-1)$, their eigencoefficients $x_k(f)$ and $y_k(f)$ can be obtained using Eqn (2). The estimated coherence is

$$\gamma_{xy}^2(f)=\frac{\left|\sum_{k=0}^{K-1}x_k(f)\,y_k^*(f)\right|^2}{\sum_{k=0}^{K-1}\left|x_k(f)\right|^2\ \sum_{k=0}^{K-1}\left|y_k(f)\right|^2} \tag{7}$$

where $K\le 2NW$ is the number of windows used and the asterisk denotes complex conjugation.

RESULTS

The MW-TFA and coherence methods [4] were used to process fMEG data recorded using the SARA instrument at the University of Arkansas for Medical Sciences [2]. One typical single-channel fMEG recording and its time-frequency (TF) distribution are shown in Figure 2, 3 and 4. Data were sampled at 312.5 Hz. The data consisted of 512 data points (as mentioned) over a 1.6 seconds duration, in which the main intervention is the fetal fMCG (the maternal MCG has been removed by bandpass filter). The vertical axis of Figure 2, shown in picoTesla (p), clearly depicts the fetal heartbeats. Both the spectrogram and MW-TFA were used in the analysis. The time-frequency distribution was obtained by sliding a 16 points window with a 1-point overlap between consecutive computations. The Hanning window was used for the spectrogram.

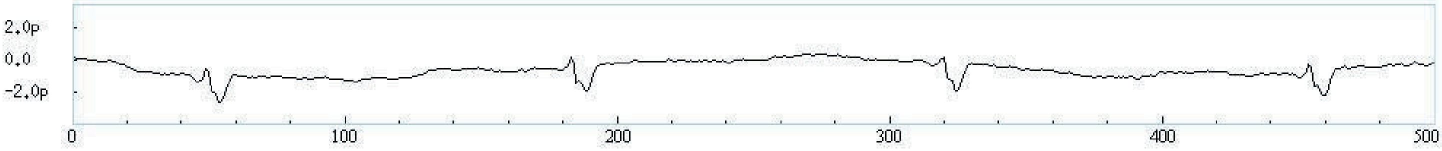

Figure 2: fMEG signal with MCG intervention

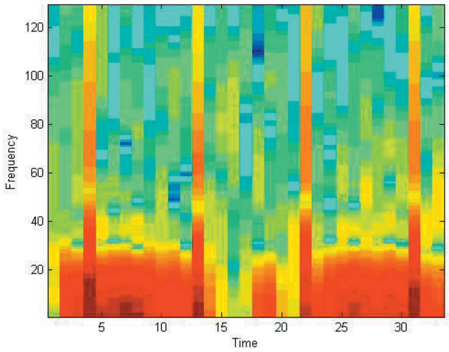

Figure 3: Spectrogram

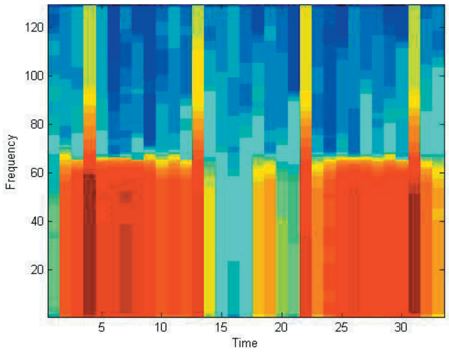

Figure 4: MW-TFA using Slepian sequences

The spectrogram (figure 3) and MW-TFA images (figure 4) show a time axis in 0.05-second increments. They show similar features of the fMEG signals, where the heartbeats are clearly identified as distinct frequency "columns." The colors represent the "power" of various frequencies. Deep red is the most intense, all the way down to blue, which is the least intense. However, the variance of MW-TFA representation is lower than that of spectrogram because of the averaging process in the MW-TFA. By looking at the MW-TFA image, we can easily observe the nonstationarity of the fMEG signal and decide whether there is an intervention. If so, when does the intervention occur (and what type of intervention)? These are very useful information in fetal status monitoring and infant-delivery prediction.

To determine the position of the intervention, TF coherence was used to examine the nonhomogeniety in multiple channels. Since the coherence measures the *similarity* between two signals, we can easily find the nonhomogeniety by computing coherences between a target sensor and its neighbours (Figure 5). Those sensors near to the intervention source (fetal heart) will obviously have low coherence with their neighbors. Since the coherence represents the *similarity* in all the frequencies, we use the mean in all frequencies to calculate the *similarity* between two channels. By choosing those channels with low coherence, the approximate position of the intervention can be found. Figure 6 shows the coherence curves of two target channels: MCK0 and MLG3. We can see that the channel with sharp drop-off in coherence—MLG3—is closer to the fetal heart.

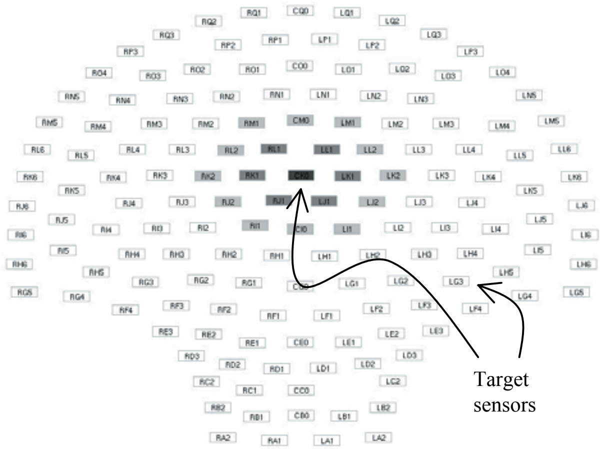

Figure 5: Target sensors and their neighbors
(Real target: black; 1st neighbors: light gray; 2nd neighbors: dark gray)

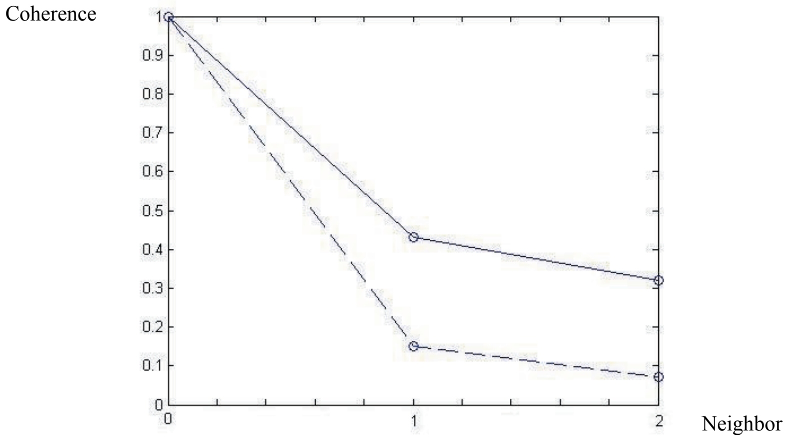

Figure 6: Coherence between target sensors and their neighbors
(MCK0: solid line, MLG3: dashed line)

CONCLUSION

We try to find interventions in fMEG signals by examining nonstationarity in single channel and nonhomogeniety in multiple channels. We apply the multiple-window time-frequency analysis to detect nonstationarity, and use coherence to measure nonhomogeniety. Preliminary results are promising, suggesting the method can identify and locate a point-source intervention such as the fetal heartbeat. The ultimate goal is to identify an unknown intervention and determinate its state. Interpreting the intervention "feature" and the associated "feature" with the fetal state are important and difficult tasks for future study. Among other techniques, spatial statistics may be a fruitful area of investigation.

ACKNOWLEDGMENT

The authors gratefully acknowledge the contributions of C. Bayrak, Q. Campbell, R. Draganova, M. Holst, J. Norton, P. Soni, and other SARA researchers toward this research. Obviously, the authors alone are responsible for the content of this paper. This work is supported the National Institutes of Health grant 1R01NS36277-03, USA.

REFERENCES

[1] T. Blum, E. Saling, and R. Bauer, "First magnetoencephalographic recordings of the brain activity of the human fetus," *British J. Obstet. Gynaecol*., 22, 1224-1229, 1985.

[2] S.E. Robinson, M.B. Burbank, A.A. Fife, G. Haid, P.R. Kubik, I. Sekachev, B. Taylor, M. Tillotson, J. Vrba, G. Wong, C. Lowery, H. Eswaran, D. Wilson, P. Murphy, and H. Preißl, "A Biomagnetic Instrument for Human Reproductive Assessment" *Biomag 2000, 12th International Conference on Biomagnetism*, Aug 13-17, 2000

[3] D.J. Thomson, "Spectrum estimation and harmonic analysis" *Proc. IEEE*, 1982

[4] Yan Xu, Simon Haykin, Ronald J. Racine, "Multiple Window Time-Frequency Distribution and Coherence of EEG Using Slepian Sequences and Hermite Functions" *Proc. IEEE*, 1999

[5] M. B. Priestley, "Nonlinear and Nonstationary Time Series Analysis" *Academic Press,* 1988

Influence of prandial state in intragastric distribution of a small volume evaluated by AC Biosusceptometry.

M. F. Américo[1], R. B. Oliveira[1], O. Baffa[1], L.A. Corá[2], F.C. Paixão[2], J.R.A. Miranda[2].
[1] Universidade de São Paulo – USP, São Paulo, Brazil [2] Universidade Estadual Paulista – UNESP, São Paulo, Brazil

Postprandial intragastric distribution of food (IDF) has a great importance in physiology and clinical studies, and currently evaluated by scintigraphy. Magnetic techniques like the Alternate Current Biosusceptometry (ACB) have been employed for studies of several parts of the gastrointestinal tract. The aim of this investigation was to evaluate the influence of prandial state in the IDF with small volume through the magnetic images obtained by ACB. Each volunteer had measurement of IDF performed on 2 separate days in different prandial state: one with the subject in fasting state and another in postprandial. In each occasion they ingested a meal test containing 60 ml of yogurt and 4g of ferrite. The multi-sensors ACB was positioned on the volunteers' abdomen and the magnetic signals were analyzed in MatLab, using Digital Image Processing. The IDF with small volume had preferential accumulation in the distal stomach for all the volunteers in fasting state. However, in the postprandial the meal test remained retained in the proximal stomach for a prolonged time before arriving at the distal stomach. These analyses were based on the interval of time to stabilization of meal test arrival curves; approximately 5,30±1,93 (mean±SD) min for the volunteers in fasting, while that in postprandial state presented 14,25±2,27 (mean±SD) min. New approach quantification was the generation of magnetic images to visualize the distribution process. The ACB also showed intense gastric activity contraction of 3 cycles/minute in the distal region. The image obtained by ACB has capability to evaluate the influence of the prandial state on the IDF with small volume in human. Our data showed that in fasting state the small meal test accumulated in the distal stomach. In summary, the ACB is a non-invasive, low cost and radiation-free technique, allowing physiological and pharmacological investigation with future clinical application. Financial Support: CAPES.

Surface-based representation of human intracranial EEG signals: electrode projection and volume conduction maps

Françoise Bauchet (1), Aurélie Bidet-Caulet (1), Catherine Fischer (2), Olivier Bertrand (1)
1-Mental Processes and Brain Activation Lab, INSERM U280, Lyon, France
2-Neurological Hospital, Lyon, France

Inflated or flattened surface-based representation of the cortex is increasingly used for the visualization of functionnal data obtained from fMRI or MEG/EEG studies. The interpretation of intracranial EEG (iEEG) data can also benefit from this approach which facilitates the visualization of cortical folds and allows group studies based on local anatomical normalization techniques. The methods presented here are more specifically dedicated to the study of the human auditory cortex explored by iEEG but could also be applied to other brain areas. They consist in:

a visualization method based on a precise 3D reconstruction of individual cortical surface and using an interactive time-varying representation of electrophysiological activity at intracranial electrode sites. This aims at providing a comprehensive spatio-temporal view of the underlying active network.

a method to project depth electrodes on flat cortical maps, allowing the coregistration of electrode locations of a group of patients on a standard auditory cortex anatomy built with a local landmark-based normalization scheme. This allows a more precise anatomo-functionnal clustering of electrode contacts.

plotting on a flat map, for each electrode location, the potentials generated at this site by dipoles located at each node of the cortical sheet. The goal here is to estimate a "cortical field of view" of each electrode contact weighted by the volume conduction effect. This facilitates the localization of local sources.

Magnetic Images of the Disintegration Process of Tablets by AC Biosusceptometry

L.A. Corá[1], F. G. Romeiro[1], M. F. Américo[2], O. Baffa[2], M. Stelzer[3], J.R.A. Miranda[1]
[1] Universidade Estadual Paulista – UNESP, São Paulo, Brazil [2] Universidade de São Paulo – USP, São Paulo, Brazil. [3]Universidade Federal de São Carlos – UFSC, São Paulo, Brazil

The oral administration is a common route in the therapy and the solid dosage forms are widely used. The drug release can occur in several human gastrointestinal tract (GIT) regions. Consequently, evaluate these formulations during the passage in the GIT contributes with information on its performance. The AC Biosusceptometry (ACB) was pioneering to characterize the behavior of magnetic tablets in the human GIT to obtain the disintegration process through magnetic recording. The aim of this work was to use a multi-sensors ACB to monitoring magnetic tablets in the human GIT and to characterize the disintegration process by magnetic images. This biomagnetic technique is based on signal recordings obtained from a high magnetic susceptibility material response by application of an alternated magnetic field in the biological milieu. Nine volunteers after an overnight fast swallowed a tablet obtained by direct compression from 1.0 g of ferrite mixed with 0.5 g of excipients and coated with Eudragit®. The multi-sensors ACB was positioned on the volunteers' abdomen and the magnetic signals were recording and analyzed in MatLab. The Disintegration Time (DT) of tablets in gastric region was 2.69 ± 0.66 (mean±SD) minutes and visualized by magnetic images. The Gastric Retention Time (GRT) was determined from the arrival of the enteric tablet in the volunteers' stomach until its output, and the values were 81.77 ± 50.71(mean±SD) minutes. The Small Intestinal Transit Time (SITT) obtained was 148.22 ± 26.10 (mean ± SD) minutes. The DT in colonic region was characterized by magnetic images, occurring 90 minutes after the tablets arrival. The images obtained by multi-sensors ACB showed accuracy in the monitoring of the tablets and to visualize the disintegration in the GIT. Moreover, ACB is non-invasive, radiation-free and harmless with applicability in the pharmaceutical investigations.

Financial Support: FAPESP.

Application of selective averaging by single trial cross-correlation for the robust extraction of transient evoked magnetic fields

P. Ferrari, M. Sussman, T.P.L. Roberts
University of Toronto-University Health Network, Toronto Canada

Single Trial (ST) evoked response data tend to display extreme variability. In so much as this variability can be attributed to random noise, the conventional application of averaging over many (+100) trials per stimulus condition is warranted. However, it can be readily observed that systematic (phase and latency) variation also contributes to the heterogeneity of ST data. Furthermore, neural activity of underlying distributed parallel systems is also implicated as a factor of ST heterogeneity [1]. Averaging across such variability may convolve multiple distinct processes and blur transient peaks. By a method of averaging trials selected on the basis of cross correlation of the time series data, we show that in a majority of cases a more robust waveform with improved signal amplitude representing the transient components may be extracted by averaging fewer (~20) but highly correlated trials, around a temporal window encompassing the transient component of interest. For the present investigation we show experimental data from neuromagnetic evoked responses to monaurally presented 1000Hz tones. In a best case scenario, this method has, in addition to improving signal to noise in the transient M100 peak, elucidated the existence of earlier M50 and later M200 components that were undetectable after many averages. The results are presented with considerations for applications and method optimization.

[1] Liu L, Ioannides AA. Brain Topogr. 1996; 8(4):385-96.

Synchronization Tomography: model calculations of spatial resolution and noise tolerance; optimization of source localization

T. Fieseler[1], J. Dammers[1], P.A. Tass[1,2]
[1]Institute of Medicine, Research Center Jülich, Jülich, Germany
[2]Department of Stereotactic and Functional Neurosurgery, University of Cologne, Cologne, Germany

Phase synchronization plays an important role both under physiological and pathological conditions. With standard averaging techniques of MEG data, it is difficult to reliably detect cortico-cortical and cortico-muscular phase synchronization processes that are not time-locked to an external stimulus. For this reason, novel synchronization analysis techniques were developed and directly applied to MEG signals. However, due to the lack of an inverse modeling (i.e. source localization), the spatial resolution of this approach is limited. To detect and localize cerebral phase synchronization, we developed the synchronization tomography: First the cerebral current source density is estimated by means of the magnetic field tomography (MFT) for each time step; then the single-run phase synchronization analysis is applied to the current source density in each voxel of the reconstruction space. We model different generators of ongoing rhythmic cerebral activity by current dipoles with time courses of slightly detuned coupled chaotic oscillators subjected to random forces. MEG signals are calculated using these generators for a whole-head MEG system, and subsequently the synchronization tomography is applied to the simulated measurements. We show advantages and limitations of the synchronization tomography. We demonstrate that the measurement noise resistance of the synchronization tomography is much higher compared to MFT alone. Furthermore, we compare different approaches to extend phase synchronization analysis, which was developed for scalar signals, on vector valued signals like the current density. The localization accuracy can considerably be improved using the strongest component of the principal component analysis of the reconstructed current density vector.

QRS-Fragmentation Detected by Filtering with Binomial Non-Recursive Filters
A new method of noise reduction using independent component analysis and wavelet transformation

G. Inoue[1], S. Honda[1], T. Kunihiro[2], A. Aoyama[1]
Department of Applied Physics and Physico-Informatics, Keio University, Yokohama, JAPAN[1]
Department of Otolaryngology, Keio University School of Medicine, Tokyo, JAPAN[2]

One of the problems in analyzing MEG is very low SNR. It requires reducing the noises in MEG data, that is, shortening the measuring time and decreasing the experimental load. This study introduced a new method using independent component analysis (ICA) and wavelet transformation for the noise reduction. Although ICA is useful method for the noise reduction, there is a fault of not being objective way to discriminate brain signal from the noise in each independent component. In this study, ICA and wavelet transformation was applied to SEF data following stimulation of the median nerve. Wavelet transformation was applied to independent components separated by ICA. It is more suitable to choose the noise or brain signal, since the intensity distribution of continuous wavelet transformation gives more precise time and frequency information. After calculating all similarities among wavelet coefficients, clustering will iterate until wavelet coefficient converge on one cluster. As a result, independent components were grouped into several clusters. The reconstructed signal from each cluster showed the electrical trigger noise, SEF signal evoked from the brain, 50 Hz artifact and outside environmental artifact. SNR of this reconstructed SEF cluster, which consisted of 200 trials, is 38.4 dB, and goodness of fit (GOF) is 96.7 %, while the conventional processed data consisted of 400 trials respectively shows 36.1 dB and 96.2 %. It noted that the data with ICA and wavelet-clustering combinations shows the same performance of doubled number of averages with conventional process. This new way shows the objective criterion to discriminate the brain signal from the noise and reduce much analyzing time and load in MEG data.

The MEG signal you record is what is

Andreas A. Ioannides and Max Burbank
Laboratory for Human Brain Dynamics, RIKEN Brain Science Institute (BSI),
2-1 Hirosawa, Wakoshi, Saitama 3510198, Japan

Modern magnetoencephalography (MEG) systems record the magnetic field with a resolution of 0.3 fT(rms)/sqrtHz over a continuous signal range of ± 160 nT(rms)/sqrtHz. The system noise is typically below 10 fT(rms)/sqrtHz at frequencies above 0.5 Hz. Although the signal produced by a neuron is still too small to measure, coherent activity of neuronal assemblies generates a signal a good fraction of a pico Tesla strong. This signal is generated by the brain and it can be separated from both environmental noise and other interference from the subject (e.g. from muscle, heart or eye). This brain-generated MEG signal has a very wide frequency spectrum with modest peaks at well-defined frequencies: rapid transitions over a few milliseconds ride on waves of much slower activity. The repeated presentation of a stimulus produces little obvious repetition in the MEG signal. The usual "processing" of the data improves the signal to noise ratio of small components, while eliminating other components, both in the low and high frequency ranges. Fast components are eliminated by averaging and slow ones by a combination of filtering, chopping of the data into small segments and overlapping responses from successive stimuli. What survives the process is an "evoked response", typically about 100 fT strong. This is a convenient summary of the neural activity elicited by the stimulus. It is also a drastic elimination of information since only a small fraction of the MEG signal generated by the brain is utilized. In this work we begin with simple estimates of what level of signal one might expect from the brain and proceed by contrasting theoretical estimates of what different brain areas may produce with what is detectable by modern instrumentation. We finally compare the resulting predictions with results from recent tomographic analysis of average and single trial MEG data

A Study on Wavelet Filtering of fMRI Multimodal Imaging with Spectral Noise

Sucheol Kang
INCOM I&C, South Korea

In this paper we proposed a simple and effective filter design for fMRI Multimodal images with spectral noise and contrast enhancement based on multi-scale wavelet adaptive shrinkage method.

Wavelet threshold algorithms replace wavelet coefficients with small magnitude by zero and keep or shrink the other coefficients. This is basically a local procedure, since wavelet coefficients characterize the local regularity of a function. After we estimate distribution of noise within fMRI, then apply to fitness Wavelet threshold algorithm.

A common way of the estimating the spectral noise level in coherent imaging is to calculate the mean-to-standard-deviation ratio of the pixel intensity, often termed the Equivalent Number of Looks(ENL), over a uniform image area. Unfortunately, we found this measure not very robust mainly because of the difficulty to identify a uniform area in a real image. For this reason, we will only use here the S/MSE ratio and which corresponds to the standard SNR in case of spectral noise.

We have simulated some brain images by specialized hardware for real-time application; processing of a 512*512 images takes about 1 min.

Our experiments show that the optimal threshold level depends on the spectral content of the image. High spectral content tends to over-estimate the noise standard deviation estimation performed at the finest level of the DWT. As a result, a lower threshold parameter is required to get the optimal S/MSE. The standard WCS theory predicts a threshold that depends on the number of signal samples only.

Imaging and Detection of Oscillatory Activity in MEG using Time-Frequency Analysis and Permutation Tests

D. Pantazis[a], M. Hough[b], T. E. Nichols[c], G. V. Simpson[b], R. M. Leahy[a]
[a]Signal & Image Processing, University of Southern California, USA [b]Dynamic Neuroimaging Laboratory, University of California, San Francisco, USA [c]Department of Biostatistics, University of Michigan, Ann Arbor, USA

Event-related components in MEG studies are often lost in background brain activity and environmental and sensor noise. The standard technique for noise reduction involves averaging over stimulus-locked responses, however this also removes higher frequency event-related components in the data that are not phase locked to the stimulus. To overcome this problem, we combine time-frequency analysis of individual epochs with minimum norm imaging to produce dynamic cortical images in multiple frequency bands. While the SNR in individual epochs is too low to see any but the strongest components, we can average signal power across epochs to find event related components in each band. To detect statistically significant differences between two conditions we use a permutation test. Under the null hypothesis there is no difference between these two conditions. Using permutations to learn the null distribution of maximum signal power in each band across the cortex, we can then determine a threshold that controls the familywise error rate, i.e. the probability of one or more false positive detections across the entire cortex [1]. Applying this test to each frequency band produces a set of cortical images showing significant event-related activity in each band of interest. We demonstrate this method in applications to high density MEG studies of visual attention. **Acknowledgement:** this work supported by NIBIB, Grant No: R01EB002010

[1] Nichols, T. E., Hayasaka, S., 2003. Controlling the Familywise Error Rate in Functional Neuroimaging: A comparative review. Statistical Methods in Medical Research 12(5), 419-446.

Movement correction in MEG

S. Taulu, M. Kajola, J. Simola
Elekta Neuromag Oy, Helsinki, Finland

Movement of the subject during the recording severely distorts MEG data. With cooperative healthy subjects this is not a problem but e.g. with small children and epilepsy patients head movements are unavoidable. The analysis of such data requires movement compensation which consists of dynamic recording of the head position and a method that takes the recorded movement into account in the analysis. The measured data is decomposed into a source model in the head coordinate system and the signals that would have been measured from a static subject corresponding to some reference head position are calculated. We use the signal space separation method (SSS) [1] as a source model. SSS contains harmonic basis functions (e.g. spherical harmonics) and is computationally fast. Earlier, minimum norm estimate [2] and spherical harmonic functions have been used in movement correction in MEG and in transforming MCG data between sensor configurations. The benefit of SSS is the separate bases for the biomagnetic signals and external interferences, and therefore it provides straightforward interference suppression along with the movement correction. The method is demonstrated by using a phantom head with movements of over 10 cm. The localization error of the dipole from raw data without movement correction was about 40 mm and only 4 mm after the movement correction.

[1] Taulu, S., Kajola, M., Simola, J. 2003. The Signal Space Separation method. Proc of the 14th Conference of ISBET (Nov 2003, Santa Fe, NM).
[2] Uutela, K., Taulu, S., Hamalainen, M. 2001. Detecting and correcting for head movements in neuromagnetic measurements. NeuroImage 14, 1424-1431.

Phase resetting tomography: A method for three-dimensional localization of stimulus-locked complex responses and transient synchronization with MEG

P.A. Tass[1,2], T. Fieseler[1], J. Dammers[1], U. Barnikol[1], K. Dolan[1], M. Schiek[3], F. Boers[1], A. Muren[1], S. Wuttich[1], K. Zilles[1,4], M. Niedeggen[5]
[1]Institute of Medicine, Research Center Jülich, Germany, [2]Department of Stereotactic and Functional Neurosurgery, University of Cologne, Germany, [3]Central Institute for Electronics, Research Center Jülich, Germany. [4]C. and O. Vogt Institute for Brain Research, Heinrich Heine University, Düsseldorf, Germany,
[5]Institute of Experimental Psychology, University of Düsseldorf, D-40225 Düsseldorf, Germany

We present a non-invasive technique to anatomically localize oscillatory neuronal populations in the human brain which react to a pulsatile stimulus either stereotypically or by switching between different responses across trials. Furthermore, our method reveals stimulus-locked transient synchronization and the transmission of the stimulus' action within a network of populations. For this, in each brain voxel we study stochastic phase resetting [1] of the reconstructed current source density obtained from magnetoencephalography measurements. We demonstrate such processes in visual brain areas in a pattern reversal experiment in ten subjects. We provide the first evidence that a brain area can switch between antiphase responses across trials. Such transient neuronal dynamics cannot be derived with neuroimaging techniques like functional magnetic resonance imaging or positron emission tomography.

[1] Tass, P.A. 2003. Stochastic phase resetting of two coupled phase oscillators stimulated at different times. Phys. Rev. E 67, 0519021-05190215

Single-trial analysis by a complex filtering approach: examination by auditory evoked M100

L. Trahms[1], A. Salajegheh[2], A. Link[1], C. Elster[1], M. Burghoff[1], T. Sander[1], D. Poeppel[2,3,4]
[1] Physikalisch-Technische Bundesanstalt (PTB), Berlin, Germany,
[2] Cognitive Neuroscience of Language Laboratory, Univ. Maryland College Park,
[3] Department of Linguistics and [4]Department of Biology, Univ. Maryland College Park

Conventional analyses of neurophysiological evoked response data rely on signal averaging across many epochs associated with specific events. The amplitudes and latencies of these averaged events are subsequently interpreted in the context of the given perceptual, motor, or cognitive tasks. Can such critical timing properties of event-related responses be recovered from single-trial data? Here we make use of the M100 latency paradigm used in previous MEG research to evaluate a novel single-trial analysis approach. Specifically, the latency of the auditory evoked M100 varies systematically with stimulus frequency over a well-defined time range (lower frequencies, say 125 Hz, yield up to 25 ms longer latencies than higher frequencies, say 1000 Hz). Here we show that the complex filtering approach recovers this key characteristic of the M100 response in the single-trials, as well as some other important response properties relating to lateralization. The results illustrate the utility of the complex filtering method and the potential of the M100 latency to be used for stimulus encoding, since the relevant variation can be observed in single trials.

This page has been intentionally left blank

A new Algorithm for Detection of Coherent Brain Areas with MEG

Belardinelli P.[1,2,3], Ciancetta L.[1,2], Pizzella V.[1,2,3], Del Gratta C.[1,2,3], Romani, G.L.[1,2,3]

[1] ITAB, Institute for Advanced Biomedical Technologies, University G. D'Annunzio, Chieti, Italy;
[2]Department of Clinical Sciences and Biomedical Imaging, University of Chieti;
[3]INFM– National Institute for the Physics of Matter, Coordinated group of Chieti

ABSTRACT

In the field of neuroscience, the study of spontaneous activity and coherence among different regions of the brain is an issue of growing interest. These studies are usually performed in the frequency domain. MEG is a particularly well suited tool for this purpose. Indeed, its temporal resolution is much higher than that of fMRI, and its spatial resolution is better than that of EEG. Starting from the work of Gross et al., we conceived an algorithm that does not call for an external reference signal for its implementation. We integrated the original algorithm with additional tools for the identification of an internal reference signal.

The possible applications of this procedure are numerous, especially in the field of cognitive studies where the activation of many different brain areas in complex sequences is studied.

KEY WORDS

Frequency domain, coherence, synchronization, localization.

INTRODUCTION

We implemented a software for distributed source estimation that uses weighted minimum norm or LORETA, and used it to detect the areas characterized by the strongest neural activity in the frequency range of interest. In this way, the grid point with maximal activity can be considered as taken as the reference for the detection of coherent areas. The study of coherence can be performed between this point and all the other grid points as well as between a suitable external reference signal and all the grid points.

METHODS

An isotropic 3D grid of constant step is placed inside a spherical model of the head. The sphere is fitted to reference points on the real head, as measured by a 3D digitizer (Polhemus). The minimum grid step in our most recent simulations was 5 mm. If an external reference signal is not available, a tomography over the whole head has to be performed. To find the peak activity, the following minimization problem has to be solved at a precise instant in time and/or in the frequency domain (study of cross-spectral matrices):

$$\min_j \| \boldsymbol{BWJ} \|^2 \qquad \text{(I)}$$

under the constraints: (1) $\Phi = \boldsymbol{KJ}$ and (2) **RJ=0**
where, in constraint (1), Φ is an N-vector comprised of magnetic field measurements; $\boldsymbol{J} = (\boldsymbol{j}_1^T, \ldots, \boldsymbol{j}_N^T)^T$ is a 3M vector comprised of the current densities **j** (3-vector) at M points with known locations within the brain volume; **K** is a transfer **N**x**3M**-matrix with α-th row $(\boldsymbol{k}_{\alpha 1}^T, \ldots, \boldsymbol{k}_{\alpha M}^T)$, where **k** is the magnetic lead field potential (3-vector); **W** is a diagonal **3M**x**3M** matrix, defined as **W**= $\boldsymbol{\Omega} \otimes \boldsymbol{I}$. **I** is the identity 3x3 matrix and Ω is a diagonal **MxM** matrix with $\Omega_{ii} = \sqrt{\sum_{\alpha=1}^{N} \boldsymbol{k}_{\alpha i}^T \boldsymbol{k}_{\alpha i}}$. **B** represents the discrete Laplacian.

For what concerns constraint (2), ***R*** is a block diagonal 3Mx3M, where each sub-block is a 3x3 matrix with the *i-th* diagonal sub-block given by:

$$\boldsymbol{R}_{ii} = \frac{\boldsymbol{r}_i \boldsymbol{r}_i^T}{\| \boldsymbol{r}_i \|^2}$$

where r_i is the position vector of the *i-th* grid point in the brain.

Constraint (2) indicates that the radial component of the current density field is silent .
This means that the solution to (I) belongs to the space spanned by the columns of (**I-R**). The solution to (I) is

$$\hat{\boldsymbol{J}} = \boldsymbol{T}\Phi ,$$

with:

$$\boldsymbol{T} = \boldsymbol{D}(\boldsymbol{DWB}^T\boldsymbol{BWD})^+ \boldsymbol{DK}^T[\boldsymbol{KD}(\boldsymbol{DWB}^T\boldsymbol{BWD})^+ \boldsymbol{DK}^T]^{-1} \qquad \text{(II)}$$

where **D= I-R**.

Solutions of (I) are superimposed over MRI brain images with 1 mm cubic voxels by interpolation at each point. Once the region with strongest activity has been localized, a map of the coherence degree (ranging from 0 to 1) between this area and all the other points within the brain is calculated.

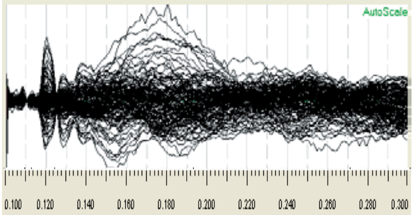

Figure 1: Time spectrum for the magnetic signal generated by the median nerve stimulation

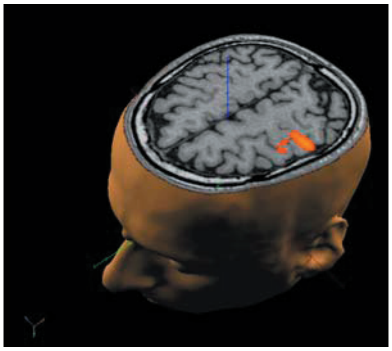

Figure 2: Localization of S1 activation with right median nerve stimulation data

This map is obtained starting from the calculation of the complex cross spectral density matrix C for all the magnetic signals. The Welch's method for spectral density estimation is used.

If we define ***F*** as the Fourier transformed data, the following problem has to be solved:

$$\min[E\{\| \boldsymbol{AF} \|^2\} + \alpha \|\boldsymbol{A}\|^2] \qquad \text{(I)}$$

under the constraint $\boldsymbol{AK}(\boldsymbol{r}) = \boldsymbol{I}$;

where $\boldsymbol{A}$ is a filter matrix that allows us to obtain the contribution to the magnetic field of a grid point in a specific frequency band, $\boldsymbol{K}$ is the transfer matrix for three independent dipoles at one grid point .

$$\boldsymbol{A}(\boldsymbol{r},f) = [\boldsymbol{K}^T(\boldsymbol{r})(\boldsymbol{C}(f))^{-1}\boldsymbol{K}(\boldsymbol{r})]^{-1})\boldsymbol{K}(\boldsymbol{r})^T(\boldsymbol{C}(f))^{-1}$$

C(f) is the cross spectral density matrix averaged across a frequency band centered at *f.* The estimates of the cross spectrum between the two dipoles placed on two different grid points are:

$$\boldsymbol{C}_{ext}(\boldsymbol{r}_i,\boldsymbol{r}_j) = \boldsymbol{A}(\boldsymbol{r}_i,f)\boldsymbol{C}(f)\boldsymbol{A}^T(\boldsymbol{r}_j,f)$$

When $i = j$ the matrix C_{ext} becomes the matrix of power estimates

$$\boldsymbol{C}_{ext}(\boldsymbol{r}_i,\boldsymbol{r}_i,f) = \boldsymbol{P}(\boldsymbol{r}_i,f)$$

The cross spectral density with an external reference at a generic $\boldsymbol{r}$ location

$$\boldsymbol{c}_s(\boldsymbol{r},f) = \boldsymbol{A}(\boldsymbol{r},f)\boldsymbol{c}_{\cdot r}(f)$$

where $c_r(f)$ is the cross spectral density between the external signal and all MEG signals.

If one singular value λ_1 of C_s, is significantly predominant with respect to the other, the cross spectrum can be considered as generated by a source with a fixed direction that is determined by the singular vectors of λ_1.

In this way, the estimates for the cross spectral density are expressed as the highest singular value:

$$c_s(\boldsymbol{r}_1,\boldsymbol{r}_2,f) = \lambda_1(\boldsymbol{C}_s(\boldsymbol{r}_1,\boldsymbol{r}_2,f))$$

The matrix of power estimates can be approximated in the same way.

The coherence matrix is calculated as follows:

$$M(\boldsymbol{r}_1,\boldsymbol{r}_2,f) = \frac{|c_s(\boldsymbol{r}_1,\boldsymbol{r}_2,f)|}{p(\boldsymbol{r}_1,f)p(\boldsymbol{r}_2,f)}$$

Then, if required, other kinds of interaction between coherent areas can be studied, such as the synchronization and the directionality index of their activities.

RESULTS

To test the localization algorithm on real data, we analysed 5 data sets acquired during right median nerve electric stimulation. As a result, we obtained the clear activations in SI (see Figure 2) and SII at the well known latencies reported in literature. Across the 5 data sets, the activated voxels with a 0.8 threshold of maximum activity, were in good agreement with the ones obtained by means of LORETA included in the Curry software.

As a test for the coherence detection procedure, we used simulated data. The coupling between an external reference signal and four different oscillating sources was studied. Two sources were placed in the SI area both in the right and the left hemisphere. The one in the left hemisphere had an oscillation frequency at 10 Hz. The other was composed of 10 Hz and 22 Hz oscillations. The other two sources were located deep in the thalamus and in the amigdala with oscillation frequencies of 18 Hz and 6Hz respectively. For each of the above frequencies, we checked the coherence map. The coherence peak was always localized at the source voxel.

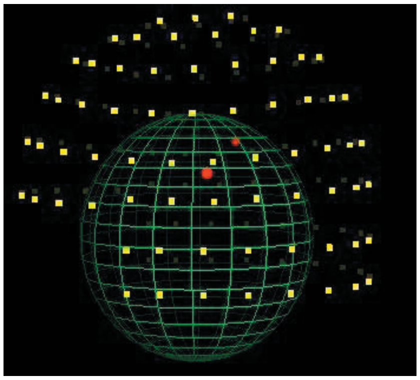

Figure 3: Coherence estimates in the 8-12Hz band with a threshold of 0.3.

DISCUSSION

A new method that integrates different techniques for studying neural activations and interactions has been presented. It can be used to model spatial distributions of sources and to calculate coherences among them in selected frequency bands.

REFERENCES

R.D. Pasqual-Marqui: Review of Methods for Solving the EEG Inverse Problem. International Journal of Bioelectromagnetism 1999. 1: 75-86.

R.D. Pasqual-Marqui: Notes on some physics, mathematics and statistics for time and frequency domain LORETA. 2002

J. Gross, J. Kujala, M. Hämäläinen, L. Timmermann, A. Schnitzler, R Salmelin. Dynamic imaging of coherent sources: Studying neural interactions in the human brain. PNAS, 2001; 98: 694-699.

J. Gross, L. Timmermann, J. Kujala, M. Dirks, F. Schmitz, R Salmelin, A. Schnitzler. The neural basis of intermittent motor control in humans. PNAS, 2002; 99: 2299-2302

Cortical rhythms in AD, LBD and old normal subjects: a quantitative MEG study

R. Franciotti[1] , D. Iacono[2], S. Della Penna[1], V. Pizzella[1], K. Torquati[1], M. Onofrj[2] and GL. Romani[1]

[1]Department of Clinical Sciences and Bioimaging – University of Chieti; and Center of Excellence on Aging, ITAB – Fondazione Università G. D'Annunzio; Chieti, Italy; [2]Department of Oncology and Neurosciences, Service of Neurophysiopathology- University of Chieti; and Center of Excellence on Aging, Ce.S.I. – Fondazione Università G. D'Annunzio, Chieti, Italy

ABSTRACT

The present MEG study evaluated the slow and fast cortical rhythms in patients affected by Alzheimer's Disease (AD) and Lewy Body Dementia (LBD) not undergoing any pharmacological therapy, and in age-matched control subjects. The absolute spectral power values of the rhythms in different regions of the brain and spectral coherence values for long and short distance were compared between the groups of subjects (15 AD patients, 7 LBD patients and 9 control subjects). The spectral power change of the alpha rhythm during spontaneous activity with open and closed eyes permitted to distinguish the control group from the patients groups. In control and LBD groups the task condition, consisting of counting the rare tone in an acoustical oddball stimulation, produced a decrease of the total spectral power in all regions and frequency bands, with respect to the rest condition. In LBD patients the neurophysiological behavior similar to controls allowed to distinguish LBD from AD patients. Coherence analysis on the alpha rhythm in closed eyes condition showed that in AD and LBD patients the loss of coherence preferentially involves the long connections that connect occipital region to frontal one. In conclusion, MEG could be an useful non invasive investigative technique that may potentially assist in the differential diagnosis of LBD and AD and consequently in a better patient management from a therapeutic point of view.

KEY WORDS: Magnetoencephalography; cortical rhythms; AD; LBD; spectral analysis; spectral coherence analysis.

INTRODUCTION

The mechanisms underlying Alzheimer's disease and Lewy Body Dementia have long been a controversial subject among scientific community [Wang, 2003]. In the clinical practice neurophysiological investigations by Electroencephalography (EEG), Quantitative EEG (QEEG), Event-Related Potentials (ERP-P300), and Choice Reaction Time Variability (CRTV) have been proposed as useful tools to discriminate patients with dementia from age-matched control subjects [Walker, 2000]. In addition QEEG coherence was used to evaluate the functionality of cortical connections in AD patients [Locatelli, 1998]. At present, no unique neurophysiological pattern has been identified in LBD that clearly differentiates it from AD [Doubleday, 2002]. In this study we utilised magnetoencephalography (MEG) to quantify absolute spectral power in a wide range of frequency band (3-47 Hz) and in different brain areas of control subjects and AD and LBD patients. In addition, we calculated spectral coherence to establish if the coherence loss in dementia preferentially involves short or long cortical connections.

METHODS

We selected 15 probable AD patients (6 males and 9 females, mean age ± SD was 73.3 ± 4.1), 7 probable LBD patients (4 males and 3 females, mean age ± SD was 72.7 ± 3.3) and 9 control subjects (4 males and 5 females, mean age ± SD was 70.3 ± 4.4). The diagnosis of probable AD was based on NINCDS-ADRDA criteria [McKhann, 1984] focusing on the multiple cognitive impairments and their temporal progression. LBD diagnosis is achieved by the consensus criteria [McKeith, 1996], focusing on the presence of hallucinations, parkinsonism and fluctuating cognition. Data were recorded using a 165 channels whole head neuromagnetic system: 153 channels are arranged over a helmet surface to record the neuromagnetic field, whereas 12 channels are used for subtraction of the magnetic field noise [Pizzella, 2001]. For all subjects of the study, magnetic field was measured in 3 different conditions: spontaneous activity with open and closed eyes, simple mental task of counting the rare tone of an acoustical oddball stimulation. At the end of each condition the head position relative to the coordinate system of the helmet was measured by energizing 4 coils attached to the subject head and digitised by means of a 3D-Digitizer (Polhemus, 3Space Fastrak). MEG data were recorded at 1024 Hz and were filtered between 0.16 and 300 Hz. For each registration condition heart and ocular contaminations were carefully removed from data, and 30 artefact free epochs of 4 s were selected. The helmet sensor was ideally divided into 4 main regions: frontal, parietal, temporal and occipital. For each epoch and for each channel the power spectrum density based on Fast Fourier Transform (FFT) was computed and finally mean power spectrum was computed for each recording condition and for each region. The spectral band ranging from 3 to 47 Hz was subdivided in 4 main bands: slow band ranging from 3 to 7 Hz, alpha ranging from 7 to 14 Hz, beta ranging from 14 to 35 Hz and gamma ranging from 35 to 47 Hz. For each main band and for each recording condition the total power spectrum was computed. Finally, considering the spontaneous activity with open eyes as rest condition, the spectral power change was computed in closed eyes condition with respect to rest (change1) and in task condition with respect to rest (change2). For statistical analysis, three-factors analysis of variance (ANOVA) was performed on the parameters change1 and change2 separately to estimate the contributions of the factors group, region and band. In addition to spectral power study, spectral coherence analysis was performed using the same 30 artefact free epochs of the closed eyes condition. Local and far coherence were calculated for channel pairs connecting two different near (occipital – parietal for the left and right hemisphere) or far (occipital – frontal for left and right hemisphere) regions. For comparison between groups, unpaired Student's t test was performed on maximal coherence values in the alpha band.

RESULTS

The statistical analysis on the parameters change1 and change2 showed a significant interaction between the factors group/region, group/band, and region/band. For the parameter change1 Duncan post-hoc test on the interaction group/region suggested that the spectral power change in the occipital region of controls was significantly larger than the occipital region of all patients ($p<0.05$). The same post-hoc test conducting for the interaction group/band revealed that for controls the parameter change1 in the alpha band was significantly larger than patients ($p<0.005$). For the parameter change2 post-hoc test distinguished AD from the other groups in frontal region by the interaction group/region ($p<0.005$) and in slow band by the interaction group/band ($p<0.005$). Fig.1 and Fig.2 show the parameters change 1 and change 2 in percentage for the occipital and frontal region respectively.

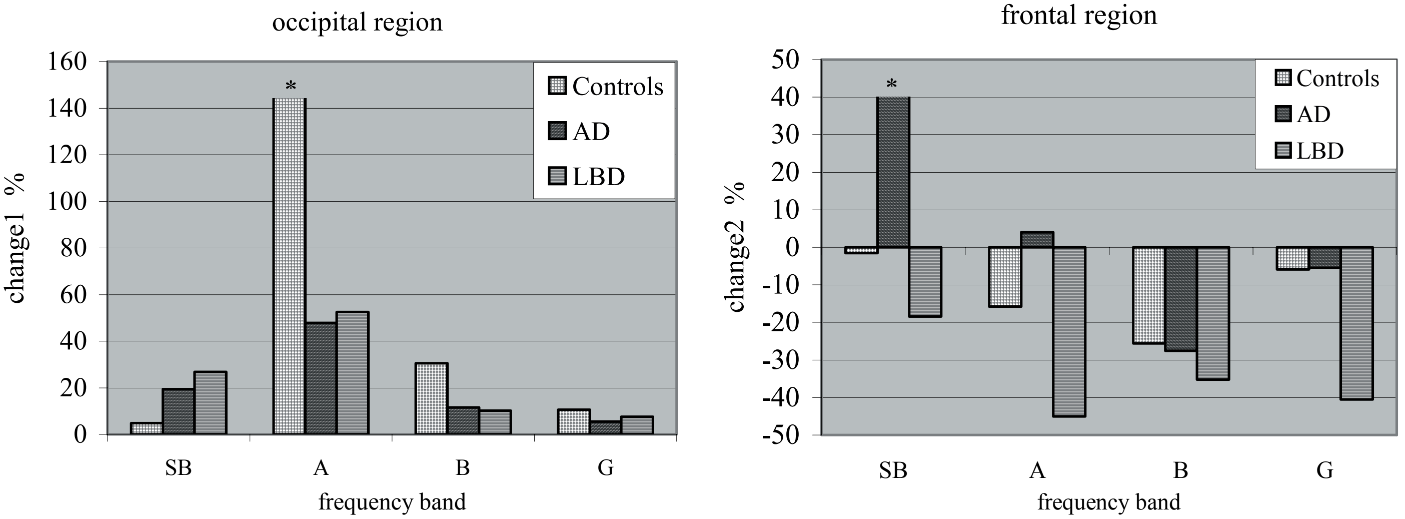

Figure 1. Spectral power change in closed eyes condition with respect to open eyes (on the left), spectral power change in task condition with respect to rest (on the right).The symbol * is used to indicate significant difference in the alpha band between the control group and the patients groups or to indicate significant difference in the slow band between AD patients group and control subjects and LBD patients groups.

Spectral coherence analysis in closed eyes condition showed that the alpha band presented coherence values greater with respect to the other bands in all groups of the study. This effect was reduced when the distance between the two regions of interest increased. For the patients group coherence values were smaller than control group for near and far regions. Statistical analysis revealed that AD patients presented coherence values significantly smaller than controls in near ($p<0.05$) and far ($p<0.01$) regions. Coherence in LBD patients was significantly smaller than controls in right near ($p<0.05$) and far ($p<0.01$) regions.

DISCUSSION

The inter-group analysis on the spectral power change in the closed eyes with respect to open eyes condition showed that the alpha activity (7-14 Hz) can be used to distinguish age-matched control subjects from patients with dementia, confirming previous QEEG studies [Bennys, 2001]. Additionally the spectral power change in task condition with respect to rest allowed us to distinguish AD patients from LBD patients. This result evidenced the differential involvement of the cholinergic system in LBD respect to AD and its relationship with the attention state [Noe, 2004]. Coherence results showed a decrease of alpha coherence in AD and LBD groups with respect to control group, consistently with previous MEG studies in AD patients [Berendse, 2000]. In addition, in our study, the coherence loss was stronger for long distance than for short distance for all patients. This result might be due to the impairment of the cortico-cortical connections that join occipital area to frontal one [Locatelli, 1998].

ACKNOWLEDGEMENTS

This work was partially supported by a grant from the Italian Ministry of Research to the Center of Excellence on Aging of the University.

REFERENCES

Bennys K, Rondouin G, Vergnes C, Touchon J. Diagnostic value of quantitative EEG in Alzheimer's disease. Neurophysiol Clin 2001;31(3):153-60.

Berendse HW, Verbunt JPA, Scheltens Ph, van Dijk BW, Jonkman EJ. Magnetoencephalographic analysis of cortical activity in Alzheimer's disease: a pilot study. Clin Neurophysiol 2000;111(4):604-12.

Doubleday EK, Snowden JS, Varma AR, Neary D. Qualitative performance characteristics differentiate dementia with Lewy bodies and Alzheimer's disease. J. Neurol Neurosurg Psychiatry 2002, 72(5):602-607.

Locatelli T, Cursi M, Liberati D, Franceschi M, Comi G. EEG coherence in Alzheimer's disease. Electroencephalogr Clin Neurophysiol 1998;106(3):229-37.

McKhann G, Drachman D, Folstein M, Katzmann R, Price D, Stadlan EM. Clinical Diagnosis of Alzheimer's disease: report of the NINCDS-ADRDA Work Group under the auspices of Department of Health and Human Service Task Force on Alzheimer's Disease. Neurology 1984; 34(7):939-44.

McKeith IG, Galasko D, Kosaka K, Perry EK, Dickson DW, Hansen LA, Salmon DP, Lowe J, Mirra SS, Byrne EJ, Lennox G, Quinn NP, Edwardson JA, Ince PG, Bergeron C, Burns A, Miller BL, Lovestone S, Collerton D, Jansen EN, Ballard C, de Vos RA, Wilcock GK, Jellinger KA, Perry RH.. Consensus guidelines for the clinical and pathological diagnosis of dementia with Lewy bodies (DLB): report of the consortium on DLB international workshop. Neurology 1996; 47(5):1113-24

Noe E, Marder K, Bell KL, Jacobs DM, Manly JJ, Stern YS. Comparison of Dementia with Lewy Bodies to Alzheimer's Disease and Parkinson's Disease with Dementia. Movement Disorders 2004;19(1):60-67.

Pizzella V, Della Penna S, Del Gratta C, Romani GL. SQUID System for biomagnetic imaging. Supercond. Sc Technol 2001;14:R79-R114.

Walker MP, Ayre GA, Cummings JL, Wesnes K, McKeith IG, O'Brien JT, Ballard CG. Quantifying fluctuation in dementia with Lewy bodies, Alzheimer's disease, and vascular dementia. Neurology 2000, 54:1616-1625.

Wang DS. From Lewy body disease to Alzheimer's disease: hypothesis and evidence. Frontiers in Bioscience 2003, 8:223-227.

P1-2

Spectral Analysis of Localized Slow Waves Observed in Patients Suspected of Cerebral Ischemia

Hatanaka, K.,[*] Tamafuri, K.,[*] Seki, S.,[†] Ohtomo, S.,[‡] Kanno, A.,[‡] and Nakasato, N.[‡]

[*]Okayama University of Science; [†]Tohoku University Graduate School of Medicine; [‡]Kohnan Hospital, Japan

ABSTRACT

Neuromagnetic source localization of slow waves is very useful for evaluation of abnormal brain activity. The present study evaluated a more efficient method for the detection of pathological slow waves based on spectral analysis. We investigated 39 inter carotid artery and middle cerebral artery stenosis patients suspected of cerebral ischemia. Measurements were made with a helmet-shaped 204 channel planar first order gradiometer system. Spontaneous neuromagnetic signals were sampled at 300 Hz, and fast Fourier transform of the detected signals was performed in consecutive time windows of 6.83 s. Power spectrum intensity of the primary and the secondary slow wave components were evaluated at the 102 sensor coil locations and then displayed as a contour map. Thirteen patients showed hemilateral distribution of the primary theta wave activity over the temporal lobe of the lesion hemisphere, though direct relation between lesion and estimated source is not apparent. Six patients also showed bilateral distribution of the secondary theta wave activities over the occipital lobe. Distribution of the occipital activity was extended in the lesion hemisphere and overlapped to the distribution of the temporal activity. We suggest that spectral analysis of neuromagnetic recording offers an efficient tool for the non-invasive evaluation of patients at risk of developing cerebral ischemia.

KEY WORDS: spectral analysis, slow wave, theta wave, cerebral ischemia, cerebrovascular disease

INTRODUCTION

Cerebrovascular disease resulting from cerebral ischemia is one of the major causes of death and disability, especially among the elderly. Cerebral ischemia is often associated with focal neurological symptoms which are reflected in abnormal localalized electrical activities. Such pathological electrical activities are usually observed as slow waves in the delta and the theta wave frequency band ranges [Vieth 1992]. Conventional neuromagnetic source analysis mainly examines time domain data. Typical source analysis involves two steps: First, the magnetoencephalography (MEG) and electroencephalography (EEG) time charts are inspected visually from the beginning to the end, looking for ‘abnormal’ waves. Experience and judgement are required to discriminate pathological waves from several channels of time waveform data, and the limited signal to noise ratio makes weak signals difficult to differentiate from noise. Second, the detected abnormal waves are inspected by magnetic fields contour mapping to check for a good ‘dipole pattern’ to confirm the physiological or artifact origin. These procedures usually demand several hours to check thoroughly all of the data recorded in the various channels and time periods, so pathological signals may be overlooked, especially by inexperienced inspectors. The present study evaluated a more efficient method for the detection and evaluation of synchronous localized slow waves based on spectral anaysis.

METHODS

Simultaneously recording of scalp EEG and MEG were performed in 39 patients (between 49 and 75 years of age, average 64.6±7.7; 32 male and 7 female) with internal carotid artery (ICA) or middle cerebral artery occlusive diseases. MEG was performed in the supine position with a helmet-shaped magnetometer incorporating 204 planar first order gradiometers at 102 positions (Neuromag System; Neuromag Ltd., Helsinki, Finland). No activation was used except for alpha blocking at the beginning of the measurements. Three 10-minute epochs consisting of 204 spontaneous MEGs and 32 spontaneous EEGs were recorded simultaneously during the resting condition with both eyes closed. The MEG signals ($\partial B_z/\partial x(t)$, $\partial B_z/\partial y(t)$; where B_z is the mean magnetic field normal to the detecting coil, x and y are the two orthogonal axes in the plane of the coil) were processed by a band-pass filter of 0.5-40 Hz and sampled at 300 Hz. Spectral analysis used a fast Fourier transform (FFT; $P_x(\omega) = \mathrm{F}[\partial B_z/\partial x(t)]$, $P_y(\omega) = \mathrm{F}[\partial B_z/\partial y(t)]$) in the frequency range from 1 to 13 Hz in consecutive time windows of 6.83 s or 2048 sampling data points. Normalized parameters $P(\omega) = \surd[P_x(\omega)^2 + P_y(\omega)^2]$ were calculated for the primary and the secondary slow wave component ω_o and ω_1 at the 102 sensor coil locations, and then superimposed as a spectral intensity contour map. Sources of slow waves were also estimated using a single equivalent current dipole model based on the best-fit sphere determined from magnetic resonance images of the subjects, and compared with the distributions of the primary and the secondary slow wave components evaluated from spectral analysis.

RESULTS

Thirteen patients showed hemilateral distribution of the primary theta wave activity (observed frequency range 6-8 Hz) over the temporal lobe of the lesion hemisphere. Six patients also showed bilateral distribution of the secondary theta wave (with lower frequency) activities over the occipital lobe. Figure 1 shows a typical example of the localization of the primary 7.7 Hz and the secondary 7.0 Hz theta wave component based on the spectral analysis of a 71-year-old male patient with a right ICA stenosis. Distributions of the primary and the secondary theta wave activities were overlapped in the lesion hemisphere. Conventional time domain source localization of the theta wave bursts in the same time epoch indicated sources of the slow wave activities were at the mesial temporal lobe of the lesion hemisphere (Fig. 2), and agreed with the distribution of the primary theta wave component (Figure. 1).

DISCUSSION

Hemilateral distribution of the primary theta wave clearly indicated the lesion hemisphere. Sources estimated from the primary theta wave component using power spectrum analysis agreed with conventional dipole source localizations using time domain data. Analysis time, however, could be reduced very effectively by skipping visual inspection of time charts. We also noticed that detectability of pathological activities was improved. This is because the dipole pattern only appears for short periods and changes very rapidly at several cycles per second for this type of rhythmic activity. For example, the 8 Hz theta wave (period of 125 ms) appears as a good ‘dipole pattern’ only for about several tens of milliseconds. Conversion of the continuous time domain data to serial time-segmented frequency domain data allows inspection of all neuromagnetic data for 6.83

s time epochs at a glance. This inspection method is much more efficient than conventional source analysis utilizing time domain data. Moreover, since the frequency spectra of pathological slow waves are different from that of noise in most cases, the pathological slow waves were clearly indicated free of artifacts over the whole brain. The primary component of the slow wave could be determined automatically from the transformed frequency spectrum. Noise might be eliminated further by time averaging effect of the 6.83 s time epoch window. The time epoch of 6.83 s seems to be the optimum for spectral analysis of pathological slow waves using present sampling frequencies because expanding the time window further reduces the detectability of pathological slow waves.

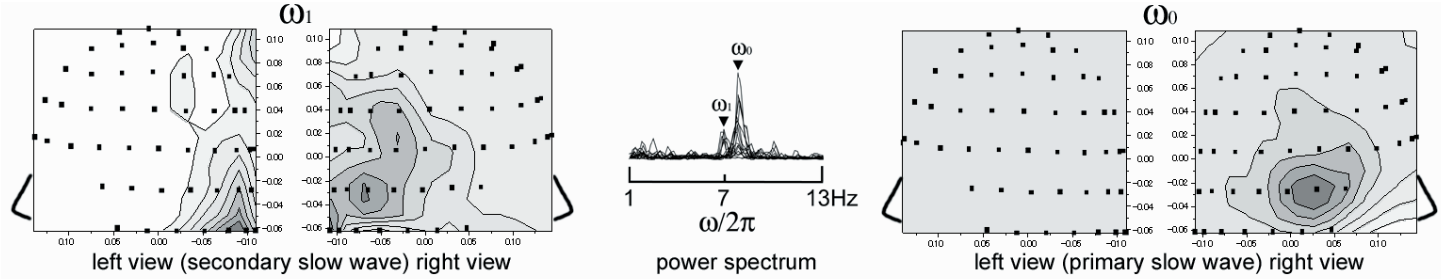

Figure 1. FFT power spectrum (middle), contour map of the primary (right) and the secondary (left) slow wave component.

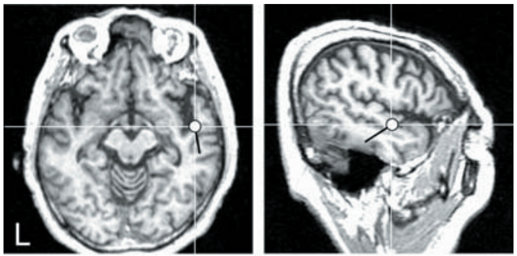

Figure 2. Source localization of the slow wave at the same epoch shown in Figure 1.

The origins of the abnormal delta wave were estimated at the margin (so-called penumbra) of the brain infarction [Hatanaka, 2000]. The present subjects had occlusive disease. Although sources estimated from the distribution of the primary theta wave agreed with the hemisphere suspected of cerebral ischemia, no direct relation between estimated source and the lesion was found. Whether the source had a cortical or subcortical origin is not clear at present. Previous EEG studies have suggested a correlation between temporal theta wave activities and cerebrovascular diseases, but the laterality of theta wave activity has not been investigated in relation to the location of the lesion. They sometimes indicated left hemisphere predominance for temporal theta wave activities [Asokan, 1987; Inui 2001]. Slow (2-6 Hz) wave activities were focused reproducibly in the primary sensorimotor cortex in six patients with transient ischemic attacks [Stippich, 2000]. The dipole source localization (Figure 2) in our case did not match the frequency (7.7 Hz) or location (more mesial location, not in the primary sensorimotor area).

Bilateral occipital theta wave was observed in about half of the patients who showed hemilateral temporal theta wave as the primary component. Distributions of the temporal and occipital theta wave component overlapped in some degree and this might indicate some interactions between these two theta wave activities. Estimated bilateral occipital localizations are different from the physiological generator of alpha activity which is supposed to originate from the parieto-occipital region. Also, alpha activity has different frequency spectrum of 8 to 12 Hz though normal aging usually reduce frequency to the upper theta band.

Alpha- or sub-alpha- like rhythmical activity of the temporal lobe was noticed by epidural EEG especially in patients with cerebrovascular disease [Niedermeyer 1990]. This temporal rhythms lies in the range of 6-11 Hz and often extends into the theta band. Since this temporal rhythm has no proven blocking-effect, it is considered as different from posterior alpha rhythms. Present investigations might suggest possible interactions of temporal and occipital synchronous activities. Further evaluations of subjects suspected of cerebral ischemia is necessary to investigate generator mechanism in the context of interconnected brain networks allowing synchoronized activities of neuronal ensembles. We suggest that spectral analysis of neuromagnetic recording is very useful for the non-invasive evaluation of patients at risk of developing cerebral ischemia and also for understanding mechanisms which lead to brain disorder caused by hemodynamic abnormality.

ACKNOWLEDGEMENTS

This work was supported by the Open Competition for the Development of Innovative Technology (No. 12208) from the Ministry of Education, Culture, Sports, Science and Technology, Japan.

REFERENCES

Asokan G, Pareja J, Niedermeyer. Temporal minor slow and sharp EEG activity and cerebrovascular disorder. Clin Electroencephalogr 1987;18:201-10.

Hatanaka K, Nakasato N, Kanno A, Ohtomo S, Seki K, Fujiwara S, et al. Origin of slow waves observed in cerebrovascular disease. In: Aine CJ, Okada Y, Stroink G, Swithenby SJ, Wood CC, editors. BIOMAG 96. Proceedings of the 10th International Conference on Biomagnetism; 1996 Feb 16-21; Santa Fe. USA. New York: Springer-Verlag; 2000. p. 1007-10.

Inui K, Motomura E, Kaige H, Nomura S. Temporal slow waves and cerebrovascular diseases. Psychiatry Clin Neurosci. 2001;55:525-31.

Niedermeyer E: Alpha-like rhythmical activity of the temporal lobe. Clin. Electroencephalogr 1990;21:210-24.

Stippich C, Kassubek J, Kober H, Soros P, Vieth JB. Time course of focal slow wave activity in transient ischemic attacks and transient global amnesia as measured by magnetoencephalography. NeuroReport 2000;11:3309-13.

Vieth J, Kober H, Weise E, Daun A, Moeger A, Friedrich S, et al. Functional 3D localization of cerebrovascular accidents by magnetoencephalography (MEG). Neurol Res 1992;14(2 Suppl):132-4.

Chaotic analysis approach in neonatal magnetoencephalography

Kotini, A., Adamopoulos, A., Koutlaki, N., * Avgidou, K., * Anninos, P., Anastasiadis P.*

Lab of Medical Physics and *Dept. of Obstetrics & Gynaecology, Medical School, Democritus University of Thrace, Dragana 68100 Alexandroupolis, Greece

ABSTRACT

The recent developments in non-linear dynamics have indicated a new understanding of many biological processes. The brain is a dynamical system that is non-linear at multiple levels of analysis. Identifying families of attractors in phase space analysis can prove valuable in describing a range of behaviours and associated neural activity including sensory and motor repertoires. For the non-linear analysis of biological signals, the parameters most commonly studied are the correlation dimension that shows the complexity of the system and the Lyapunov exponents that show the reactivity of the system to the deterministic external stimuli. The aim of this study was to measure the complexity of brain activity using MEG recordings in neonates born to preeclamptic and uncomplicated pregnancies, in order to determine whether non-linear MEG dynamics could be able to find out changes in these groups. Our study population consists of 40 respective term neonates who were delivered normally, without any clinical signs of brain damage. Thirty of them had a normal pregnancy and labor with normal values of Apgar scores, umbilical cord pH and birth weight, while 10 neonates had preeclamptic pregnancy. MEG recordings from neonates corresponding to normal pregnancies were of lower magnetic power spectral amplitudes (163.2 ± 22.6 fT/√ Hz) compared with those gained from neonates corresponding to pregnancies complicated with pre-eclampsia (236.7 ± 8.9 fT/√ Hz). The difference between the two groups was statistically significant ($p<0.005$). The above analysis of the MEG in neonatal preeclamptic brain shown lower dimension complexity in compare with normal neonatal brain and lower the first Lyapunov exponent, which means lower information processing. The non-linear analysis of the MEG activities in neonates may offer important perspectives to understand significant features of their brain function.

KEY WORDS: Neonatal brain, biomagnetic measurements, normal pregnancy, pre-eclampsia, perinatal asphyxia, nonlinear analysis

INTRODUCTION

In recent years there is a growing body of evidence from laboratory and clinical studies that at least 2% of newborns have been exposed to an asphyxial insult during labor and delivery, which may affect their outcome. Despite all the progress achieved in obstetric and neonatal care, intrapartum fetal asphyxia as a condition of impaired blood gas exchange leading to progressive hypoxemia and hypercapnia with a significant metabolic acidosis is still a major cause of hypoxic-ischaemic brain injury in term newborns. Early assessment of the degree of the resulting hypoxic-ischaemic encephalopathy (HIE) is essential for the clinical management and is considered a prognostic factor for the newborn's neurodevelopmental outcome. Preeclampsia is a complication of pregnancy that can cause birth asphyxia at or near term, due to influence on uteroplacental circulation, resulting in brain damage. Electroencephalography (EEG), Ultrasound examination, Computed Tomography (CT) and Magnetic Resonance Imaging (MRI) have been widely applied in high risk infants for prognostic purposes. In the last decade, Magnetoencephalography (MEG) has been utilized as an alternative method for assessing the brain function because directly records the extremely weak magnetic fields associated with electrical activity of cortical and subcortical neuronal groups, has high temporal and spatial resolution and is completely safe and non-invasive [Anastasiadis et al., 1997]. The aim of this pilot study was to measure the complexity of brain activity using MEG recordings in neonates born to preeclamptic and uncomplicated pregnancies, in order to determine whether non-linear MEG dynamics measured by dimensional complexity and first Lyapunov exponent could be able to find out changes in these groups.

METHODS

We performed a prospective study on 40 neonates (birth weight 2250 – 4100 grams) who were delivered normally between 37-41 weeks of gestation. Maternal age ranged from 16 to 39 years. Ten neonates had pregnancies complicated by pre-eclampsia delivered at our Hospital from January 1997 to December 2000 while 30 neonates had a clinically uncomplicated pregnancy randomly selected in the same time-period. All participants met the following criteria: a) gestational age >37 weeks b) normal delivery and c) no clinical sign of HIE on neurologic examination. Informed consent was obtained from all parents prior to the procedure. The study was approved by the hospital Ethics Committee. MEG recordings were obtained from the temporal region bilaterally with one-channel biomagnetometer (model 601, San Diego) from four specified points on each side of the scalp, with the babies lying supine during quiet sleep. Biomagnetic recordings from the two study populations were obtained between 24 and 72 hours after birth. The selection of the measurement points was based on the 10-20 International Electrode Placement System, with the T3-T4 standard EEG recording positions being the centers of two respective circles, and all 4 measurement points on each side being placed diametrically opposite on two vertical diameters going through T3-T4, 1cm distant from the center. The sensor was placed 3mm above each particular point. Using t-test assessed statistical analysis of our results. The non-linear analysis was estimated for the MEG signals using the proper mathematical algorithms.

RESULTS

MEG recordings from neonates corresponding to normal pregnancies were of lower magnetic power spectral amplitudes (163.2 ± 22.6 fT/√ Hz) compared with those gained from neonates corresponding to pregnancies complicated with pre-eclampsia (236.7 ± 8.9 fT/√ Hz). The difference between the two groups was statistically significant ($p<0.005$). Table 1 shows the correlation between clinical diagnostic criteria of pre-eclampsia and birth-weight percentiles for all 10 neonates of pre-eclamptic pregnancies, which had high amplitudes, cord pH between 7.14-7.19 and 1′ Apgar scores between 5-7. We notice that there is a strong correlation between the severity of pre-eclampsia with birth-weights ($p=0.003$) and MEG values ($p=0.002$) (Table 2). Table 3 presents the correlation of perinatal variables (birth weight: $p<0.0001$; gestational age: $p=0.1$; pH: $p<0.0001$ and Apgar scores: $p<0.0001$) in the two study groups. All 30 neonates in normal pregnancies had low amplitudes, birth weights over the 75th percentile, umbilical cord pH between 7.25-7.50 and Apgar scores between 7-9. The average values of D from both neonatal brains from normal and preeclamptic pregnancies are summarized in Table 4. It can be seen that neonates from preeclamptic pregnancies had a lower D at the right ($p<0.0001$) and left ($p<0.0001$) temporal regions compared the ones from normal pregnancies. It means that the chaotic activity of preeclamptic brain in the temporal area is lower than that in normal brain. The first Lyapunov exponents (L1) were significantly greater than 0 in these groups (Table 4).

The preeclamptic infants had lower values of L1 compared with the controls at the right (p=0.0002) and left (p=0.05) temporal lobes, which means lower information processing.

Table 1. Gravidae with pregnancies complicated with pre-eclampsia

Gestational age (weeks)	Pre-eclampsia	Blood pressure	Proteinuria	MEG (fT/√ Hz)	Neonatal Weight (percentile)
37	severe	200/110	2+	234	w< 10^{th}
	severe	190/95	3+	243	$10^{th} < w < 25^{th}$
	severe	210/115	3+	233	$10^{th} < w < 25^{th}$
38	severe	195/105	2+	244	$50^{th} < w < 75^{th}$
	mild	155/100	1+	228	$50^{th} < w < 75^{th}$
	mild	160/90	1+	224	$50^{th} < w < 75^{th}$
	severe	195/110	2+	243	$25^{th} < w < 50^{th}$
	mild	155/90	1+	225	$50^{th} < w < 75^{th}$
39	severe	185/115	3+	248	$25^{th} < w < 50^{th}$
	severe	210/115	2+	245	$50^{th} < w < 75^{th}$

Table 2. Correlation of pre-eclampsia's severity with birth weights and MEG values

Pre-eclampsia	Severe	Mild	Statistical significance
Birth weight (gr)	2542±191	3054±132	p=0.003
MEG (fT/√ Hz)	241±5	225±2	p=0.002

Table 3. Correlation of perinatal variables in the two study groups

Perinatal variables	Normal	Pre-eclampsia	Statistical significance
Birth weight (gr)	3653±372	2681±274	p<0.0001
Gestational age (fT/√ Hz)	38.5±1.1	37.9±0.7	p=0.1
pH	7.35±0.06	7.16±0.01	p<0.0001
Apgar	8	6	p<0.0001

Table 4. Mean MEG attractor dimension (D) and first Lyapunov exponent versus examined groups

	Right temporal		Left Temporal	
	D	L1	D	L1
Preeclamptic (10)	3.06±0.17	1.19±0.16	3.21±0.23	1.23±0.15
Normal (30)	4.19±0.21	1.49±0.13	4.23±0.25	1.42±0.24

DISCUSSION

Our study revealed the complexity in the temporal regions of neonates born with preeclamptic pregnancies. This may be due to the decreased information processing and less flexible neural networks in the area of the preeclamptic brain. It is notable the significant difference among the mean values of biomagnetic recordings from normal and pre-eclamptic pregnancies. The high spectral amplitudes in the pre-eclamptic group could be related to the comparatively lower pH values (7.14-7.19), which might affect brain function, temporarily or permanently. Our results fit in well with previous studies, in which normal states of lowered vigilance and pathological conditions showed decreased EEG dimensional complexity, whereas normal attentional states tended to increased dimensional complexity [Elbert et al., 1994]. While the first Lyapunov coefficient (L1) and attractor dimension are related, the exact nature of the relationship is unproven, it is obvious that both parameters measure different aspects of a system's dynamics. The low values of L1 in the temporal hemispheres express a decrease in the information processing and indicate less flexible neural networks in these areas [Rosenstein et al., 1993]. New techniques for the visualization of spatiotemporal dynamics in neural ensembles provide opportunities for observing coherent spatial structures, and the natural basis functions of neural population activity involved in the control of movement and perception. New developments in complex systems can be a source of power new analytical tools and insight into the dynamics of neural systems. Particularly the inference of the complexity the MEG activities in the brain may elucidate the significant features of the neonatal brain's development and function.

REFERENCES

Anastasiadis P, Anninos P, Diamantopoulos P, Sivridis E. Fetal magnetoencephalographic mapping in normal and pre-eclamptic pregnancies. J Obstet Gynaecol 1997; 17: 123-126

Elbert T, Ray WJ, Kowalik ZJ, Skinner JE, Graf KE, Birbaumer N. Chaos and physiology: deterministic chaos in excitable cell assemblies. Physiol Rev 1994 ;74:1-47.

Rosenstein MT, Collins JJ, Juca JD. A practical method for calculation largest Lyapunov exponents from small data sets. Physica D 1993; 65:117-134

Alterations in Power Distributions Reflect Symptom Changes in Schizoaffective Disorder

Schulman, J.J., Ramirez, R., Cancro, R., Ribary, U., and Llinas, R.

Department of Physiology and Neuroscience, New York University School of Medicine, New York, NY, USA

ABSTRACT

Studies have indicated that the pathological conjunction of theta (4-8 Hz) and gamma (25-50 Hz) thalamocortical activity serves as the physiological underpinning for thalamocortical dysrhythmias. Syndromes including Parkinson's disease, tinnitus, central pain, OCD, depression and schizoaffective disorder are proposed to be generated by local theta oscillations underlying negative symptoms and gamma-related positive signs. Current results demonstrate changes in theta-range localizations reflecting changes in symptom state.

Spontaneous whole-head magnetoencephalograms were recorded from subjects with schizoaffective disorder, including one who had undergone stereotactic anteromedial pallidotomy and centrolateral thalamotomy. Independent components (ICs) were derived using an algorithm based on Infomax principles. ICs with theta-range peaks were localized in a probabilistic sourcespace using a recursive weighted minimum-norm algorithm; results were interpolated onto a common brain.

Localization of activity indicated a correlation between increased symptom intensity and power distributions to medial frontal and temporal areas. Conversely, symptom diminution was mirrored by a decrease in the number and intensity of theta-range ICs and their localization to control-like locations. These results suggest the applicability of MEG to physiological phenotyping in neurological and psychiatric disorders.

KEY WORDS

Thalamocortical dysrhythmia, schizophrenia, theta, gamma, MEG, independent component analysis, multi-taper, minimum-norm

INTRODUCTION

Advances in neuroscience and innovations in signal processing have begun to provide electrophysiological models for normal cognition and its aberrations. MEG studies have shown an increase in low-frequency activation in cases of Parkinson's disease, tinnitus, depression, central pain, obsessive-compulsive disorder, and psychosis. [Llinas 1999] [Schulman 2000, 2001, 2002] [Van Marle 2002] We have conceptualized this mode of common pathophysiology – in which aberrant ongoing oscillatory activity exists in anatomically-relevant regions – as thalamocortical dysrhythmias (TCDs). In particular, the observation of theta-range oscillations is consistent with deinactivation of low-threshold Ca^{++} channels in thalamocortical circuits. Thus, the TCD syndromes may be viewed as an abnormal expression of intrinsic thalamocortical rhythms.

METHODS

Spontaneous, eyes-closed neuromagnetic activity (bandpass filtered 1-100 Hz; sample rate 508 Hz) was recorded from six subjects with chronic schizoaffective disorders (SZA). Average age was 37.8±4.01 SE; all were male, and all right-handed. Diagnoses were made by an experienced psychiatrist based on DSM-IV criteria. [American Psychiatric Association, 2000] In addition, identical recordings were performed on an age- and gender-matched group of nine controls with no reported neurological or psychiatric history. Recordings were performed with a 148-channel whole-head neuromagnetometer system (4-D Neuroimaging, San Diego CA) in a magnetically-shielded room, and electrocardiograms were recorded for heartbeat-artifact minimization. One subject was also studied following the placement of bilateral stereotactic lesions which led to marked and ongoing symptom diminution. [Jeanmonod, 2003]

Following removal of cardiac and distant-source artifacts, multi-taper spectral analysis was used to derive a spectral profile for each subject. This was quantified by a mean spectral energy (MSE) ratio which compared relative theta and alpha power by dividing the total spectral power in each of two bands by the bandwidth in Hz.

In addition, each MEG time series was processed with temporal Independent Component Analysis (ICA) using the Infomax implementation of EEGLAB. [Makeig, 1997] This blind source separation method uses an iterative approach to isolate the raw MEG signal into spatially stable and temporally independent components. Noisy channels and timeslices were removed prior to spectral calculations and ICA. A component of interest containing increased theta-range power and dipolar spatial distribution was selected for localization from each subject.

A single spherical sourcespace was constructed from a probabilistic atlas (MNI-152) and scaled to the dimensions of each subject's head. A recursive weighted minimum-norm approach, [Ramirez, 2001] based on the FOCUSS algorithm, [Gorodnitsky, 1995] was used to compute inverse solutions from the mixing matrix of the IC of interest. For visualization, results were smoothed with a three-dimensional Gaussian kernel and interpolated onto a common high resolution structural MRI previously segmented into gray and white matter and inflated with the FreeSurfer software package. [Fischl, 2002]

RESULTS

Multi-taper spectral analysis revealed group spectral differences between SZA and control groups (Figure 1a). Spectral quantification with theta:alpha MSE ratios (Figure 1b) verified that the spectral energy differences were statistically-significant (Mann-Whitney; $p<0.05$). Furthermore, localization of a normalized and averaged IC for the SZA group demonstrated theta activation in limbic and executive areas (Figure 1c).

One subject was studied on an additional occasion three months following the placement of bilateral stereotactic lesions based on independent neurosurgical criteria. The pre-surgical recording revealed a leftward shift in spectral energy, while the post-surgical spectrum for this subject was consistent with well-established control profiles. Similarly, pre-surgical theta activity recovered with ICA was localized to the limbic and frontal regions, while post-surgical theta activity was minimal, sparse, and diffusely-localized.

DISCUSSION

The theta-range oscillations observed in this study are distinct from theta activity which occurs as part of normal task responses and drowsiness. In cases of TCD, these oscillations are statically-located and persistent, though in either case, they can be generated by hyperpolarization-induced deinactivation of the low-threshold Ca^{++} conductance (I_T) in thalamocortical neurons. Furthermore, the particular localization of theta activity in the

SZA subjects studied is supported by findings of gray matter decreases in both medial frontal cortex and mediodorsal thalamus in schizophrenia-spectrum disorders. These anatomical changes are capable of inducing hyperpolarization via disfacilitation.

Our findings in the post-treatment domain further suggest that changes in global electrophysiology are the root of effective therapies, and that such changes may be observed with MEG.

ACKNOWLEDGEMENTS

Supported by the NYU SoM General Clinical Research Center (NCRR M01 RR00096) and a pre-doctoral NRSA (NINDS F31 NS42973) to JJS.

Figure 1a

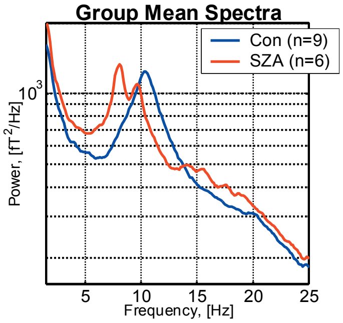

Figure 1b

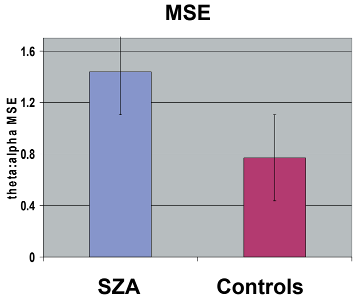

Figure 1c

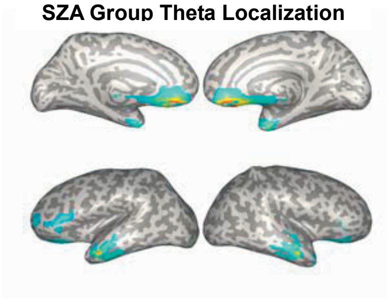

Figure 2a

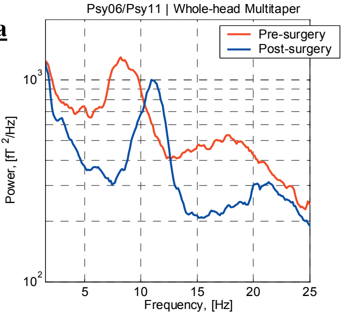

Figure 2b

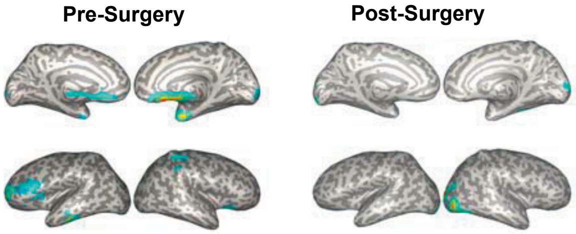

REFERENCES

American Psychiatric Association. Diagnostic and statistical manual of mental disorders. 4th ed. Washington, D.C.: American Psychiatric Association; 2000.

Fischl B, Salat DH, Busa E, Albert M, Dieterich M, Haselgrove C, et al. Whole brain segmentation: automated labeling of neuroanatomical structures in the human brain. Neuron 2002; 33 :341-55.

Gorodnitsky IF, George JS, Rao BD. Neuromagnetic source imaging with FOCUSS: a recursive weighted minimum norm algorithm. Electroencephalogr Clin Neurophysiol 1995; 95:231-51.

Jeanmonod D, Schulman J, Ramirez R Cancro R, Lanz M, Morel A, et al. Neuropsychiatric thalamocortical dysrhythmia: surgical implications. Neurosurg Clin N Am 2003; 14:251-65.

Llinas RR, Ribary U, Jeanmonod D, Kronberg E, Mitra PP. Thalamocortical dysrhythmia: A neurological and neuropsychiatric syndrome characterized by magnetoencephalography. Proc Natl Acad Sci U S A 1999; 96:15222-7.

Makeig S, Jung TP, Bell AJ, Ghahremani D, Sejnowski TJ. Blind separation of auditory event-related brain responses into independent components. Proc Natl Acad Sci U S A 1997; 94:10979-84.

Ramirez R, Horenstein C, Kronberg E, Ribary U, Llinas R. Anatomically-constrained iterative algorithm for MEG-based mapping of electrical activity. Neuroimage 2001; 14:s893.

Schulman JJ, Ramirez R, Horenstein C, Ribary U, Kronberg E, Cancro R, et al. Thalamocortical dysrhythmia in depression and obsessive-compulsive disorder. Society for Neuroscience Abstracts 2001; Program No. 111.4.

Schulman JJ, Ramirez RR, Ribary U, Kronberg E, Horenstein C, Cancro R, et al. MEG of Thalamocortical Dysrhythmia in Obsessive-Compulsive Disorder. Society for Neuroscience Abstracts. 2002; Program No. 397.2.

Schulman JJ, Zonenshayn M, Mogilner AY, Rezai AR, Kronberg E, Ribary U, et al. The role of thalamocortical dysrhythmia in chronic pain. Society for Neuroscience Abstracts 2000; Program No. 241.3.

Van Marle H, Kronberg E, Schulman JJ, Ribary U, Llinas R, Shulman A, et al. Magnetoencephalographic recordings from tinnitus patients during masking procedures. In Biomag 2002. Jena: VDE Verlag; 2002. p. 191.

Dynamic Statistic Parameter Maps of Spontaneous Alpha and Mu Rhythms

Chih-chuan Chen[1,2], Anders M. Dale[1], Eric Halgren[1,3]
[1]Athinoula A.Martinos Center for Biomedical Imaging, MGH/MIT/HMS, Charlestown , MA, USA [2]Department of Neurology,
National Taiwan University Hospital, Taipei,Taiwan, [3]Radiology, UCSD, USA

We studied the spatial-temporal evolution of spontaneous alpha and mu rhythms in humans using distributed source estimates. *Methods*: 306 channels of MEG data were collected under five states: rest with eyes closed, rest with eyes open, clenching left hand with eyes open, clenching right hand with eyes open and backward calculating with eyes open. The cortical surface was reconstructed from T1-weighted 3D-MRI, and used to constrain the noise-normalized minimum norm, yielding dynamic statistical parametric maps (dSPM) [1]. dSPM maps were calculated during sessions characterized by strong alpha and mu rhythms; noise estimates were calculated during the control states. *Results*: (1) alpha rhythm: The dSPM of alpha rhythm shows periodic activities in occipital cortex, strongest in the calcarine fissure, but with weak spread to occipito-temporal and occipito-parietal regions. This is consistent with the single dipole fitting result. (2) mu rhythm: dSPM is maximal in the central sulcus, with mu activities also in pre- and post-central sulci. The mu rhythm could be suppressed by contra-lateral and ipsilateral hand movement, although more effectively on the contralateral side. *Conclusion*: Our dSPM results suggest that alpha rhythm may be mainly generated in primary visual cortex, rather than in the occipital-parietal regions that have previously been suggested [2]. Both sensory and motor cortex may contribute to mu rhythm generation, as has been suggested by intracranial recordings [3].

Supported by NS44623.

[1] AM Dale et al, *Neuron* 2000 , 26 :55-67, [2] R Hari & R Salmelin, *TINS* 1997, 20(1):44-9 [3] J Klopp et al, *NeuroImage* 2001, 14:391-405

The influence of brain tumor treatment on pathological activity in MEG

J.C. de Munck1) , A. de Jongh1), J.C. Baayen2), R.M. Heethaar1), W.P. Vandertop2), C.J. Stam3)
VU University medical center, Amsterdam, The Netherlands, Department of
1) Clinical Physics, MEG center; 2) Neurosurgery; 3) Clinical Neurophysiology

Interictal spikes represent only a very small part of the MEG/EEG data. It has been proposed in the literature to use another pronounced property of the MEG/EEG data of patients with epilepsy: the enhanced delta band activity. It was investigated whether pathological delta activity can be localized using simple dipole models, and in how much this delta activity is influenced by tumour treatment (neurosurgery and/or radiotherapy).

MEG and MR recordings were made both before and after the treatment in 17 patients. Patients with malignant tumors exhibited more delta activity than patients with low graded tumors and meningiomas. In all patients with high grade tumors the delta power was lower after the treatment.

Preoperatively 14 clusters of equivalent dipole sources describing focal activity were found in 12 out of 17 patients. Thirteen of these clusters were located near the tumor, and one cluster near an edema border. After the operation 13 such clusters were found in the same 12 patients (one exception). Eleven clusters were located near the lesion border and 1 cluster near the edema border. The shift in source locations after operation was in general considerably smaller than the dimension of the preoperative tumors. This finding indicates that similar areas generate the pre- and postoperative delta activity. Furthermore, focal delta sources were found in a case without tumor recurrence and also in cases that most tumor tissue was removed. These findings suggest that the pathology underlying the slow waves is the irreversible structural damage to the surrounding white/grey matter.

MEG Imaged Brain Activation during the Transition from Wake to Sleep

Drake[1], CL, Moran[2], JE, Scofield[1], H, Tepley[2,3], N, Roth, T[1]
[1]Henry Ford Hospital Sleep Disorders and Research Center Detroit, Michigan, USA.
[2]Henry Ford Hospital, Detroit, Michigan, USA. [3]Oakland University, Rochester, Michigan, USA.

Neuroimaging studies show differences in brain activity between wake and specific sleep stages. However, few studies have measured the patterns of change during the transition form wake to sleep reported in this MEG imaging study. Further, we describe the use of ICA techniques for both artifact elimination and imaging of MEG data to obtain changes in brain activation patterns that occur during the transition from awake to sleep.

Six normal healthy subjects (mean age 31 ± 9 years, 3-female) were studied. Both electroencephalographic (EEG) and magnetoencephalographic (MEG) data were recorded simultaneously during a 1-hour nap (10:30-11:30AM). For brain imaging analysis, one 15-second epoch of wake, one 15-second epoch of sleep and one 15-second epoch of the transition to sleep (approximately 7.5 seconds of wake and 7.5 seconds of sleep) was extracted from the MEG recording for each subject. Imaged activity was averaged across subjects for wake, transition, and sleep states. In addition, a state independent reference level of brain activation was obtained by averaging the imaging results across subjects and states.

Compared to the reference level of brain activation, during sustained wakefulness, activity in the occipital cortex and region of the posterior thalamus dominated subjects averaged brain activation. During the transition from wakefulness to sleep onset, this activation pattern changed to one showing greater activation in the right frontal cortex and region of the anterior thalamus. During stage 1 sleep, maximum activity was primarily in brain regions near the anterior thalamus.

Acknowledgement Research supported by NIH/NINDS Grant RO1-NS30914.

The temporal dimension of functional links

K. Linkenkaer-Hansen
Netherlands Institute for Brain Research, The Netherlands

The conscious perception of sensory stimuli depends on distributed processing in dynamically linked networks in anatomically distinct areas of the brain—a process that in most instances require only a few hundred milliseconds. In contrast, neuronal operations that originate largely endogenously require a great deal of integrity over time scales of typically tens of seconds or even minutes. Examples include attentional processes, or the production and understanding of language. Functional neuroimaging has, nevertheless, paid little attention to the dynamic patterns of neuronal activation on time scales longer than a few seconds. In this talk I describe a variety of filtering and correlation-analysis techniques that have proved useful in revealing functional links in MEG signals that are distributed over time scales of seconds to hundreds of seconds [1, 2]. Moreover, I will present evidence that long-range temporal correlations analysis may be useful in detecting abnormal dynamics of ongoing oscillatory activity in patients suffering from neurodegenerative diseases. In conclusion, by analyzing the correlation structure of the amplitude envelope of neuronal oscillations we may detect functional dependencies embedded in complex physiological signals such as the ongoing MEG. It is argued that long-range functional links in time are important for the integrity of neuronal processing and possibly crucial for a variety of cognitive processes. Financial support from the Danish Research Agency is gratefully acknowledged.

[1] Linkenkaer-Hansen, K., Nikouline, V.V., Palva, J.M., Ilmoniemi, R.J. 2001. Long-range temporal correlations and scaling behavior in human brain oscillations. J. Neurosci 21, 1370–1377. [2] Nikouline, V.V., Linkenkaer-Hansen, K., Huttunen, J., Ilmoniemi, R.J. 2001. Interhemispheric phase synchrony and amplitude correlation of spontaneous beta oscillations in human subjects: a magnetoencephalographic study. NeuroReport 12, 2487–2491.

The effect of body mass on insulin sensitivity in the cerebral cortex of humans

H. Preissl[1], O. Tschritter[1], H. Marx[1], R. Frost[1], A. Fritsche[1], W. Lutzenberger[1], H.-U. Häring[1], M. Stumvoll[2], N. Birbaumer[1]
[1]University of Tübingen, Germany, [2]University of Leipzig, Germany

Subjects with type 2 Diabetes show Insulin resistance in several peripheral tissues. In contrast, it is not know whether there is a similar effect in the central nervous system (CNS). In mice knock-out of the CNS insulin signal leads to hyperphagia, obesity and insulin resistance. To investigate the role of cortical insulin effects in human obesity we measured spontaneous and evoked auditory cortical activity.

10 lean (m/f: 6/4, BMI 21±1) and 15 overweight (m/f: 8/7, BMI 30±1) subjects were studied in a placebo controlled design. Cortical activity was recorded with a whole-head magnetoencephalographic (MEG) system. The MEG recordings were performed on 2 different days (starting 7 am) separated by 1 week in-cluding three levels of insulin under constant glucose level or saline solution (placebo). When a stable state after the insulin infusion was reached spontaneous and evoked magnetic fields (auditory mismatch) were recorded. Difficulties in weight control were evaluated using a visual analogue scale (VAS). We found significant effects in the theta band (TW) for spontaneous activity and for the mismatch negativity (MMN).

In lean subjects TW and MMN showed a significant enhancement during insulin administration compared to the placebo condition. In overweight subjects there was no change. The net change in TW was negatively correlated with VAS and positively correlated with the insulin sensitivity index (ISI) for peripheral glucose uptake. In a multivariate analysis BMI was correlated with TW while ISI was not.

Cortical insulin response is different in lean and overweight human subjects. Self reported tendency to weight gain is associated with low insulin mediated changes in cortical activity, suggesting that insulin resistance of the CNS plays a key role in development of human obesity and insulin resistance.

This work is supported by the DFG (Clinical Research Group 114).

Tinnitus related distress correlates with fronto-temporal alpha reduction and delta enhacement as measured by magnetencephalography

N. Weisz, S. Moratti, A. Keil, M. Meinzer, T. Elbert
Dept. of Psychology, University of Konstanz, Germany

The neurophysiological mechanisms underlying tinnitus perception are not well understood. Surprisingly, there have been no group studies comparing abnormalities in the ongoing, spontaneous neuronal activity in subjects with and without tinnitus perception. Methods: A data stream of five minutes, was recorded with a whole head neuromagnetometer under a resting condition from 17 tinnitus sufferers and 16 normal hearing controls. After noise-reduction and for eye-artefacts correction, the data was transformed to source space by applying the Minimum Norm Estimate [1,2]. The spectral power at each source was investigated by calculation of mean FFTs. Results: Tinnitus sufferers produced more delta (1.5-4 Hz) in the MEG, generated in temporal regions than normal controls. At the same time a decrease in the alpha (8-12 Hz) band could be observed over the same regions in the patient group. Moreover, correlations with tinnitus-related distress revealed strong associations with abnormalities in both frequency bands, particularly in right temporal and left frontal areas. Overall, effects were stronger for the alpha than for the delta frequency band. Conclusion: Tinnitus is associated with marked changes in the neuromagnetic spontaneous activity pattern. It remains to further studies to explore whether the regional pattern found here might indicate a tinnitus-related cortical network. This study was supported by a grant from the Deutsche Forschungsgemeinschaft (EL 101/20). We thank Thomas Hartmann for help during data acquisition and Horst Böttcher (ProAkustik) for providing a high resolution audiometer.

[1] Hämäläinen M, Hari R, Ilmoniemi RJ, Knuutila J, Lounasmaa OV: MEG - theory, instrumentation, and applications to noninvasive studies of the working human brain. Reviews of Modern Physics 1993; 65: 413-497. [2] Hauk O, Keil A, Elbert T, Muller MM: Comparison of data transformation procedures to enhance topographical accuracy in time-series analysis of the human EEG. J Neurosci Methods 2002; 113: 111-22.

Working Memory Processing In Normal Subjects and Subjects with Dyslexia

Bowyer S.M.[1,2,3], Lajiness-O'Neill R. [1,3], Weiland B. [1,2], Mason K.M. [1], and Tepley N. [1,2]

[1]Henry Ford Hospital, USA; [2]Oakland University, USA; [3]Wayne State University, USA.

ABSTRACT

MEG was used to determine the neuroanatomical location of working memory processes and their underlying neuronal pathways. Differences between subjects with dyslexia and normal readers were studied during a spatial and verbal working memory tasks. Differences in regions of activation between normal subjects and subjects with dyslexia are described. This study demonstrates the possibility of identifying differences in memory processing in subjects with and without learning disorders and creates an avenue for memory-based remediation and non-invasive testing.

KEYWORDS: Memory, Dyslexia, MEG, MR-FOCUSS

INTRODUCTION

Early studies of verbal and spatial working memory processes described the organization as content specific and as occurring through distinct processing pathways or streams [Courtney, 1997; D'Esposito, 1997].]. For example, verbal working memory is more lateralized to left hemispheric regions and spatial working memory is more lateralized to the right hemisphere. In addition, recent fMRI investigations have also suggested that process specific organization occurs [Crosson, 1999; D'Esposito, 1998]. That is, encoding and storage may be more strongly lateralized to left rather than right hemispheric processes, regardless of whether it is a verbal or visual task. Working memory, a critical aspect of initial learning, may reorganize in a more contralateral manner in patients with learning disorders, consistent with findings in episodic learning and facial memory in epilepsy [Golby, 2002]. MEG [Pizzagalli, 2002; Ioannides, 2000; Halgren, 2000] has been used to explore the mesial temporal aspects of memory functioning such as object and facial memory, which have greater hemispheric specialization and localization. Working memory was mapped with MEG in patients with and without dyslexia to determine if similar areas of activation suggest similar substrates for working memory or if contralateral reorganization of these processes occurs in dyslexia. The difference between results from fMRI and MEG involve the temporal resolution and the activation of source points. fMRI results display a static picture that incorporates source activity averaged over a long time interval. MEG can provide a precise picture of neuronal activation at different instants of both memory and language processing. MEG results illuminate the pathways of cortical processing involved in memory. MEG also provides information regarding the onset of encoding and retrieval processes so that we can examine the question regarding content relative to process organization, and whether this is different in individuals with dyslexia.

METHODS

Our 148 channel whole head Neuromagnetometer (4D Neuroimaging) was used to measure magnetic fields from five individuals with dyslexia, between 9 and 50 years of age and five age, gender, and handedness, matched controls. Measurements were taken inside a magnetically shielded room located in the Neuromagnetism Laboratory at Henry Ford Hospital (HFH), utilizing a protocol approved by HFH's Internal Review Board (IRB). All subjects were administered the Edinburgh Handedness test [Oldfield, 1971] and underwent a neuropsychological evaluation to diagnose dyslexia. Individuals with dyslexia were recruited by a Ph.D. level neuropsychologist from the Division of Neuropsychology in the Department of Behavioral Health at HFH. The diagnosis of dyslexia was determined following the Diagnostic and Statistical Manual of Mental Disorders [American Psychiatric Association, 1994] diagnostic criteria that include individuals who display reading achievement (measured by individually administered standardized tests of reading accuracy or comprehension) substantially below that normally expected of persons of similar chronological age, measured intelligence, and age appropriate education. Normal (reading) individuals were used for the controls. Members of this group had normal, age appropriate, reading ability. They were also matched based on age, gender, handedness, and estimate of intellectual ability to subjects with Dyslexia. Normal reading individuals underwent the same neuropsychological evaluation as subjects with Dyslexia.

Each subject signed an informed consent form approved by the HFH Internal Review Board. In the case of children, a parent/guardian give informed consent. Each subject was prepped for the MEG study in the usual manner [Bowyer, 2003]. The subject then lay comfortably on the bed inside the magnetically shielded room. (A parent was allowed to remain with a minor child inside the shielded room. After removing all metallic objects, the parent remained seated in a corner of the room.) Standard automatic probe position routines were used to locate the subject's head with respect to the neuromagnetometer detector coils. The neuromagnetometer helmet containing the detector array was placed around the subject's head in close proximity to the skull surface. The subject was asked to avoid excessive eye blinks and body movements during data collection. Data collection runs lasted 8-12 minutes. Each subject was monitored by video camera and two-way audio speaker system during the time he/she was in the shielded room. All MEG data was band-pass filtered 0.1 to 100 Hz, and digitally sampled at 508.63 Hz.

MEG Test 1: Spatial working memory was studied by measuring the subject's MEG field responses to visual presentations of a series of white squares presented for 2 seconds every 3 seconds [D'Esposito, 1998]. A square was presented in one of 12 different locations around an imaginary circle (all 12 locations are shown in figure 1). During each presentation the subject was asked to mentally determine whether each square being presented was in the same position as the square presented two prior images ago. Subjects were instructed to respond only to displays in which this was the case by pushing a keypad with their right fore finger. This test was made up of two trials lasting ~7-minutes each.

MEG Test 2: Verbal working memory was studied by measuring the subject's MEG field responses to visual presentations of a series of upper case letters (figure 2) for 2 seconds presented every 3 seconds [D'Esposito, 1998]. During each presentation the subject was asked to mentally determine whether the letter being presented was the same as the letter presented two images ago. Subjects were instructed to respond only to correct targets by pushing a keypad with their right finger. This test was made up of two trials lasting ~7-minutes each.

Data Analysis:. Data analyses were performed using a PC after the data had been filtered 1-50 Hz and exported

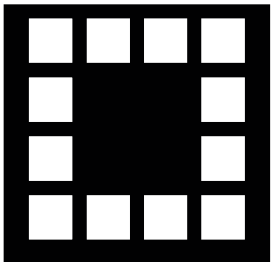

Figure1. Spatial working memory stimuli.

A

Figure2. Verbal working memory stimulus.

from the Sun acquisition computer. The averaged epoch data was analyzed with MR-FOCUSS [Moran, 2001] a non-linear current density imaging technique. For each subject the latency (in ms), location (x,y,z coordinates) and average amplitude of response (nanoAmp-meter) was extracted from the MR-FOCUSS imaging results for each memory process step. Also an image of the averaged cortical activity from 0-600 ms was created to determine the most dominant cortical areas during these tasks. To correlate MEG areas of cortical activity with specific anatomical structures, each subject's MRI was co-registered with their head digitization points collected at the beginning of the MEG study.

RESULTS

Cortical activation between 0-650 ms was analyzed by MR-FOCUSS, to determine the latency and source of neuronal activity of spatial and verbal working memory processes. All subjects showed occipital lobe activity at ~100ms after onset of visual stimulation in both memory tasks, this is consistent with visual activation. Analysis of the location of activity in the subjects without dyslexia during the spatial working memory showed cortical activity at approximately 200 ms after stimulus onset in the right superior temporal gyrus (STG) and right angular gyrus (AG). Subjects with dyslexia were similarly activated with a slight delay of approximately 20 ms. These latency and location differences were not statistically significant between the subjects with and without dyslexia (p=0.37, student t-test).

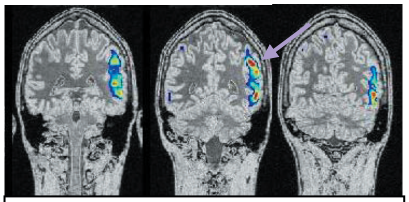

Figure 1. MR-FOCUSS analysis of the MEG recordings from a subject without dyslexia during the verbal working memory task. Averaged MEG image activation results of cortical activity, over 30 ms from 200-230ms after onset of stimuli. Note the cortical areas of activation in the left hemisphere (arrow).

During the verbal working memory task, activity was seen in the **LEFT** STG and left AG, in subjects without dyslexia, at approximately 200ms after stimulus onset. Figure 1 displays the cortical localization of averaged activity from 200-230 ms in one subject. Subjects with dyslexia were not similarly activated. Activation was in the **RIGHT** STG and right AG. Figure 2 displays the cortical activation seen in a subject with dyslexia. Note the activity is in the opposite hemisphere as the normal control seen in figure 1. These differences were statistically significant between the subjects with and without dyslexia (p=0.001, student t-test).

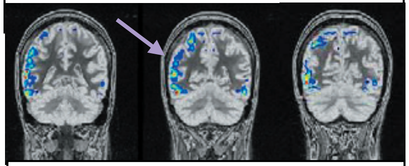

Figure 2. MR-FOCUSS analysis of the MEG recordings from a subject with dyslexia during the verbal working memory task. Averaged MEG image activation results of cortical activity, over 30 ms from 200-230ms after stimulus onset.Note the cortical areas of activation in the right hemisphere (arrow).

DISCUSSION

This study supports the hypothesis that there are differences in how memory is proccessed in subjects with dyslexia compared to normal reading subjects. The current findings reveal a core deficit in verbal, but not nonverbal working memory in dyslexia as demonstrated by MEG. This suggests that the addition of intervention modalities to specifically address auditory attention and working memory in conjunction with traditional methods used to treat phonological deficits should be considered in treatment. It also demonstrates the ability of MEG, utilizing MR-FOCUSS, to detect cortical pathways involved in processing memory. Further studies of MEG data may reveal the cortical network involved in memory processing and possibly provide a key to the variants of dyslexia observed clinically. MEG may be able to discern the more accurate theoretical model of memory. The promise of this study is that biomagnetic field mapping will increase our understanding of memory, a critical aspect of initial learning.

ACKNOWLEDGEMENT: This research was supported by NIH/NINDS Grant RO1-NS30914 and LEARN.

REFERENCES

American Psychiatric Association, Committee on Nomenclature and Statistics: Diagnostic and Statistical Manual of Mental Disorders, 4th Edition, American Psychiatric Association, Washington, D.C., 1994.

Bowyer SM, Mason K, Tepley N, Smith BJ, Barkley GL. MEG Validation Parameters for Clinical Evaluation of Interictal Epileptic Activity. J Clin Neurophysiol 20(2):87-93, 2003.

Courtney SM, Ungerleider LG, Keil K, Haxby JV. Transient and sustained activity in a distributed neural system for human working memory. Nature. 10;386(6625):608-11, 1997.

Crosson B, Rao SM, Woodley SJ, Rosen AC, Bobholz JA, Mayer A, Cunningham JM, Hammeke TA, Fuller SA, Binder JR, Cox RW, Stein EA. Mapping of semantic, phonological, and orthographic verbal working memory in normal adults with functional magnetic resonance imaging. Neuropsychology. 13:171-87, 1999

D'Esposito, Ballard, Aguirre & Zarahn, Human prefrontal cortex is not specific for working memory: a functional MRI study. Neuroimage 8:274-282, 1998.

Golby, A.J., Poldrack, R.A., Illes, J., Chen, D., Desmond, J. E., Gabrieli, J.D. Memory lateralization in medial temporal lobe epilepsy assessed by functional MRI. Epilepsia 43: 855-863, 2002.

Halgren , E, Raij T, Marinkovic K, Jousmaki V, Hari R. Cognitive response profile of the human fusiform face area as determined by MEG. Cereb Cortex 10: 69-81, 2000.

Ioannides AA, Liu LC, Kwapien J, Drozdz S, Streit M. Coupling of regional activations in a human brain during an object and face affect recognition task. Human Brain Mapping 11:77-92, 2000.

Moran JE, Bowyer SM, Tepley N: Multi-Resolution FOCUSS source imaging of MEG Data. 3rd International Symposium on Noninvasive Functional Source Imaging within the Human Brain and Heart, Biomedizinische Technik 46, 112-114, 2001.

Oldfield RC: The assessment and analysis of handedness the Edinburgh Inventory. Medica Neuropsychologia. 9:97-113, 1971.

Pizzagalli DA, Lehmann D, Hendrick AM, Regard M, Pascual-Marqui RD, Davidson RJ. Affective judgments of faces modulate early activity (approximately 160 ms) within the fusiform gyri. Neuroimage, 16:663-377, 2002

Neural Correlates of Event Related Distractions During A Driving Task Using MEG

Bowyer S.M.[1,2,3], Hsieh L.[2], Moran J.E.[1], Chiang Y.R.[2],Young R.A.[2,4], Tepley N,[1,3]

[1]Henry Ford Health Systems, USA; [2]Wayne State University, USA; [3]Oakland University, USA; [4]General Motors, USA.

ABSTRACT

Performance of a secondary task, such as a cell phone conversation, may change attention to an automobile driving task. In this study, MEG imaging was applied to an automobile driving simulation paradigm to identify the cortical regions engaged in the primary driving task. Subjects viewed a driving video and responded (foot pedal) to red light stimuli (events) presented either centrally or peripherally in the driving scene. Cortical activation was imaged from MEG data averaged on the foot pedal response. MEG temporal resolution enabled the determination of sequential cortical activations. Orbital frontal gyrus activation was observed throughout the interval. Red light onset evoked occipital cortex activity that was followed by activation in the superior frontal gyrus and anterior cingulate gyrus. Peaks of motor and pre-motor cortex activation were detected during eye fixation movements (light on), and motor activity in the precentral gyrus preceding foot and leg activation of the pedal response pad. This action turned off the light and produced a visual evoked response in the occipital cortex. Occipital activation occurred when the light was turned off with the pedal response. These were brief intervals and correlated with known locations for visual and specific motor cortex locations. Frontal activation was dominant throughout this driving task with prominent peaks associated with the red light onset and the pedal push. Our findings suggest driving tasks recruit neural systems known to be involved in visual-motor multimodal processing and integration. The use of event-related MEG in investigating neural processing during simulated driving tasks is quite promising.

KEYWORDS: Driving, Attention, MEG, MR-FOCUSS

INTRODUCTION

An essential issue for human factors research is to examine and evaluate the design of human-machine interfaces for the safe and efficient operation of complex equipment under multi-tasking conditions [Russo, 2004]. Multi-tasking is required for both primary driving (steering, braking, navigation) and secondary tasks (e.g. a cell phone conversation). Very little is currently known about how the brain functions at the neuronal level during driving tasks with or without distractions from non-driving related in-vehicle devices. This has proven to be a difficult question to answer with indirect measurement techniques. For example, self-reports of attending to the road require that drivers be aware of being distracted – and yet drivers may be unaware that they are missing things on the road [Rensink, 1997]. Measurements of eye movement behavior cannot account for drivers who look right at something and do not see it [Underwood, 2003]. Response time measurements are purely behavioral, and do not elucidate underlying neural mechanisms [Zheng, 2002]. MEG studies of driving performance have not been attempted until now. To determine exactly how and why the performance of secondary tasks such as answering a cell-phone and conversing using a hands-free telematics system can affect primary driving requires knowledge of neural pathways involved in these tasks. Design of a telematics or navigation system to reduce driver distraction, or improve situation awareness probably cannot be accomplished if the fundamental nature of driver distraction is not known. The scientific goal of this study was to determine the neural basis of mental attention shifts that underlie driver errors (i.e., driver distraction). Hopefully, this will provide insights on brain mechanisms that can be used to develop telematics or navigation systems with less impact on driving awareness.

METHODS

Our 148 channel whole head Neuromagnetometer (WH2500 Magnes, 4D Neuroimaging), was used to measure magnetic fields in five individuals, between 30 and 55 years of age (4 females) all of whom possessed a current driver's license. Measurements were taken inside a magnetically shielded room located in the Neuromagnetism Laboratory at Henry Ford Hospital (HFH).

Details of the MEG study: Each subject signed an informed consent form approved by the HFH Internal Review Board. Subjects were prepped for the MEG study with magnetic dipole coils fixed to the subject's head [Bowyer, 2003]. These coils were activated before and after tests to generate signals for calculating the location of the subject's head with respect to the neuromagnetometer detector array. The subject then lay comfortably on the bed inside the magnetically shielded room with the neuromagnetometer array surrounding the subject's head in close proximity to the skull surface. A mirror system was used to enable the subject to view projected driving video. Two red LEDs were affixed to the viewing screen, one in the lower central region, and the second one on the left side of the screen (Fig 1). The subject was asked to avoid excessive eye blinks and body movements during data collection. Data collection runs lasted approximately 4 minutes. Each subject was monitored by video camera and two-way audio speaker system during the time he/she was in the shielded room. The MEG data were band-pass filtered 0.1 to 100 Hz, and digitally sampled at 508.63 Hz.

MEG Test: While in a supine position each subject attended to surrounding vehicle activity, traffic signals, signs and city scenery in a driving video projected directly in front of him/her. At random intervals either the central or peripheral red light stimulus was turned on and the subject was required to detect the light and push a foot pedal with his/her right foot. Subsequent pedal activation turned the light off and produced a click sound. For the duration of time between turning the light on, to pedal push, a trigger high code was recorded simultaneously with the MEG data. A different code was used for central and peripheral lights. There were 40 red light stimuli during each study. The test was repeated three times to obtain a total of 120 pedal activation events.

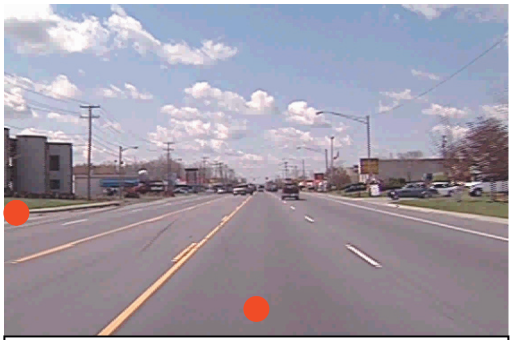

Figure 1. Driving scene and red lights (on) as viewed by the subject.

MRI Scan: To correlate MEG areas of cortical activity with specific anatomical structures, each subject's MRI was co-registered into each subject's head digitization points collected at the beginning of the MEG study [Bowyer, 2003]. The techniques for co-registration of MEG and MRI are well established and used in all HFH clinical MEG studies. This allows precise correspondence between anatomical structures and MEG areas of cortical activation. The MRI scan was performed on a 3-Tesla GE whole body MRI scanner. This volumetric scan was a 3D inversion recovery spoiled gradient echo sequence with TE:4.5ms, TI:300ms, and TR:10.4 ms, the imaging matrix was 256x256x200.

Data Analysis: MEG data was analyzed using MR-FOCUSS [Moran 2001, Bowyer 2004] for imaging MEG data to a cortical model of the subject's brain created from the MRI image sequence. For each of the three runs, the 40 windows of MEG data centered on the pedal push response were averaged. Next, the three runs for each subject were averaged and imaged using MR-FOCUSS. For these subjects, the sequence of image activity included extended source activation in the frontal cortex and focal activation events in other brain regions. The imaging results were combined into a single five-subject average by rescaling x,y,z coordinates of imaged activity for each subject to a common MRI head model.

RESULTS

Cortical activation between –500 and 500 ms of pedal activation was imaged by MR-FOCUSS. In Fig. 2, the average MEG data for all five subjects is displayed. The high frequency component in these data has a frequency of 28 Hz and was primarily imaged in the right motor and premotor cortex. In some subjects this component was more prominent than others. During the entire epoch the orbital frontal gyrus activation was active with peaks associated with light onset and pedal activation. In Fig. 3, average brain activation for one subject is shown. Red light on (t=-580ms) evoked occipital cortex activity (Fig. 4a), followed by activation in the superior frontal gyrus and anterior cingulate gyrus (t=-470ms) (Fig. 4b). Motor activity (t=-270ms) in the precentral gyrus (Fig. 4c), corresponding to foot and leg control was followed by foot pedal response pad (t=0). This action turned off the light and produced a visual evoked response (t=95ms) in the occipital cortex and a bilateral auditory response (t= 111ms) in auditory cortex. MEG temporal resolution enabled the determination of sequential cortical activations. Occipital activation was seen with light on, and light off. Motor cortex activation was detected during eyeball movement (light on), and foot movement. These were brief intervals and correlated well with known locations for visual and specific motor cortex locations. Frontal-parietal networks were dominant during the driving task.

DISCUSSION

Our findings suggest driving tasks recruit neural systems known to be involved in visual-motor multimodal processing and integration. The use of event-related MEG in investigating neural processing during simulated driving tasks is quite promising. Further studies of MEG involving simulated cell phone conversations may reveal the cortical network involved in driver distraction during telemetric distractions.

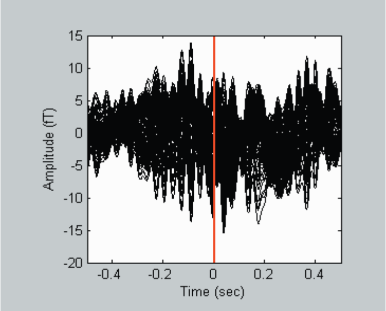

Figure 2. 148 channels of averaged MEG data from all five subjects average on pedal response.

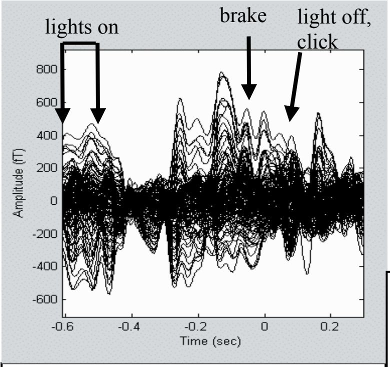

Figure 3. MEG graph of all 148 MEG channels with significant events marked from one subject.

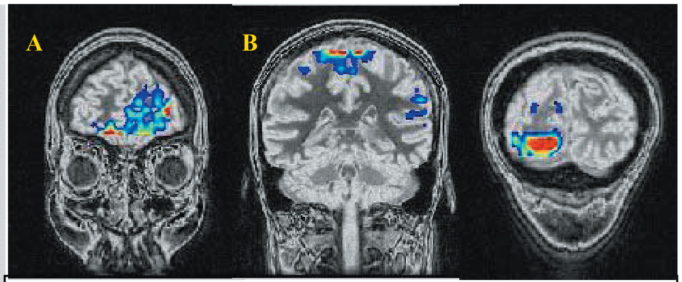

Figure 4. MR- FOCUSS localizations of activity in A) the frontal lobe (t= -300ms), followed by B) activity in the motor cortex (t= -180ms), followed by C) visual cortex activation (t= 80ms) corresponding to light off from subject in fig. 3.

ACKNOWLEDGEMENT: This research was supported by NIH/NINDS Grant RO1-NS30914.

REFERENCES

Bowyer SM, Mason K, Tepley N, Smith BJ, Barkley GL. MEG Validation Parameters for Clinical Evaluation of Interictal Epileptic Activity. J Clin Neurophysiol 2003, 20(2):87-93.

Bowyer SM, Moran JE, Mason KM, Constantinou JE, Smith BJ, Barkley GL, Tepley N. MEG Localization of Language Specific Cortex Utilizing MR-FOCUSS. In press Neurology June, 2004.

Moran JE, Bowyer SM, Tepley N: Multi-Resolution FOCUSS source imaging of MEG Data. 3rd International Symposium on Noninvasive Functional Source Imaging within the Human Brain and Heart, Biomedizinische Technik 2001; 46:112-114.

Rensink RA, O'Regan JK, Clark JJ. To see or not to see: The need for attention to perceive changes in scenes. Psychological Science, 8(5):368-373, 1997.

Russo MB, Sing H, Santiago S et. al. Visual Neglect: Occurrence and pattern in pilots in a simulated overnight flight. Aviation, Space, and Environamental Medicine 2004; 75:4:323-332.

Underwood G, Chapman P, Brocklehurst N, Underwood J, Crundall D. Visual attention while diving: sequences of eye fixations made by experienced and novice drivers. Ergonomics 2003; 46(6):629-646.

Zheng XS, McConkie GW, Tai Y. Dynamic monitoring of traffic flow: the driver's situation awareness. In Proceedings of 2nd Human Performance, Situation Awareness and Automation Technology, Daytona FL 2002.

An MEG Study of the Spatiotemporal Dynamics of Feature Binding

Filbey, F. M., Holroyd, T., Slack, K., Maltzman, L., Coppola, R., Sunderland, T., and Cohen, R. M.

National Institute of Mental Health, USA

ABSTRACT

Feature binding (FB) is the memory formation of a whole event from multiple parts. Previous literature, mostly from functional magnetic resonance imaging (FMRI) studies, show that FB processes elicit a neural circuit involving hippocampal, thalamic, and fronto-temporo-parietal areas. This is the first study, to our knowledge, that investigates FB using MEG. Thirteen healthy volunteers were presented with a FB task previously described [Mitchell, 2000] while a whole cortex MEG system recorded neural activities during one- and two-feature memory challenges. Synthetic aperture magnetometry analysis was used to localize sources of activities in the α, β, γ and θ bands during working memory (WM) for one feature and WM for two features. As expected, sources of activation during FB were observed in the thalamus, fusiform gyrus, parietal lobe, and dorsolateral prefrontal cortex, which support the FMRI literature. Additional significantly activated areas during FB were found in the parahippocampal gyrus, cingulate gyrus and caudate nucleus.

KEY WORDS

MEG, memory, thalamus, cingulate gyrus, dorsolateralprefrontal cortex, parietal lobe, caudate nucleus, parahippocampal gyrus

INTRODUCTION

Working memory (WM) has been widely studied in the functional magnetic resonance imaging (FMRI) literature. Of those key brain regions associated with WM functions, the dorsolateral prefrontal cortex (DLPFC; BA 8, 9, 45, 46, 47.) is thought to underlie organization, maintenance and manipulation of information [Levy, 2000], and the medial temporal cortex particularly the anterior portion of the hippocampus [Mitchell, 2000] and the posterior parietal cortex, particularly the intraparietal (IPS) to be associated with tasks requiring feature binding [Donner, 2002]. In a combined EEG-FMRI study, Kraut et al. reported γ synchronization in the thalamus, particularly in the pulvinar, during FB [Kraut, 2003]. The same was found by Ward et al. in a patient with unilateral damage to the rostral part of the pulvinar. In this case study, they reported that damage to the pulvinar led to errors in FB, in this case, of shape and color [Ward, 2002]. The aim of this study is twofold. The first goal is to characterize the dynamics of neural activity related to FB. Secondly, this study examines the use of MEG as a tool for the investigation of processes that have previously been reported in the FMRI literature, such as FB. MEG provides a finer temporal resolution than FMRI, and with current development in MEG data analysis (e.g. source mapping techniques), comparable spatial resolution.

METHODS

Continuous MEG signals sampled at a rate of 600 Hz were recorded using a 275-channel third-order gradiometer whole-cortex CTF Omega 2000 system (VSM MedTech Ltd., Coquitlam, Canada) from 13 healthy, right handed, seated controls (mean age = 26.4; 6 females) while they performed a previously described FB task [Mitchell, 2000]. Subjects participated in three separate runs of 510 s each. Each run contained sequential presentations of two of the three FB conditions. In the object (OBJ) and location (LOC) conditions, Ss were instructed to remember only the objects or the locations of the objects within a nine-square grid, respectively. In the combination condition (COMBO), Ss were asked to remember both the objects and their locations. For each 17 s trial, Ss were asked to respond to a single probe by button-pressing. Data analysis was carried out by a source mapping technique called synthetic aperture magnetometry (SAM) using CTF software. The data was parsed into control and working memory (WM) epochs. Periods prior to stimuli (6.04 seconds) were considered control epochs; WM epochs were those prior to the test cue (8.04 seconds). Changes in power between control and WM epochs were measured in the θ (3.5 – 7 Hz), α (7.5 – 13 Hz), β (14 – 30 Hz), and γ (30 – 80 Hz) bands. Following SAM analysis, the data were normalized into z-scores and transformed into Talairach space using Analysis of Functional NeuroImages (AFNI; Cox, RW). To look for the effect of feature binding, an analysis of variance (ANOVA) was performed to compute differences in cortical power between FB and OBJ plus LOC. Maps of statistically significant power changes were displayed on individual anatomical scans acquired using a magnetization prepared rapid gradient (MP-RAGE) sequence on a 3.0 Tesla Signa MRI scanner (124 x 1.2 mm slices, TR = 9.7 ms, TE = 4 ms; GE Medical Systems, Milwaukee, WI).

RESULTS

Changes in power appeared to be significantly greater ($F=3.16$, $p<0.05$) during the FB conditions (COMBO) compared to both non-FB conditions (OBJ, LOC) in several areas. Increased θ-band power was found in the L thalamus, L parahippocampal gyrus, and L and R anterior cingulate. De-synchronization in θ activity associated with FB was found in the L pulvinar, R inferior parietal lobe, and R posterior cingulate. In the γ-band, synchronization in the R thalamus, L fusiform gyrus, and L dorsolateral prefrontal cortex (DLPFC / BA 46), in addition to de-synchronization in the L caudate and R cingulate gyrus were found to correspond with FB. In the α-band, FB was associated with increased power in the R parahippocampal gyrus, L DLPFC (BA9), while de-synchronization was found in the R superior parietal lobe, R caudate and L posterior cingulate gyrus. β-band synchronization was found in the L DLPFC (BA 8), while de-synchronization in the R superior parietal lobe appeared to underlie FB. Synchronization in the L DLPFC (BA 8, 9 and 46) during FB was found in the α, β and γ bands. On the other hand, consistent de-synchronization was found in the R parietal lobe in the θ, α and β bands.

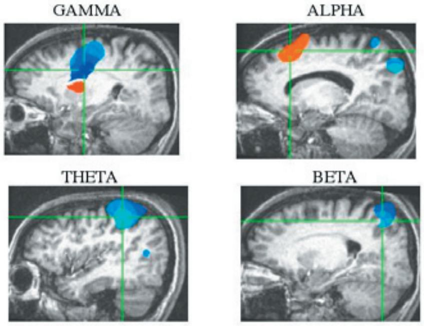

Figure 1. The largest sources per band during FB are: γ = R cingulate gyrus (27, -7, 32); α = L DLPFC (BA 6) (-16, 23, 55); θ = R inferior parietal lobe (41, -41, 51); β = R superior parietal lobe (22, -70, 46).

DISCUSSION

These MEG findings indicate similar regions of neural activities during FB processes previously reported in the FMRI literature. In addition to those areas previously identified in fMRI studies, activity in the cingulate gyrus and caudate nucleus were also found. The cingulate gyrus has been shown to be involved in attention control and management [Luks, 2002], and response monitoring [Milham, 2002]. In a study by Postle, the caudate nucleus was reported to be a key area in spatial WM. It was postulated that the caudate is responsible for the integration of spatial information and motor response preparation [Postle, 2003]. Of interest is the synchronization across multiple frequency bands in the L DLPFC and de-synchronization in the R parietal lobe during FB. The DLPFC is well known to underlie working memory processes, particularly in the maintenance and manipulation of coded information. The parietal area has also been linked to FB processes. It is posited that the parietal lobe plays a role in the efficiency of attention [Nobre, 2003]. Thus, it is not surprising that both of these regions were robustly activated in several of the frequency bands. Although we did not find a significant difference in hippocampal activation as expected, an increase in power in the parahippocampal gyrus in the α and θ bands was found. It is possible that the lack of hippocampal activation may indicate that there is no difference in the maintenance of one feature versus two features, but that there is a difference in the recognition of the information between the two conditions [Ranganath, 2001]. It is also possible that the MEG technique might not be sensitive to the type of activation that is detected in the FMRI studies. The greatest activity in terms of size and number was found in the γ and θ bands. γ-band activity during attention and memory have often been reported in both EEG and MEG literature [Kraut, 2003]. In a meta-analysis by Bastiaansen, θ-band oscillations were postulated to be involved in cell assembly formations that lead to WM [Bastiaansen, 2003]. These results are for a fairly wide time window (i.e., 6 - 8 s); therefore, further analyses are planned to utilize the temporal resolution of MEG. In conclusion, this study gives evidence for the usefulness of MEG in investigating WM processes in terms of FB.

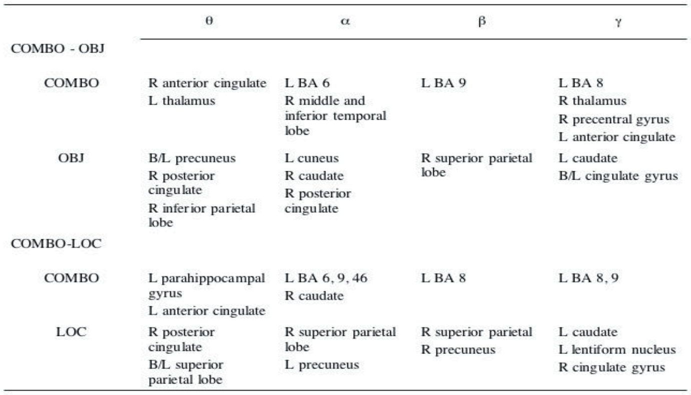

	θ	α	β	γ
COMBO - OBJ				
COMBO	R anterior cingulate L thalamus	L BA 6 R middle and inferior temporal lobe	L BA 9	L BA 8 R thalamus R precentral gyrus L anterior cingulate
OBJ	B/L precuneus R posterior cingulate R inferior parietal lobe	L cuneus R caudate R posterior cingulate	R superior parietal lobe	L caudate B/L cingulate gyrus
COMBO-LOC				
COMBO	L parahippocampal gyrus L anterior cingulate	L BA 6, 9, 46 R caudate	L BA 8	L BA 8, 9
LOC	R posterior cingulate B/L superior parietal lobe	R superior parietal lobe L precuneus	R superior parietal R precuneus	L caudate L lentiform nucleus R cingulate gyrus

Figure 2. Significant power increases (per condition) when COMBO was compared separately with OBJ and with LOC conditions.

REFERENCES

Bastiaansen M, Hagoort P. Event-induced theta responses as a window on the dynamics of memory. Cortex 2003;39:967-992.

Donner TH, Kettermann A, Diesch E, Ostendorf F, Villringer A, Brandt SA. Visual feature and conjunction searches of equal difficulty engage only partially overlapping frontoparietal networks. Neuroimage 2002;15:16-25.

Kraut MA, Calhoun V, Pitcock JA, Cusick C, Hart J, Jr. Neural hybrid model of semantic object memory: implications from event-related timing using fMRI. J Int Neuropsychol Soc 2003;9:1031-1040.

Levy R, Goldman-Rakic PS. Segregation of working memory functions within the dorsolateral prefrontal cortex. Exp Brain Res 2000;133:23-32.

Luks TL, Simpson GV, Feiwell RJ, Miller WL. Evidence for anterior cingulate cortex involvement in monitoring preparatory attentional set. Neuroimage 2002;17:792-802.

Milham MP, Erickson KI, Banich MT, Kramer AF, Webb A, Wszalek T, et al. Attentional control in the aging brain: insights from an fMRI study of the stroop task. Brain Cogn 2002;49:277-296.

Mitchell KJ, Johnson MK, Raye CL, D'Esposito M. fMRI evidence of age-related hippocampal dysfunction in feature binding in working memory. Brain Res Cogn Brain Res 2000;10:197-206.

Nobre AC, Coull JT, Walsh V, Frith CD. Brain activations during visual search: contributions of search efficiency versus feature binding. Neuroimage 2003;18:91-103.

Postle BR, D'Esposito M. Spatial working memory activity of the caudate nucleus is sensitive to frame of reference. Cogn Affect Behav Neurosci 2003;3:133-144.

Ranganath C, D'Esposito M. Medial temporal lobe activity associated with active maintenance of novel information. Neuron 2001;31: 865-873.

Ward R, Danziger S, Owen V, Rafal R. Deficits in spatial coding and feature binding following damage to spatiotopic maps in the human pulvinar. Nat Neurosci 2002;5:99-100.

P1-3

A Study of Visual Tasks to Measure MEG Signals Associated with Memory Functions

Masanori Higuchi, Natsuko Hatsusaka.

Applied Electronics Laboratory, Kanazawa Institute of Technology, Japan

ABSTRACT

We are developing diagnostic protocols to find out the early stages of dementia such as Alzheimer's disease by using a MEG system. In relation between brain functions and dementia, memory defects are characterized as the most obvious signs of dementia. Therefore, to measure MEG signals associated with memory functions seems to be helpful for developing the protocol. As a preliminary study, we tried to identify the components of memory functions in the visual evoked magnetic field by using simple visual tasks. Subjects were instructed to memorize one figure in a few seconds, and to count the number of the memorized figure which appeared in a sequence of figures presented randomly. In a control task, figures were presented randomly without memorization. Evoked responses by visual stimuli were averaged for each session. We compared the results of the control and memory task sessions, and identified components which seem to be related to memory functions. For practical protocols, the task was required to evoke reliable and robust responses in normal subjects. We also discussed how to improve the task in order to detect more significant signals.

KEY WORDS

MEG; Alzheimer’s disease; memory function; visual evoked magnetic field.

INTRODUCTION

We are developing diagnostic protocols to find out the early stages of dementia such as Alzheimer's disease (AD) by using a MEG system. Although there are some studies about AD by means of MEG [Osipova, 2002] [Pekkonen, 2002], most of them deal with primitive responses such as N1m of auditory evoked response. In relation between brain functions and dementia, memory defects are characterized as the most obvious signs of dementia. Considering these points, we have developed a 320-channel whole-head MEG system which has a potential to detect magnetic field signals from the cerebral cortex and deep brain areas. As a preliminary study, we tried to measure the visual evoked magnetic field related to a memory function by using a simple memory task. We compared the results of the control and memory task, and identified the components that seem to be related to a memory function.

METHODS

We have developed a new-type 320-channel whole-head MEG system, which has a potential to detect magnetic field signals from the cerebral cortex and deep brain areas. For deep brain measurement, our MEG system has magnetometers that are more sensitive to the magnetic field caused by deep source. Our MEG system can operate 320 channels, which consists of 160 channels for magnetometers and the rest for 50mm base-lined co-axial gradiometer [Higuchi, 2003].

Three neurologically normal subjects (2 males, 1 female) participated in this study. Visual stimuli were presented to each subject on a screen by projection from outside of a magnetically shielded room. The image size was about 5cm^2 at a 20cm distance from the eyes. In memory task, subjects were instructed to memorize one figure in a few seconds, and to count the number of the memorized figure which appeared in a sequence of figures presented randomly. The figures were 3 simple symbols (circle, triangle, square). To suppress primary visual evoked responses, we used a gray colour for the background of the figures, and reduced the contrast in brightness.

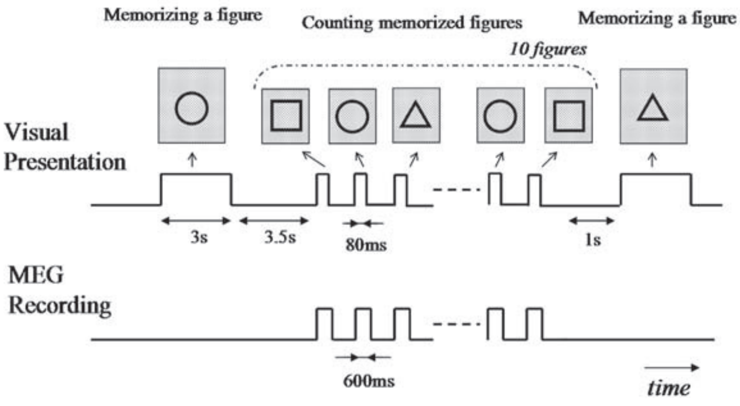

Figure 1. Time sequence of visual presentation and MEG recording.

The time sequence of visual presentation and MEG recording is shown in Figure 1. One figure to memorize was presented for 3s. After 3.5s, 10 figures were presented randomly at 1.2s intervals with 80ms duration. Appearance probability of each symbol was equal to 1/3. Subjects were counting the appearance of the memorized figure among these figures. The correct answer was presented on a screen before next trial started. This trial was repeated 10 times in one session. In this task, any response equipment was not used. It was carried out only in mind. MEG signals were recorded from 100ms before to 500ms after visual onset (pass-band 0.1-200Hz, sampling frequency 1kHz).

RESULTS

Figure 2 shows averaged MEG signals of one subject. The upper waveforms are the results of the memory task, the middle waveforms are the results of the control task and the lower waveforms are the difference between the two tasks. In the control task, visual stimuli were presented randomly without memorization. As the figure shows, significant visual evoked responses were observed from 100ms to 250ms after visual onset in both tasks. We observed a distinct response at about 300ms in the memory task. This response was not so significant in the control task. Therefore, clear peaks appear at this latency in the difference waveforms. We found similar responses in another subject. Figure 3 shows isofield contour maps at this latency. These maps suggested there are two dipole sources related to a memory function. Using the difference field, we applied the dipole fitting procedure. The dipoles were estimated at the right frontal area and the left parietal area as shown in Figure 4.

DISCUSSION

C. L. Grady et al. have reported significant activation was found in the right prefrontal cortex, including the inferior and middle prefrontal regions, and the right parietal cortex during face recognition by using positron emission tomography [Grady, 1995]. In our study, the results suggest recognition process has some relation to the right frontal cortex and the left parietal cortex. While our results on the source in the right frontal cortex were compatible with their study, those on the left parietal cortex were opposite in hemisphere. We speculate it was caused by the difference between face and symbol used as visual stimulation.

For the practical diagnostic protocols, more significant responses are needed. The signal of the memory function is generally supposed to be unstable and affected by attention level of the subject. Before this study, we used slightly complicated illustrations for the visual stimuli. But we could not identify significant responses related to the memory function because of complex and long-continued visual responses. For this reason we used very simple symbols in this study. Furthermore, we need to search the optimum conditions of the measurement to obtain robust signals.

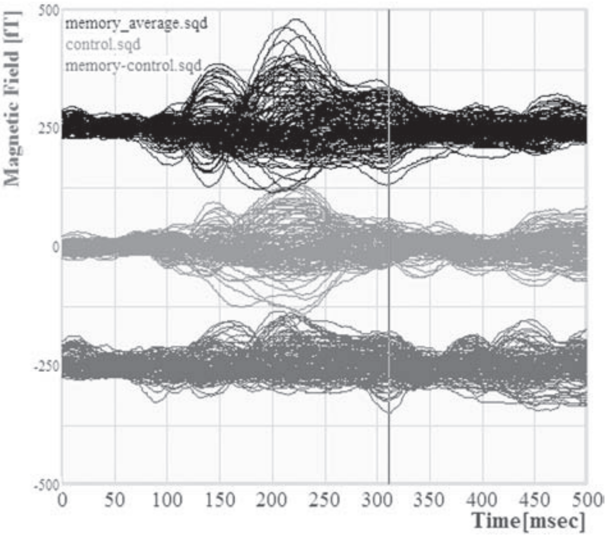

Figure 2. MEG waveforms. *Upper*: memory task, *Middle*: control task, *Lower*: difference waveforms.

ACKNOWLEDGEMENTS

This study was carried out as part of the Cooperative Link of Unique Science and Technology for Economy Revitalization “Ishikawa Hi-tech Sensing Cluster” supported by MEXT Japan.

REFERENCES

Osipova D, Ahveninen J, Jaaskelainen I. P., et al. Cholinergic modulation of spontaneous MEG activity: implications for Alzheimer’s disease. Biomag2002 Proceedings, 2002. p. 170-172.

Pekkonen E, Osipova D, Jaaskelainen I. P., et al. Cholinergic System Modulate Preattentive Auditory Processing in Ageing and in Alzheimer’s Disease. Biomag2002 Proceedings, 2002. p. 176-178.

Higuchi M, Ogata H, Uehara, et. al. Development of a 320 channel MEG system for deep source measurements. The Journal of Japan Biomagnetism and Bioelectromagnetics Society 2003; 16(1); 96-97 (in Japanese).

Grady CL, McIntosh AR, Horwitz B, et al. Age-Related Reductions in Human Recognition Memory Due to Impaired Encoding. Science 1995; 269(5221);218-221

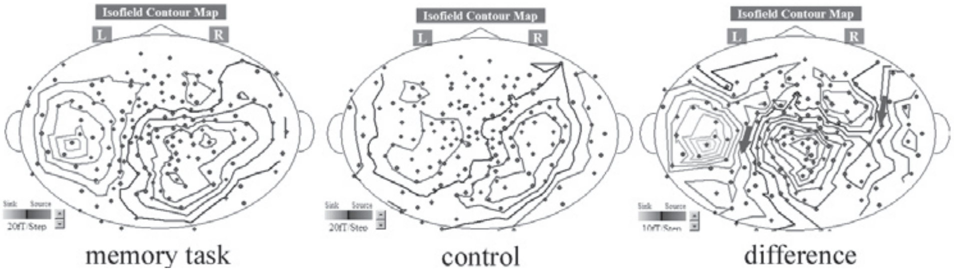

memory task control difference

Figure 3. Isofield contour maps at 300ms after visual onset. *Left*: memory task, *Middle*: control task, *Right*: difference field.

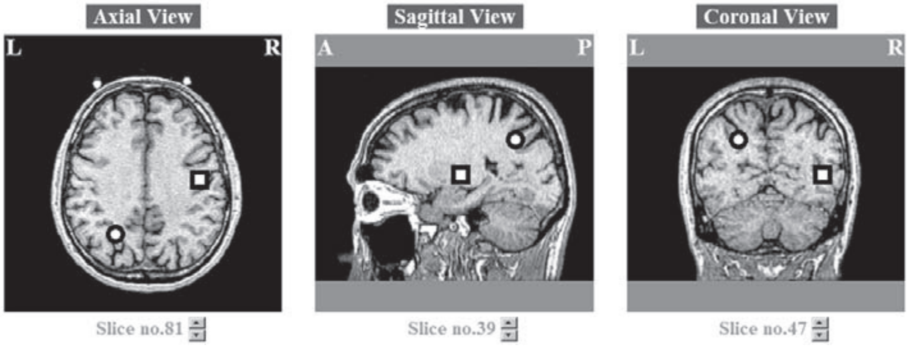

Figure 4. Current dipole estimation by using the difference field data at 300ms

Probing awareness by regional neural-coupling based on linearly independent beamformer projection of MEG data

Holroyd, T.[1], Hendler, T.[2], Eapen, M.[2], and Ungerleider, L.G.[2]

[1]MEG Core Facility, NIMH, Bethesda, MD, USA; [2]Laboratory of Brain and Cognition, NIMH.

ABSTRACT

In this study, we characterized the neuronal dynamics that underlie perceptual competition during binocular rivalry (BR) in humans. Faces presented to one eye, competing with a house presented to the other eye, were studied with and without their conscious percepts. It has been shown that conscious percepts are associated with increased firing within high order visual areas and with increased correlated activation among various cortical regions. It is an open question, whether or not the actual selection into awareness requires neural coupling between thalamic and cortical regions. 275-channel MEG was recorded from 10 subjects while participating in a BR task and reporting by a key press the changes in percept (either face or house). Group SAM analysis in AFNI identified estimated sources of activation in the thalamus and inferior temporal regions for increased power of the MEG signal during the rivalry period. Phase-locking values (PLV) quantifying coherence between these estimated sources were computed from the Stockwell transform of linearly independent (dual basis) virtual channels. The PLVs showed increased coherence during periods of awareness of face percepts relative to periods of face suppressions. Hence this novel approach for calculating the virtual channels and the PLVs probes neural coupling between deep sources in thalamus and cortical sources in high order visual cortex that are involved in conscious perception.

KEY WORDS

Amygdala, Binocular Vison, Brain Mapping, Facial Expression, Fear, Magnetoencephalography, Temporal Lobe, Thalamus, Visual Perception.

INTRODUCTION

How do brain processes cause conscious states and how are those states realized in brain structures? This question encapsulates in essence the neurobiological problem of consciousness [Searle, 2000]. Or, more particularly, What are the principles according to which phenomena such as neuron firing bring about subjective states of awareness? It has been hypothesized that neural correlates of consciousness consist of synchronized neuron firing in the general range of 40Hz in various networks of the thalamocortical system, specifically in connections between the thalamus and layers IV and VI of the cortex. This type of organized neural event can bridge between multiunit neural activity and the holistic mental experience of consciousness.

One way to look for the neural correlates of consciousness is using binocular rivalry (BR). In BR, two images are presented separately to each eye, but only one is perceived at any given time. This controls for the merely stimulus-related processing of early vision and allows identification of neural structures related to both conscious and unconscious processing of the percept itself. Furthermore, the high temporal resolution of MEG makes it possible to study the dynamics of the (spontaneous) switch from one percept to another. Edelman et al. [Tononi, 1998][Srinivasan, 1999] were able to demonstrate evidence for population synchronization in MEG recordings of subjects experiencing BR. However, one important aspect of the dynamics of this system is synchronization of subcortical regions such as the thalamus. Because the sources involved are relatively deep, their magnetic fields are expected to cover wide areas of the MEG sensor, making simple between-sensor coherence difficult to interpret.

We hypothesize that source-based coherence measured between neural populations will reflect more accurately the cortical-subcortical aspect of unifying neural events. More so, we presume that changes in coherence will reflect the (re)organization of the networks supporting the different percepts. Thus, we expect that percepts in awareness will generate coherence between subcortical and cortical sources and that this coherence will reflect the competition between the percepts. In addition, we assume that unique frequency bands will characterize different aspects of the competing images. We manipulated the stimuli on two levels: one of perceptual category (i.e., face vs. house) and the other of emotional valence (i.e., neutral or negative facial expression).

Coherence was calculated at the source level using linear beamformers optimized for the individual sources. Because the projections from each beamformer are just different linear combinations of the same data, it is important to perform the projection in a way that takes linear dependencies among the beamformers into account. A dual-basis construction is used for this purpose.

The objectives of this study are two-fold. Firstly, we seek an understanding of the neural dynamics underlying the experience of awareness; and secondly, we wish to illustrate how MEG may be most effectively used to achieve this goal.

METHODS

Ten healthy, normal volunteers (age 30±5 yr; 7 males) took part in this study. All subjects (Ss) were right-handed with normal symmetric or corrected visual acuity.

Stimuli were prepared using black and white photographs of 4 individuals (2 males and 2 females) each with fearful and neutral expressions, taken from standardized sets of stimuli. Each face was presented simultanously with one particular house. Face and house were color filtered to allow dichoptic presentation through non-metalic red-green glasses. Contrast and luminance were adjusted per image to allow only one percept at a time while Ss were wearing the glasses.

Eight combined face-house stimuli were presented in 40 sec Rivalry epochs. Each epoch consisted of either fearful or neutral faces contrasted against the same house. The Ss' task was to press one of two buttons when the dominant percept was a face, and to press the other button when the dominant percept was a house. Each Rivalry epoch was followed by a 40 sec Replay epoch in which separate (non-rivalrous) images of either the face or the house were presented using interstimulus interval times recorded during the previous Rivalry epoch. Rest periods of fixation on a gray square with a fixation point appeared for 10 sec between epochs and for 30 sec at the beginning (Baseline) and end of the run. Responses were recorded using a fiber-optic response pad (Current Designs, Inc., Philadelphia, USA). The Ss were seated during the task presentation.

Continuous MEG signals were recorded in a magnetically shielded room (Vacuumschmelze, Hanau, Germany) using a 275-channel whole-cortex MEG system (CTF Omega 2000, VSM MedTech Ltd., Coquitlam, Canada). Data were digitized at 600 Hz with a bandwidth of 0–150 Hz. Synthetic 3rd-order gradiometer balancing was used to subtract magnetic background signals.

Synthetic Aperture Magnetometry (SAM) was used in the differential mode to compute volumes showing relative power changes in 500 msec windows between Fear vs. Neutral, Face vs. House, and Rivalry vs. Replay, for each S in the θ (4–8 Hz), β (14–24 Hz), and γ (24–50 Hz) frequency bands. The SAM volumes were z-scored to eliminate intersubject variability in relative power levels, co-registered with the Ss' structural MRI, and transformed into Talairach space. The Talairached volumes were then averaged and subjected to a 3D t-test for each condition. Voxels significant at the $p < .05$ level were then selected from the amygdala complex, inferior temporal cortex, and thalamus, and transformed back into the individual Ss' MRI coordinates. These voxel's coordinates were then used to create SAM beamformers in windows from -2 to $+1$ sec around the responses in the Rivalry condition.

Linearly independent virtual channels were computed for each of the beamformers simultaneously by dual-basis projection. If $\mathbf{V}$ is the matrix with the beamformers as column vectors, then the dual basis $\mathbf{V}^*$ can be written as the pseudo-inverse $\left[\mathbf{V}^{\mathrm{T}}\mathbf{V}\right]^{-1}\mathbf{V}^{\mathrm{T}}$ where the dual vectors are the rows of $\mathbf{V}^*$. Projection of the bandpassed raw data using the dual vectors yields timeseries for each of the original beamformers that are linearly independent from all the other beamformers.

The resulting timeseries were decomposed into a complex-valued time-frequency representation z using the Stockwell transform, which maintains an absolute phase origin and thus preserves relative phase. The amplitudes of the complex values at each t-f point were normalized and the relative phase between channels averaged across trials to form the Phase Locking Value (PLV), for each pair of virtual channels: $\mathrm{PLV}_{ij} = \frac{1}{N}\sum \bar{z}_i^* \bar{z}_j$ where $\bar{z} = z/|z|$ and the sum is over trials. A bootstrap procedure was then applied in which the trials for one of the channels were shuffled and the PLV recalculated, 200 times. PLV values larger than 2.5 standard deviations from the mean of the shuffled PLVs were considered significant.

RESULTS

The figure shows the θ-band PLVs between right fusiform and thalamus, averaged across 8 Ss (two Ss were removed because their switching times were too short) and averaged per perceived category. Left; independent beamformers do not adequately resolve the activity. Right; projections using the dual basis reveal strong thalamocortical phase locking for face only, though the physical stimulus is identical in both cases.

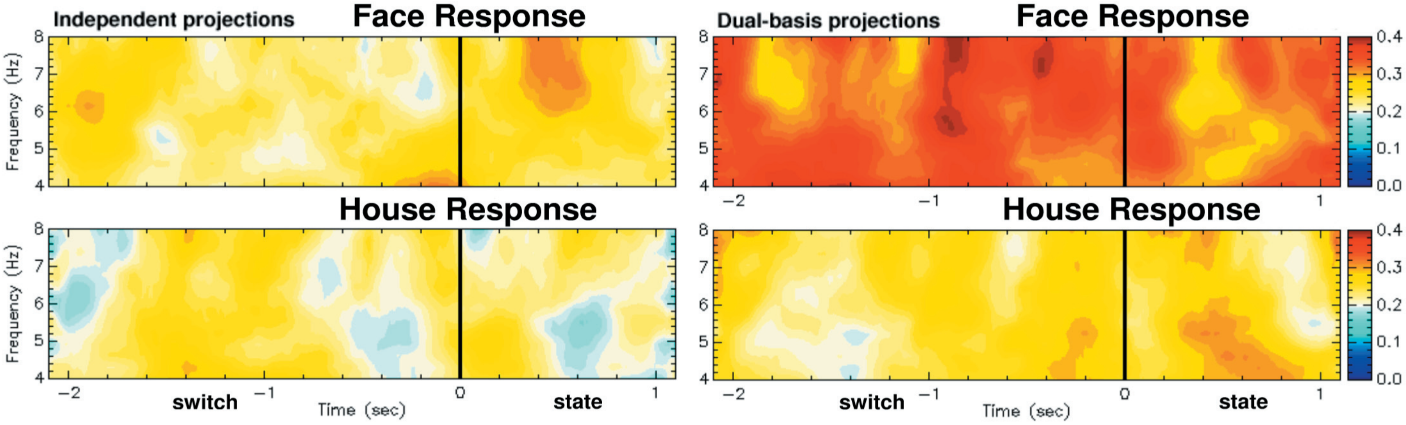

DISCUSSION

Brains contain many reciprocal connections and loops between functionally related areas. It has been suggested that synchronization of activity plays an important role in the integration of different features of a stimulus (binding). MEG allows us to observe the activity of different areas, to test this hypothesis. However, some care must be taken when analyzing MEG data from this point of view, because of the linear mixing of magnetic fields.

Beamforming is an effective technique for optimally isolating the activity of a given source. This optimality is subject to certain assumptions, one of them being that noise sources are uncorrelated. In this case, we are explicitly interested in correlated sources, and a straightforward comparison using independent beamformers may miss important correlations due to cancellation by the beamformer itself. Thus, it is critical to perform the beamformer projections simultaneously, in order to resolve the linearly independent portions of the signal. Beamformers also amplify noise, making the detection of correlations more difficult. An important difference between the PLV and coherence is that the PLV is normalized prior to averaging. That is, only the relative phase is used, irrespective of the power. The PLV is thus more sensitive to phase coupling than coherence. This is especially important in the case of systems with flexible, intermittent dynamics, where "phase gathering" may be more important than "phase locking."

Finally, we have shown evidence that phase synchronization between areas may play a role in the dominance of competing percepts.

REFERENCES

Searle, JR. Consciousness. Annu Rev Neurosci 2000;23:557–578.

Tononi, G, Srinivasan, R, Russell, PD, and Edelman, GM. Investigating neural correlates of conscious perception by frequency-tagged neuromagnetic responses. Proc Natl Acad Sci USA 1998;95:3198–3203.

Srinivasan, R, Russell, PD, Edelman, GM, and Tononi, G. Increased Synchronization of Neuromagnetic Responses during Conscious Perception. J Neurosci 1999;19:5435–5448.

MEG analysis of “Theory Of Mind” in Emotional Vignettes Comprehension

Ishii R.[1], Gojmerac C.[2,6], Stuss D.T.[2,6], Gallup G.G. Jr[3], Alexander M.P.[4], Chau W.[2], Pantev C.[5]

[1]Department of Psychiatry and Behavioral Neuroscience, Osaka University Graduate School of Medicine, Japan. [2]The Rotman Research Institute, Baycrest Centre for Geriatric Care, Canada. [3]Department of Psychology, State University of New York at Albany, USA. [4]Department of Neurology, Harvard University, Beth Israel Deaconess Medical Center, USA. [5]Institute of Biomagnetism and Biosignalanalysis, University of Munster, Germany, [6]University of Toronto.

ABSTRACT

[Objective] Several studies suggested that an impaired “theory of mind” might play a key role in psychiatric disorders, such as autism and schizophrenia. Medial frontal lobe lesions of the right frontal lobe were reported to impair this ability. The aim of our study was to locate areas of the brain associated with the process of “theory of mind” in normal subjects. [Methods] In order to index the activity of brain areas related to "theory of mind" reasoning in sixteen normal adults, we administered an emotional (“happy”, “sad”, “angry” and “neutral”) vignettes comprehension task during magnetoencephalography (MEG) recordings and analyzed these data by using SAM (synthetic aperture magnetometry), SPM99 and the permutation method. Subjects were presented with eight different videotaped social situations (each emotion has two vignettes) and were asked to indicate which emotion they represented. [Results] Statistically significant activation in the comparison of “happy”-“sad” and “angry”-“sad” was observed in the bilateral medial prefrontal cortices in the alpha frequency band. There were no significant differences in comparisons of each type of emotional vignette to the neutral vignettes, “happy”-“angry” comparison, and male-female comparisons. There was no significant difference in other frequency bands. [Conclusion] This result suggests that bilateral medial prefrontal cortex are involved in the comprehension of emotional states of others.

KEY WORDS

MEG, Theory of Mind (ToM), spatial filter, autism, schizophrenia, emotion, SPM, permutation, synthetic aperture magnetometry (SAM).

INTRODUCTION

“Theory of mind” is the ability to explain and predict the behavior of others in terms of their mental states [Perner, 1988]. Several studies have suggested that an impaired theory of mind may lie at the heart of psychological disorders that are characterized by deficits in social understanding. It has been reported that patients with autism have deficits in performance on theory of mind tasks, i.e., requiring the interpretation of mental states of others [Happe, 1995]. Schizophrenia is also a biologically based disorder that appears to be characterized by a specific impairment in this theory of mind process [Corcoran, 1995].

Medial frontal lobe lesions, with a particular preeminence for the right front lobe, impaired performance on theory of mind tasks [Stuss, 2001]. A recent PET study showed that a language-based “theory of mind” task activated an extensive neural network that included the medial frontal cortex, the superior frontal cortex, the anterior and retrosplenial cingulate, and the anterior temporal pole [Calarge, 2003]. Although several other brain regions have been implicated in theory of mind, the frontal lobes have been considered to play a special role in human behavior, with damage in this region affecting high-level cognitive functions but also social behavior, personality, personal memories and self-awareness.

Our study used MEG to locate areas of brain associated with the process of theory of mind in normal subjects. To index the activity of neural systems that are engaged during theory of mind reasoning in normal adults, we measured MEG recordings during the emotional vignettes comprehension task (Stuss, Gallup, & Alexander, in preparation) and analyzed the data by using SAM, SPM99 and permutation.

METHODS

Sixteen normal subjects (eight males and eight females, all right-handed, age 25 to 37) participated in this study. After explaining the nature of the study, informed consent was obtained. Experimental procedures were in accordance with the Ethics Commission of the Baycrest Centre for Geriatric Care and the Declaration of Helsinki. The subjects had no history of neurological and psychiatric disorders. During recording the subjects sat relaxed under the MEG helmet-shaped device and kept their eyes open and their arms relaxed.

To index the activity of neural systems that are engaged during theory of mind reasoning in normal adults, we employed the emotional videotaped vignettes comprehension task (Stuss, Gallup, & Alexander, in preparation). These emotional vignettes depicted four types of emotions (happy, sad, angry and neutral), two vignettes for each emotional type. The time length of those vignettes varied from 25sec to 50sec. After viewing each scene, subjects were asked to indicate which emotion was represented in the vignette by pointing to one of four face pictures, each representing one of the four emotions.

MEG data were obtained using a whole head helmet-shaped 151-channel SQUID sensor array (Omega 151, CTF Systems Inc.) within a magnetically shielded room. MEG signals were digitized at 625 Hz and filtered using a 60 Hz notch filter and 200 Hz low pass filter.

The tomographic distributions of the current source density in alpha, beta and gamma frequency bands were determined from the MEG data, using synthetic aperture magnetometry (SAM) [Robinson, 1992][Ishii, 1999]. SAM is a spatial filtering technique based on the nonlinear constrained minimum-variance beamformer. This technique overcomes the nonuniqueness of generalized inverse solutions, such as the minimum norm, and thereby permits unambiguous three-dimensional source mapping during task performance.

SAM images were generated by subtracting each emotional vignette (25 seconds during happy, sad, angry and neutral vignettes x 2 trials) from the other: e.g., “happy”-“neutral”, “angry”- “neutral”, “sad”-“neutral”, “happy”- “sad”, “angry”- “sad” and “happy”- “angry”. We also compared these activation images between male and female subjects. This was done for each voxel divided by their ensemble standard error of instrumental (SQUID sensor) and environmental noise. The distributions of the SAM images were transformed to the SPM T1 template space. A nonparametric permutation technique was applied to the normalized SAM results to determine the statistical significance of the results. The omnibus null hypothesis of no activation anywhere in the brain was rejected if at least one t-value was above the critical threshold for $P<0.05$ determined by 1024 permutation. Voxels with t-values above this critical 0.05 threshold were considered as a region of activation.

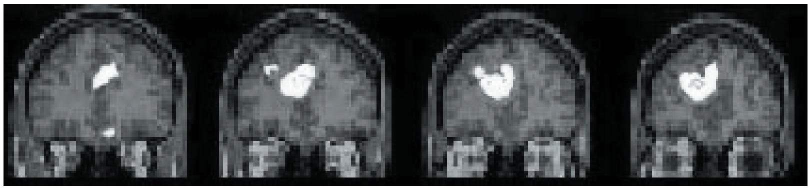

Fig.1: SAM-SPM99-Permutation images of the comparison “happy”-“sad”. (n=16, $p<0.05$)

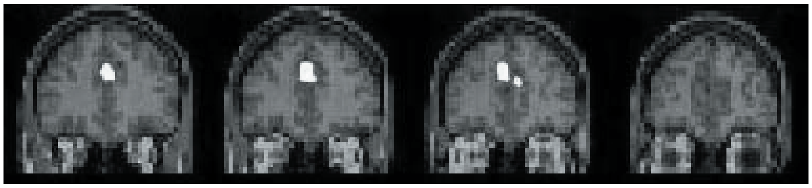

Fig.2: SAM-SPM99-Permutation images of the comparison “angry”-“sad”. (n=16, $p<0.05$)

RESULTS

After viewing the emotional vignettes, all subjects were able to identify correctly the emotional state represented in the vignette. SAM-SPM99-permutation revealed statistically significant activation difference in comparison of the “happy”-“sad” and “angry”-“sad” in the bilateral medial prefrontal cortices in alpha frequency band (fig.1 and 2). We could not find any difference in comparisons of each emotional vignette to neutral vignettes, the “happy”-“angry” comparison, or in the male-female comparison. There were no significant differences in other frequency bands.

DISCUSSION

The major finding of this study was that statistically significant activation in the comparison of “happy”-“sad” and “angry”-“sad” was observed in the bilateral medial prefrontal cortices in the alpha frequency band. Like the previous studies using rCBF methods to investigate “theory of mind” [Calarge, 2003], our MEG study also showed that the medial prefrontal region is activated when subjects tried to imagine and estimate the mental states of others. Frith and colleagues had suggested that there might be a “theory of mind system” in the human brain like the language system and the facial recognition system, and this system might be composed of medial prefrontal, superior temporal and inferior frontal regions [Frith & Frith, 1999]. We suggest that the bilateral medial prefrontal cortices have an important role for comprehension of emotional states of others.

The significant bilateral medial prefrontal activation was found only in the comparison of “happy”-“sad” and “angry”-“sad” scenes. . The sad vignettes represented quite depressing scenes (e.g., people crying at a gravesite). The sad scenes might evoke and prolong the emotional states more easily than other emotional vignettes. We speculated that the subjects might be more in the empathic mode during the sad vignettes.

We could not find any difference in the comparisons of each emotional vignette to neutral vignettes. Post hoc questioning suggested that the subjects tried to extract emotional clues from these neutral vignettes and found that there was no emotional significance in these vignettes only after analyzing of the entire vignette. We speculated from these insights that the neutral vignettes were not an appropriate comparison, because the subjects may have still engaged theory of mind processing in trying to find an emotional significance that was not present. There was no difference between the 8 male and 8 female subjects. Increasing the subject number and analyzing correlations of MEG in relation to personality variables of individuals may be a future avenue of research.

This study provides experimental evidence for an independent cerebral implementation of self-perspective in the context of theory of mind. Our study design using the relatively non-invasive MEG imaging procedure might be useful as an experimental tool in the study of patient populations who are reported to have theory of mind deficits, e.g., autism and schizophrenia.

REFERENCES

Calarge C, Andreasen NC, O'Leary DS. Visualizing how one brain understands another: a PET study of theory of mind. Am J Psychiatry. 2003;160:1954-64.

Corcoran R, Mercer G, Frith CD. Schizophrenia symptomatology and social inference: investigating “theory of mind” in people with schizophrenia. Schizophre Res 1995;17:5-13.

Fretcher PC, Happe F, Frith U, Baker SC, Dolan RJ, Frackowiak RS, Frith CD. Other minds in the brain: a functional imaging study of “Theory of mind” in story comprehension. Cognition, 1995;57:109-128.

Frith CD, Frith U. Interacting minds—a biological basis. Science, 1999;286:1692–1695.

Happe FG. The role of age and verbal ability in the theory of mind task performance of subjects with autism. Child Dev 1995;66:843-855.

Ishii R, Shinosaki K, Ukai S, Inouye T, Ishihara T, Yoshimine T, et al. Medial prefrontal cortex generates frontal midline theta rhythm. Neuroreport 1999;17:675-679.

Perner J, and Wimmer H. Misinformation and unexpected change: testing the development of epistemic-state attribution. Psychol Res 1988;50:191-197.

Robinson SE, Rose DF. Current source image estimation by spatially filt1ered MEG. In: Hoke M, Eme SN and Okada YC, eds. Biomagnetism: Clinical Aspects: Proceedings of the 8th International Conference on Biomagnetism. New York: Elsevier, 1992:761-765.

Stuss DT, Gallup GG Jr, Alexander MP. The frontal lobes are necessary for ‘theory of mind’. Brain 2001;124:279-286.

Cortical Processing Differences in Attention-Deficit Hyperactivity and Normal Control Subjects

Nagel S.M.[1,2], Bowyer S.M.[2,3,4], Moran J.E. [2], and Tepley N.[2,3]

[1]Saginaw Valley State University, USA; [2]Henry Ford Hospital, USA; [3]Oakland University, USA; [4]Wayne State University, USA.

ABSTRACT

Magnetoencephalography (MEG) was used to investigate the cortical activity differences in cognitive processing in subjects with Attention-Deficit Hyperactivity Disorder (ADHD) and normal controls. Using MR-FOCUSS, we compared MEG images of the localization of cortical activity measured from the ADHD patients and control subjects. Although the results should be interpreted cautiously, this study suggests the presence of functional defects in the frontal and parietal cortex in ADHD patients. Analysis of one subject pair indicated an absence of frontal cortex activation in ADHD at ~200 ms. during both selective attention and response preparation. A shift from left to right hemispheric activation in ADHD was indicated during vigilance, along with a difference in cortical activity at ~300 ms. Processing delays, hemispheric differences, and frontal and parietal cortex deficits were found during response error detection and response control in ADHD.

KEY WORDS Attention-Deficit Hyperactivity Disorder, ADHD, MEG, MR-FOCUSS.

INTRODUCTION

Attention-deficit hyperactivity disorder (ADHD) is the most common psychiatric disorder of childhood and continues into adulthood for approximately 30% of the cases. Attention to this public health problem has increased in recent years. In 1998, the National Institutes of Health held a consensus development conference on the diagnosis and treatment of ADHD ***[http://consensus.nih.gov/cons/110/110_statement.htm]***. The members of this panel called for research to improve the understanding of the diverse causes of ADHD to aid the prevention, diagnosis, and treatment. We present here the results of one 49 year old male diagnosed with ADHD-Combined Type compared with the results of an age, sex, and IQ matched normal control in an attempt to begin to understand differences in the cortical activation associated with this diagnosis during vigilance, selective attention to visual stimuli, and the executive control over verbal responses.

METHODS

To date, seven patients diagnosed with ADHD (4 with Combined Type, 2 with Inattentive Type, and 1 Hyperactive Type) and two normal control subjects have been recruited via an ad placed in a hospital publication and then tested. Mean age of the ADHD participants was 26 years old, range was 18 – 48, 4 males and 3 females. ADHD diagnosis (DSM-IV criteria) was assessed through multiple methods [American Psychiatric Assoc, 1994]. The exclusion criteria for all participants were a medical history of organ, mental, and neurological disease and/or medication use that could affect the test results. The Institutional Review Board of Henry Ford Hospital approved the protocol for this study and informed consent was obtained. The MEG data were collected using a whole-head neuromagnetometer (4D Neuroimaging WH2500). The participants were prepared for studies in the lab's customary way [Bowyer, 2003].

A Visual Continuous Performance Test (Visual-CPT) [Ricco, 2002] was used to measure the participant's MEG field responses while he/she maintained vigilance and engaged processes of selective attention. Random letters were shown for a brief 150 ms each with a 1.8 second inter-stimulus interval (4 blocks of 100 trials). The participant was instructed to respond as quickly possible by pressing a switch to the "X" target stimulus when it followed the "A" cue stimulus.

The Stroop Interference Test (SIT) [Stroop, 1935] was used to measure the participant's MEG field responses during a task that necessitates the use of higher executive control over behavior. Stimuli were presented individually for 500 ms, with a 1.5 second inter-stimulus interval (3 Conditions, 40 trials each). Condition 1 involved the verbal identification of color stimuli. Condition 2 involved reading the names of colors written in the congruent color text. In Condition 3, words were presented in a text color that was incongruent to the name of the color, and the color of the text was identified.

Each participant was asked to have an MRI scan performed. The MRI scans were used to co-register the MEG data to specific locations in the cortex of each participant. This allowed for a precise localization of the anatomical landmarks and cortical activation areas associated with the tasks (0-650 ms following stimulus presentation). All MEG study data were digitally filtered 1-50 Hz. For each subject the latency (in ms.), location (x,y,z coordinates), and average amplitude of response (nanoAmp-meter) were extracted from the MR-FOCUSS [Moran, 2001] imaging results for each cognitive process step. VECMF's were analyzed at the time of data collection by ECD.

RESULTS

The results collected during the Visual-CPT and the SIT distinguished a 49 year old male ADHD patient and matched normal control (NC) along several dimensions of cortical activation. The following results highlight the findings for Frontal and Parietal cortical regions known to be involved in the control of attention and executive control [Nagel-Leiby, 1990]: L=Left, R=Right, B= Bilateral, F= Frontal Cortex, P= Parietal Cortex, I= Inferior, S= Superior, D= Dorsolateral.

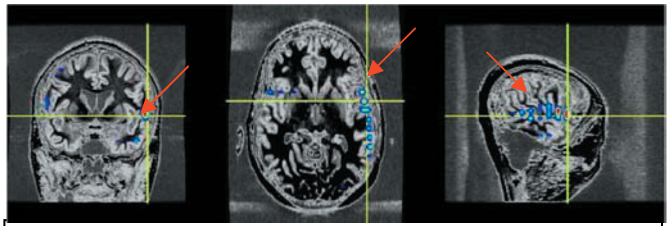

Figure 1A Coronal (L), Axial (Center), and Sagittal (R) views of Left Inferior Frontal and Parietal activation in NC at 303 ms following a cue to attend.

Visual Continuous Performance Test: In Condition 1 (vigilance) the NC showed greater activation overall of the L hemisphere (Amp=-16.7, Time= -47.7ms), whereas the ADHD showed greater activation overall of the R hemisphere (Amp= +10.7, Time= +28.3ms). The NC showed activation in LIF (238-334 ms) with a shift to RIF activation at 442 ms (some LIFactivation remained at 442 ms). Conversely, the ADHD showed activation in BSP at 300 ms with a shift to the LDF and RIF at 344 ms. In Condition 2 (selective attention) the NC showed activation of LF (204 ms), followed by activation of LIF and LP at 303 ms (FIG 1A). LIF remained activated until 338 ms. RSF was activated at 436 ms. Conversely, the ADHD showed activation of RIF from 318 - 360 ms (FIG. 1B). In Condition 3 (response preparation) the NC showed activation of RIF from 218-318 ms with anterior movement, and activation of LIF at 413 ms. Conversely, the ADHD showed activation of LSP and LSF at 301 ms, followed by activation of RDF, RP, and BIF at 350 ms.

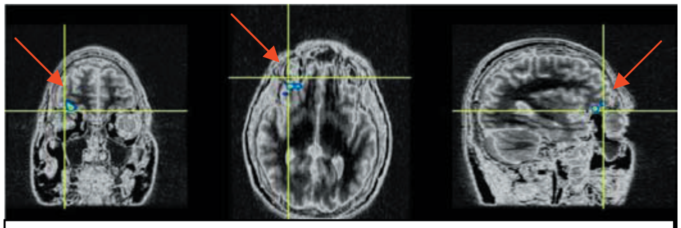

Figure 1B Coronal (L), Axial (Center), and Sagittal (R) views of activation in ADHD at 320 ms following a cue to attend.

Stroop Interference Test: In Condition 1, the NC showed activation of L > RIP (179 ms.), followed by activation of BIP and RSF from 323 – 423 ms. Conversely, the ADHD showed no activation of P or F. In Condition 3a (high error rate reflecting poor executive control), the NC showed BIP and BSP activation at 220 ms. BIF was activated at 320 ms. The ADHD showed activation of LF at 405 ms. and LIP at 482 ms. In Condition 3b (low error rate reflecting good executive control), the NC showed activation of LIF at 209 ms (FIG 2A), followed by LIP activation at 258 ms (FIG. 2B). The ADHD showed activation of the LSF at 313 ms (FIG. 2C).

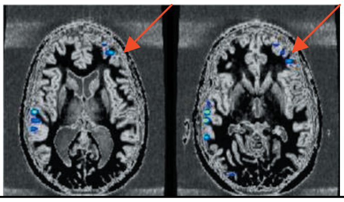

Figure 2A Axial view of Left Frontal Activation in NC at 209 ms. during challenged but effective response control.

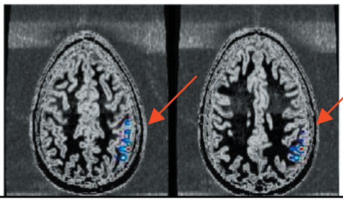

Figure 2B Axial view of Left Inferior Parietal Activation in NC at 258 ms in same condition shown in Figure 2A.

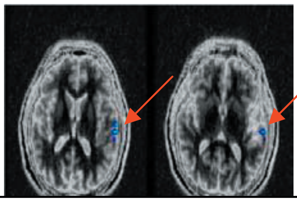

Figure 2C Axial view of Left Superior Frontal Cortex in ADHD at 313 ms during challenged but effective response control.

DISCUSSION

ADHD may be associated during vigilance (CPT-Condition 1) with right rather than left hemisphere activation and a lack of activation of the Left Inferior Frontal and Bilateral Parietal Cortex at ~300 ms. relative to normal. When selective attention is engaged (Condition 2), ADHD may be associated with a lack of activation of Left Frontal Cortex at ~200 ms. relative to normal. Normal activation of Left Frontal and Parietal Cortex at ~300 ms. (Fig. 1B) may be associated with activation of Right Frontal Cortex in ADHD (Fig. 1B). ADHD may also be associated during selective attention with an absence of normal Right Frontal Cortex activation at 400 ms. When a response is prepared to a cued target (Condition. 3), ADHD may be associated with a lack of Right Frontal Cortex activation at ~200 ms relative to normal. In addition, ADHD may be associated with a greater activation of Left Parietal and Frontal Cortex at ~300 ms. relative to normal, as well as more widespread activation in Right Frontal and Parietal Cortex at 400 ms, when only the Left Inferior Frontal Cortex is activated in normal processing.

The SIT findings suggest that ADHD may be associated with a lack of activation of attention processing in Bilateral Inferior Parietal Cortex (~300 ms) and Right Superior Frontal Cortex (~300-400 ms.) relative to normal. When the executive control of responses is dysfunctional due to task demands, ADHD may be associated with a lack of normal activation of Bilateral Inferior and Superior Parietal Cortex at ~200 ms. In addition, ADHD may be associated with a lack of normal activation of Bilateral Inferior Frontal Cortex at ~300 ms, as well as late (~350 – 480 ms.) activation of Left Frontal Cortex and Left Inferior Parietal Cortex. When the executive control of responses is functional, ADHD may be associated with reduced overall right hemispheric activation. Normal activation of Left Inferior Frontal Cortex at ~200 ms may be absent or reduced in ADHD. Finally, there may be a delay (from ~200 ms in NC to ~300 ms in ADHD) and shift (Inferior in NC and Superior in ADHD) of Frontal Cortex activation in ADHD relative to normal during the executive control of responses under challenging circumstances.

This study establishes the efficacy of specific MEG imaging techniques in determining the structure, activation sequence, and strength of neuronal interaction during visual attention and the executive control of responses. In addition, this study indicates that MEG should increase the understanding of how attention and other forms of executive control occur in those diagnosed with ADHD. MEG studies may help refine the diagnosis of subtypes of ADHD, leading to selective and more effective behavioral and pharmacological treatment of these subtypes. In addition, MEG studies may help to elucidate the generators of the neurophysiological event-related potentials.

ACKNOWLEDGEMNT: Supported by NIH/NINDS Grant RO1-NS3091.

REFERENCES

Committee on Nomenclature and Statistics: Diagnostic and Statistical Manual of Mental Disorders, 4th ed. Washington, D.C.: American Psychiatric Association; 1994.

Bowyer SM, Mason K, Tepley N, Smith BJ, Barkley GL. MEG validation parameters for clinical evaluation of interictal epileptic activity. J Clin Neurophysiol 2003; 20(2):87-93.

Ricco, CA, Reynolds, CR, Lowe, P, Moore, JJ. The continuous performance: a window on the neural substrates for attention? Archives of Clinical Neuropsychology 2002;17:235-72.

Stroop, JR. Studies of interference in serial verbal reactions, Journal of Experimental Psychology 1935; 28: 643-62.

Moran JE, Bowyer SM, Tepley N. Multi-resolution FOCUSS source imaging of MEG data. 3rd International Symposium on 7 Noninvasive Functional Source Imaging within the Human Brain and Heart, Biomedizinische Technik 2001;46: 112-14.

Nagel-Leiby, S, Buchtel, HA, Welch, KMA. (1990). Cerebral control of directed visual attention and orienting saccades. Brain 1990;113:237-76.

MEG study on the perception of rhythm and its expression in authentic music

Popescu, M.[1,2], Otsuka A.[1,3], and Ioannides A. A.[1]

[1] Laboratory for Human Brain Dynamics, Brain Science Institute (BSI), RIKEN, Wako-shi, Japan
[2] Hoglund Brain Imaging Center, University of Kansas Medical Center, Kansas City, Kansas, USA
[3] Center for Evolutionary Cognitive Sciences, University of Tokyo, Tokyo, Japan

ABSTRACT

Studies on music perception generally rely on contrasting brain responses evoked by different types of artificially introduced violations of the musical syntax, and/or comparison of the responses from subjects with different musical ability. However, understanding the neural correlates of authentic music appreciation cannot be achieved through the study of music errors alone. We have used magnetoencephalography (MEG) to unscramble from the dynamics of brain activations features related to music rhythmical properties, when subjects listened to an authentic musical piece. To achieve this, we developed a combination of multiresolutional wavelet decomposition and self-similarity measures that enable characterizing the temporal sequencing of an authentic musical piece and brain activations. These methods can show when and where in the brain the activity reflects the rhythmical expressiveness of authentic musical stimuli. We show that music perception triggers a large spectrum of cerebral responses that span different temporal scales: bilateral activations within and around the auditory cortices and motor related areas faithfully respond to onset and rhythmic properties of the stimuli while activations in frontopolar, ventrolateral prefrontal, and anterior temporal areas grow in strength as the music unfolds and last well beyond the end of the stimulus, thus seemingly tracking the global contour of accumulating interest or tension. The results show that rhythmical structure of the music is correlated with activity changes in motor related areas (supplementary motor area, premotor areas, and somatomotor areas) in each hemisphere. These findings bring to focus what the quintessential factors might be that allow expressive temporal deviations (of an aggogic character) to be internalized.

KEY WORDS

Magnetoencephalography (MEG); wavelet; rhythm; music

INTRODUCTION

While formal similarities and dissimilarities of music and language suggest that music predates language by a long way, the neural basis of music perception is still far less understood than that of language. An increasing number of imaging studies have recently focused on identifying brain regions involved in music perception; findings, however, were generally restricted by the physical principles of the imaging devices and/or by the analysis tools. The formidable problems that such a study of brain processes entails has limited most earlier MEG/EEG studies to contrasting brain responses to congruent versus incongruent terminal notes in short note sequences. The present study aimed to make a step forward by exploring the *dynamics* of neuronal activity elicited by changes in rhythmical attributes of a piece of authentic music. To achieve this, we developed a novel technique aiming to bridge the structural analysis of score representations of music to the time course of regional brain activations. This is done via the music analysis at the signal level, thus incorporating the expressiveness of the musical performance. Specifically, we designed a technique based on multiresolutional wavelet decomposition of the amplitude modulation of the sound signal and self-similarity measures of the wavelet coefficients to extract measures of music rhythmicity and correlate them with the analogous measures derived from the induced regional brain activity.

METHODS

SUBJECTS, MEASUREMENTS, AND STIMULI

Five male, right-handed subjects, with no formal musical training, volunteered for the experiment. The MEG signals were recorded in a magnetically shielded chamber using the CTF whole head Omega system. The subjects were requested to listen to a music stimulus consisting of a part of Frantz Liszt's *Etudes d'execution transcendante d'apres Paganini*, S.141-No. 5, which is a solo piano piece with a moderate tempo. The analysis reported in this paper is based on a motif component lasting 10 s, which was selected because its different segments had distinct changes in the performance rhythm that could be quantified by the degree of temporal deviations from the reference interval ratio (DRIR). The piece is driven by three note-based groups throughout and the rhythmic and metrical values are the same on all segments. The interval ratio of the three-notes group component defined by the score is 1:1:2. The mean interval ratios in performance, however, reveals two switches in note duration ratios: the first switch marks the transition from a close to metrical segment (1:1.2:2.0, segment A) to a segment characterized by higher DRIR (1:1.3:2.4, segment B), whereas the second switch marks the transition to a segment with the smallest DRIR (1:1.1:2.1, segment C).

BEAT TRACKING ALGORITHM

The first step of the beat tracking algorithm segregated the prominent rhythmical features of the musical motif by extracting the amplitude modulation (AM) component of the acoustic signal. The AM component was subsequently parameterized using a pseudocontinuous wavelet transformation [Grossmann and Morlet, 1984]. Similarity measures between feature vectors (matrices) were computed from successive temporal windows of the AM scalogram. The distance measure was embedded in a two-dimensional similarity matrix referred to as a *rhythmogram*. The beat spectra were then separately computed for the three segments (A, B, C, 2.4 s each) of the musical motif using the autocorrelation of the rhythmogram matrix [Foote and Uchihashi, 2001].

MEG DATA ANALYSIS

The MEG data were pre-processed (digitally filtered, baseline corrected, averaged) using standard techniques. The current density throughout the brain was reconstructed using the CURRY 4.5 source localization software (Philips Res. Lab.), with a minimum L2 norm constraint for the currents and L-curve regularization [Hämäläinen and Ilmoniemi, 1994]. For tracking the time course of the brain activations, the modulus of the current

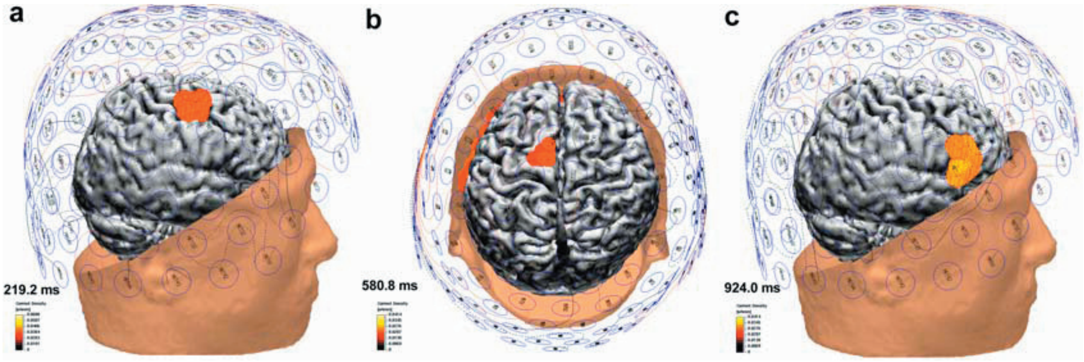

Figure 1. Representative instantaneous current density estimates for one subject, showing snapshots of activations in motor related regions consistently identified in the study. (a) Activations in the right somatomotor area. (b) Activations in the left supplementary motor area. (c) Activations in the right lateral premotor area.

density estimate was integrated over spherically shaped volumes of interest (VOIs). The beat spectra were computed for the activation curves (ACV) and correlated with the beat spectrum of the music signal.

RESULTS

The reconstruction results first proved that music perception triggers a wide spectrum of cerebral responses spanning different temporal scales [Popescu et al., 2004]: from activations reflecting the fine rhythmical structure of the stimulus (within and around the auditory cortices and motor related areas), to activations tracking the global contour of accumulating interest or tension, growing in strength as the music unfolds and lasting well beyond the end of the stimulus (in frontopolar, ventrolateral prefrontal, and anterior temporal areas). Particularly, these findings confirmed predictions of psychophysical studies, which suggested that activity in motor related regions accompanies music perception (figure 1). While the activation of PMA and SMA is consistent with previous results reported by studies on music perception. [Halpern and Zatorre, 1999, Maess et al., 2001], the activation of SM1 in the absence of overt motor behavior (such as finger or foot tapping) supports the hypothesis that it is also involved in the perception of the temporal patterns embodied in the musical rhythm. The beat-spectrum was therefore used to study the dynamic properties of the activation in motor-related areas and their relationship with the temporal patterns of the musical rhythm. The changes in the mean correlation coefficients between the beat spectrum of the sound signal and those of the regional activation curves show a decrease in the performance–rhythm tracking ability of motor-related regions of the left hemisphere for the second segment of the motif. This was particularly evident for the SM1 and PMA areas. Statistical testing revealed a significant decrease in the mean correlation coefficients after the first switch in musical rhythm, from segment A to segment B, for all left motor areas ($t = 4$, $P = 0.008$ for left SMA; $t = 2.28$, $P = 0.042$ for left SM1; and $t = 3.45$, $P = 0.013$ for left PMA). Moreover, a significant increase in the mean correlation coefficient was noticed after the second switch (marking the transition from high DRIR on segment B to small DRIR on segment C) in left SM1 ($t = 2.13$, $P = 0.05$). The increase for the left PMA approached significance ($t = 1.90$, $P = 0.06$), while no difference was found for the same comparison of the left SMA ($t = 0.11$, $P = 0.46$). These lateralized findings suggest dynamic changes in rhythm tracking performance while listening to the motif, which are hemisphere specific.

DISCUSSION

Our results demonstrate that metrical rhythms preferentially drive a coherent mode of oscillatory activity in the motor regions of the left hemisphere. This result relates to the previously reported good performance in memorization and reproduction of these rhythmical patterns [Essens and Povel, 1985; Sakai et al., 1999]. The change to a high DRIR decreases the left hemisphere performance in rhythm tracking, which in turn determines a right hemisphere dominance in the representation of rhythms characterized by high DRIR. Our study supports and qualifies earlier claims [Peretz, 1990] that processing of rhythm is not confined to only one hemisphere.

REFERENCES

Essens PJ, Povel DJ. Metrical and nonmetrical representations of temporal patterns. Percept Psychophys 1985; 37; 1– 7.

Foote J, Uchihashi S. The beat spectrum: a new approach to rhythm analysis. Proceedings of the IEEE International Conference on Multimedia and Expo 2001.

Grossmann A, Morlet J. Decomposition of Hardy functions into square integrable wavelets of constant shape. SIAM J Math 1984; 15; 723–36.

Hämäläinen MS, Ilmoniemi RJ. Interpreting magnetic fields of the brain: minimum norm estimates. Med Biol Eng Comput 1994; 32; 35– 42.

Popescu M, Otsuka A, Ioannides AA. Dynamics of brain activity in motor and frontal cortical areas during music listening: a magnetoencephalographic study. Neuroimage 2004; 21; 1622-1638.

Halpern AR, Zatorre RJ. When that tune runs through your head: a PET investigation of auditory imagery for familiar melodies. Cereb. Cortex 1999; 9; 697–704.

Maess B, Koelsch S, Gunter TC, Friederici AD. Musical Syntax is processed in Broca's area: an MEG study. Nat. Neurosci. 2001; 4; 540–545.

Peretz I. Processing of local and global musical information in unilateral brain damaged patients. Brain 1990; 13; 1185– 1205.

Sakai K, Hikosaka O, Miyauchi S, Takino R, Tamada T, Iwata NK, Nielsen M. Neural representation of a rhythm depends on its interval ratio. J Neurosci 1999; 19; 10074–81.

Effect of Working Memory Load on MEG coherence

Tanaka, K[1], Kawakatsu, M.[1], Yunokuchi K.[2]

[1] Tokyo Denki University, Japan, [2] Kagoshima University, Japan

ABSTRACT

We examined magnetoencephalography (MEG) coherence in the 5 bands (alpha1, alpha2, beta1 and beta2) while the subjects were performing working memory tasks. MEG signals were recorded from 5 healthy males using the whole-head SQUID system. The tasks required comparing each of the current stimulus to the one that appeared on either verbal or spatial attributes 1～3 trials previously. The results showed that coherence in the beta2 (19 - 30Hz) band between regions of left hemisphere dominance significantly increased with increasing memory load during verbal working memory tasks. On the other hand, no significant changes of coherence with increasing memory load during spatial working memory tasks were obtained between any pair of sensor sites in the beta2 band. These results suggest that the spatial and verbal working memory tasks differently modulate the component of the neural circuit, and greater connections between the cortex regions of the left hemisphere increase with verbal working memory load.

KEY WORDS

Working memory, MEG, Coherence

INTRODUCTION

The human frontal cortex helps mediate working memory, a system that is used for temporary storage and manipulation of information and is involved in many higher cognitive functions, such as language, planning and problem-solving. Goldman-Rakic argues that these working memory circuits are modality-specific, with prefrontal and parietal activation for spatial processing, and prefrontal and temporal activation for non-spatial or pattern information [Wilson, 1993]. However, these studies have not focused on the functional coupling between activated brain areas during working memory processing. Thus, we used MEG coherence, which provide a functional measure of corticocortical communication. The purpose of the present study is to examine the task-related changes in magnetoencephalography (MEG) coherence during working memory loads. An increase in coherence is interpreted as increases of functional connection between two different brain areas [Miltner,1999].

METHODS

A. Experimental paradigm

Subjects were seated in front of a screen at a distance of 173cm. They performed 6 versions of continuous matching tasks (Figure 1). Matches occurred on 50% of the trials. Each stimulus item was drawn from a set of 6 capital letters. The letter on a given trial appeared at one of 6 imaginary hexagon centered in the screen. The distance from each position to the center was 3.3 cm. Presentation of letter name and position were designed so that each letter and position occurred with equal probability. Critical stimuli were presented for 250ms once every 4.5s. A fixation point appeared at the center of the screen 1.5s before the stimulus. The tasks require comparing each of the current stimuli to the one that appeared on either verbal or spatial attributes 1～3 trial before. In 6 conditions, the subjects were required to respond by lifting the right-hand index finger for non-matching stimuli (those that did not match the name or spatial position of the comparison stimulus) and lifting the right-hand middle finger for matching stimuli. Subjects were instructed to respond as quickly and accurately as possible.

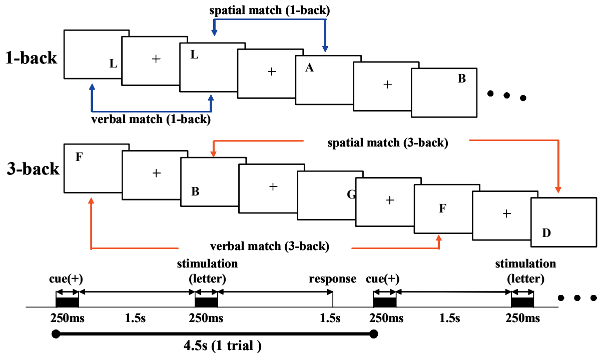

Figure 1. Diagram of working memory task.

B. Data acquisition and analysis

MEG data were recorded from 5 subjects (5 males, aged 23-27 years). Informed consent was obtained from each subject. Magnetic signals measured were using the 122-channel whole-cortex-type DC-SQUID system located in a magnetically shielded room, Tokyo Denki University. The signals were band passed filtered for 0.03-100 Hz, and digitized at 512 Hz. Fast Fourier transforms and Coherence computed 50% overlapped 2048 sample Hanning windows were calculated for all artifact-free MEG segments for correctly performed trials. Averaged power spectra and Coherence ware then computed across segments for each task condition in each subject. Coherence was defined as, $C(f)^2 = \left|S_{xy}(f)\right|^2 / S_{xx}(f) \cdot S_{yy}(f)$ where is $S_{xy}(f)$ the cross-power spectral density and $S_{xx}(f)$ and $S_{yy}(f)$ are the respective auto-power spectral densities. Coherences were calculated between censor pairs 28 of regions, following frequency bands: theta (4 – 7.5 Hz), alpha1 (7.5 – 10.0 Hz), alpha2 (10.0 – 12.5 Hz), beta1 (12.5 – 19.0 Hz) and beta2 (19.0 – 30.0 Hz).

RESULTS

A. Behavior

Mean reaction time increased significantly as the task difficulty increased (1-back=722ms, 2-back=827ms, 3-back=839ms). Accuracy decreased significantly as the task difficulty increased (1-back=0.92, 2-back=0.84, 3-back=0.80). However, there was no significant effect of task-type (Accuracy: verbal=0.84, spatial=0.86, RT: verbal=804ms, spatial=788ms). Lack of any overall difference in the speed or accuracy of performance between the spatial and verbal versions of the tasks indicates that the task types were of equal difficulty.

B. Power and coherence

Figure 2 shows significant changes in alpha1, alpha2, beta1 and beta2 band of coherence and power during (i) verbal and (ii) spatial working memory tasks. Both alpha1 and alpha2 signals were larger in the easy task conditions (1-back) than in the difficult task conditions (3-back). In addition, significant increase or decrease with the increasing difficulty of the task was observed at positions common to verbal and spatial tasks. In the beta bands, the power increased with increasing task difficulty during the verbal and spatial working memory tasks. The difference of coherence pattern was observed between verbal and spatial tasks in the beta2 (19－30Hz) band. During verbal task, coherence between regions of left hemisphere dominance significantly increased with increasing memory load. On the other hand, No significant changes in coherence with increasing memory load during spatial working memory tasks was observed between all regions.

DISCUSSION

No differences in power pattern in alpha bands between verbal and spatial modalities have been observed. This result agrees with our previous study by EEG [Tanaka, 2002]. On the other hand, the neuronal activity of the beta band has been proposed as a physiological indicator of the modality of cognitive task [Pulvermuller, 1997]. Our main result was that greater connections in beta2 between the cortex regions of the left hemisphere increase with verbal working memory load. Thus, our results support the concept that the increase of working memory load can induce the functional connection of widely extended regions. However, in spatial tasks, no significant changes in beta2 band have been observed. Bhattacharya et al reported significant increase of coherence in the gamma band (>30 Hz) between posterior and frontal cortex with increasing task difficulty during mental rotation tasks [Bhattacharya, 2001]. Thus, the effect of working memory load during spatial tasks may be present in a higher frequency band than beta2 band.

ACKNOWLEDGEMENTS

The research was financially supported by the Sasakawa Scientific Research Grant from The Japan Science Society.

REFERENCES

Wilson FO, Scalaidhe S, Goldman-Rakic P. Dissociation of object and spatial processing domains in primate prefrontal cortex. Science 1993; 260: p.1955-8.

Miltner WHR, Braun C, Arnold M, Witte H, Taub E. Coherence of gamma-band EEG activity as a basis for associative learning. Nature, 1999; 397: p. 434-6

Tanaka K, Wang G, Yunokuchi K. Properties of EEG Power Spectrum Relating to Working Memory. Trans. Jap. Soc. BME, 2002; 40-1: p. 7-13.

Pulvermuller F, Birbaumer N, Lutzenberger W Mohr B. High-frequency brain activity, its possible role in attention, perception and language processing. Progress Neurobiology, 1997; 52: p.427-45.

Bhattacharya J, Petsch H, Feldmann U, Rescher B. EEG gamma-band phase synchronization between posterior and frontal cortex during mental rotation in humans. Neuroscience Letters, 2001; 311: p.29-32.

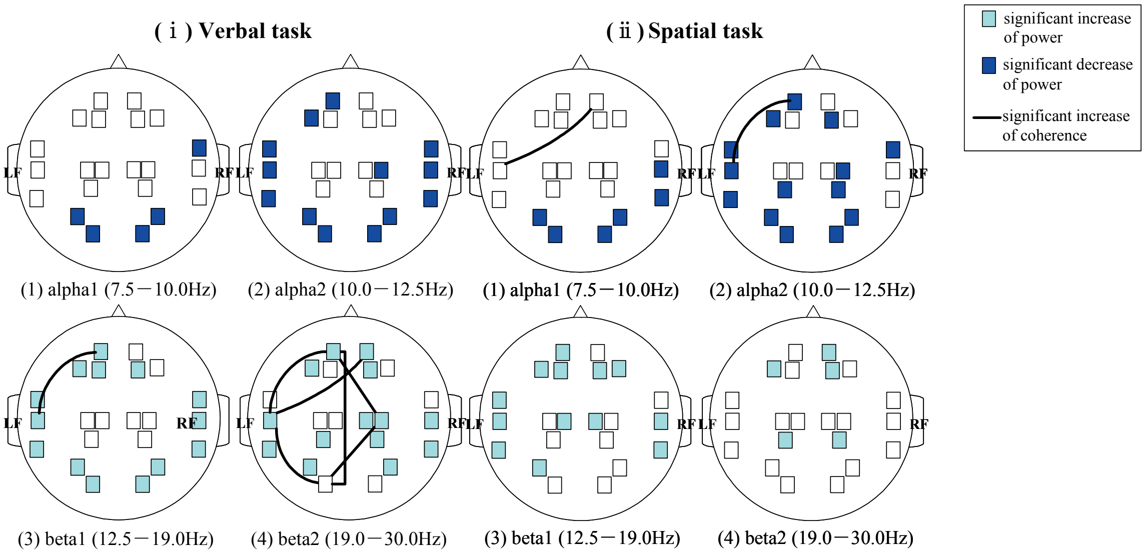

Figure 2. Significant changes of coherence and power spectrum during (i) verbal and (ii) spatial working memory tasks. The solid lines connecting sensor sites indicate significant increases of coherence with increasing memory load. Black squares, decreases; gray squares, increases of power spectrum with increasing memory load.

An Analysis of Logical Process of 3D Virtual Imaging Creation
- A Parametric fMRI Study

Li-qun Wang

Applied Superconductivity Research Laboratory, Tokyo Denki University, Japan

ABSTRACT

In the present study, a 1.5T fMRI was used to investigate that which brain areas contribute to creative imagination. The BOLD effect activations of a creative imagination task (referring to the two side views of an object, then creating the 3D image) were compared with those of a plane figure task (watching a 2D presentation and distinguish the shape). Sixteen right-handed volunteers performed the both tasks during EPI fMRI. In the creative imagination task, the activations were detected in both cerebrums of the superior, inferior parietal lobule, the superior, middle frontal gyrus, and the anterior, posterior lobe of the cerebellum. The activations in the left temporal lobe (including the fusiform gyrus) were also found during this task. In contrast, during the plane figure task, the activations were discerned in inferior occipital lobe, right middle occipital gyrus, and both cerebrum of parietal lobe. In the creative imagination process, the activation detected in the left parietal lobule suggested a logical creation analysis such as memory retrievals. The activation in the right parietal lobule suggested assistance from spatial cognition and a spatial judgment operation. The activations of the cerebellum may relate to an operation for changing position face to the 3D virtual image. We suggest that the fusiform gyrus may work as an implement object properties encoding system and support the visual buffering structure to make high spatial resolutions in imagery while multiple parts are visualized. In addition, the process of image creation is similar to the process of building blocks. They use every well-known part to make a new object.

KEY WORDS

fMRI, Human brain mapping, 3D Virtual Imaging, Creative imagination, Fusiform gyrus, Cerebellum

INTRODUCTION

In the past 10 years, fMRI has become an important tool in the study of the imaging brain function, and it has brought great changes in the estimation of visual imagery. Many studies have been conducted on the neural foundations of visual perception [Lumer, 1998 and Kosslyn, 1994;] using fMRI, and tremendous progress has been achieved. However, some questions still remain open, such as creative imagery.

In the present study, the author used a 1.5T fMRI to investigate that which brain areas contribute to creative imagination. The Blood Oxygenation Level Dependent (BOLD) effect activations of a creative imagination task (referring to the two side views of an object, then creating the 3D image) were compared with those of a plane figure task (watching a 2D presentation and distinguish the shape).

METHODS

Sixteen right-handed volunteers (ages: 20 to 36, 8 males and 8 females) participated in this experiment. They were instructed to perform both the creative imagination task and the plane figure task in silent rime during multi-slice echo-planar (EPI) T2*-weighted fMRI.

A. Equipment: A 1.5 T superconductivity magnet MRI scanner with super high speed switching EPI Gradient RF coils was used in the present study.

B. Scanning parameter: The entire brain was covered by 28slices, and the scanning parameters were:

FOV: 240×240 mm,
Matrix: 64×64,
Slice thickness: 4 mm,
Slice gap: 1 mm,
TR/TE: 4600/47.2 ms,
Total scan time: 6.0 min.

C. Design: The Boxcar alternative sequence design was adopted in this experiment. There were 3 on/off cycles in each task section. These 3 cycles were made by 6 epochs, and each epoch has 12 scans, which consists of 28 slices. Therefore, we have:

Each section = 28 slice × 12 scan × 6 epoch = 72 volume.

D. Tasks

Task 1: The participants were asked to set the creative imagination tasks (referring to the two side views of an object, then creating the 3D image of the object) as stimuli, watch a 2D presentation of the object, and then to distinguish the shape as a control.

Task 2: They were also asked to set a plane figure task (while watching a 2D presentation) and distinguish the shape as a specific task, using the white screen as their control.

E. Ex-post Processing: Image format was transformed from DICOM III to Analyze. Following the official procedures (Realign and Movement correction, Normalization, Smoothing, fMRI model estimation), statistics processing using SPM99 was performed to examine the significant difference between the activation and the control.

RESULTS

In the creative imagination task (**Figure 1.**), the activations were detected in both cerebrums of the superior, inferior parietal lobule, the superior, middle frontal gyrus, and the anterior, posterior lobe of the cerebellum. The activations in the left temporal lobe (including the fusiform gyrus) were also found during the creative imagination task ($P < 0.001$, $Z = \mathrm{Inf}$).

In contrast, during the plane figure task (**Figure 2.**), the activations were discerned in inferior occipital lobe, right middle occipital gyrus, and both cerebrum of parietal lobe ($P < 0.001$, $Z > 5.82$).

DISCUSSION

A logical thought model that builds a 3D virtual image from two side views was designed to observe logical process of creative imagination, and to visualize the activated patterns with fMRI. We focused our attention on the visual imagery and components of image creation in this study. In order to reduce the noise of visual cognitions, we also compared the activations of the creative imagination task with those of the plane figure task.

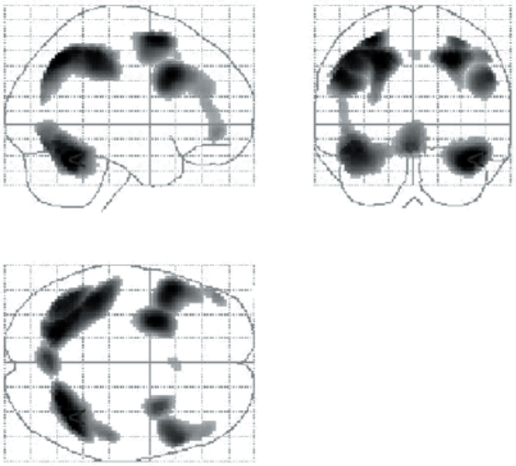

Figure 1. The activations in both cerebrums of the superior, inferior parietal lobule, the superior, middle frontal gyrus, the left temporal lobe (including fusiform gyrus), and anterior, and posterior lobe of cerebellum (in dark colour) in the creative imagination task ($P<0.001$, Z □ Inf) observed with fMRI. The results are shown in Talairach's 3D proportional system. The SPM99 final version was applied to statistics processing in the official procedure

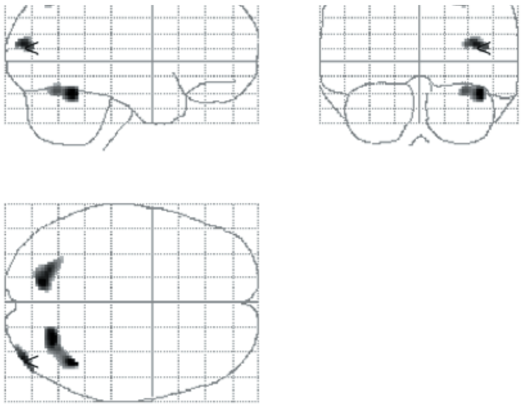

Figure 2. The activations in both cerebrums of the inferior occipital lobe, right middle occipital gyrus, and both cerebrum of parietal lobe including precuneus (in dark color) during the plane figure task ($P<0.001$, $Z>5.82$) observed with fMRI. The results are shown in Talairach's 3D proportional system. The SPM99 final version was applied to statistics processing in the official procedure.

In the creative imagination process, the activation detected in the left parietal lobule suggested a logical creation analysis such as library searching or memory retrievals. The activation in the right parietal lobule suggested that the 3D image creation, which makes spatial judgment, needs assistance from spatial cognition, such as spatial memory. The activations in both cerebrums of frontal gyrus demonstrated that an associate working memory operation is required in this processing [Author, 2000]. The activations of the cerebellum may relate to an operation for changing position face to the 3D virtual image. Activations of the fusiform gyrus suggest that the fusiform gyrus may play an important role in maintaining details of virtual images that built and memorized the properties of each part. This structure may enable one to see the shapes of different parts and how they should be put together to form the whole.

We suggest that the fusiform gyrus may work as an implement object properties encoding system and support the visual buffering structure to make high spatial resolutions in imagery while multiple parts are visualized. In addition, the process of image creation is similar to the process of building blocks. They use every well-known part to make a new object.

REFERENCES

Author AB. Neural systems activated during visual mental imagery. In Toga, A.W., Massiotta, J.C. Eds., Brain Mapping-The System. London: Academic Press; 2000

Kosslyn, S. M., Alpert, N. M., Thompson, W. L., et al. Identifying objects seen from different viewpoints: A PET investigation. Brain 1994; 117: 1055-71.

Lumer, E. D., Friston, K. J., Rees, G. Neural correlates of perceptual rivalry in the human brain. Science 1998; 280: 1930-34.

Activity in the Cingulate Region Immediately Prior to Making Response in a Working Memory Task

M. Altamura[1], B. Elvevåg[1], T. Holroyd[2], F.W. Carver[2], L. Pezawas[1], J.R. Cohen[1], V. Mattay[1],
T.E. Goldberg[1], D.R. Weinberger[1], & R. Coppola[12]
[1]Clinical Brain Disorders Branch, NIMH, Bethesda, MD, USA. [2]MEG Core Facility, NIMH.

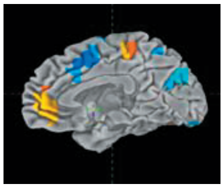

Oscillations in the theta band in anterior cingulate (AC) have been described during the N-back working memory task. Jensen [1], using a Sternberg paradigm, demonstrated that theta activity appears particularly robust following the presentation of the probe. In this study, we explored the level of AC activity immediately prior to the subjects making a response. Seven healthy subjects underwent MEG in a CTF 275-channel whole-head system while they performed two versions of the Sternberg paradigm: a delay of 1 and 6 seconds between stimulus items and the probe, with a fixed set-size of 5 letters (36 trials per each condition). Synthetic Aperture Magnetometry was used to analyze task activation in the theta band (5-8Hz) using a 500 msec time window prior to each individual's response. Analysis of Variance in AFNI yielded significant synchronization ($p<0.001$) of the rostral right AC (BA 32) that was greater for the 1-sec delay relative to the 6-sec delay (orange in figure). Additionally, a relative desynchronization (blue) was noted in the caudal portion of the right AC (BA 24). AC activity changes in the theta frequency sprior to response are consistent with the hypothesis that this region is involved in action selection. We also demonstrate that caudal and rostral portions of the AC are differentially engaged depending on how long the information has to be stored online. Activity in other frequencies and time windows are also being explored.

[1] Jensen, O., Tesche, C. 2002. Frontal theta activity in humans increases with memory load in a working memory task. European Journal of Neuroscience, 15, 395-399.

Working memory impairments after severe Traumatic Brain Injury: What does MEG reveal

Asloun S (1-2)., Croizé A.C.(2), Ducorps A.(3), Schwartz D.(3), Garnero L.(4), Azouvi P.(1)
(1) : Neurological Rehabilitation unit, R. Poincaré Hospital, Garches, France
(2) : Inserm U.483, University of Paris VI, France
(3) : MEG centre, la Salpêtrière Hospital, Paris, France
(4) : LENA-CNRS UPR 460, la Salpêtrière Hospital, Paris; France

Many studies of working memory (WM), both in healthy subjects and severe Traumatic Brain Injury (sTBI) patients, with fMRI suggested the involvement of a prefrontal and parietal network activation. To our knowledge, no study of WM after sTBI has been reported with MEG imaging. This technique is however well suited to assess the slowing down of information processing observed in TBI patients. The aim is to assess the spatial and temporal profiles of brain activity during a WM task in sTBI compared to controls. Ten healthy subjects and five sTBI were submitted to a n-back task, with three conditions of increasing WM load. First results are in agreement with cortical networks described in previous fMRI studies. Both patients and controls showed a prefrontal and parietal network activation. The novelty of these results was to reveal that all stages of information processing, involving early visual sensory signals, were slowed down in the patients group. This slowing down increased with later cognitive stages of information processing. Furthermore, patients showed a higher signal intensity than controls. Finally, while controls showed an activation involving mainly the left hemisphere, activation was bilateral in sTBI. MEG appears thus to be an interesting technique for the study of impairments in WM after sTBI. It reveals that these patients showed both a global slowing down of information processing and a higher and more widespread level of activation, presumably as adaptative mechanisms.

This poster will be presented also in symposium S2, see full paper on Page 8.

MEG and fMRI Evidence of Working-Memory Networks in Children

K.T. Ciesielski[1,2], P.G. Lesnik[1,2], S.P. Ahlfors[1]
[1]MGH/MIT/HMS Athinoula A. Martinos Center for Biomedical Imaging, Charlestown, USA.
[2]Department of Psychology, University of New Mexico, Albuquerque, N.M., USA

We investigated developmental changes within frontal-cerebella and parietal-striatal neural networks related to executive control of information manipulation, particularly inhibitory control during working memory (WM) tasks: Our hypotheses were: (1) in different stages of development different components within these networks may become activated, (2) the pattern of activation within the two networks depends on both neural tissue maturation and task strategies employed by children and adults. fMRI and MEG were used to examine spatiotemporal patterns of network activation in ten year-old children and young adults performing a categorical N-back working memory task, which required rapid and accurate categorization of a visual event, based on correct classification of two preceding events. Semantic feature selection plays an important role in this task. fMRI data was analyzed with SPM99 (Welcome Dept of Cognitive Neurology, UK). MEG sources were estimated with a minimum-norm solution on the cortical surface. Three major regions were specifically activated in children: 1) lateral and posterior cerebellum, 2) premotor and supplementary motor cortex, and 3) anterior insula and putamen/caudate nuclei. In adults the predominant activation occurred about 30 ms earlier than in children and involved dorsolateral prefrontal (BA 9 & 10), inferior/ventral prefrontal (BA 47, 45, 11; L>R) cortex, posterior cingulate (BA 31) and to a lesser degree lateral cerebellum. MEG suggested major activity within the time window of 360-400 ms post-stimulus. The primary involvement of the cerebellum and premotor cortices in children and inferior/ventral prefrontal areas in adults suggests a developmental shift in strategies used to solve the categorization task: from action knowledge used by children, to semantic-feature selection strategies in adults, who are able to utilize later maturing prefrontal cortices. Supported by The MIND Institute.

MEG activation comparison to fMRI BOLD for a working memory task

R. Coppola[12], J.H. Calicott[2], T. Holroyd[1], B.A. Verchinski[2], S. Sust[2], D.R. Weinberger[2]
[1]MEG Core Facility, NIMH, Bethesda, MD, USA. [2]Clinical Brain Disorders Branch, NIMH.

Cognitive tasks have been explored with metabolic and electrophysiological activation measures. Here we examine the relation between BOLD fMRI and MEG to a working memory task in the same group of normal volunteers. Subjects performed a run of sixteen 22 second blocks alternating between a 2-back and a 0-back visually presented task. Stimuli were one of 4 numbers; response was a button press to match the current number (0-back) or the number from 2 trials previous. MEG was recorded on a CTF 275 channel system. Synthetic aperture magnetometry was used to analyze task related activation differences in theta, alpha, beta, and gamma frequency bands. SAM creates an optimum spatial filter from the covariance between the active state (2-back) and control state (0-back) to calculate a 3-d source image comparing the source strength for specified time windows for the two states. In this case we used time windows comprising either 500 msec after the stim, 500 msec centered on the response, or the middle 14 sec of the block. Group t-maps were created in AFNI by aligning to Talairach the individual z-scored SAM volumes registered to their structural MRI. BOLD fMRI was collected at 3T (GE EPI-RT) to identical task design. Data were structurally aligned, smoothed, and normalized to MNI space using SPM99. Single subj block design contrast maps for 2b>0b were followed by a group second level analysis and thresholded at approximately p<.001. This map showed activation of the working memory network as described in several studies. Of the 12 SAM maps (4 freq bands by 3 time windows) only the beta band for the response window showed very high agreement with the BOLD activation. At comparable p level threshold the MEG showed beta desynchronization with a very similar spatial extent to the BOLD activation. This relationship will be important for better understanding of the physiological basis of neuroimaging activation.

Spatio-temporal organisation of frontal cortical areas underlying different levels of cognitive control

A.C. Croizé[1,2] and Y. Burnod[1,2]
[1] INSERM U483, Université Pierre et Marie Curie, Paris, France; [2] IFR 49

The aim of the present study is to determine the specific function of frontal regions at different levels of cognitive control. Four tasks have been used to specify the spatio-temporal dynamics of frontal activation patterns: 1) A simple visuo-spatial delayed-task guided by a single rule of response; 2) A switching delayed-task including two rules of response; 3) A predictive branching task [2] : the subjects had to respond according to a single rule, so the sequences were predictive; 4) An unpredictive branching task: two different rules were introduced pseudo-randomly into the sequences, so the subjects could not predict the rule required. Event-related magnetic fields were recorded in 15 healthy volunteers. Computation of magnetic generators was performed using Minimum Norm algorithms [3]. Encoding and retrieval processes involved in the simple delayed-task are accompagnied by activation (450 msec) in the right premotor (BA 6) and superior frontal regions (BA 8/9) [1]. The comparison between switching and simple delayed-tasks reveals an early frontal activation, involving the right dorsolateral prefrontal cortex (BA 46 - 200-400 msec). Both branching tasks involve activation of the fronto-polar regions (BA 10), with a medial prefrontal activation in the predictive branching task, and an increased early activation of the dorsolateral prefrontal cortex (BA 46) in the unpredictive branching. These observations suggest a hierarchical antero-posterior organization of the frontal cortex consisting of top-down interactions between prefrontal regions and premotor area [2, 3]. Moreover, frontopolar and dorsolateral cortex was engaged when subjects performed sequences of goals contingent to an external event, while medial prefrontal cortex was involved in predictive sequences of goals. These results are consistent with the idea that processing predictive and unpredictive sequences of goals are mediated by distinct prefrontal networks along the medial-lateral axis [4]. [1] Croizé A.C., et al.. (in press).. Neuroimage. [2] Koechlin E., Basso G., et al. 1999. Nature, 399, 148-151. [3] Koechlin E., Ody C., Kouneiher F. (in press). Science. [4] Dreher J.C., Koechlin E., Ali S.O., Grafman J. 2002. Neuroimage, 17, 95-109.

Neural Dynamics Underlying Time Estimation in an Auditory Oddball Task

B. Elvevåg[1], F.W. Carver[2], M. Altamura[1], T. Holroyd[2], V. Mattay[1], T.E. Goldberg[1], D.R. Weinberger[1] & R. Coppola1[2]
[1] Clinical Brain Disorders Branch, NIMH, Bethesda, MD, USA. [2] MEG Core Facility, NIMH.

Understanding real-time dynamics in subcortical and cortical brain structures at a basic level may provide a useful framework with which to examine clinical disorders that alter the synchrony of the underlying neural populations. We used 275 channel MEG to explore the spatiotemporal dynamics underlying simple time estimation. Eight subjects listened to 250 1kHz tones of which 50 were target tones (600ms), requiring a right button press. The remaining 1200ms tones were to be ignored. We analyzed the 500ms after target tone offset (during response preparation), as compared to 500ms prior to tone onset. Synthetic Aperture Magnetometry was used to examine activation in the theta (5-8Hz), alpha (8-12Hz), beta (14-30Hz) and gamma (30-50Hz) frequency bands, and t-tests ($p<0.001$) were computed in AFNI. In the theta band an increase in power (synchronization) occurred in right medial frontal gyrus, bilateral middle frontal gyri and left inferior frontal gyrus. In the alpha band there was an increase in power in anterior and posterior cingulate and right medial prefrontal regions, and a decrease in power (desynchronization) in left parietal region (BA 7), bilateral superior temporal gyri and occipital areas. In the beta band there was an increase in power in bilateral medial frontal gyri and cerebellar vermis, and a decrease in power in left motor and premotor areas. In the gamma band there was synchronization in right caudate and bilaterally in the cerebellum, and desynchronization in left parietal regions. These data complement recent fMRI studies and demonstrate the viability of examining both cortical and subcortical structures on a millisecond time-scale.

Object Priming-Related Changes in Cortical Synchronization

J. Gilbert,[1] T. Holroyd,[2] F. W. Carver,[2] P. Bellgowan,[1] and A. Martin[1]
[1] Laboratory of Brain and Cognition, NIMH, USA
[2] MEG Core Facility, NIMH, USA

We used magnetoencephalography (MEG) to study the neural system involved in repetition priming using an object-naming paradigm. During scanning, subjects (n=9) were shown rapidly presented pictures of animals (stimulus duration=300 msec; ISI=1700 msec), and asked to respond with a button press as they named the animal to themselves. Subjects viewed 50 exemplars of differing animals (e.g., dog, cat, mouse), with each picture repeating 5 times over the duration of the scan. In this way, we could look at the neural effects of novel stimuli (first presentation) to repeating stimuli (second, third, fourth, and fifth presentations) over the course of one experimental run. The MEG data were analyzed in both beta (BB, 14-30Hz) and gamma (GB, 30-50Hz) bands using Synthetic Aperture Magnetometry (SAM), an adaptive beamformer technique that provides continuous, 3-dimensional images of cortical power changes. These power changes, reflecting cortical firing synchrony or asynchrony, were analyzed during a time window beginning 100 msec prior to stimulus onset and lasting 100 msec post offset (duration=500 msec), for each of the five conditions. Individual subject data were then normalized and averaged for each condition, and compared across conditions using random-effects ANOVA. In agreement with previous functional MRI studies [1], our analysis revealed posterior ventral temporal decreases in BB synchrony with stimulus repetition, coupled with increases in left insula. In addition, we found GB decreases in occipital and posterior parietal areas, and increases in left frontal regions, including BA 10. These findings are consistent with the claim that posterior and anterior cortical regions make unique and different contributions to object priming; a long-lasting, implicit form of memory.

[1] van Turennout, M., Ellmore, T., and Martin, A. 2000. Long-lasting cortical plasticity in the object naming system. *Nature Neuroscience* 3, 1329-1334.

Equivalent current dipole estimation from human brain magnetic evoked responses to visual and auditory stimuli as part of a short-term memory task

Klevest Gjini, Takashi Maeno, Keiji Iramina, Shoogo Ueno
Department of Biomedical Engineering,
Graduate School of Medicine, University of Tokyo, Japan

A delayed matched-to-sample short-term memory task with visual and auditory stimuli was used during magnetoencephalolographic measurements to assess the brain activity related to basic visual and auditory stimulation, and further, encoding of the presented visual stimuli in short-term memory. In the delayed match-to-sample task with visual stimuli each trial consisted in the presentation of a sample visual pattern (composed of four colored basic shapes) for 500ms. In the delayed match-to-sample task with auditory stimuli each trial consisted in the presentation of a sample auditory stimulus (combination of the names of four colors used in visual stimulation). After an interval of 3.5 seconds a test stimulus was presented for comparison. The subjects were instructed to make a comparison and later give a response when a third stimulus (mark) was presented 1.5s later. This sequence was used in control condition, too (without memorizing the sample; giving a response after each mark). Magnetic measurements were carried out using a 204-channels whole head device. Averaged evoked responses were obtained from around 100 trials. ECD (equivalent current dipole) fitting procedure was used to estimate the activity related to basic visual and auditory stimulation during the first 200 ms from the stimulus onset, and further, to encoding of the presented stimuli in short-term memory. ECDs representing activation to basic visual and auditory sensory stimulation were estimated in primary visual and auditory cortices, respectively. Regarding the process of encoding of the presented visual stimuli, a possible activation of the Wernicke’s area and the inferotemporal cortex were evaluated. In the case of auditory modality a post-activation of visual association cortex around 300ms was estimated.

Electrophysiological Correlates and Neuronal Substrates of the Perception of Musical Phrase Structure

T. R. Knösche[1], C. Neuhaus[1,2], J. Haueisen[2]
[1] Max-Planck-Institute for Human Cognitive and Brain Sciences, Leipzig, Germany
[2] Friedrich Schiller University, Jena, Germany

The processing of phrase boundaries is crucial for the perception and understanding of sequential information, such as music or speech. We investigate EEG and MEG components related to these processes in music perception and identify the underlying neural networks. Twelve right-handed musicians listened to 100 different melodies, differing in phrase structure. ERP (32 electrodes) and MEG (whole-head, 148 magnetometers) were recorded. Significant neural correlates to the processing of the phrase boundaries were identified and analyzed using ANOVA. The Multiple Signal Classification (MUSIC) method was employed to identify potentially active brain regions. EEG revealed a centro-parietal deflection peaking at about 550 ms after pause offset in response to the phrase boundary. The analysis of the MEG waveforms resulted in a longer period of time with significant differences between both conditions. Source analysis revealed active regions include posterior and anterior cingulate, retrosplenial cortex, and the posterior part of the hippocampus. The topology of the ERP effect suggests that it is related to the closure positive shift (CPS) reported for language [1]. Its likely origin from limbic structures such as cingulate cortex and parahippocampal region points towards an interplay of attentional and memory processes being involved in the processing of musical phrase structures. Hence, it seems that the CPS reflects processes that are necessary for shifting resources from the previous phrase to the next one. The different time course of the EEG and MEG effects within the investigated time window proves that several subprocesses involving different neural networks are activated sequentially.

This work was supported in part by the European Union and the Thuringian Ministry of Science.

[1] Steinhauer K, Alter K, Friederici AD. *Nature Neuroscience* 2(2), 191-196 (1999)

Encoding of Visual Features and Their Conjunctions: An fMRI and MEG Study

S. Kovacevic*, V.P. Clark*, Y. Okada*, L.D. Partridge*, and C.J. Aine †*
*University of New Mexico; † New Mexico VA Health Care System, Albuquerque, NM, USA

Previous studies in both human and non-human primates suggest that dorsal higher-order visual regions are specialized for processing spatial information and ventral regions for object information, although less is known about how spatial and object information is combined. In this study, we were interested in determining whether encoding conjunctions of color and location information will enhance activity in dorsal extrastriate regions that are predominantly involved in location processing, e.g. the supramarginal gyrus and the inferior parietal lobule. Both fMRI and MEG data were collected on the same healthy young subjects (25-35 years of age) in a counterbalanced design using the same stimuli and timing parameters. Stimuli consisted of a 4x4 matrix of different colored squares, in which one square was probed at a time. Subjects were instructed to encode color only, location only, or both color and location of the probed squares during different runs. The encoding tasks were followed by a dot detection task, which served as a baseline for the fMRI data analysis, and then recognition tests for the encoded feature or features. Active brain regions and their associated time-courses were characterized by using the multi-start spatial-temporal algorithm (MSST) on MEG data. Subjects performed equally well on all recognition conditions. In agreement with previous studies both fMRI and MEG data suggest that the encode location task, when compared to the encode color task, elicited stronger activity in the inferior parietal lobule/supramarginal gyrus. Activity in this region was strongest during the encode both color and location task. Differences in the time-courses of the MEG sources associated with different encoding conditions, localized in the vicinity of this parietal region were apparent as early as 130 ms poststimulus. Our findings suggest that the inferior parietal lobule/supramarginal gyrus is important in processing and perhaps binding of spatial and object information together. This work was supported by a grant from The MIND Institute.

Transient and Steady-State magnetic fields following combined audio-electrical stimulation

Matthias Schulz[1,2,3], Bernhard Ross[2,3] and Christo Pantev[2,3]
[1]Department of Psychiatry, and [2]Institute of Biomagnetism and Biosignalanalysis, University of Muenster, Muenster, Germany; [3]The Rotman Research Institute for Neuroscience, Baycrest Centre for Geriatric Care, Toronto, Ontario, Canada

Multisensory integration has been defined by Meredith and Stein [1] as the increase of a neuron's responses to a stimulus combination compared with its response to an individual stimulus. Multimodal representations are possibly generated through the convergence of information from different sensory systems onto a common group of neurons. To understand the dynamics of multisensory integration in humans by means of Magnetoencephalography is a methodical enterprise. In this study we introduce and assess a stimulation paradigm allowing the combined measure of the steady-state field (SSR) and the transient evoked field exploring at the same time auditory and somatosensory brain responses. To this end nine adults were investigated by whole-head MEG using a single equivalent current dipole (ECD) approximation and synthetic aperture magnetometry (SAM). Electrical and auditory stimuli were presented either alone or in combination. The electrical stimulation comprises a 27-Hz amplitude modulation stimulus and the acoustic stimulus consists of a 500-ms tone burst with 39-Hz amplitude modulation of the carrier frequency. We demonstrate here that the distinct sources of steady-state and transient responses can be reliably measured without significant spatial distortion with this combined stimulation paradigm for both the auditory and somatosensory modality, enabling the exploration of audiotactile interaction effects on the primary and secondary cortical level. [1] Meredith MA and Stein BE. 1983. Science 221, 389–391.

Cortical rhythms of rhythmical tune tapping

Matthias Schulz[1,2,3], Bernhard Ross[2,3], Andreas Wollbrink[2,3], Wilkin Chau[3], Takako Fujioka[3], Ryouhei Ishii[3] and Christo Pantev[2,3]
[1]Department of Psychiatry, and [2]Institute of Biomagnetism and Biosignalanalysis, University of Muenster, Muenster, Germany; [3]The Rotman Research Institute for Neuroscience, Baycrest Centre for Geriatric Care, Toronto, Ontario, Canada

Music is a universal tongue; simple tunes are ubiquitously whistled or tapped. Music can be performed solely from memory (internally-cued) or played in the concert with auditory cues (externally-cued). The motivation of this MEG study was to explore the neuronal correlates of internally-cued and externally-cued rhythmical tune tapping. Ten subjects with no former musical training tapped the rhythm of a well-known tune from Carmen either *(a)* self-generated by recalling the tune merely from memory (internally-cued) or *(b)* externally controlled by tapping in synchrony to the simultaneously presented tune (externally-cued). An imperative stimulus informed the subjects prior to the task which of the conditions *(a or b)* will follow in order to obtain brain responses *(1)* in preparation to the task and as well *(2)* during the task. Magnetic fields where recorded using a 151-channel MEG whole-cortex system and analyzed using synthetic aperture magnetometry (SAM). Our study shows that a complex cognitive function like the performance of music is orchestrated by the interplay of numerous cortical areas. Delta, alpha and beta oscillatory activity was found in the posterior parietal cortex particularly during the preparation of the internally-cued tune tapping *(1a)*. Throughout the internally-cued tune tapping *(2a)* theta and delta band activity was found in the dorsolateral prefrontal cortex and as well in the left inferior temporal cortex. Whereas for the externally-cued simultaneous tune tapping mainly high gamma band activity in the primary motor cortex, supplementy motor cortex and the gyrus cingulum *(2b)* was found.

Coherence Analysis Reveals Brain Networks Associated with Learning to Entrain Movement to Visual Cues

C.D. Tesche[1], T. Martin[1], J.M. Houck[1], R.J. Ilmoniemi[2]
[1]University of New Mexico, USA [2]BioMag Laboratory, HUCH, Finland

Movements cued by a train of visual stimuli shift from reaction to the stimuli to anticipation of presented stimuli after only a few cues. Entrainment of movement requires attention to the timing of presented stimuli, estimation of inter-stimulus intervals, and execution of motor responses guided by the temporal pattern of stimuli. We investigated the interaction between cerebellum and motor cortex during the development of entrained finger movements with MEG. A train of 10 white circles with foveal presentation (stimulus duration 750 ms, inter-stimulus interval 350 ms) served as cues for right index finger movement. Data were recorded from 5 subjects for 100 stimulus trains (inter-train interval 4.25 s). An L1 Minimum-Norm Current Estimate algorithm (MCE) was used to identify the spatio-temporal pattern of brain activity. Source locations/orientations for activity in contralateral motor cortex were extracted on an individual-subject basis from data time-locked to the movements. Spectra characterizing coherent activation of motor cortex and cerebellum were computed from data time-locked to stimulus presentation. Coherent activity occurred at frequencies of 0.6-14 Hz. The distribution of sources within cerebellum and associated brainstem structures depended on the location of the cue in the sequence of stimuli. A unique set of sources emerged as the movement shifted from reactive to anticipatory. Coherent oscillatory activity has been reported within and between cortical areas during stimulus processing and between motor cortex and muscle. The present results suggest that coherent phenomena may be observed also in cortico-cerebellar networks, and this coherence may reflect processing of temporal information.

Supported by a grant from the MIND Institute

The study of working memory with a novel method of stimulus presentation

M.P. Weisend[1,3,5], F.M. Hanlon[2,5], M.X. Huang[1], R.J. Thoma[2,5], R.R. Lee[1], G.A. Miller[6], and J.M. Canive[2,5].
Department of Radiology[1] and Psychiatry[2] New Mexico VA Health Care System. Depts of Radiology[3], Psychiatry[4], and Psychology[5], University of New Mexico, Albuquerque, NM, USA; Depts of Psychology, Psychiatry, and The Beckman Institute[6], University of Illinois, Urbana-Champaign, IL, USA

A major difficult in the study of cognitive functions with magnetoencephalography (MEG) is the characterization of a large and unknown number of sources with activations that overlap in time. The stimuli in most studies of cognitive phenomena are presented with rapid onset. This produces excellent time locked responses in sensory cortices and typically less robust responses in higher order cortices. This is less than optimal since higher order cortices are often the targets of study in cognition while sensory sources are subtracted out as “noise.” In this study we demonstrate a method of stimulus presentation that tightly controls activations in sensory cortices while preserving activity in higher-order cortices. 122-channel MEG data was collected while subjects performed a delayed match-to-sample working memory task. The subjects were presented with a sample letter and after a delay, distractors and a match for the sample. Stimuli were presented with rapid onset or with smooth “movie-like” transitions between stimuli. Spatial-temporal source analysis was done with the multistart spatial temporal dipole fitting method. When stimuli were presented with rapid onset 42.5% of all sources localized to primary visual cortices. With smooth transitions between stimuli only 20% localized to primary visual cortex. Similar numbers of were elicited by stimulus presentation with rapid onset and smooth transitions. However, the sources in higher order cortices, including dorsal lateral prefrontal cortex, posterior parietal cortices and temporal lobe sources, were found with greater frequency and reliability when stimuli were presented with smooth transitions. A NARSAD Young Investigator Award to MPW supported this work.

P1-4

Cortical Hyperexcitability in a Migraine patient before and after Sodium Valproate Treatment

Bowyer S.M.[1,2,3], Mason K.M.[1], Moran J.E.[1], Tepley N.[1,2], and Mitsias P.D. [1,3]

[1]Henry Ford Health System, USA; [2]Oakland University, USA; [3]Wayne State University, USA.

ABSTRACT

DC-MEG waveforms arising during migraine aura were utilized to determine effectiveness of prophylactic medication therapy on neuronal hyperexcitability. Seven patients were prescribed valproate (Depakote) for migraine prophylaxis. MEG scans were recorded during visual stimulation before commencing medication and again after 30 days of daily use of Depakote. Cortical brain activity was recorded during stimulation with a black and white circular checkerboard pattern alternating at 8 Hz and analyzed with MR-FOCUSS. Large amplitude DC-MEG signals, imaged to extended areas of occipital cortex, were seen prior to therapy. After 30 days of prophylactic treatment, reduced DC-MEG shifts in the occipital cortex and reduced incidence of migraine attacks were observed. Using visual stimulation, we have confirmed the hyperexcitability of widespread regions throughout occipital cortex in migraine patients, explaining the susceptibility for triggering SCD and migraine aura. This study confirmed that MEG can non-invasively determine the status of neuronal excitability pre and post therapy. This may be helpful in determining which prophylactic medications will be most effective in reducing hyperexcitability in particular patients.

KEYWORDS

DC-MEG, Migraine, valproate, MR-FOCUSS

INTRODUCTION

Excitability of cell membranes appears to be a fundamental factor in the brain's susceptibility to migraine attack [Welch, 2003]. We have previously used MEG to study the DC-MEG shifts that arise in visually stimulated Migraine patients [Bowyer, 2001]. DC-MEG shifts provide direct measurement of neuronal excitation and suppression. We demonstrated DC-MEG field shifts arising during spontaneous and visually induced migraine aura, resembling those previously reported from spreading cortical depression (SCD) crossing a sulcus in animal models, in which electrocorticography (ECoG) was used to confirm SCD depolarization [Bowyer, 1999,1999].

We present a preliminary study of patients with migraine who received prophylactic treatment with sodium valproate and underwent MEG studies prior to start of treatment and at follow up, in an attempt to define MEG waveform characteristics that are associated with good response to treatment.

METHODS

Seven patients with migraine (3 with aura and 4 without aura) as diagnosed based on the International Headache Society [IHS, 2004], were recruited from the outpatient headache clinic at Henry Ford Hospital. Mean age was 37±13 years old, 5 women and 2 men. The treating physician had prescribed sodium valproate (Depakote®) 125 mg twice daily, for migraine prophylaxis, as part of their routine clinical care. Each patient gave written informed consent to participate in this study, which was approved by the Institutional Review Board of Henry Ford Hospital.

The MEG studies were performed using a 148-channel Neuromagnetometer (4D Neuroimaging WH2500). Patients were prepared for studies in our customary way [Bowyer, 2001]. The visual stimulus pattern, a circular checkerboard, was previously described in Bowyer [2001]. The stimulus pattern alternated black and white at 8 Hz. DC MEG fields were recorded during visual stimulation by the checkerboard pattern, prior to commencement of medication. Patients returned to the MEG laboratory 30 days later after continuous daily use of the prescribed dose of sodium valproate and the same visual stimulations and MEG recordings were performed.

All data were digitized at 254 samples per second, band passed at 0-100 Hz. Data were filtered at 0.001-100 Hz to remove equipment drift, which was coherent in all 148 channels. The data were then decimated from 254 to 11 samples per second to simplify computer analysis. These two steps eliminated most of the high frequency signals and artifacts without significantly affecting the slowly varying DC shifts, which occurred over minutes. The data were analyzed for DC-MEG shifts. To correlate MEG areas of cortical activity with specific anatomical structures, a standard volumetric MRI scan was manually rescaled to the patient's digitized head shape [Moore, 2000]. The magnetic resonance imaging (MRI) scan was a sagittal T1 image, 124 slices, and 256x256 matrix that included the entire skin surface of the head. The MRI was used to constrain cortical images obtained by MR-FOCUSS [Moran, 2001] to lie within the cortical gray matter. The results were then displayed on the volumetric MRI scan which was co-registered to the subject's MEG x, y, z coordinate system. These coordinates were established during data acquisition.

MR-FOCUSS provides whole brain images of both focal and extended sources, which may be simultaneously active. The MR-FOCUSS results were displayed on the subject's MRI scan. Selection of significant activation is determined by setting the display threshold to 25 % (color coded white, see figure 1) of the maximum cortical source amplitude and for significant locations 80–100% (color coded black). For the MR-FOCUSS solution in this study, approximately 60 percent of all source locations have amplitudes less than 0.5% of the maximum amplitude. For the 25 % display threshold, the most active 5 to10 percent of the cortex is depicted in each gray scale color-coded functional image of figure 1, with black representing approximately the top 0.3 percent most active sites (9 out of 2900 sites).

RESULTS

Prior to initiation of treatment with sodium valproate, DC-MEG shifts were seen in the extended occipital and parietal cortex, as well as frontal cortical regions in all seven patients, confirming the hyper-excitability of the occipital cortex to visual stimulation. Figure 1A shows the DC-MEG results prior to medication in one patient. Note the extended cortical areas of activation in the occipital, parietal, and frontal cortex. Average MR-FOCUSS analysis of the imaged MEG activation data are displayed on a standard anatomical MRI scan. The average is over the first 400 seconds.

Thirty days after initiation of sodium valproate treatment, migraine attacks in three out of four patients were much less frequent. The other three of the initial seven subjects did not return for the follow up study. Following 30 days of continuous treatment, MEG recordings revealed a reduction of DC shifts in three patients, an indication that the medication inhibited the cortical hyper-excitability or changed the threshold for induction of SCD or an SCD like event. In these three patients there were corresponding reductions of migraine occurrence over the month. The one subject who did not have a reduction in DC shifts also did not have a reduction in migraine occurrence. Figure 1B displays the DCMEG results seen after 30 days of prophylactic migraine treatment in the same patient displayed in figure 1A. Reduced cortical activity in the occipital cortex is seen in the averaged MR-FOCUSS analysis of the imaged activation results on the coronal MRI scans. The average is again over the initial first 400 seconds. Frontal cortical activation was noted, likely from temporal muscle clenching during the visual stimulation. This appears on both pre and post medication MEG studies.

We compared the finding from this patient to those of normal controls. Control subjects displayed no DC-MEG shifts as previously reported in [Bowyer, 2001].

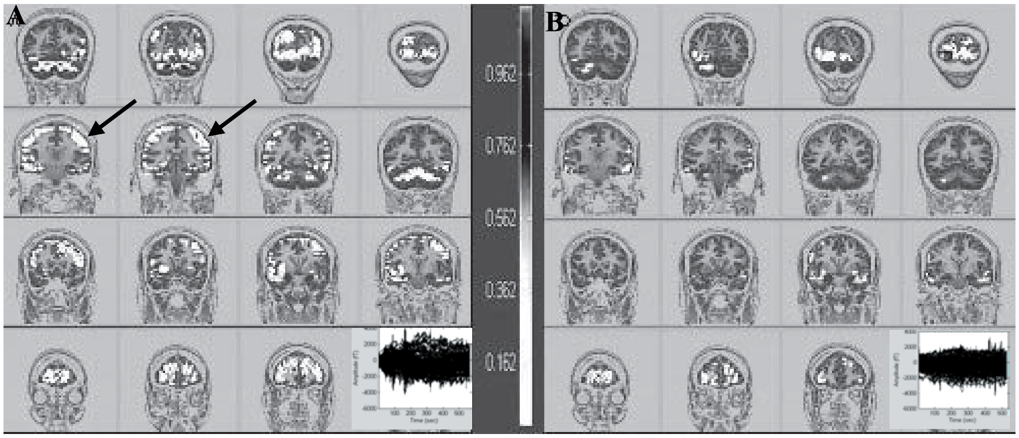

Figure 1. A) MR-FOCUSS analysis of the MEG recordings from a migraine patient prior to start of treatment with sodium valproate. Averaged MEG image activation results of cortical activity, over the initial 400 seconds, are overlaid onto a standard coronal MRI scan. Scale is in nanoAmp-Meters. Note the extended cortical areas (light color) of activation in the occipital, parietal (large arrows), and frontal cortex. 148 channel MEG graph in lower right hand corner displays DC shifts. B) MR-FOCUSS analysis of the MEG recordings from the same migraine patient after 30 days of treatment with sodium valproate. Averaged image activation MEG results of cortical activity are overlaid onto a standard coronal MRI scan. Note the reduced cortical activity in the extended occipital and parietal cortex. 148 channel MEG graph in lower right hand corner displays reduced DC shifts.

DISCUSSION

This study confirmed the hyperexcitability of the occipital cortex in patient's with migraine. It also supported the hypothesis that cortical excitability was reduced after 30 days of prophylactic drug treatment, which could correlate with the patient's clinical response to prophylactic therapy.

Using visual stimulation techniques, we have confirmed the hyperexcitability of widespread regions throughout occipital cortex, similar to our previous report [Bowyer, 2001]. This helps explain the susceptibility for triggering SCD or SCD-like events in migraine sufferers, and suggests that such neuroimaging studies pre and post migraine drug therapy may increase understanding of how sodium valproate, and perhaps other anti-migraine drugs, exert their antimigrainous action. We have shown that the use of MEG can determine the status of neuronal excitability pre- and post-prophylactic medication therapy non-invasively. If further studies reveal a reduction in DC shifts or normalization of the VECMF after other prophylactic drug therapy has been initiated, then the relationship between the drug used and the underlying hyper-excitability will be established.

The MEG DC shift changes observed from the baseline to the post-treatment study are likely linked to the use of sodium valproate as migraine prophylaxis, and correlate well with the patient's clinical response to the treatment. A concern here could be that the observed change after sodium valproate is a reflection of normal fluctuations in brain excitability and not a response to the drug. However, in previous studies of migraine patients and controls [Bowyer 2001] we have not observed any significant fluctuations, therefore ruling out this possibility and confirming that the change is indeed linked to the sodium valproate use. This is an important finding because MEG may offer information about response to prophylactic therapy early in the course of treatment, and thus could be used as a tool for selecting the appropriate prophylactic medication for each patient. MEG could be used through out the treatment process to adjust medication therapy accordingly for the benefit of the patient. Since patients may indicate a reduction in headache occurrences, which may or may not be the result of the prophylactic medication therapy they are usually kept on the same medication for several months before a change in medication is implemented. MEG can be used to guide therapy after the initial 30-day drug intervention by indicating the actual impact of the drug on cortical excitability. This should be demonstrated in the context of a larger study, in which patients are subjected to a variety of prophylactic agents.

ACKNOWLEDGEMNT: Research supported by NIH/NINDS Grant RO1-NS30914.

REFERENCES

Bowyer SM, Aurora SK, Moran JE, Tepley N, and Welch KMA. MEG Fields from Patients with Spontaneous and Induced Migraine Aura. Annals of Neurology 2001;50:582-587.

Bowyer SM, Okada YC, Papuashvili N, Moran, J.E., Barkley, G.L., Welch, K.M.A., and Tepley, N. Analysis of MEG signals of spreading cortical depression with propagation constrained to a rectangular cortical strip: I. Lissencephalic rabbit model. Brain Research 1999; 843:71-78.

Bowyer SM, Tepley N, Papuashvili N, Kato, S., Barkley, G.L., Welch, K.M.A., and Okada, Y.C. Analysis of MEG signals of spreading cortical depression with propagation constrained to a rectangular cortical strip: II. Gyrencephalic swine model. Brain Research 1999; 843:79-86.

Headache Classification Subcommittee of the International Headache Society. The International Classification of Headache Disorders 2^{nd} Edition. Cephalalgia 2004; 24 (S1).

Moore CI, Stern CE, Corkin S, Fischl B, Gray AC, Rosen BR, Dale AM Segregation of somatosensory activation in the human rolandic cortex using fMRI. J Neurophysiol 2000; 8:558-69.

Moran JE, Bowyer SM, Tepley N. Multi-Resolution FOCUSS source imaging of MEG Data. 3rd International Symposium on Noninvasive Functional Source Imaging within the Human Brain and Heart, Biomedizinische Technik 2001; 46 : 112-114.

Welch KMA. Contemporary concepts of migraine pathogenesis. Neurology 2003;61:S4: 2-8.

Tonic motor cortex activation during fast and slow finger movements analyzed by simultaneous DC-Magnetoencephalography and DC-Electroencephalography

Leistner, S.[1], Sander, T.[2], Burghoff, M.[2], Curio, G.[1], Trahms, L.[2], Mackert, B.M.[1]

[1] Neurophysics Group, Campus Benjamin Franklin, Charité-University Medicine, Berlin, Germany
[2] Physikalisch-Technische Bundesanstalt, Section Biomagnetism, Berlin, Germany

ABSTRACT

Functional neuroimaging studies on repetitive finger movements show a positive correlation between movement frequency and cortical activation. During very fast movements this correlation is abolished probably because of automation. Methodologically, these studies visualize neuronal activation indirectly via concomitant vascular/metabolic changes.. Here, activation characteristics for fast and slow finger movements were analyzed intraindividually using two electrophysiological techniques, DC-MEG as well as DC-EEG, simultaneously. 7 healthy subjects performed self-paced finger movements using the right hand: to prevent automation the subjects bent alternatingly the 2. and 3. finger twice (30 s fast/slow separated by 30 s rest). DC-fields were recorded over the left hemisphere using a modulation-based MEG technique. DC-EEG was recorded using an custom-made DC-amplifier and 16 DC-surface electrodes covering the left primary motor cortex. In 6/7 subjects motor-related DC-fields were recorded reproducible above noise level and closely related to the movement periods. Fast finger movements revealed significantly stronger magnetic field amplitudes than slow movements. DC-EEG revealed a tonic DC-shift over the left hemisphere during the activation; notably, the time curves were prolonged when compared to the DC-MEG. In this study DCEEG is applied in combination with DCMEG to test the feasibility of combined measurements for the investigation of neurovascular coupling in long lasting paradigms. In the exemplary simple finger movement paradigm, stronger cortical activation during fast, non automatized finger movements in comparison to slow movements was demonstrated.

KEY WORDS

Magnetoencephalography, Electroencephalography, Finger movements, Direct current recordings, Primary somatosensory cortex

INTRODUCTION

Functional neuroimaging studies with Magnetic Resonance Imaging or Position Emission Tomography showed a linearly stronger motor cortex activation with increasing rates of finger tapping, both in terms of volume and strength of activity [VanMeter, 1995] [Schlaug, 1996]. This rate-effect is thought to reflect increased motor control demands during higher rates of finger movements [Jancke, 1998]. On the other hand, no further increase of motor cortex activation was reported at very fast rates of finger movements, probably because of automation [Sadato, 1996]: Whereas for slow finger movements, each individual finger movement is controlled, for fast movements, mostly the rhythm of movements is controlled [Jancke, 1998] [Toma, 2002].

Methodologically, functional neuroimaging methods visualize neuronal activation indirectly via concomitant vascular/metabolic changes. In a complementary approach, DC-Magnetoencephalography (DC-MEG) as well as DC-Electroencephalography (DC-EEG) can be measured simultaneously. Here, the long-time course of activation characteristics for fast and slow finger movements were analyzed intraindividually using these two electrophysiological techniques simultaneously.

METHODS

The study was approved by the local Ethical Committee. 7 healthy right-handed subjects (three females and four males; aged 24-28 years) performed self-paced finger movements using the right hand. Alternating periods of 30 s fast or slow finger movements triggered by an acoustic command, always separated by 30 s rest periods, were performed for a total of 30 min recording time. To prevent automation the subjects bent alternatingly the second and third finger twice. Finger movement rate was determined using a custom-made light barrier.

Prior to the measurements, the somatosensory evoked magnetic response “N20m” was recorded and served as a functional “landmark” identifying in each subject the location of the postcentral gyrus. The N20 response was elicited by electrical right median nerve stimulation (8,9/s, 0.1 ms constant-current square-wave pulses above motor threshold) over 60 s.

The DC-MEG was recorded in a magnetically shielded room with a multichannel planar SQUID-device positioned tangentially over the pericentral hand cortices in the left hemisphere. Subjects were lying supine on a bed moving sinusoidally in a horizontal direction, their eyes were fixated onto a cross attached to the bed (for protocol details see [Mackert, 2001]). The hydraulically driven modulation transposed cranial DC-fields to the modulation frequency of 0.4 Hz where the magnetic noise is lower. Independent component analysis (ICA) identifying field components with statistically independent time evolution separated motor-related DC-fields from ferromagnetic contamination and brain background fields (for details: [Wubbeler, 2000]). In each subject the intensity of the task-related ICA component, as identified via its spectral energy peak at 1/min corresponding to the stimulation protocol, was calculated as the mean global field power recorded by the 49 SQUID channels.

DC-EEG was recorded on the left scalp using a custom-made DC-amplifier (Physikalisch-Technische Bundesanstalt, Berlin, Germany; bandwith DC-125 Hz) with 16 sintered Ag/AgCl electrodes clustered around C3. Ag/AgCl electrodes were filled with electrode gel (Abralyt, Easy Cap, Germany). Amplitudes of the DC-shifts were quantified with the reference electrode at FCz. DC-signals were aquired at 250 Hz by a 20 bit data acquisition. For data analysis the software Brain Vision Analyzer (Brain Products, Germany) was used. All trials with artefacts caused by head or body movements were excluded from analysis. After segmentation of the movement and rest periods respectively, DC-detrending and baseline correction were performed.

RESULTS

Fast finger movements were performed at 1.5-2.0 Hz and slow finger movement at 0.5-0.7 Hz.

In 6 of 7 subjects fast finger movements and slow finger movements revealed motor-related DC-MEG as well as DC-EEG signals clearly above noise level. The movement related DC-activity followed closely the movement periods and decayed to baseline during the rest periods over the entire length of the recording sessions, i.e., 30 minutes.

Fast finger movements revealed statistically significant stronger magnetic field amplitudes and electric potentials than slow movements: The mean DC-MEG field strength associated with fast finger movements was significantly higher compared with slow finger movements (all subjects: 179.1 fT ± 20.2 versus 154.7 fT ± 22.0; t-test $p<0.05$) The mean amplitudes of the DC-EEG potentials were significantly greater for fast finger movements compared with slow finger movements (all subjects: 15.5 µV ± 1.3 versus 12.4 µV ± 1.3 t-test; $p<0.05$).

DC-MEG-activity showed a slow decay after the end of the movement. DC-EEG time curves were somewhat prolonged when compared to the DC-MEG time curves (figure).

The reconstructed motor-related spatial pattern of the DC-MEG-fields were basically bipolar with extrema directed from the parietal to the frontal areas as shown previously [Mackert, 2001].

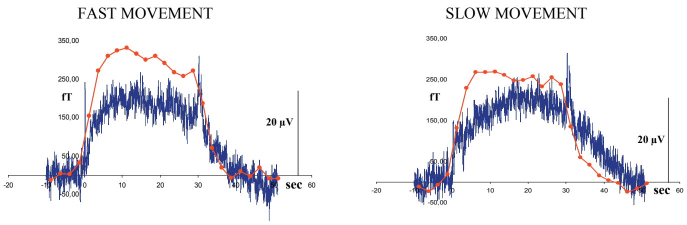

Figure 1. One examplary subject: DC-MEG mean field strength (dotted line) and DC-EEG potentials for slow and fast finger movements in one examplary subject (the EEG-peaks at 0 and 30 sec are probably acustically generated, e.g. N 100)

DISCUSSION

This study confirms the feasibility of noninvasive long-term DC-monitoring using simultaneously electroencephalography and SQUID-based magnetoencephalography. The long-term baseline stability of the modulation-based DC-MEG was already shown in our previous studies [Wubbeler, 2000] [Mackert, 2001]. Prolonged DC-EEG-recordings were reported by the group of Vanhatalo and Voipio et al., who recorded sustained voltage shifts during 3 min hyperventilation using a custom-designed DC-EEG amplifier [e.g. Voipio, 2003]. From a technical point of view, simultaneous DC-MEG and DC-EEG might be extended to arbitrarily long durations. Therefore this combined technique provides a non-invasive neurophysiological reference for the interpretation of neuroimaging results especially in long lasting, tonic neuronal activation paradigms.

In the exemplary simple finger movement paradigm with reduced automation, stronger cortical activation during fast finger movements compared to slow movements was demonstrated. This result confirms electrophysiologically that the movement rate affects the magnitudes of activation in primary motor cortex.

The origin of the prolonged decay of DC-MEG as well as DC-EEG signals is unclear but might be attributed to the regenerational processes in the extracellular space. Its time course is similar to that of the electrically measured intracortical DC-potentials in animals after electric stimulation. The somewhat retarded and prolonged DC-EEG time curves compared to DC-MEG need to be confirmed in further studies.

Based on the long-term baseline stability and the good signal-to-noise ratio appears feasible to extend the measurements to stroke patients with potentially pathologic neuro-vascular coupling.

ACKNOWLEDGEMENTS

Supported by BMBF Grant 01 GO 0208 and DFG Cu 36/1-5

REFERENCES

Jancke L, Specht K, Mirzazade S, Loose R, Himmelbach M, Lutz K, Shah NJ. A parametric analysis of the 'rate effect' in the sensorimotor cortex: a functional magnetic resonance imaging analysis in human subjects. Neurosci Lett. 1998;252:37-40.

Mackert BM, Wubbeler G, Leistner S, Trahms L, Curio G. Non-invasive single-trial monitoring of human movement-related brain activation based on DC-magnetoencephalography. Neuroreport 2001;12:1689-1692.

Sadato N, Ibanez V, Deiber MP, Campbell G, Leonardo M, Hallett M. Frequency-dependent changes of regional cerebral blood flow during finger movements. J Cereb Blood Flow Metab. 1996;16:23-33.

Schlaug G, Sanes JN, Thangaraj V, Darby DG, Jancke L, Edelman RR, Warach S. Cerebral activation covaries with movement rate. Neuroreport. 1996;22:7:879-883.

Toma K, Mima T, Matsuoka T, Gerloff C, Ohnishi T, Koshy B, Andres F, Hallett M. Movement rate on activation and functional coupling of motor areas. J Neurophysiol 2002;88:3377-3385.

VanMeter JW, Maisog JM, Zeffiro TA, Hallett M, Herscovitch P, Rapoport SI.. Parametric analysis of functional neuroimages: application to a variable-rate motor task. Neuroimage. 1995;2:273-283.

Voipio J, Tallgren P, Heinonen E, Vanhatalo S, Kaila K. Millivolt-scale DC shifts in the human scalp EEG: evidence for a nonneuronal generator. J Neurophysiol. 2003;89:2208-2214.

Wubbeler G, Ziehe A, Mackert BM, Muller KR, Trahms L, Curio G. Independent component analysis of noninvasively recorded cortical magnetic DC-fields in humans. IEEE Trans Biomed Eng. 2000;47:594-599.

P1-4

Technique for the Direct Measurement of DC-like Magnetic Biosignals Demonstrated by the Cold Reflex of the Abdomen

Schnabel A., Thiel F., Mueller W. and Burghoff M.

Physikalisch-Technische Bundesanstalt (PTB), Abbestr. 2-12, 10587 Berlin, Germany

ABSTRACT

Very low frequency dc-like signals, such as the cold reflex, could only be measured up to now by moving the subject repeatedly, up to the magnetic detector. PTB's novel magnetically shielded room BMSR 2, together with a low noise 16 channel SQUID magnetometer, allow the recording of dc-like signals without moving the subject; these are direct measurements. The total observed magnetic drifts are limited by 1/f-noise and external disturbances to a value below 6 pT/h. The measurement is continuous in time, therefore provides frequency resolution from dc to several kHz. This allows us to also observe the changing pattern between two different static magnetic states. As an example, the measurement of the cold reflex of the abdomen is shown and discussed. Not only the expected cold reflex, but other periodic and spontaneous signals from the human body can be seen with this method.

KEY WORDS

dc-like magnetic fields, biomagnetic measurements, vector magnetometer, magnetically shielded room, cold reflex of the abdomen

INTRODUCTION

The measurement of biomagnetic fields of the human body below 0.1 Hz could up to now only by carried out by indirect measurement. There are two reasons which have restricted the direct measurements of human magnetic fields. The first is the low frequency behaviour of magnetically shielded rooms; the shielding factor drops rapidly with the frequency. The second reason is the 1/f noise of the detector system leading to a strong increase of the noise at low frequencies. To overcome both problems, measurements were performed by moving the subject or body part repeatedly up to the magnetic detector. The introduced modulation shifts the signal to a higher frequency where the measuring system is able to resolve such weak magnetic field changes. By demodulation, the magnetic field, changes can be observed down to the DC level [Wübbeler, 1998].

The disadvantage is that non-magnetic mechanical equipment is needed, as well as additional software for the interpretation of the measured signal. Due to the movement, only frequencies up to half the modulation frequency can be resolved in such a measuring setup. Further, if a trigger event leads to a change in the magnetic field, the rise time can only be measured if it is slow enough. For processes with rise times of several minutes and more, or for the measurement of weak static fields from material tested for the use inside a good magnetically shielded room, this indirect technology is very good.

However, because there are biological processes in the frequency range of 0.01 Hz to 1 Hz that could not be measured this way, PTB tried a new method to allow direct recordings. These factors were included in the requirements for its new magnetically shielded room BMSR-2.

The example used here, for this direct measurement, is the cold liquid reflex of the abdomen. It was measured for the first time in the 1970s by D. Cohen et al. [Cohen, 1983] with the in-out modulation technique, which was introduced to biomagnetic measurements by his MIT group. However, the higher frequencies could not be seen, because of the modulation method used.

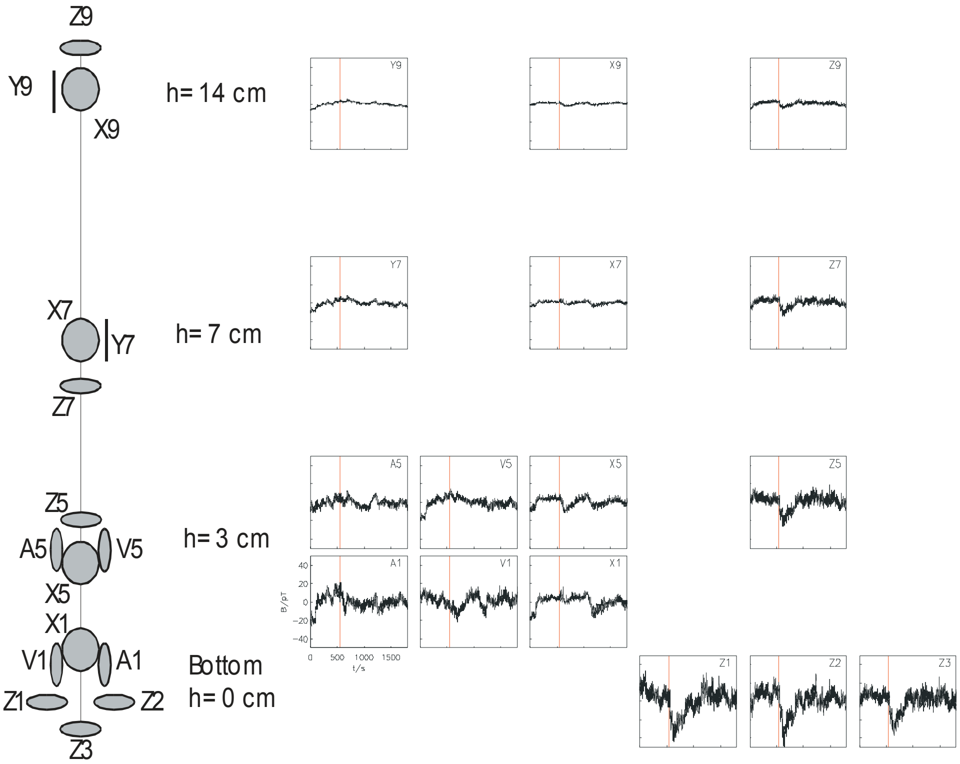

Figure 1. Left: Sensor arrangement of the 16 channel SQUID magnetometer. The subject lies horizontally just below Z1, Z2, and Z3. Right: Measured magnetic fields at the abdomen, showing falloff with distance. The time, when 400 ml of cold liquid was swallowed, is marked as a (red) vertical line. The sensor used for each trace is indicated in each box.

METHODS

The measurements where performed in the BMSR 2 of PTB. To increase the shielding factor of the passive shielding consisting of 7 MU-metal layers [Bork, 2000], at frequencies below 5 Hz, the chamber is equipped with active shielding. Both methods together achieve a shielding factor of more than 7 million for frequencies >0.01 Hz. A 16 channel SQUID vector magnetometer module with W9A SQUIDs of PTB [Drung, 2002][Drung, 2003] was used for all measurements. The arrangement of the SQUIDs is illustrated in figure 1. The chamber together with the detector was tested for its long time stability without a subject inside the chamber. The data was always digitized with a sampling frequency of 250 Hz, an anti-aliasing filter of 100 Hz, and without a low pass filter.

The investigated subjects were males (mean age 40 years), lying in the supine position with the detector vertical and close to the center of the stomach. The body of the subject was stabilized with the help of a vacuum mattress. The recording was started at least 15 min before drinking about 400 ml cold apple juice of about 8°C, with a straw to avoid movement artifacts. In one experiment the influence of possible movements was tested in advance as well as the effect of drinking the same amount of apple juice at 37°C.

RESULTS

The test of the magnetic field of the chamber without a subject showed that the settling of the doors of the chamber lead to an e-functional like field change with a time constant of about 2 min after closing. Ten min after closing, the observed drifts are less than 6 pT/h in all channels. This already includes the external disturbances which are 5 times stronger in the vertical direction than in the horizontal directions. The 1/f noise of the SQUIDs would lead to uncorrected drifts in each channel which is not observed in the background measurement. The first attempt to measure the cold reflex was immediately successful. Figure 1 gives a channel overview within 30 min of the recording in a bandwidth from dc-100 Hz. The heart signal with an amplitude of about 10 pT at the bottom level h=0 cm dominates the noise floor and decreases with increasing distance to the heart. The time where the drinking started is marked in all channels.

A cold reflex of up to 40 pT and almost 10 minutes duration is clearly seen in the channels close to the body and is strongest in the z-channels. These values varied from 20 – 40 pT amplitude and 10 – 20 minutes duration between the recordings. In contrast to these findings, the experiment with drinking of warm liquid showed also a reflex but with duration of only 5 minutes and amplitude of about 30 pT.

Figure 2 shows the band-pass filtered signal of channel Z1 from Figure 1 between 0.02 Hz and 0.5 Hz. After this filtering the magnetogastrogram (MGG), with a frequency of around 0.04 Hz and amplitude of about 1/5 of the cold reflex signal, can be seen. The amplitude of this MGG activity is increased about 50 % after drinking the liquid and lasts about 15 min independent of the temperature of the liquid.

In addition we detected strong slow temporal activity with a period of 150 sec duration with amplitudes in the same range as the cold effect. Due to the decrease of these signals with increasing sensor to body distance, we assumed that the origin is also physiological. The MGG did not increase during these periods.

DISCUSSION

The experiment to measure the cold reflex of the abdomen demonstrates the capability of the new PTB equipment to directly measure magnetic signals at less than 0.001 Hz and 10 pT amplitude. The vector structure of the module helps to distinguish between signals from the subject and the backgroundt. The cold reflex of the abdomen as a triggered signal could be measured directly, without position modulation. The experiments also show that other spontaneous signals of the subject produce magnetic fields of similar structure. But the mechanism and exact location of the sources of such activity is still unknown. Future experiments with our new 304 channel SQUID vector magnetometer will have the localization power to find the sources of the different observed signals.

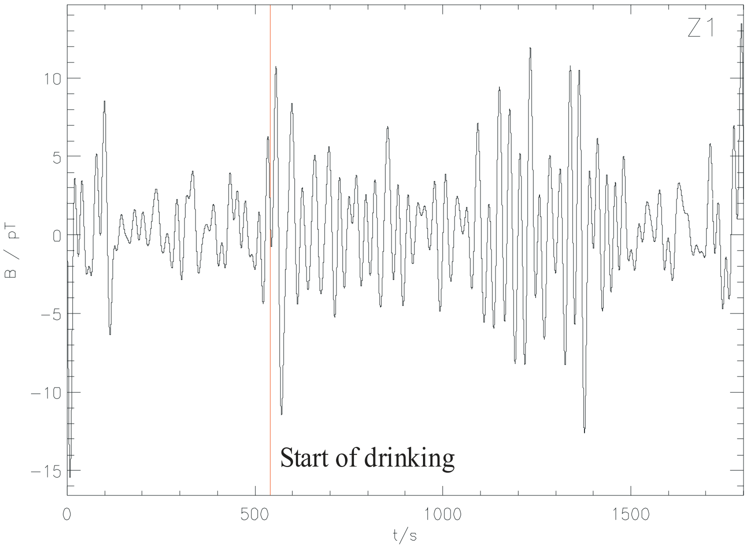

Figure 2. Magnetogastrogram (MGG) with a frequency of about 0.04 Hz obtained by a 0.5 Hz low pass filter of channel Z1 from Figure 1. After drinking 400 ml of cold apple juice at 540 msec, the amplitude about doubles for 20 minutes.

ACKNOWLEDGEMENTS

We thank Prof. D. Cohen for presenting his results and experience of his dc-like measurements to PTB.

REFERENCES

Bork J, Hahlbohm H-D, Klein R., The 8-Layered magnetically shielded room of the PTB: Design and construction. Biomag 2000, Helsinki: 2000.

Cohen D, Steady fields of the body, in Biomagnetism, S.J. Williamson, G-L Romani, L. Kaufman and I. Modena eds., Plenum Publishing Corporation: 1983.

Drung D., High-performance DC SQUID read-out electronics, Physica C 368: 2002; p. 134-140.

Drung D., High-T_c and low-T_c dc SQUID electronics, Supercond. Sci. Technol. 16: 2003; p. 1320-1336.

Wübbeler G., Mackert J., Armbrust F., Burghoff M., Trahms L., Mackert B.-M., Wolff K.-D., Ramsbacher J., Curio G., and Trahms L., SQUID Measurements of Human Nerve and Muscle Near-DC Injury-Currents Using a Mechanical Modulation of the Source Position, IEEE Applied Superconductivity 6/10-12: 1998; p. 559-565.

DC-Magnetoencephalography: direct measurement in an extremely magnetically shielded room

M. Burghoff[1], T.H. Sander[1], A. Schnabel[1], D. Drung[1], B.-M. Mackert[2], G. Curio[2], and L. Trahms[1]
[1]Physikalisch-Technische Bundesanstalt (PTB), Berlin, Germany [2]Neurophysics Group, Dept. of Neurology, Campus Benjamin Franklin Charité – University Medicine Berlin, Germany

Slow biological processes, i.e. neuronal currents with time constants longer than one second can be recorded during long-lasting physiological tasks, but, in particular, are expected in metabolic injuries to brain cells in stroke or migraine. Non-invasive magnetical or electrical recordings in this frequency range are dominated by low-frequency noise or drift artefacts. The development of a modulation-based DC-MEG technique allowed sensitive DC-field recordings in this frequency range. However, the time resolution of this technique is limited to the inverse of the modulation frequency (~5 sec). Now, we report on a new approach of measuring the dc-MEG directly without mechanical modulation. The measurements are performed in PTB's novel magnetically shielded room BMSR-2 with a passive shielding factor of 75000 at 0.01 Hz. Using 16 SQUIDs in a vector arrangement, a peak-to-peak noise of less than 1.2 pT was measured in a bandwidth from DC to100 Hz for an interval of 90 s. Due to this extremely low noise floor in the DC frequency range, DC-fields of several hundred fT related to prolonged motor or auditory activations (averaging n=30 epochs) could be resolved directly over the head. By omitting the sensor-to-source modulation a high time resolution allows the short term dynamic characteristics of long lasting neuronal processes. In particular, the beginning and the end of neuronal activations could be resolved down to the millisecond range, revealing that the sharp onset slope immediately at the motor activation initiation is much steeper than the relaxation after offset.

Imaging of the liver iron concentration by using an AC bio-susceptometer

S. Della Penna[1,2,3], A. Pentiricci[1,2,3], F. Cianflone[1,2,3], C. Del Gratta[1,2,3], S.N. Erné[4] and G.L. Romani[1,2,3]
[1]Department of Clinical Sciences and Biomedical Imaging, and [2]ITAB, Fondazione Università "G. D'Annunzio", Chieti, Italy; [3]INFM, Gc Chieti, Italy; [4]ZIBMT, University of Ulm, Germany

SQUID based bio-susceptometers are routinely used to measure liver iron concentration (LIC) in patients affected by haematological diseases causing iron overload. These systems actually provide a LIC assuming a homogeneous iron distribution in the liver [1]. Nevertheless, studies based on qMRI or post-mortem biopsy reported on the existence of clusters with an iron content up to 3 times the average storage in patients' livers [2], [3]. Here we present an algorithm for the absolute imaging of the LIC suited to operate on a specifically designed bio-susceptometer. In this design, a 7-channel sensor array detects the signal of the sample immersed in a homogeneous and a constant gradient magnetic fields. The homogeneous field sets the position of the point with zero applied field. By varying the zero field position, a set of lines are obtained. The line parameters are analyzed by a linear fit to retrieve a set of magnetic susceptibilities to be associated with regions in a piecewise homogeneous liver. The limits of these regions are changed according to the values of a total cost function and to the trend of a suitable partial cost function. We successfully tested the algorithm by means of a simulation using part of a sphere as the liver containing a small cluster with down to 1.25 times the average LIC. Further simulations, including the use of a realistic model of the liver and of the surrounding tissues, will be made to test the method robustness.

[1] Fischer R. 1998 Liver Iron susceptometry in *Magnetism in Medicine.* Andrä W., Nowak H. eds.Wiley-VCH Verlag, Berlin, 286-301.[2] Clark P.R., St. Pierre T.G. 2000. Quantitative mapping of transverse relaxivity (1/T(2)) in hepatic iron overload: a single spin-echo imaging methodology. Magn. Reson. Imaging. May; 18(4):431-8.[3] Ambu, R., Crisponi, G., Sciot, R., VanEyken, P., Parodo, G., Iannelli, S., Marongiu, F., Silvagni, R., Nurchi, V., Costa, V., Faa, G., & Desmet, V. J. 1996. Uneven hepatic iron and phosphorous distribution in beta-thalassemia. J Hepatol, 23, 544-9.

Concurrent DC-Magnetoencephalography and Near-Infrared Spectroscopy for the Study of Slow Brain Activity

T.H. Sander[1], A. Liebert[1], H. Wabnitz[1], M. Burghoff [1], R. Macdonald[1], L. Trahms[1], S. Leistner[2], G.Curio[2], B.M. Mackert[2]
[1]Physikalisch-Technische Bundesanstalt, Section Biomagnetism, [2]Neurophysics Group, Campus Benjamin Franklin, Charite; Berlin, Germany

Functional brain imaging methods, such as fMRI and PET, map neuronal activation indirectly through the accompanying neurovascular response. At present it is not clear how these indirect effects relate to electrophysiological activity of the brain. To elucidate this relation is rather difficult, because, firstly, simultaneous measurements of MRI or PET and EEG or MEG are technically difficult, if not impossible, and, secondly, the frequency range covered by the modalities differs by at least one order of magnitude. This study presents an attempt to measure slow electrophysiological activity simultaneously to its neurovascular correlate by applying two novel measurement techniques. Modulation DC-magnetoencephalography (mDC-MEG) is a tool specifically developed for the direct monitoring of cortical activity on the scale of seconds to minutes. Multichannel time-resolved near-infrared spectroscopy (mtNIRS) monitors cortical activity related changes in blood oxygenation on a similar time scale and is compatible with the mDC-MEG. The concurrent mDC-MEG and mtNIRS response profiles were measured over the motor cortex of nine subjects performing a standard sustained motor stimulation paradigm. It consisted of alternating 30 s of finger movement with 30 s of rest for a duration of 30 mins. The mtNIRS and mDC-MEG signals follow the stimulation rhythm as is visible in the average and even in the single epoch data. In 5/9 subjects having good data quality the response of the oxyhemoglobin reaches the maximum level significantly later on a scale of seconds compared to the DC-field signal. The measurements and the analysis procedure were tested for consistency using synthetic data in the case of the mDC-MEG.

This poster will be also presented in Workshop 1. For the full paper, see Page 75.

Imaging DC MEG Fields Associated with Epileptic onset in Rat

B. Weiland[1,2], S.M. Bowyer[1,2,3], J.E. Moran[1], K. Jenrow[1,2], and N. Tepley[1,2]
[1]Henry Ford Hospital, Detroit, Michigan, USA.[2]Oakland University, Rochester, Michigan, USA. [3]Wayne State University, Detroit, Michigan, USA.

Complex partial epileptic seizures are characterized by hypersynchronous neuronal activity that is believed to arise from a zone of epileptogenesis. Action potential generation associated with this hypersynchronous bursting increases the extracellular potassium ion (K+) concentration via the opening of voltage sensitive potassium channels. Interference with this K^+ efflux produces excessive neuronal excitability and seizures. This study investigated the characteristics of direct current (DC) magnetoencephalogram (MEG) shifts arising from a putative zone of epileptogenesis. MEG data were acquired using a six channel system with first order gradiometers, (4mm coil diameter, 20 mm baseline - Tristan Associates model 606), nominally located 6.5mm above the rat skull. Limbic status epilepticus was induced by intra-arterial (femoral) administration of kainic acid (10 mg/kg, in saline), and evolved within approximately 30 minutes of injection. Two picoTesla DCMEG shifts, lasting 10 to 20 seconds, were observed at the onset of epileptic spike train activity and status epilepticus. In addition, absolute DC MEG field measurements were performed before kainic acid administration, and during epileptic burst activity, by recording the change in DC MEG associated with increasing the distance between the rat skull and the sensor array by 2 mm. These DC fields were higher in amplitude during seizure relative to the baseline recordings. This investigation was able to non-invasively detect and characterize DCMEG waveforms associated with kainic acid-induced seizure activity.

Acknowledgement Research supported by NIH/NINDS Grant RO1-NS30914. We would like to also thank Dr. Yoshio Okada for his expert assistance.

This poster will be also presented in Workshop 1, see Page 69.

Cell Magnetometry for an Evaluation of Toxicity of Man-Made Mineral Fibers

Y. Aizawa, Y. Kudo, H. Shinji, M. Okada, Y. Sugiura, Y. Komatsu and M. Kotani*

Kitasato University School of Medicine, *Tokyo Denki University, Japan

ABSTRACT

Alveolar macrophages are considered to play a major role in the pathophysiology of lung diseases caused by exposure to various kinds of pathogens and particles. In this study, the cytotoxic effects of different man-made mineral fibers (MMMF) on macrophages were evaluated using a magnetometry, lactate dehydrogenase (LDH) release assay in extracellular medium, DNA ladder detection for apoptosis and ultrastructure observation. Alveolar macrophages obtained from Fischer rats by bronchoalveolar lavage were incubated in vitro for 18 h with Fe_3O_4 as a magnetometric indicator and either chrysotile fibers (CF) as positive control or one of MMMF including silicon carbide whisker (SiC), titanium oxide (TO), potassium octatitanate whisker (PT), rock wool (RW) and microglass (MG).

In the control cells incubated in phosphate-buffered saline (PBS) alone, rapid attenuation of the residual magnetic field, so-called relaxation was observed immediately after cessation of the external magnetic field. A delay of relaxation was observed in alveolar macrophages exposed to CF, SiC, TiO_2 or PT. Slight delay of relaxation was observed in those exposed to MG, while no delay was found in RW-exposed cells. The release of cytoplasmic enzyeme, LDH corresponded with the delay of relaxation except in SiC-exposed cells. Relaxation is thought to occur due to the random rotation of phagosomes containing magnetized iron oxide particles in an intracellular environment. Since impaired cyotoskeletal movement causes delayed relaxation, this phenomenon indicates cell damage due to exposure to fibers, while LDH release indicates damage of cell membrane. For safety screening of MMMFs, cell magnetometry appears useful in in vitro examination. Apoptosis was not shown by DNA ladder detection and ultrastructure observation except for the cells exposed to SiC. Precise mechanism of fibers causing delayed relaxation are still to be clarified to confirm the usefulness of this technique for evaluation of fiber toxicity.

KEY WORDS

Cytotoxicity, cell magnetometry, man-made mineral fibers, asbestos, chrysotile

INTRUDUCTION

Asbestos fibers are known to cause fibrotic diseases in lungs, chronic inflammatory reactions and respiratory dysfunction. Since the use of asbestos is legally prohibited in many countries, development of non-hazardous substitutes for asbestos is needed. There are several man-made mineral fibers (MMMFs) available on the market, such as silicon carbide whisker (SiC), titanium oxide (TO), potassium octatitanate whisker (PT), rock wool (RW) and microglass (MG).

Alveolar macrophages are considered to play a major role in the pathophysiology of lung diseases caused by exposure to various kinds of pathogens and particles. In this study, the cytotoxic effects of five MMMFs were evaluated on macrophages using a magnetometry and lactate dehydrogenase (LDH) release assay in extra-cellular medium, ultra-structure and apoptosis. Cell magnetometry is a modification of pneumomaganetometry conducted first by Cohen [1973]. Administered iron oxide particles are engulfed by macrophages and an external field magnetizes iron oxide particles located in phagosomes of macrophages. Relaxation, a rapid decrease of the remanent magnetic field strength (RMF) radiated from phagocytized iron oxide particles in macrophages after the cessation of external magnetization, was used as an indicator of cellular function.

METHODS

Iron oxide (Fe_3O_4) particles with a mean geometric diameter of 0.26 μm were used as the magnetometric index. The CF and 5 MMMFs were provided by the Japan Fibrous Materials Research Association. The materials were suspended in phosphate-buffered saline (PBS) and mixed by ultrasonic oscillation before use.

Male F344/NS1c rats were anesthetized with an intraperitoneal injection of pentobarbital and bonchoalveolar lavage fluid was collected. The cells were divided into 3 groups: group 1 exposed to chrysotile fibers (CF), group 2 exposed to one of MMMFs and group 3 exposed to PBS as an control. All groups included Fe_30_4 as an indicator of magnetometry.

Cell disks were removed from the wells after 18 hours in a 5%-CO_2 incubator. Glass tubes containing a medium and a cell disk on the bottom were installed on a stage and magnetized in 70 mT for 10 ms. Then the stage was turned at 10 rpm above the probe of a fluxgate magnetometer and maintained at 37℃ by a heater with a thermostat.

We evaluated cellular enzyme release by measuring LDH activity using LDH-UV test. Triton-X 100 was added to the control group to measure the total LDH activation index derived from both the intracellular and the extra-cellular matrices. The LDH release rate (%) was calculated using the following equation: (LDH activation index from CF or MMMF exposed-cells) x 100 / (total LDH activation index).

Macrophages that adhered to glass were used for the observation by scanning electron microscopy (SEM) and transmission electron microscopy (TEM) respectively. The DNA ladder method was performed by using 2 steps, DNA extraction and agarose gel-electrophoresis.

RESULTS

In the control (PBS), rapid attenuation of the residual magnetic field, so-called relaxation was observed immediately after cessation of the external magnetic field. A delay of relaxation was observed in alveolar macrophages exposed to CF, SiC, TiO_2 and PT. A slight delay of relaxation was observed in the cells exposed to MG, while no delay was found in RW-exposed cells. The release of cytoplasmic enzyme, LDH corresponded well with the delay of relaxation except in SiC-exposed cells.

No fragmentation of DNA was observed in all MMMF-exposed macrophages. Morphological examination by TEM demonstrated phagocytic vacuoles, surrouded by a clearly membranous structure with decreased microvilli in exposed cells. Cells with a condensed nucleus suggestive of apoptosis were observed only when exposed to SiC.

Table Results of cytotoxicity evaluation by magnetometry, LDH release, ultra-structure and apoptosis

	Delayed Relaxation by Magnetometry (threshold)	LDH release (threshold)	Ultra-structure	Aoptosis	Reference
Asbestos					
CF	Moderate (<20µg/ml)	Moderate*	Mild	Negative	Keira, 1998, *un-published
MMMFs					
SiC	Moderate (<29µg/ml)	Negligible	Mild nuclear change	Slight	Watanabe, 2000
TO	Moderate (<20 µg/ml)	Mild (<=20 µg/ml)	Mild	Negative	Watanabe, 2002
PT	Moderate (<=10 µg/ml)	Mild (<=10 µg/ml)	Mild	Negative	Watanabe, 2002
RW	Negligible	Negligible	Mild	Negative	Kudo, 2003
MG	Mild (<160 µg/ml)	Mild (<160 µg/ml)	Mild	Negative	unpublished

DISCUSSION

The delay of relaxation generally corresponded with the release of cytoplasmic enzyme. Comparing the thresholds of magnetometric behavior with those of LDH release in the cells exposed to various MMMFs, the former appears more sensitive than the latter. Relaxation is thought to occur due to the random rotation of phagosomes containing magnetized iron oxide particles in an intracellular environment. Since delayed relaxation is considered due to impaired cyotoskeleton, this phenomenon indicates impaired motion system due to exposure to fibers. The LDH release indicates damage to the cell membrane. Apoptosis was suspected in the cells exposed to SiC, but negative for other fibers. Necrotic change is more possible in cytotoxicity due to fibers than is apoptosis. For the screening of safety for MMMFs, cell magnetometry appears useful for in vitro examination. The final conclusion should be made by in vivo exposure study or epidemiological study. Also, the precise mechanism of delayed relaxation due to fiber exposure should be clarified to confirm the usefulness of this technique for evaluation of fiber toxicity.

REFERENCES

Cohen D. Ferromagnetic contamination in the lungs and other organs of the human body. Science 1973;180:745-748.

Keira T, Okada M, Katagiri H, Aizawa Y, Okayasu I, Kotani. Magnetometric evaluation for the effect of chrysotile on alveolar macrophages. Tohoku J Exp Med 1998;186:87-98.

Watanabe M, Okada M, Aizawa Y, Sakai Y, Yamashina, Kotani. Magnetic evaluation for the effects of silicon carbide whisker on alveolar macrophages. Ind Health 2000;38:239-45.

Watanabe M, Okada M, Kudo Y, Tonori Y, Niitshuya M, Sato et al. Difference in the effects of fibrous and particulate titanium dioxide on alveolar macrophages of Fischer 344 rats. J Toxicol Environ Health, Part A 2002;65:1047-60.

Watanabe M, Shibata K, Okada M, Kudo Y, Niitsuya M, Satoh T et al. Magnetometric evaluation for cytotoxicity of potassium octatitanate whisker on alveolar macrophages of Fischer 344 rats. J Occup Health 2002;44:321-8.

Kudo Y, Watanabe M, Okada M, Shinji, Niitsuya M, Satoh T et al. Comparative cytotoxicity study of rock wool and chrysotile by cell magnetometric evaluation. Inhalation Toxicol 2003;15:1275-95.

In vivo tissue characterization using magnetic techniques

Carneiro, A. A.[1], Fernandes, J. P.[1], Araújo D.[1], Baffa, O.[1], Elias, J. Jr.[2], Pierre, G. St.[3], Ribeiro, L. T.[2], Santos, A. C. [2], Covas, D. T.[2]

[1]Departamento de Física e Matemática, FFCLRP, Universidade de São Paulo, 14040-901, Ribeirão Preto-SP, Brazil;
[2]Faculdade de Medicina de Ribeirão Preto, Universidade de São Paulo, 14049-900, Ribeirão Preto – SP, Brazil;
[3]Department of Physics, The University of Western Australia, Nedlands, Western Australia 6907, Australia

ABSTRACT

Among the few non-invasive methods to quantify liver iron deposits, magnetic resonance imaging (MRI) and biomagnetic liver susceptometry (BLS) have been considered the best to evaluate iron overload in the body. This diagnosis is necessary in patient that receives transfusion of blood regularly and that has a genetic disorder known as hemochromatose. In this work, we present the evaluation of the clinical usefulness of MRI and BLS of hepatic tissue to quantify iron deposits in non-blood transfused and transfused patients, and the utility of MRI to evaluate iron overload at spleen and heart and to characterize hippocampal sclerosis. Liver iron evaluation by MRI and SM were performed in a group of 48 patients and hippocampal sclerosis by MRI was performed in a group of 21 patients. The MRI images weighted in T2 were acquired using multi-slice single-spin-echo (SSE) and single-slice multi-spin-echo (MSE), conducted on a 1.5 T whole body scanner. SM measurements were performed using an ac superconducting susceptometer based on SQUID. As results, typically MRI is able to evaluate iron overload as high as 30 mg/g $_{\text{dry tissue}}$ when using a MRI scanners provided with specially designed pulse sequences. Susceptibility measurement work better than MRI to evaluate higher iron overloads in the liver, but it needs special equipment.

KEY WORDS Susceptometry; Magnetic resonance; Hemochromatose; hippocampal sclerosis; SQUID.

INTRODUCTION

Iron overload: Iron overload in the body may occur secondary to increased gastrointestinal absorption or from repeated blood transfusions [Olivieri, 1994]. When chronically transfused and inadequately chelated patients develop cellular injury, skin hiperpigmentation and growth fail. This is followed in adolescence by pubertal failure, insuline-dependent diabetes, hypothyroidism, cardiac failure and arrhythmias [Fosburg, 1990 and Davis, 2000]. Practical management of iron overload requires a reliable estimation of body iron content and distribution, as well as understanding how iron overload translates into clinical consequences [Britteham, 2001].

The most used method to evaluate total amount of body iron, in the majority of the clinical centers, is the measurement of the serum ferritin concentration in the blood. However, the correlation between serum ferritin and body iron is not sufficiently precise to be of strong prognostic value, mainly in situations of inflammation or tissue damage. Serum ferritin is also influenced by chelation and vitamin C treatment in a complex relationship with body iron content. Moreover, the relationship between serum ferritin and body iron appears to be different for different haematological conditions [Angelucci, 2002]. Another alternative to evaluate body iron overload consists in the measurement of liver iron concentration (LIC). Liver is the main iron storage in the body, containing approximately 70% of the total content [Angelucci, 2000]. Liver iron correlates closely with total body iron and can be assessed by biopsy or, more recently, by non-invasive magnetic resonance imaging (MRI) and biomagnetic liver susceptibility (BLS). Although the liver iron is more commonly investigated to estimate iron overload in the body due to the large size of this organ and its easy assessment, heart iron overload is the main cause of death in most transfused patients. So, its measurement is very useful to guide the control of chelation therapy to avoid heart failure. Recently, it was observed that it is possible to estimate the heart iron level in relation to LIC by MRI image [Anderson, 2001].

Hippocampal sclerosis: The *Hippocampal sclerosis* represents 60% of the cases of epilepsy of the temporary mesial lobule, and 75% of these patients develop epilepsy form clinically untreatable. In these cases, the surgical dismissing of the epileptogenic area can lead to a good control of crises, varying from 60 to 80%. In most of the cases the simple visual qualitative evaluation is enough for the diagnosis. However, in about 10 to 15% of the cases, the difference is not visually perceptible. In these cases, the quantification of the relaxation time T2 of the hippocampal area allows the information about the brain lesion at level lower than that observed by human eyes in the conventional MRI imaging [Jackson, 1993 and Von Oertzen]. In an ideal way, a good evaluation of relaxometry demands a great number of echoes, however, this demands a long time of acquisition, hindering your accomplishment in patient, mainly with multi-slices sequences. In practice clinic, the quantification of the relaxometria T2 hipocampal has been accomplished with sequences of the type Spin echo with double echo, being used only two points to compose the relaxation curve [Grunewald, 1994 and Ducan, 1996].

MATERIALS AND METHODS

BLS procedure to body iron assessment: The biomagnetic liver susceptometry (BLS) was evaluated using a susceptometer based on RF- SQUID (Superconducting Quantum Interference Device). This system uses an almost homogenous AC magnetizing field with low intensity and low frequency (114 μT and 7.7 Hz) applied on the hepatic region. The field detector consists of a second order gradiometer coil with 2.5 cm of diameter and 4 cm of baseline [Carneiro, 2003]. A water bag of approximately 5 liters surrounding the torso was used to minimize other tissues contribution. And it is positioned by a special vacuum mattress that sets the subject. A simplified drawing of the BLS system and the patient positioning is present in Figure 1. The ultrasound image to evaluate the depth and size of liver and distance between the liver and the lung was made with the patient already laid down in the position of the susceptometric measurement (supine position with the body rotated about 35^{o} relative to vertical axis), and personal data (age, weight, height) were also recorded. During the measurement, the bed was moved down 8 cm with a velocity of 2 mm/s. The patient or volunteer was dressing non-magnetic clothes.

From the BLS signal (ΔV_{BLS}) the LIC is calculated using the following equation:

$$LIC = \frac{1}{\chi_{m,ftn}\Delta \mathrm{int}_{liver}}\left[\frac{\mu_o\left(\Delta V_{BLS} - \Delta V_{system} + \delta\right)}{C} - \left(\chi_{air} - \chi_{tissue}\right)\Delta \mathrm{int}_{lung}\right], \qquad (1)$$

where ΔV_{system} is the system (bed, bag, etc) contribution, measured keeping the same position and displacement of the bed, but without the patient; δ is correction factor to compensate the small difference in the signal caused mainly by small difference of susceptibility between the water in the bag and the biologic tissue; C is the calibration factor; $\chi_{m,ftn}$ is the iron susceptibility of mass (1.6 10^{-6}); χ_{air} is the susceptibility of the volume of the lungs (0.36 x 10^{-6}); μ_o is the vacuum permeability and Δint is the variation of the integral volume (see equation below) calculated over the liver and lung volume when the torso is displaced. The integral *int* is given by

$$\text{int}_{vol} = \int_{Vol} \vec{B}_m(r) \cdot \frac{\vec{B}_d(r)}{I_d} d^3r \ , \qquad (2)$$

where $\vec{B}_m(\vec{r})$ is the magnetizing field density, and $\vec{B}_d(\vec{r})$ is the magnetic field density that the detector coils would generate in the element of volume (d^3r) if energized with a current I_d.

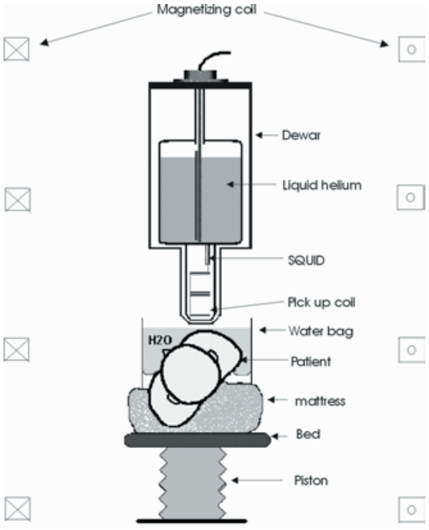

Figure 1: Simplified profile of the susceptibility system and positioning of the patient.

MRI procedure to iron assessment: MRI images to evaluate liver iron overload were acquired using two different spin-echo (SE) and two gradient echo (GRE) sequences, conducted on a 1.5 T whole body scanner (Siemens MAGNETOM Vision Plus). The SE sequences were multi-slice single-spin-echo (SSE) (TR=2500 ms, TE=6,7,8,9,12,15,18 ms and slice thickness = 5 m) and single-slice multi-spin-echo (MSE) (TR=2000 ms, TE = 22.5,45,..,300 ms and slice thickness = 8 mm). The images using SSE sequence were reconstructed in a 192x256 matrix and for each TE 19 slices covering all liver, all spleen and part of the heart volume, were acquired. The seven repeated sequences were acquired under fixed gain. Each sequence has a 4 minutes duration and lasting approximately 30 minutes. This SSE sequence with short TE is a specially developed sequence, by Siemens and collaborators, to evaluate liver iron overload using transverse relaxation evaluation. The images using MSE sequence were reconstructed in 256x256 matrix and lasts approximately 5 minutes. A saline solution bag was used as a reference. The bag used has one liter volume and was placed on the left side of the torso as was indicated by Clark *et al.* [Clark, 2000]. These SE sequences were performed without attempting to respiratory gating or breath-holding techniques.

As TR is significantly large when compared to typical T2 relaxation time of the liver tissue, the transverse relaxation rate R2 (=1/T2) was calculated fitting the image signal intensities by the following mono exponential equation :

$$S_{SE}(TE) = S_{SE}(0)e^{-R_2 TE} + S_{LO} , \qquad (3)$$

where S_{LO} is the signal level offset, $S_{SE}(0)$ is the signal intensity at TE=0 ms.

The transverse relaxation rate R2 was evaluated on a pixel wise basis only from images acquired by SSE sequences of a selected region of interest (ROI) and a histogram was used to assess its distribution (Fig. 2). The ROI was selected on the entire liver area, avoiding vein regions. A Gaussian distribution was assumed with its peak value representing the liver R2 value. In SSE images, the slice chosen to select the ROI was that with the greatest liver area. Fluctuations in voxel intensity, caused mainly by respiratory motion, were accommodated using a 5x5 smoothing window as progressively centered on each voxel in the ROI. Smoothing was applied in all images. In this case, attention was also given to avoid vein regions. Variations of liver signal intensity (SI_{liver}) between the images acquired with different TE in the SE sequence were corrected by the signal intensity of the water bag imaged together with the patient ($SI_{water\ bag}$). It is expected that the signal intensity coming from the water imaged should have almost same intensity for all TE. These same procedures were applied to evaluate relation rate R2 at spleen and heart tissue. For this last organ, the ROI was drawn on the left ventricular myocardium.

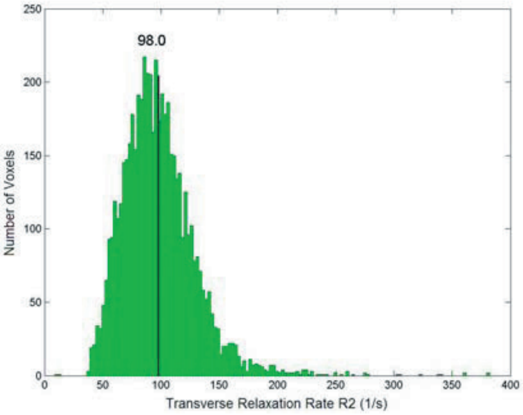

Figure 2: Distribution map of the transverse relaxation rate R2=1/T2 of the liver evaluation from images acquired by SSE sequence.

MRI procedure to evaluate hippocampal sclerosis: MRI images to evaluate hippocampal sclerosis were acquired using two different spin-echo (SE) sequences: a conventional spin echo (CSE) with two TE (30 and 120 ms) and a turbo Spin Echo (TSE) also with two TE (30 and 90 ms). These images were performed in the same scanner already related above. For each sequence, three slices distanced of 8 mm were obtained in the hippocampal region. Similarly to the LIC evaluation, the brain damaged region was analyzed evaluating relation rate R2 of the tissue from relaxometry procedure. In these cases only two images were obtained with two different TE, the R2 value was determined by a liner fit of the naperian logarithm of the pixel intensity versus TE value. The analysis was made over two symmetric regions of the brain in the hippocampal area.

RESULTS

The correlation found between the T2 value by MRI and LIC by BLS was 93% when using SSE sequence. The logarithm of signal intensity from MSE sequence versus the BLS results shows a better correlation (95%). The T2 value calculated from MSE images presented a poor correlation with the LIC by BLS. The main motive of this was the long TE used to acquire the images. No correlation was observed between the T2 value from the liver tissue versus T2 from the spleen tissue. But a low correlation (73%) was found between T2 values from the liver tissue versus T2 from the heart tissue. The high heart iron level has been the main cause of death of the patients regularly transfused that present a very high liver iron level.

A correlation of 84% was observed between T2-values of the tissue evaluated on the hippocampal sclerosis area using the two sequences (CSE and TSE).

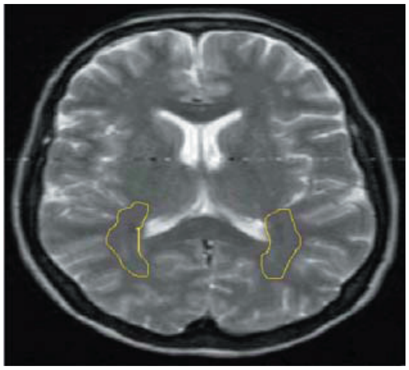

Figure 3: Illustration of the ROIs drawning in the symmetric region of the brain to evaluation of the hippocampal sclerosis by relaxometry from MRI images.

DISCUSSION

This work confirms the feasibility of using two non-invasive methodologies to quantify liver iron concentration at levels from normal to the highest found in clinical diagnostic. Having potential application to follow and guide the control of the tissue iron balance in patients submitted to blood transfusion and iron chelation treatment, including the need to evaluate the efficacy of the new oral chelants.

The studies on hippocampal sclerosis by T2 relaxation time with MRI indicated this methodology as having good potential to evaluate epileptic patients. The considered correlation observed between two sequences (CSE and TSE) suggests this second one as best alternative to assessment of the T2-value of hippocampal tissue in practice clinic because of the advantage of your reduced acquisition time (aprox. 2 minutes).

REFERENCES

Olivieri NF, Nathan DG, MacMillian JH, Wayne AS, Liu PP, McGee A, Martin M, Koren G and Cohen AR. Survival in medically treated patients with homozygous beta-thalassemia. N Engl J Med 1994; 331: 574-8.

Fosburg MT, Nathan DG. Treatment of Cooley's Anemia. Blood 1990; 76(3):435-444.

Davis BA, Porter JB. Long-term outcome of continuous 24-hour deferoxamine infusion via indwelling intravenous catheters in high-risk beta-thalassemia. Blood 2000; 95: 1229-36.

Brittenham GM, Sheth S, Allen CJ and Farrel DE. Noninvasive Methods for quantitative assessment of transfusional iron overload in sickle cell disease. Seminars in Hematology 2001; 38(1): 37-56.

Angelucci E, Muretto PO, Nicolucci A, Baronciani D, Erer B, Gazlev J, Ripati M, Sodani P, Tomassoni S, Visane G and Lucarel G. Effects of iron overload and Hepatitis C virus positivity in determining progression of liver fibrosis in thalassemia following bone marrow transplantation. Blood 2002; 100(1): 17 – 21.

Angelucci E, Brittenham GM, McLaren CE, Ripalti M, Baronciani D, Giardini C, Galimberti M, Polchi P and Lucarelli G. Hepatic iron concentration and total body iron stores in thalassemia major. New England Journal of Medicine 2000; 343, 51.

Anderson LJ, Holden S, Davis B, Prescott E, Charrier CC, Bunce NH, Firmin DN, Wonke B, Walker JM and Pennell DJ. Cardiovascular T2-star (T2*) magnetic resonance for the early diagnosis of myocardial iron overload. Eurpean Heart Journal 2001; 22, 2171-2179.

Jackson, G.D. Connelly A, Duncan JS, Grunewald RA, Gadian DG.. "Detection of hippocampal pathology in intractable partial epilepsy: Increased sensitivity with quantitative magnetic resonance T2 relaxometry." Neurology 43: 1993; 1793-1799.

Von Oertzen J, Urbach H, Blumcke I, Reuber M, Traber F, Peveling T, Menzel C, Elger CE. "Time-efficient T2 relaxometry of the entire hippocampus is feasible in temporal lobe epilepsy." Neurology 58(2): 2002; 257-64.

Grunewald RA, Jackson GD, Connelly A, Duncan JS. "MR detection of hippocampal disease in epilepsy: factors influencing T2 relaxation time." American Journal of Neuroradiology 15(6): 1994; 1149-56.

Duncan, JS Bartlett P, Barker GJ 1996. "Technique for measuring hippocampal T2 relaxation time." American Journal of Neuroradiology.

Carneiro AAO, Fernandes JP, Zago MA, Covas DT, Angulo IL and Baffa O, Superconductor Susceptometric System to evaluate liver iron overload. Review of Scientific Instrument 74(6): 2003; 3098-3103.

Clark P.R., St. Pierre T.G. 2000, Quantitative mapping of transverse relaxivity ($1/T_2$) in hepatic iron overload: a single spin-echo imaging methodology. Magnetic Resonance Imaging 18: 2003; 431-438.

The Colon Transit Time in Different Phases of the Menstrual Cycle: Assessed with Biomagnetic Technique

Córdova-Fraga, T.[1], Huerta-Franco, R.[2], Gutiérrez-Juárez, G.[1], Sosa-Aquino, M.[1], and Vargas-Luna, M.[1]

[1]Instituto de Física, Universidad de Guanajuato, Loma del Bosque 103, Lomas del Campestre, 37150 León, Gto., México
[2]Instituto de Investigaciones sobre el Trabajo, Universidad de Guanajuato, Cerro Gordo 220, Lomas del Campestre, 37150 León, Gto., México

ABSTRACT

Twenty measurements of the colon transit time (CTT) were performed by biomagnetic technique in five young women. Subjects were assessed during 12 hours a day four phases of the menstrual cycle (MC): early follicular (EF), days 1-4 of the MC; late follicular (LF), days 9-14; early luteal (EL), days 15-18; and late luteal (LL), days 23-28 of the MC. Comparison intra and inter-subjects were made. The results of a *t* test for dependent samples, demonstrate that women with regular MC had higher CTT on LF (3.29 ± 1.40 m/hr) than on LL phases of the MC (1.28 ± 0.4 m/hr) t =3.22, $p = 0.04$. Also we found differences from EL to LL phases of the MC (4.49 ± 1.72 m/hr *vs.* 1.29 ± 0.35 m/hr, $t = 3.05$, $p = 0.05$). However, in a patient with polycystic ovary syndrome (PCOS), we found a CTT of 3.1 m/hr on day 3; 2 m/hr on day 15; and 0.8 m/hr on day 30 of the MC. The time of the magnetic marker displacement was higher on days 3 of the MC, if we compared these values with those from women with regular MC (1.8 ± 0.67 m/hr). We demonstrate that biomagnetic technique is a powerful method to assess changes in CTT presented in female subjects during the MC. Furthermore, the results found for the CTT in different phases of the MC of the females subjects, are in agreement with those reported by using other techniques.

KEY WORDS

Biomagnetic Technique, Magnetic Marker, Colon Transit Time, Menstrual Cycle

INTRODUCTION

Large intestine is part of the gastrointestinal tract. In adult subjects it has a length around 1.5 m. It performs three kinds of movements: austral propulsion, peristaltic frequency, and mass movement. The first is the expulsion of the content of an austral when it was filled; the second has a range of frequencies from 2 to 12 contractions per minute; and the third is a gastric reflex associated with the arrive of the food to the stomach [1]. It is known that CTT is larger in women than in men [2]. Furthermore, it has been reported that CTT is altered during the MC, probably due to the effects of the sexual hormones [3]. On the other hand, very recently the biomagnetic technique has been used for the measurements of CTT in humans [4,5]. However, as far as we know there are not reports on the use of these techniques for the CTT measurements in female subjects during the MC.

METHODS AND PROCEDURE

A group of five women from 19 to 21 years were recruited after the protocol was approved by the Human Ethical Committee of the Instituto de Física (Universidad de Guanajuato, México) and written informed consent was obtained from the subjects to participate in this work. The study was conducted according to the Declaration of Helsinki. Four women had clinical history of regular MC (from 21 to 35 days) and ovulation was confirmed with progesterone (P_4) serum levels > 5 ng/mL on days 21 to 23 of the MC, and they did not suffer from diabetes or other endocrine alterations. A woman had PCOS with MC lengh higher than 35 days. Height and weight were measured by standard procedures, and the subject ´s body mass index (BMI), was calculated. Skinfold thickness was measured at three different anatomical sites (triceps, suprailium, and thigh) using a Lange skinfold caliper (Cambridge Scientific Industries, Inc. Cambridge, MD). The mean of three measurements on each site was used in order to calculate the percentage of body fat according to Jackson and Pollock method [6].

The assessment of the CTT (displacement of a magnetic marker in meters per hour, m/hr) was performed on the four phases of the MC, and subjects were assessed during 12 hours a day in five conditions: 1) fasting state, 2) post-prandial state, 3) after breakfast, 4) after dinner, and 5) after defecating.

A magnetic marker was swallowed by each subject 13 hours previously to the CTT assessment. Biomagnetic modality is based on the detection of this magnetic marker. The magnetic signal was recorded using a first order gradiometer, assembled with two digital tri-axial fluxgate sensors from Applied Physics Systems. They work at room temperature and have a range of resolution from 3 nT to 100 µT. Biomagnetic signal from a magnetic dipole changes as $1/r^3$, while the same signal, recording with a gradiometer changes as $1/r^4$ [7]. This allows us to eliminate the static magnetic sources localized relatively far from the gradiometer. Hence, it is possible to detect magnetic sources to distance around the baseline when a magnetometer gradiometer is used. This consideration allows to localize a magnetic marker while the magnetic probe is moving. In this research, a magnet of cylindrical shape, 3 mm of radius and 4 mm height was used as magnetic marker, this had a magnetic moment around 0.014 $A \cdot m^2$. The magnet was encapsulated into a sphere of polycarbonate of 6 mm diameter in order to avoid interaction with gastric juice. This magnetic marker produces enough amplitude on the magnetic signal to be detected by the gradiometer while it was displaced through the colon. Localization of the magnetic marker during 12 hours a day (with intervals from 3 to 4 hours) was used to estimate the CTT of the intestine lumen content.

RESULTS

The mean values of the age, BMI, and percentage of body fat for the subjects evaluated were: 20.6 ± 1.1 years (mean ± standard deviation), 22.5 ± 1.2 Kg/m^2 and 24 ± 0.66 %, respectively. In figure 1, we present the mean values of CTT of four women with regular MC. It is important to observe that the CTT values were statistically different (when we made a *t* test for dependent samples), from LF to LL phases of the MC (3.30 ± 1.22 m/hr *vs.* 1.29 ± 0.35 m/hr, $t = 3.22$, $p = 0.04$). Also we found differences from EL to LL (4.49 ± 1.72 m/hr *vs.* 1.29 ± 0.35 m/hr, $t = 3.05$, $p = 0.05$). However, in a patient with PCOS (who has higher androgen serum levels with anovulatory menstrual cycles), we found 3.1 m/hr on day 3; 2 m/hr on day 15; and 0.8 m/hr on day 30 of the MC). The time of the marker displacement was higher on day 3 of the MC if we compare this value with those observed in regular females (1.8 ± 0.67 m/hr).

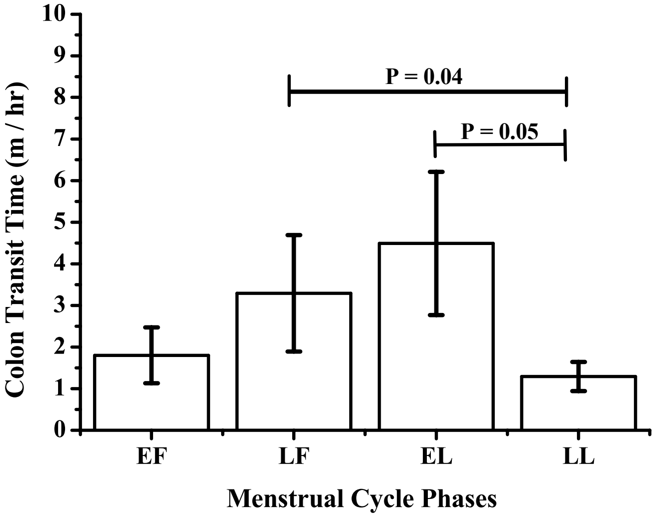

Figure 1. Mean and standard deviation values of the Colon Transit Time of women with regular menstrual cycle. Differences between Late Luteal (LL) with Early Luteal (EL) and Late Follicular (LF) phases were statistically significant. EF = Early Follicular.

DISCUSSION

In this work we demonstrate that biomagnetic technique is a powerful method to assess changes in CTT presented in female subjects during the MC. Also, we demonstrate that this technique could be used to assess and diagnose CTT alterations in different pathologies related to sexual hormone alterations such as PCOS, late onset adrenal hyperplasia, peri- and post-menopause periods, and others such as andropause. One of the principal advantages of this technique is the lack of deleterious effects. Furthermore, the results found for the CTT in different phases of the women´ s MC, are in agreement with those observed using other techniques.

ACKNOWLEDGEMENTS

This work was partially supported by CONACyT (No. 38749-E) and CONCyTEG (No. 97-16-02-027). We want to thank J.C. Martínez and M. Muñoz, M. Noriega and R. Rodríguez for technical support. Finally, we thank all the volunteers.

REFERENCES

[1] Libro de fisiología de Tortora

[2] Bouchoucha M and Thomas SR. Error analysis of classic colonic transit time estimates. Am J Physiol Gastrointest Liver Physiol 2000; 279: G520-7

[3] Gill RC, Murphy PD, Hooper HR, Bowes KL, Kingma YJ. Effect of the Menstrual Cycle on Gastric Emptying. Digestion 1987; 36: 168-74

[4] Basile M, Neri M, Carriero A, Casciardi S, Comani S, Del Gratta C, Di Donato L, Di Luzio S, Macri M, Pasquarelli A, Pizzella V, Romani G. Measurement of segmental transit through the gut in man. A novel approach by biomagnetic method. Digestive Diseases and Science 1992; 37: 1537-43

[5] Córdova-Fraga T, Carneiro AAO, Araujo DB, Oliveira RB, Sosa M, Baffa O. Spatial and temporal evaluation of the human colon motility. Submitted to Physiological Measurements 2004

[6] Jackson AS, Pollock ML. Practical Assessment of Body Composition. Physic Sports Med 1985; 13: 76-90

[7] Brown BH, Smallwood RH, Barber DC, Lawford PV, Hose DR. Medical Physics and Biomedical Engineering. 1st Ed. Bristol (UK): IOP Publishing Ltd; 1999

Binding kinetics of magnetic nanoparticles on latex beads and yeast cells studied by magnetorelaxometry

Eberbeck, D.[a], Bergemann, C.[b], Hartwig, S.[a], Steinhoff, U.[a] and Trahms, L.[a]

[a] Physikalisch-Technische Bundesanstalt, Berlin, Germany
[b] Chemicell GmbH, Berlin, Germany

ABSTRACT

The ion exchange mediated binding of magnetic nanoparticles (MNP) to modified latex spheres and yeast cells was quantified using magnetorelaxometry. By fitting subsequently recorded relaxation curves, the kinetics of the binding reactions was determined. The amount of MNP with weak ion exchanger groups bound to latex and yeast cells scales linearly with the concentration of latex beads or yeast cells whereas that of MNP carrying strong ion exchanger groups is proportional to the square root of concentration. This latter binding apparently leads to a much stronger aggregation of yeast cells.

KEY WORDS

magnetic nanoparticles; magnetrelaxometry; binding reaction kinetics

INTRODUCTION

The study of binding reactions between bio-molecules is important for many fields of bio-sciences, e.g. for monitoring the effectiveness of drug applications or the selective coupling of an antibody or a particular protein structure to specific binding sites. Molecular binding is characterised by its stability, i.e. the degree of reversibility, by the relative amount of realised bindings, and by the kinetics of the reaction.

A tool for characterising these aspects of bio-molecular binding reactions is the Magnetic Relaxation ImmunoAssay (MARIA) [Kötitz, 1995, Weitschies, 1997] which is based on the method of Magneto-RelaXometry (MRX), i.e. the measurement of the relaxation of the net magnetic moment of magnetic nanoparticles (MNP) using Superconducting Quantum Interference Devices (SQUIDs).

This work deals with the quantification of the kinetics of ion exchange coupling. First the binding of magnetic nanoparticles (MNP) carrying cation exchange groups and positively charged latex spheres was studied. In addition we have investigated the binding of MNP to yeast cells in order to find out possible differences in the coupling behaviour between purely chemical systems and living biological systems.

METHODS

Latex beads of 5 µm diameter, which were coated with a polymer presenting an amino group, were suspended in water with an original concentration $n_L=1.84\cdot10^{14}$ m^{-3}. To this aqueous solution the ferrofluid Resovist was added with a particle density of about $n_{MNP}=2.75\cdot10^{22}$ m^{-3}. MNP of Resovist consist of magnetite cores surrounded by a surfactant layer which contains carboxyl groups serving as cation exchanger groups. The binding of MNP to yeast cells (original concentration: $n_y=2.48\cdot10^{14}$ m^{-3} was studied with MNP loaded with either weak anion exchanger groups diethylaminoethyl (DEAE) ($n_{MNP}=4.8\cdot10^{22}$ m^{-3}) or strong anion exchanger groups polyethylenimine (PEI) ($n_{MNP}=2.8\cdot10^{21}$ m^{-3}).

To start a coupling reaction, 50 µl of the MNP-suspensions were filled into a vial containing 100 µl of an aqueous latex or yeast cell suspension. Then, the sample was placed into the MRX-device, so that the first relaxation measurement began some 30 s later. Relaxation curves were then measured every 10 s for several minutes.

Measurement device and measurement procedure were described earlier in detail [Matz, 1999]. In short, a magnetising field of 1300 A/m was applied for t=1 s. Some 500 µs after switching off the field, a highly sensitive SQUID-device recorded the magnetic induction $B_r(t)$ at a distance of 10 mm above the sample. The remanent induction of the sample was determined by the difference between measurement curves of the sample and that of the empty sample holder.

The observed relaxation of MNP, suspended in water is much faster than that of MNP which are immobilised on large targets like yeast cells or latex. After the addition of MNP to a latex suspension, the relaxation curve $B(t)$ of the magnetic moments of the MNP consists of two contributions: the slow relaxation of bound MNP, $B_b(t)$, and the faster one of the MNP which are not bound on latex, $B_{ub}(t)$, i.e.

$$B(t)=\beta B_b(t)+(1-\beta)\, B_{ub}(t). \quad (1)$$

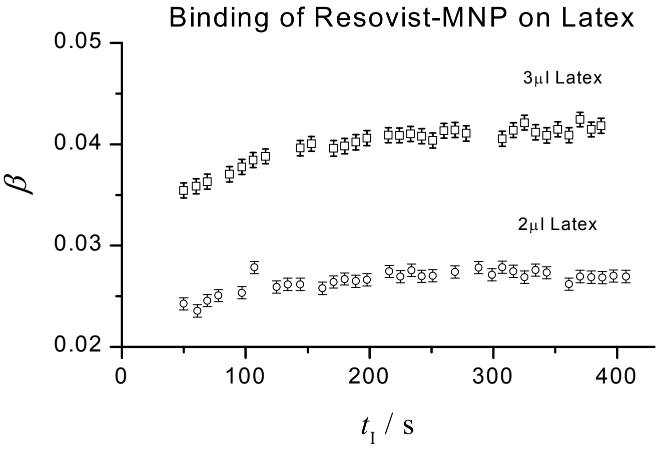

Figure 1: Time dependence of binding parameter β measured for two different latex concentrations.

Fitting the data with (1) we obtain the quantity of interest, β, representing the amount of bound particles contributing to the total signal.

RESULTS

The sequence of 60 relaxation curves measured subsequently after the incubation displays the reaction kinetics in terms of $\beta(t_I)$, where t_I is the time after incubation (figure 1). For small amounts of targets the immobilisation of MNP saturates about 100…200 s after the incubation. For higher target concentrations of latex or yeast cells the saturation time exceeds the observation time and the description of $\beta(t_I)$ by a straight diffusion model, derived from the classical Smoluchowski model, does no longer apply [Eberbeck, 2004].

Measurements of $\beta(t_I)$ were performed on different concentrations of latex and yeast cells whereas the MNP-concentration remained constant. The titration curves are displayed in (figure 2).

DISCUSSION

In the case of the binding of MNP to latex as well as the binding of DEAE-modified MNP to yeast cells we measure a nearly linear titration curve. This was expected for free movable fully suspended particles. Interestingly, we have found a different relation between binding signal and concentration for the strong ion exchanger, i.e. the PEI-MNP: $\beta_f \propto c_y^{0.5}$. These differences may be attributed to different degrees of aggregation of latex beads and yeast cells after incubation, which are evident from light microscopy (figure 3).

Apparently, the tendency of the yeast cells to aggregate is stronger in the presence of nanoparticles with a higher ion charge. It is plausible, that by this aggregation the effective, relative target surface for the MNP decreases with increasing concentration of target particles. This could explain the reduced scaling exponent.

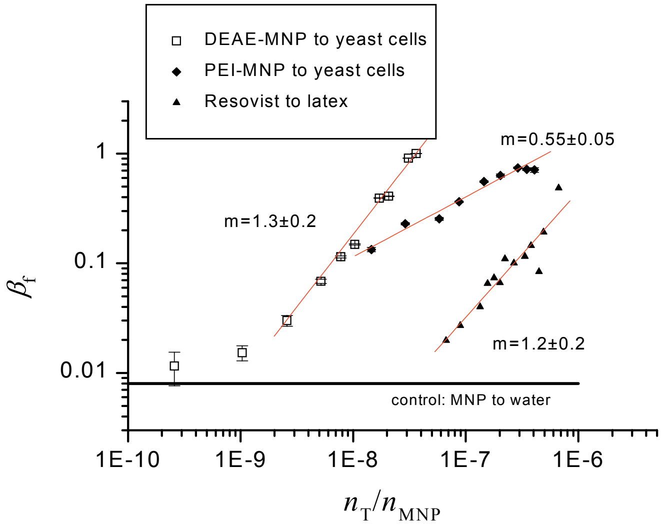

Figure 2: Dependence of the final value of binding parameter β_f, on the ratio of the target concentration n_T to concentration of the MNP. The lines are linear fits the slopes of which are indicated by *m*.

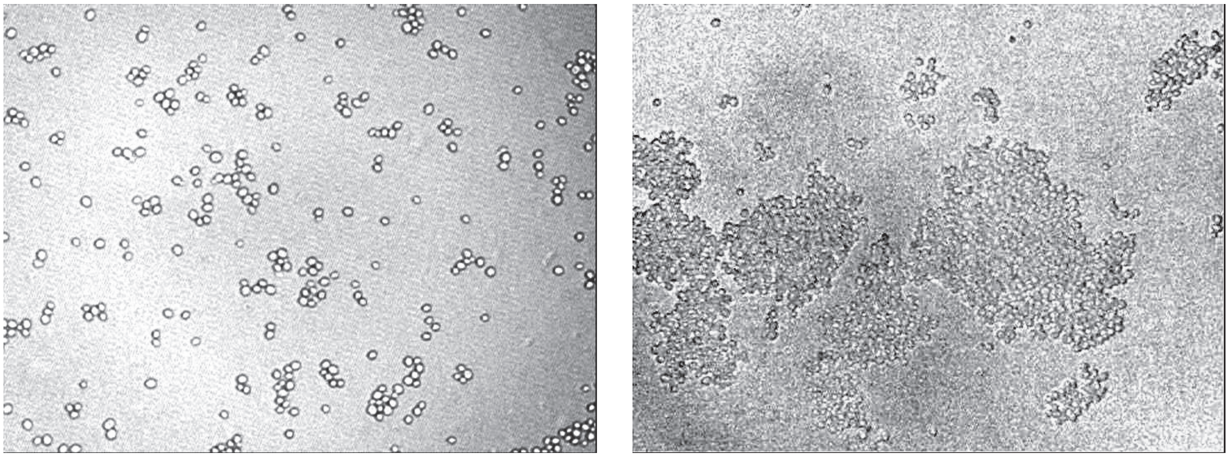

Figure 3: Microscopy picture of yeast cells after incubation with DEAE-modified MNP (left) with $n_y/n_{MNP}=4.13\cdot10^{-8}$ and PEI-modified MNP with $n_y/n_{MNP}=2.34\cdot10^{-6}$ (right.)

ACKNOWLEDGEMENTS

Technical support by C. Aßmann and T. Schurig for the microscopy measurements is gratefully acknowledged. This work was supported by the priority program 1104 of the Deutsche Forschungsgemeinschaft.

REFERENCES

Kötitz R, Trahms L, Koch H, Weitschies W. In: Baumgartner C et al., editors, Biomagnetism: fundamental research and clinical applications, Elsevier Science, 1995, p. 785-788.

Weitschies W, Kötitz R, Bunte T, Trahms L. Pharm. Pharmacol. Lett. 1997, 7, p 1-4.

Matz H, Drung D, Hartwig S, Groß H, Kötitz R, Müller W, Vass A, Weitschies W, Trahms L, Appl. Supercond. 1999, 6, p 577-583.

Eberbeck D, Bergemann C, Hartwig S, Steinhoff U, Trahms L, J of Organometallic Chemistry, submitted.

Interaction of Artificial Metallic Objects with Biosusceptometric Measurements

Engelhardt, R.[1], Fung, E.B.[2], Kelly, P.[3], Biehl, T.R.[4], Pakbaz, Z.[2], Nielsen, P.[1], Harmatz, P.[2], Fischer, R.[1,2].

[1]University Hospital Hamburg-Eppendorf, Germany; [2]Children's Hospital & Research Center at Oakland; [3]Children's Hospital, Cincinatti; [4]Virginia Mason Hospital, Seattle, USA.

ABSTRACT

In human subjects, metallic objects cause distortions of the magnetic fields used by magnetic resonance imaging (0.5 – 3.0 T) or by SQUID biomagnetic liver susceptometry (BLS: 0.1 – 30 mT) and may lead to artifacts in the measurement of the relaxation rate or the magnetic susceptibility. In BLS, the measured signal will depend not only from the magnetic susceptibility of the object, but also from its distance to the sensor assembly, and in case of ferromagnetic objects, from the direction of its remanent field. The magnetic susceptibility of a vascular access port-a-cath and of surgical clips have been measured by a SQUID biosusceptometer. Additionally, the impact from port-a-caths and dental braces on liver iron concentration (LIC) measurements was measured in vivo with respect to their radial distance from the gradiometer center axis. For the port-a-cath, a mean magnetic volume susceptibility of $(83.5 \pm 0.3)\cdot 10^{-6}$ SI-units was found, which may be compared with the magnetic susceptibility of titanium at room temperature of $(180 \pm 2)\cdot 10^{-6}$ SI and of ferritin/hemosiderin iron as found in the human liver of $(1550 \pm 50)\cdot 10^{-6}$ SI. At a radial distance of 5 cm from the gradiometer center axis, the voltage amplitude is similar to the signal generated by a normal liver. Modern surgical clips have nearly no impact on LIC measurements. However, dental braces although further away from the center axis, often superimpose the signal even from an iron overloaded liver. Depending on the Ni-content, these objects reveal ferromagnetic properties, making measurements unstable and analysis difficult.

KEY WORDS

Implant, port-a-cath, dental brace, staple, surgical clip, magnetic susceptibility, biosusceptometry.

INTRODUCTION

In human subjects, the interaction of metallic implants such as surgical clips (staples), orthopedic implants, stents, pace makers, dental braces, and vascular access ports with magnetic fields as applied in magnetic resonance imagers (MRI) or in biomagnetic measurements with SQUID biosusceptometers always create technical difficulty. Of greatest concern are ferromagnetic objects because of their excessive magnetic interactions (magnetic volume susceptibility 10^6 SI-units) and their remanent fields. In the strong magnetic fields of MRI systems (0.5 – 3.0 T) these implants may cause either a hazardous situation due to the generation of torque and deflection forces on these objects [Shellock, 1988] or may at least cause magnetic field distortions leading to image artifacts around these objects. Often the magnetic properties of these implants are not known, especially, older implants and antimagnetic stainless steel implants may contain tiny ferromagnetic contaminants leading to a contraindication of using MRI [Nowak, 1997]. Although, in current practice, most implants are manufactured from titanium and plastic materials, which do not show any deflection nor torque in a magnetic field of 3.0 T (Shellock, 2002), these implants may cause field distortions in the weak magnetic field of a SQUID biosusceptometer (0.1 – 30 mT) leading to artifacts in the measurement of the magnetic susceptibility within the human body.

In patients with iron overload from blood transfusions (e.g., thalassemia) often a vascular access port (port-a-cath) is applied for the continuous infusion of the iron chelator deferoxamine or surgical clips (staples) have been used for splenectomy or cholecystotomy. The position of these implants may vary relative to the field of view (FOV) of a biosuceptometer for the assessment liver iron. Therefore, the impact on the measured magnetic signal will depend not only from the magnetic susceptibility of the implant, but also from its relative distance to the FOV and in the case of ferromagnetic dental braces, also from the orientation of the remanent magnetic field.

METHODS

An apheresis port-a-cath and surgical clips (staples) have been measured by a SQUID biosusceptometer (Ferritometer®). The port-a-cath (Triumph I, Horizon Medical Products Inc.,USA) manufactured from titanium and polysulfone has a volume of 2.9 cm^3, which can be approximated by a hemisphere with a radius of 1.4 cm. Surgical clips were made of titanium with a length of 10 mm and a volume of 10 mm^3 (TIM-20, Ethicon Endo-Surgery Inc., USA).

The two LT_C-SQUID biosusceptometers, Hamburg Biosusceptometer (UKE: Biomagnetic Technologies Inc., San Diego, USA) and the Ferritometer® at Children's Hospital Oakland (CHO: model 5700, Tristan Technologies Inc., San Diego, USA) have been described elsewhere [Paulson, 1991] [Starr, 2000]. The sensor assembly, situated in a vacuum space inside the dewar tail of the biosusceptometers, comprise two sets of superconducting magnetic field coils (1st order gradiometer) and 2 (UKE) or 3 (CHO) different symmetrically coaxial detector coils (2nd order gradiometers A, C and planar B). The underlying principles of liver iron measurements with SQUID biosusceptometers have been published over the last 20 years [Farrell, 1983] [Fischer, 1998]. Usually, a measurement is performed by moving an object or patient away from the sensor assembly either versus air or water as reference medium. However, also horizontal scanning versus air can be applied.

In a first setup, the magnetic susceptibility of the port-a-cath and the surgical clip was measured on an empty wine bottle, which produced nearly no magnetic signature when measured versus air, below the sensor assembly of the Ferritometer® at CHO. Measurements were performed by vertical movement and horizontal scanning versus air reference.

In a second setup, biomagnetic liver susceptometry (BLS) with and without a port-a-cath, with and without dental braces was performed. At CHO, a port-a-cath was attached to the skin of an iron overloaded patient at a standard medio-clavicular position on the right upper thorax, which is 10 – 20 cm away from the position of liver iron measurements. At UKE, a patient (β-thalassemia major) was measured before and after dismounting the dental braces.

RESULTS AND DISCUSSION

In a first test, the port-a-cath was scanned in the horizontal plane (x-direction) at two distances relative to the lower pick-up coils of the sensor assembly (z = 2.4 and 3.4 cm). Thereby, the setup was moved manually by 20 cm within 10 seconds, which corresponds with the inner diameter of the bellows of the water coupling membrane. The SQUID voltage patterns for the most critical detector with the largest gradiometer pick-up coil

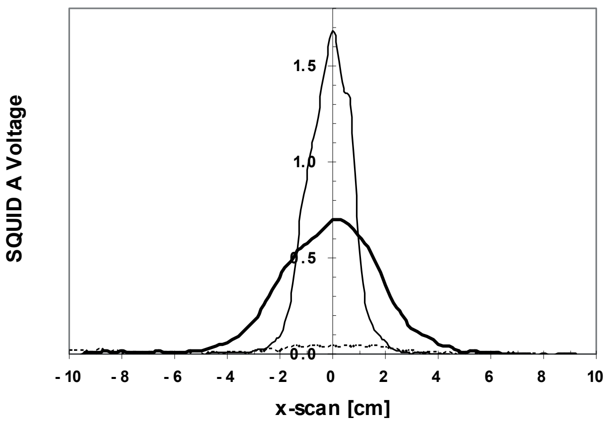

Figure 1. Horizontal scans of a vascular access port-a-cath at sensor distance z = 2.4 cm (thin solid line), at z = 3.1 cm (thick solid line) and of 3 surgical clips at z = 2.6 cm (dashed line).

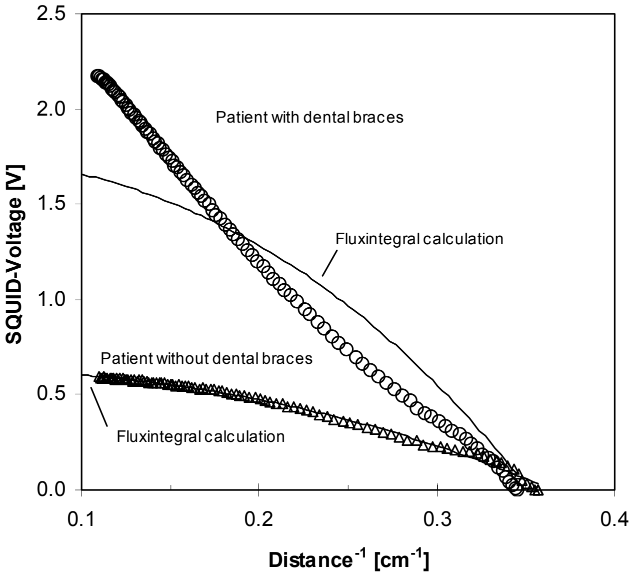

Figure 2. Biomagnetic liver susceptometry (SQUID channel A) in a patient with (circles) and without dental braces (triangles). With braces, the fluxintegrals do not fit the measured data, while, without braces the fluxintegral fit is perfect.

diameter are shown in Figure 1. Close to the dewar tail, the sensitivity volume of the sensor assembly is more restricted by the radius of the field coil of 1.7 cm, while further away, the radius of the gradiometer A of 2.5 cm determines the measurable signal from the port-a-cath in a range of x = ± 5 cm. This coincides with the outer diameter of the dewar tail. The signal patterns of the other two detector channels were even more restricted by the smaller size of their gradiometer coil radii.

The magnetic susceptibility was measured directly by lowering the port-a-cath in the central position (x = 0). The transformation of the vertical distance z into magnetic flux integrals for the 3 SQUID detector channels was performed by a hemisphere with a volume of the port. A mean magnetic volume susceptibility of $(83.5 \pm 0.3) \cdot 10^{-6}$ SI-units was achieved, which may be compared with the susceptibility of titanium at room temperature of $(180 \pm 2) \cdot 10^{-6}$ SI. The size of the susceptibility clearly shows the paramagnetic property of the investigated port-a-cath model and may be compared with the susceptibility of the paramagnetic ferritin/hemosiderin iron in the human liver of $(1550 \pm 50) \cdot 10^{-6}$ SI.

The in vivo experiment with the port-a-cath mounted at the standard medio-clavicular position of the right upper thorax on a patient (β-thalassemia major, 31 y, mean LIC = 1100 ± 200 $\mu g/g_{liver}$) revealed no significant magnetic contribution. With and without port-a-cath, a LIC of 1063 ± 166 and 1171 ± 128 $\mu g/g_{liver}$ was determined, which is in the range of variation for this patient. In a recent measurement, a patient with an implanted port-a-cath at an even closer distance of 6-7 cm was measured without any significant additional magnetic contribution. This is in agreement with the findings from the horizontal scanning.

The influence of dental braces on a SQUID-measurement in a patient is shown in Figure 2. The measurement with braces shows a strong distortion on the measured SQUID-voltage (circles). The measured data disagree with the calculated fluxintegrals (line through the data) indicated by a huge chi-square (~1200). The data without braces 5 weeks later (triangles) show no magnetic distortion and the chi-square (~5) indicates a good agreement between the measured data and the fluxintegral calculation.

In the final analysis of BLS-measurements, weak magnetic distortions can be considered by a one parameter error-function. In the shown measurement with braces, the huge error-term would cause the final LIC to range between 1450 and 2700 $\mu g/g_{liver}$. In the subsequent BLS-measurement without braces, the final analysis of the LIC results in 1120 ± 120 $\mu g/g_{liver}$. Further magnetic field-measurements by a Hall probe revealed a remanent magnetic field on the braces clearly above 2 mT.

However, patients with dental braces of smaller ferromagnetic signature (micro Tesla) can be measured, although in practice, this may become difficult to judge in advance.

ACKNOWLEDGEMENTS

We would like to thank Hannes Nowak for helpful discussion. This work was supported in part by Cooley's Anemia Foundation.

REFERENCES

Farrell DE, Tripp JH, Brittenham GM, Danish EH, Harris JW, Tracht AE. A clinical system for accurate assessment of tissue iron concentration. In: Romani GL, Williamson SJ, editors. Proceedings of the 4th International Workshop on Biomagnetism. Il Nuovo Cimento 1983; 2D:582-93.

Fischer R. Liver iron susceptometry. In: Andrä W, Nowak H, editors. Magnetism in Medicine - A Handbook. Berlin: Wiley-VCH; 1998. p. 286-301.

Nowak H, Michaelsen S, Giessler F, Huonker R, Haueisen J, Kaiser WA. Patient screening for MRI with SQUID biomagnetometers. Biomed Tech 1997;42 Suppl:233-4.

Paulson DN, Fagaly RL, Toussaint RM, Fischer R. Biomagnetic susceptometer with SQUID instrumentation. IEEE Trans Magnetics 1991;MAG-27: 3249-52.

Shellock FG. MR imaging of metallic implants and materials: a compilation of the literature. Am J Roentgenol 1988;151:811-4.

Shellock FG. Magnetic resonance safety update 2002: implants and devices. J Magn Reson Imaging 2002;16:485-96.

Starr TN, Fischer R, Ewing T, Longo F, Engelhardt R, Trevisiol E, Fagaly RL, Paulson DN, Piga A. A new generation SQUID biosusceptometer. In: Nenonen J, Ilmoniemi RJ, Katila T, editors. Biomag 2000 – Proceedings of the 12th International Conference on Biomagnetism. Helsinki: University of Technology; 2001. p. 986-9.

P1-5

Magnetocardiography of animals in magnetically shielded environment with active compensation

H.E. Horng[1,2], S.H. Liao[1], S.J. Hsu[2], H.C. Yang[2,3], Chih-Chen Chen[3],C.H. Wu[3], Chau-Chung Wu[4]

[1]. Department of Physics, National Taiwan Normal University, Taipei 116, Taiwan
[2]. Institute of Electro-Optical Science and Technology, National Taiwan Normal University, Taipei 116, Taiwan
[3]. Department of Physics, National Taiwan University, Taipei 106, Taiwan
[4]. Department of Internal Medicine (Cardiology Section), National Taiwan University Hospital, Taipei 106, Taiwan

ABSTRACT

High-T_c 1st-order electronic superconduting quantum interference device (SQUID) gradiometer system is constructed to study the magnetocardiography (MCG) of rabbits in moderately magnetically shielded environment with active compensation. In the noisy hospital environment, the noise cannot be completely reduced with the 1st-order gradiometer, therefore, a reference SQUID with active compensation is used to further reduce the noise level leaking into the room. The MCG system is equipped with the X-Y translation bed. We used a low-pass filter with the cut off frequency at 44 Hz, high-pass filter with the cut off frequency at 0.1 Hz and the 60 Hz notch filter to reduce the power line interference. The noise level of 1st order gradiometer MCG system in this moderately magnetically shielded room was about 1 pT/Hz$^{1/2}$ at 1 Hz. MCG of normal and hypercholesterolemic rabbits are performed in the moderately magnetically shielded environment. The results are discussed.

KEYWORDS

Interference Device Gradiometers, Magnetocardiogram, Magnetometer

INTRODUCTION

Superconducting Quantum interference device (SQUID) has been used to measure small magnetic field. One important application of SQUID is the field of biomagnetism [1-9] like magnetocardiogram. These biomagnetic fields range about several tens of picotesla from the human heart or several picotesla from small animal heart. The high-T_c SQUID magnetometer is suitable to detect the magnetic field in these ranges. In order to study magnetic cardiac signal and provide useful clinical information the high-T_c SQUID MCG system must be installed in moderately magnetically shielded environment to raise the signal-to-noise ratio and reduce the measuring time for average.

In this work, the first order electronic high-T_c SQUID gradiometer system was set up and used to examine the magnetocardiogram of the rabbits in moderately magnetically shielded room. The moderately magnetically shielded room was constructed of mu-metal layers and aluminum layers. The shielding factor of the magnetically shielded room was measured. The active feedback compensation is also established to reduce the magnetic field noise inside the magnetically shielded room.

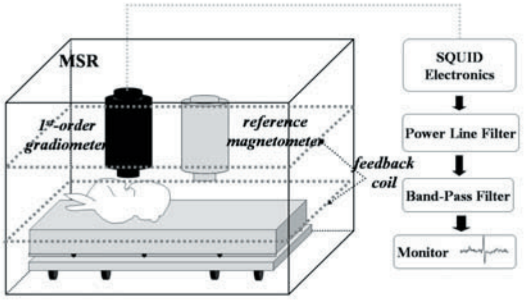

Figure 1. Block diagram of the first order gradiometer MCG system in the magnetically shielded room with the active compensation. The power-line filter and the band-pass filter are necessary to get rid of the noise from the environment.

EXPERIMENTS

The first order electronic high-T_c SQUID gradiometer system consists of two commercially available high-T_c radio-frequency (rf) SQUID magnetometers from the

Jülich SQUID Company. The magnetometers were mounted in axial arrangement with their sensing planes oriented along the z-axis and separated by a baseline distance of 8 cm. The magnetometers show a white noise level of about 300 fT/Hz1/2 and low frequency noise level of about 1 pT/Hz1/2 at 1 Hz. Figure 1 shows the block diagram of the magnetocardiogram (MCG) system in the magnetically shielded room. The shielding factor of the magnetically shielded room is about 50 dB at 1 Hz, 70 dB at 10 Hz and 95 dB at 100 Hz. Subtraction electronics is used to subtract the environmental noise in the shielded room. The output of the gradiometer is filtered with the notch filter (60 Hz) and the band-pass filter (0.1 Hz – 44 Hz). Figure 2 shows the noise spectrum inside the magnetically shielded room. The external interference of induces the low frequency noise of 4 pT/Hz$^{1/2}$ at 20 Hz. In order to cancel this noise the active feedback compensation system was established. The compensation system [10-12] consists of an extra SQUID magnetometer to detect the noise inside the shielded room. With this feedback compensation, the noise level in the shielded room is reduced to 1 pT/Hz$^{1/2}$ at 20 Hz.

The rabbit specimen with a maximum signal strength of around 12 pT is seated on a computer-controlled X-Y translation bed which is shielded by a piece of mu-metal between the X-Y translation stage in the bottom of translation bed and the mattress on the top of translation bed. The X-Y translation stage is used to move the specimen to be tested. Using this translation bed, the specimen can be moved easily and accurately between tested points.

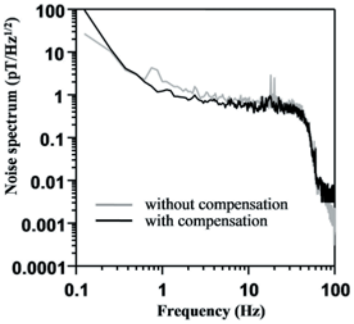

Figure 2. Noise spectrum of first order gradiometer MCG system in the magnetically shielded room with and without active compensation.

RESULTS AND DISCUSSION

Figure 3 shows the averaged MCG and electrocardiography (ECG) signal of a rabbit. The ECG was measured between the arm and the leg of the rabbits. The ECG was simultaneously recorded during the MCG measurement. The ECG signal is used as a time reference for averaging to improve the signal-to-noise ratio of MCG signal. An averaging of about 100 times can achieve a signal-to-noise ratio of 9. The QRS complex and T wave of MCG signal can be observed clearly. The weakest P-wave in a cardiac cycle also can be observed. The peak value of the R-wave is about 5 pT.

Using the X-Y translation bed, we obtain the two-dimensional MCG signal over a scanned area of 10.5 × 10.5 cm^2 and the data are shown in figure 4. The distance between two measuring points is 1.5 cm. The QRS complex and the T-wave of MCG signal can be observed clearly in two-dimensional MCG imaging. The upper part shows a positive R-wave while the lower part shows a negative R-wave. Figure 5 shows the contour map corresponding to the peak of the R-wave of two-dimensional MCG signals. The sign + and the sign – can show that MCG signal can be generated from the dipoles around the heart.

Figure 6 shows the evolution of MCG signal in the magnetically shielded room for strong and weak MCG signals [13] measured at two different positions above the chest with different averaging times. The averaging times are 40, 60, 80 and 100. The signal-to-noise ratio of the strong point is about 9. The signal-to-noise ratio will not be further improved if the averaging times are increased over 80 times. The same condition was also found at the weak point.

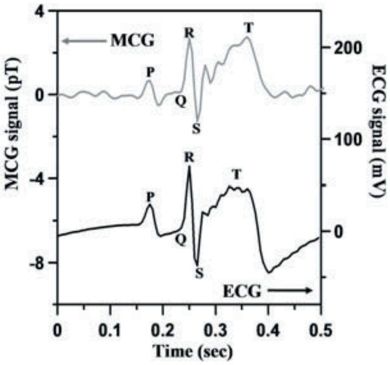

Figure 3. Average MCG and ECG signals of the rabbit (~100 average times). The P wave, QRS complex and T wave of MCG signal can be observed clearly.

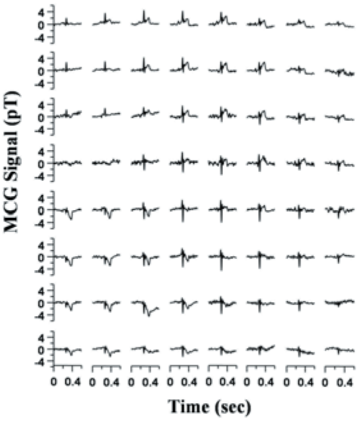

Figure 4. Two-dimensional mapping of the MCG signal obtained from a first order gradiometer in moderately magnetically shielded environment. The scanned area is 10.5×10.5 cm^2 (8× 8 points).

Figure 7 shows the comparison between the normal rabbit (A) and the hypercholesterolemic rabbit (B). The QTc [14] can be used to differentiate the normal rabbit form the hypercholesterolemic one. The QTc is defined as the QT interval divided by the square root of the RR interval in seconds. The QTc of the hypercholesterolemic rabbit (311 ± 11 ms) is longer than the normal rabbit (289 ± 9 ms). In our data of the normal rabbit, the QTc value for both ECG signal and MCG signal is 292 ms. From the MCG signal of the hypercholesterolemic rabbit, we get the value of QTc is 302 ms. However, the QTc value of the ECG is difficult to observe. Some of the data [14] also shows the unclear T wave of the hypercholesterolemic rabbit. The data may indicate MCG signal providea extra information which is useful for some clinical applications in future.

CONCLUSION

We have set up an electronic gradiometer MCG system with active compensation in moderately magnetically shielded room. The noise of electronic gradiometer system was reduced to about 1 $pT/Hz^{1/2}$ in the low frequency regime. The suitable averaging time is about 40 seconds in in each measurement. Comparing the normal rabbit with the hypercholesterolemic one, we can identify the hypercholesterolemic rabbit from the MCG data even though the T wave was unclear in the ECG data.

ACKNOWLEDGMENT

This work is supported by the grants: 91-N-FA01-2-4-2 and NSC92-2112-M002-046

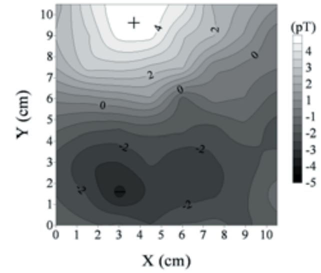

Figure 5. Two-dimensional MCG mapping at the instant of the R-wave obtained from a first order gradiometer.

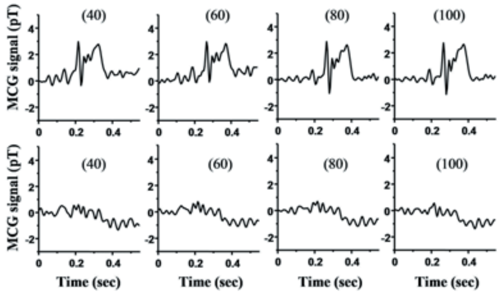

Figure 6. Evolution of the strong and weak MCG signals measured at two different positions with 40, 60, 80 and 100 times of averaging.

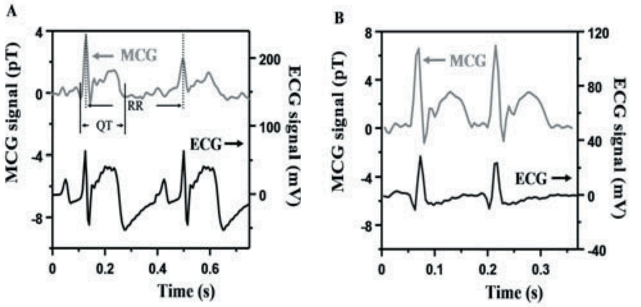

Figure 7. Averaged MCG and ECG signals of the normal rabbit (A) and the hypercholesterolemic rabbit (B). The QT, RR and QTc of the normal rabbit are 180 ms, 380 ms and 292 ms for both MCG signal and ECG signal. The QT, RR and QTc of the hypercholesterolemic rabbit are 115 ms, 144 ms and 303 ms for MCG signal. However, ECG is not observed in the rabbit B.

REFERENCE

1. Achenbach S and Moshage W Physiol. Meas. 1993:14:A61.
2. Borgmann J, David P, Ockenfuss F, Otto R, Schubert J, Zander W and Braginski A I, Rev. Sci. Instrum. 1993:68:730.
3. Cohen D, Science 1968:161:784.
4. Zhang Y, Panaitov G, Wang S G, Wolters N, Otto R, Schubert J, et al. Appl. Phys. Lett. 2000:76:906.
5. Borgmann J, David P, Ockenfuß G, Otto R, Schubert J, Zander W, et al. Rev. Sci. Instrum. 1997:68:2730.
6. Yang H C, Wang S Y, Chen C H, Jeng J T, Chen J H and Horng H E, J. Low Temp. Phys. 2003:131:509.
7. Yang H C, Wang S Y, Jeng J T, Horng H E, IEEE Trans. Appl. Supercon. 2003:13:360-363.
8. Horng H E, Hung S Y, Jeng J T, Liao S H, Hsu S C, Hwang J H, et al. IEEE Trans. Appl. Supercond. 2003:13:381-384.
10. Borgmann J, David P, Ockenfuss G, Otto R, Schubert J, Zander W, et al. Rev. Mod. Sci. Instrum. 1997:68:2730.
11. He D F, Krause H-J, Bick M, Solnter H, Woltner N, Wolf W , et al. IEEE Trans. Appl. Supercond. 1999:9:3684.
12. Zhang Y, Panaitov G, Wang S G, Wolters N, Otto R, Schubert J, et al. Appl. Phys. Lett. 2000:76:906.
13. Liao S H , Hsu S C, Lin C C, Horng H E, Chen J C, Chen M J, et al. Supercond. Sci. Technol. 2003:16(12):1426.
14. Liu Y B, Wu C C, Lu L S, Su M J, Lin C W, Lin S F, et al. Circulation Research 2003:92(10):1145.

On-line localization magnetic markers for clinical applications and drug delivery studies

Kosch[1] O., Weitschies[2] W., and Trahms[1] L.

[1]Physikalisch-Technische Bundesanstalt Berlin, Germany
[2]Institut für Pharmazie, Universität Greifswald, Germany

ABSTRACT

We have extended the method of magnetic marker monitoring (MMM), to allow the tracking of the transport of solid drug forms through the gastrointestinal tract during the recording. To this end, the tools of on-line field visualization and on-line localization of the magnetic marker were developed. This additional option enables to display the actual position of the magnetic marked pharmaceutical dosage form as well as its state of disintegration via the decrease of its magnetic moment during the measurement. This information helps the operator to minimize the distance between the marker and the sensor position, so that the quality of the measurement can be improved.

KEY WORDS

magnetic marker monitoring, on-line localization, drug delivery

INTRODUCTION

The spatiotemporal sequence of the gastrointestinal transport of solid pharmaceutical dosage forms is not yet fully understood. The number of reports about esophageal damage due to ingested medication in solid drug forms has steadily increased since first descriptions by [Pemberton, 1970], [Evans, 1976], [Bonavina, 1987].

In the past we have shown the performance of magnetic marker monitoring using biomagnetic measurement equipment for tracking of solid drug forms during the gastrointestinal passage with high spatiotemporal resolution [Kosch, 2002]. Up to now these measurements were analyzed off-line, so that the information of the actual position and state of the dosage form was unknown during the measurement, thus preventing any corrective interaction of the operator. With the development of on-line field visualization and on-line localization the handling of MMM is considerably improved.

METHODS

These additional tools were developed for the 63 channel SQUID system manufactured by PTB [Drung, 1995] working in a standard shielded room. This system includes 83 SQUID sensors combined electronically to 63 gradiometer channels and a data acquisition system consisting of a master and a slave unit. On the master unit the measurement can be stored with sampling rates ranging from 250 Hz up to 20 kHz. For MMM-measurements, usually sampling rates of 250 Hz are used. Details about the acquisition system can be found in [Müller, 2003].

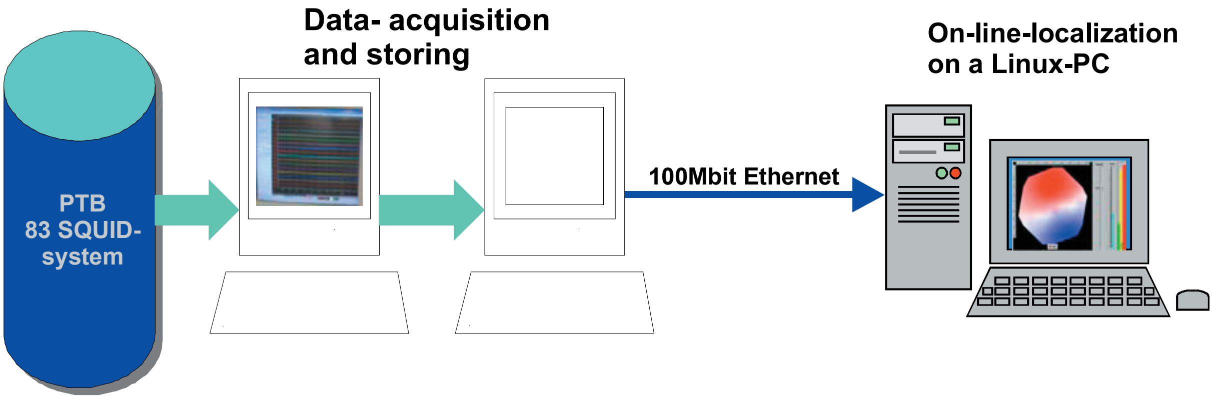

Figure 1. Binding of the on-line localization to the measurement system

The on-line localization and visualization is done on a separate Linux-PC as shown in Fig. 1. The measurement data for the localization are transferred from the master to a RAM-disk of the Linux-PC via a 100Mbit ethernet interface. The RAM-disk is exported to the master unit by the open source software SAMBA. Before transfer, the data rate is sampled down to 125 Hz by the master unit.

For the localization all of the 63 channels are used, i.e. 49 Bz gradiometer channels with vertical direction and 14 gradiometer channels in horizontal direction. Position and disintegration state of the magnetically marked dosage form are determined by fitting the field of a magnetic dipole to the measurement data in inverse field calculation. The inverse solution is found by the Levenberg-Marquardt algorithm [Press, 1995]. During one iteration the new parameter vector (position and moment of the magnetic dipole) is calculated by adding the vector Δdetermined with (1), where J is the Jacobian matrix, J^T the transposed of J and $[B_{mes} - B_{fit}]$ the difference vector of measured and fitted field values which is to minimize.

$$\Delta = A'^{-1} \cdot g \quad \text{with} \quad g = J^T \cdot \left[B_{mes} - B_{fit}\right] \qquad (1)$$

$$A = J^T \cdot J \quad \text{and} \quad a'_{jj} = a_{jj}(1+\lambda); \quad a'_{jk} = a_{jk} \quad (j \neq k) \qquad (2)$$

According to [Press, 1995] A' is calculated by (2) where the diagonal elements of A (the normalized Jacobian) are scaled by $(1+\lambda)$ to vary between the inverse-Hessian method and the steepest descent method. In our implementation the analytical derivatives of the magnetic dipole field are used for calculating the Jacobian matrix J rather than simple numerical derivatives. This causes more computational effort but increases the stability of the inverse field solution. If A is singular the matrix A' is calculated by

$$a'_{jj} = a_{jj} + \lambda; \quad a'_{jk} = a_{jk} \quad (j \neq k) \qquad (3)$$

This is equal to the Tikhonov zero-order regularization [Tikhonov, 1977]. Further, in every iteration step the value for λ is optimized to reduce the total number of iteration steps. The on-line localization and visualization is running with a frequency of 25 Hz.

RESULTS AND DISCUSSION

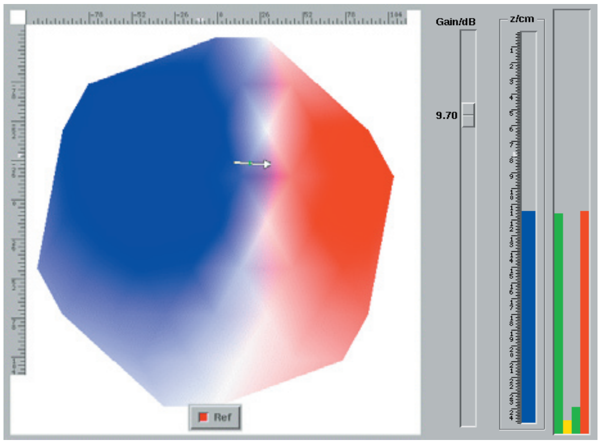

Figure 2. Visualization of the online localization

The visualization of the on-line localization shows the actual position and the moment of the magnetically marked dosage form. Additionally the goodness of fit reflects the contribution of possible field components from sources other than the magnetic dipole. Together with position and magnetic moment this information provides an overview on the measurement and enables the operator to assess its quality. For the practical application, this on-line information is of enormous value for improving the measurement by identifying and eliminating possible sources of perturbation and by increasing the signal to noise ratio during the measurement after minimizing the distance between the marker and the central sensor position. Further, by this feedback the angle between the area covered by the sensor array and magnetically marked capsule can be optimized and the conditioning of the inverse problem can be improved. As a result, it was only rarely necessary to use the Tikhonov regularization (3) for evaluating the data.

Using on-line visualization it was possible to investigate more than 300 esophageal transports for a comprehensive statistical analysis [Osmanoglou]. Moreover, the information provided by on-line visualization enables the medical operator to influence the transport of the dosage form interactively via exogenous factors, like body position and additional volume of liquid bolus. With these additional on-line tools, magnetic marker monitoring becomes a versatile method for clinical studies and for a wide range of diagnostic applications.

ACKNOWLEDGEMENTS

This work is supported by Deutsche Forschungsgemeinschaft in the project MMM für Gastro-Intestinal-Transport TR408/3-1.

REFERENCES

Pemberton J. Oesophageal obstruction and ulceration caused by oral potassium therapy, Br Heart J (322) , 1970, pp. 267-268

Evans KT, Roberts GM. Where do all the tablets go?,1. Lancet, 1976, 2(799), pp.1237-1239

Bonavina L, DeMeester TR, McChesney L, Schwizer W, Albertucci M, Bailey RT. Drug-induced esophageal strictures, Ann Surg 206(2), pp173-183, 1987

Kosch O, Osmanoglou E, Hartmann V, Strenzke A, Weitschies W, Wiedenmann B, et. al. Investigation of gastrointestinal transport by magnetic marker localisation, Biomedizinische Technik, 47, Ergänzungsband 1 (2002), pp. 506-509

Drung D. The PTB 83-SQUID System for Biomagnetic Applications in a Clinic, IEEE Trans. on Appl. Superconductivity, Vol. 5, No. 2, June 1995, pp. 2112-2117

Müller W, Grunwald P, Riedel W, Burghoff M. Mehrkanal - Aufnahmesystem für Biosignale mit bis zu 512 analogen Eingängen, Biomedizinische Technik, 48, Ergänzungsband 1 (2003), pp. 40-41

Press WH, Teukolsky SA, Vetterling WT, Flannery BP. Numerical Recipes in C, Cambridge University Press, New York, USA, 1995, pp. 681-688

Tikhonov AN, Arsenin VY. Solution off Ill-Posed Problems, Washington: Wingston, 1977

Osmanoglou, E., van der Voort, I.R., Fach, K., Kosch, O., Bach, D., Hartmann, V., Strenzke, A., Weitschies, W., Wiedenmann, B., Trahms, L., Mönnikes, H., Magnetic Marker Monitoring of solid Dosage Forms Neurogastroenterology and Motility, in press.

Development of a magnetic field measurement system for small animal lungs

M. Kotani[1], Y. Zheng[2], K. Aizawa[3] and Y. Kudou[3]

[1]Faculty of Engineering, Tokyo Denki University, Tokyo, 101-8457, Japan. [2]School of Information Environment, Tokyo Denki University,Chiba, 270-1382, Japan. [3]Dept. Hygiene & Prev., School of Med., Kitasato Univ. kanagawa, 228-8555, Japan

ABSTRACT

Magnetic field measurements have been used to evaluate the retention of occupational dusts in the lungs, such as welding fumes and asbestos fibers. The study in the magnetic measurement of ferromagnetic particles in small animal lungs, such as mouse, should facilitate the determination of these particles accumulated in human lungs. The remanent magnetic fields produced by ferromagnetic particles in the lungs decrease rapidly with time. This phenomenon is due to the relaxation and the clearance of these ferromagnetic particles, which has been experimentally observed by using many animals, such as rabbits and mice. The relaxation is primarily attributed to the rotation of the particles in macrophages.

A new system to measure accurately magnetic fields produced by mice lungs with ferromagnetic particles has been developed by us. This system consists of two parts, one is a magnetic measurement apparatus, which have a conventional fluxgate magnetometer, a magnetizing coil and a turntable onto which 3 mice can be put, and another is a shield box, which is made of new materials. The weight of the shield box is lighter than the conventional one. Finally, we will explain how to use this magnetic measurement system and how this shield box is excellent.

KEY WORDS

measurement system, shield box, ferromagnetic particles, magnetopneumography

INTRODUCTION

At present, pneumoconiosis is mainly diagnosed by using X-rays. However, X-rays are unable to find most micro particles accumulated in lungs. Therefore, the illness can not be discovered until the change of organization of lungs occurs. As the particles continuously accumulate into the lungs, after a long time, the pneumoconiosis becomes remarkable and serious eventually. Once pneumoconiosis of a labor is discovered through X-rays, reshuffling his work place is already too late. Therefore, it is necessary to know the amount of accumulation particles in lungs at the early stage of the illness. The magnetopneumography (MPG) measurement, which utilizes the magnetism characteristic of ferromagnetic particles in the lungs, is just an effective method for discovering the problem at the early stage of pneumoconiosis.

Magnetic shield must be used because the lung magnetic field of a small animal is feeble, and the influence of geomagnetism, city noise, etc. is large. Therefore, the shied room is significant for this study. However, it is expensive and cumbersome, so we attempt to develop a new shield box, which is inexpensive and much smaller than the conventional shied room.

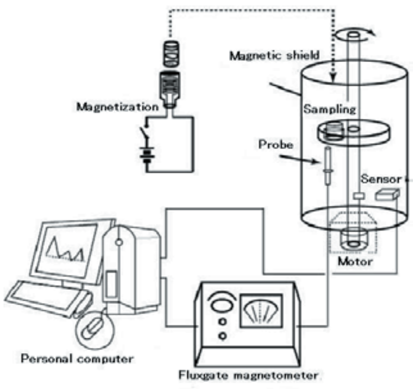

Fig.1. Outline figure of lung magnetic field measurement system

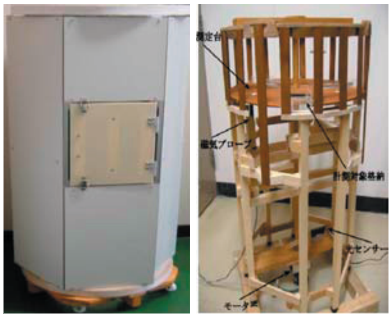

(a) (b)

Fig.2. (a) Magnetic shield box. (b) Magnetic field measurement system.

Fine helmet is soft-magnetic material. It uses three basic ingredients, Fe, Si, and B, five very small quantity ingredients, Cu, Nb, Ta, Mo and Zr and adds metal-arc welded alloy, then by using the single rolling method and super quenching method, forms amorphous metal thin belts. These belts become eventually fine helmet by hot process and crystallizing. The characteristics of the fine helmet:

1. High saturation magnetic density
2. High magnetic permeability
3. Low magnetostrictive
4. Good temperature characteristic
5. Good high-frequency characteristic.
6. Good time stability.
7. Thin, light, and good rigidity.

In this study, we first determine the magnetic characteristics of the shield box, which is made of the manufactured fine helmet. Then, in order to determine the quantity of the accumulated particles and investigate the relation between the quantity and the magnetic field, we have developed a simple model to simulate a small animal lung injected by ferromagnetic particles, and used a magnetic field measurement system to do the experiment. Furthermore, the inverse problem analysis has been performed to determine the distribution of articles

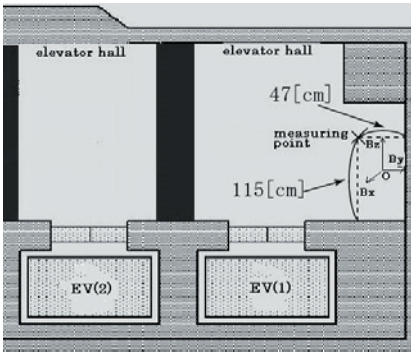

Fig. 3. A experimental arrangement for investigating the characteristics of the shield box.

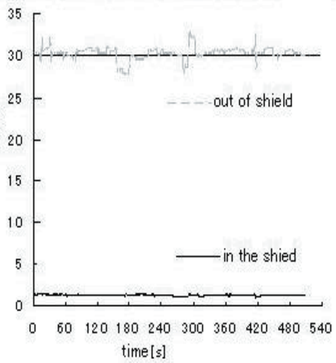

Fig.4. Magnetic shields measured with and without shield.

CONSTRUCTION OF MEASUREMENT SYSTEM

The shape of a magnetism shield box developed by the authors is of a hexangular prism, the height of it is 147 cm, and the maximum diameter is 57 cm; the exterior of the shield box is shown in Figure 2 (a). The wall of magnetism shield box consists of two layers. The outside layer of the shield box is 0.3 mm thick aluminum plate, while the inside is made of the fine helmet material. The inside layer contains 15 sheets of the fine helmet, which has a thickness of 0.25 μm, and the texture direction of two adjacent sheets is perpendicular each other in order to enhance the effect of the magnetic shield. There is a window in the shield box for taking out the model. The window is attached by a resin composition material in order to prevent from the inflow of the magnetic flux. The magnetic field measurement system is composed of three parts, they are a magnetism probe, a light sensor, and a turn table at which the measurement sample is located, and rotated by using a motor. This structure, shown in Figure 2 (b), makes the measurement of a very small magnetic density feasible.

In order to investigate the effect of the shield box for preventing from environmental noises, we have measured the variations of magnetic field in a moving elevator by using a gauss meter for the two cases, i.e. with and without shield box. Here, the varying magnetic shield is realized by the movement of the elevator. The measurement was performed in en elevator hall of the third floor of building No. 11 in the Tokyo Denki University, which is shown in Figure3. The experimental results, with and without shield, are shown in Figure 4, and the magnitudes at the different directions are listed in table 1. It can be seen that the magnitudes at vertical direction, Bz, is larger than that at other directions, and that the absolute value with shield is much smaller than that without shield. In the electronic system laboratory of the Tokyo Denki University, we have also investigated the discrepancy of the magnetic field at different places within the shield box. It has been found that the magnetic field, measured by a gauss meter, at the center of the shield box is larger a little bit than that at the position, at which the probe aims. Therefore, the shield effect is improved further. The results are shown in Table 2.

Table 1 The magnitudes at the different directions with and without shield

	Bx[μT]	By[μT]	Bz[μT]	|B|[μT]
Without shield	15.32	9.76	27.01	32.56
With shield	0.54	0.14	1.31	1.43

Table 2. Effect of the terrestrial magnetism on magnetism fields of the center and side of turntable

	Bx[mμT]	By[mμT]	Bz[mμT]	|B|[mμT]
Center of turntable	0.63	0.37	0.25	0.77
Side of turn table	0.67	0.27	0.17	0.74

MEASUREMENT RESULTS AND INVERSE PROBLEM

We have used ferromagnetic particles (Fe3O4) of 10mg to form two dipoles. The two dipoles are separate with a distance of 2.5cm. Magnetization was performed in a height of 5 cm above a coil. A fluxgate magnetic meter was used to measure the magnetic fields of the two dipoles, and the position of the measurement probe is shown as Fig. 1. The experiments result is shown in Fig. 5 and Fig.6. A matrix-inversion method is used in this study for determining the distribution of the magnetic dipoles or sample, which simulates the small animal lung. The values of the magnetic field around the sample are used in the solution of the inverse magnetic problem. The magnetic density generated by the dipoles is

$$B_{zn} = T_{n1}D_1 + T_{n2}D_2 + \cdots T_{nm}D_m$$

where, n is the number of measuring points and m is the number of magnetic dipole, ***T*** is a transfer function, which is given by the following equation,

$$T_{nm} = \frac{1}{4\pi}\frac{2(z_n - z_{Dm})^2 - (x_n - x_{Dm})^2 - (y_n - y_{Dm})^2}{\{(x_n - x_{Dm})^2 + (y_n - y_{Dm})^2 + (z_n - z_{Dm})^2\}}$$

Then, the distribution of the magnetic field of dipoles, D_s, can be determined by using a least-squares method with these measured data. The calculation formula is

$$[D_s] = [T^T T]^{-1}[T^T][B_z]$$

where, $[T^T]$ is the transposition procession of [T]. The evaluation result calculated by the inverse problem method is shown in Figure 7. It can be seen from the evaluation result that estimation of the value and site of dipole have been showed the peak after [trigger] 2.6 seconds and 3.2 seconds. There peak overlapped are the positions of magnetic dipoles.

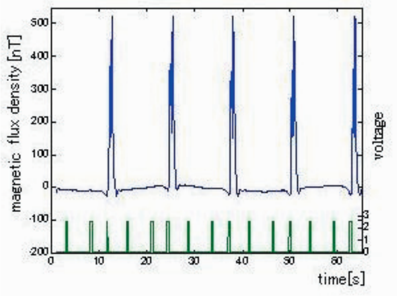

Fig.5. Measurement result of magnetic dipoles.

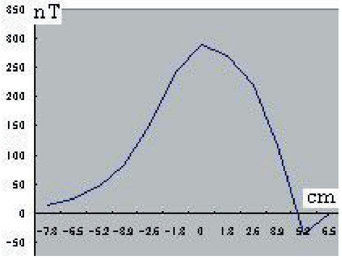

Fig. 6 The expansion of measurement data.

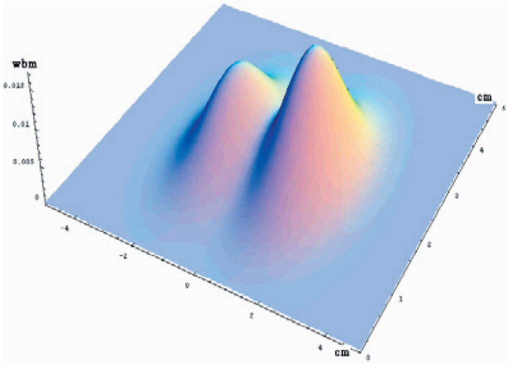

Fig.7 Calculated values of two dipoles.

CONCLUSIONS

A magnetic field measurement system for small animal lungs has been developed successfully. This study indicates that the magnetic noise decreases by 7% or less due to using the shied box designed specially for measuring the magnetic field of small animal lungs. It is also indicated that the magnetic field at the center of the shield box is larger a little bit than that at the side of the box. It is found from the experiments of dipoles that for the case of large signals, an average of 100 continual data has been used in order to decrease the effect of noise, while for feeble signals, further study is needed.

REFERENCES

1. D. Cohen, M. Kotani and N. Cuffin, “Magnetic Fields of the lungs”, Report of the Low-Field Group, Magnet. Lab. M. I. T., Feb. 1-268. 1978.
2. “Comparative Cytotoxicity Study of Rock Wool and Chrysotile by Cell Magnetometric Evalation,”Y. Kudo and M. Kotani, Inhalation Toxicology, 15:1275-1295, 2003. Copyringht Taylor & Francis.
3. The Ministry of Labor work hygiene department, “The Journal of Japan Working Hygiene”, Vol.9, 30-35, 1995.
4. Y. Zheng, M.Sato, and M. Kotani, “Research of Laborer’s Magnetopneumography”, The Journal of the JBBS, Vol.13-1, 86-87, 2000.

Cytomagnetometric Study of Interactions of the Cytoskeletal Filaments

Nemoto, I., and Kawamura, K.

Tokyo Denki University, Japan

ABSTRACT

The purpose of this study is to investigate the interactions between microtubules and microfilaments in living cells by cytomagnetometry. About half a million J774A.1 cells were incubated with Fe_3O_4 particles of diameter 1.92μm, with the average ratio of <1 particle/cell. The cells were treated with cytoskeletal drugs; colchicine, vincristine and nocodazole which disrupt microtubules, cytochalasin B, latrunculin A to disrupt microfilaments, Y-26732 to inhibit actomyosin contraction, and taxol to stabilize microtubules. In this study E_r measurement in cytomagnetometry was performed for 2 hours after treatment with drugs. E_r is considered to be the energy imparted to the phagosomes from the surrounding tissues within the cell. It was found that disruption of microtubules by any of the 3 drugs above caused drasctic increase in E_r. Fluorescent microscopic observation showed that the distribution of microfilaments within the cells became quite nonuniform under the influence of these drugs. When drugs disrupting microfilaments were given simultaneously with colchicine, the increase in E_r was completely inhibited. Also redistribution of microfilaments was much suppressed. These results seem to be in agreement with the recent finding that microbules and microfilaments actively inhibit each other in order to perform their functions in coordination.

KEY WORDS

cytoskeleton, microtubules, microfilaments, cytomagnetometry, colchicine, cytochalasin

INTRODUCTION

Microfilaments(**MF**) and microtubules(**MT**) are two important members of the so-called cytoskeleton of the cell. They play various roles in intracellular movements and keeping the cell shape. Recent works[Benink, 2000][Canman, 1997][Mandato, 2000] show that they sometimes actively inhibit each other so that disruption of one sometimes increases the amount and activity of the other. These studies were mostly carried out using *Xenopus* oocytes and their extracts, which implies the difficulty in studying such phenomena in living cells. Briefly, cytomagnetometry is a method to investigate the mechanical properties of living cells by measuring the magnetic field from cells (cell field, hereafter) into which magnetic particles have been introduced through phagocytosis[Nemoto, 1982][Valberg, 1985]. Other than mechanical parameters such as viscosity and elasticity[Nemoto, 2000][Moeller, 2000], this method can measure the kinetic energy (denoted E_r here) imparted to the particles probably through the cytoskeleton[Nemoto, 1989]. E_r randomizes the direction of the magnetic moments of the particles. Previously, we also noted changes in E_r after treatment with cytoskeletal drugs. The purpose of the present study is to further investigate the change in E_r when MT were depolymerized and when MT and MF were simultaneously depolymerized to see whether their interactions are inhibitory or promotive.

METHODS

J774A.1 cells were incubated with spherical magnetic particles of diameter 1.92μm and magnetic moment $4.6\times10^{-14}\,\mathrm{Am}^2$ (generous gift of Dr. Moeller, GFS, Germany), average ratio being 1 particle/cell. About 5×10^5 cells which phagocytized particles made a monocellular layer on the bottom of a 12mm diameter bottle. The cells were treated with cytoskeletal drugs: colchicines (**Col**), nocodazole (**Noc**), and vincristine (**Vnc**) to disrupt MT; cytochalasinB (**CytB**), and LatrunculinA (**LatA**) to disrupt **MF**; Taxol (**Tax**) to stabilize MT; Y-26732 to inhibit actomyosin systems.

To measure E_r, we put the cells having magnetic particles with magnetic moment μ in a weak magnetic field H (typically 0.5×10^{-4} T). We assume that in equilibrium, the distribution of the angle θ between the direction of H and μ follows the Boltzmann distribution: $p(\theta)\propto\exp(\mu H\cos\theta/E_r)$. Then the cell field in the equilibrium state under H is proportional to $L(a)=\coth(a)-1/a,\ a=\mu H/E_r$. Therefore measurement of cell field yields E_r. We applied the weak field H throughout one experiment lasting for 2 hours except for brief (about 10s) periods of cell field measurement which took place every 10 minutes. Therefore, we may assume that we are following the slow change of equilibrium state caused by drugs.

RESULTS

Fig. 1 shows the change of E_r after treatment with MT-disrupting drugs. It is seen that every drug causes increase in E_r implying that depolymerization of MT causes it. Fig. 2 shows the dependency of the rate of change on the concentration of the drug; colchicine was used in this case. It is seen to be sensitive to the concentration between 1-5 μM. Fig. 3 shows the effects of other drugs. It is seen that those which depolymerize MF lowered the E_r curve compared to the control curve. Fig. 4 shows the result when colchicine was combined with another drug. It is seen that the colchicine-induced increase in E_r was completely suppressed by the MF-disrupting drugs. Taxol caused a delay in the increase.

DISCUSSION

We have the follwing idea about the phenomena we observed, taking into consideration the results obtained with *Xenopus* oocytes and their extract[Mandato, 2000]. MT in normal states inhibit MF directly (by physical contact) or actomyosin contraction through some chemical process.

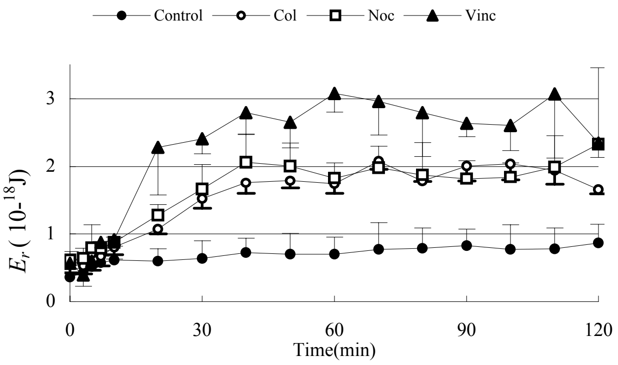

Figure 1. Change of E_r after treatment with MT-disrupting drugs.

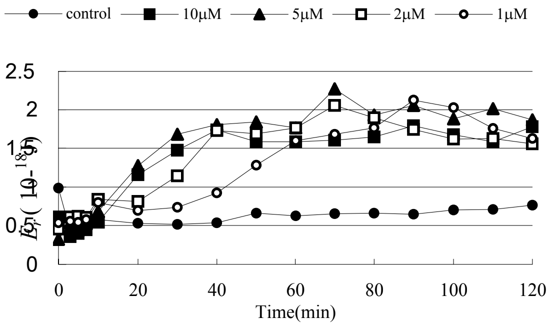

Figure 2. Time course of E_r after treatment with colchicine of various concentrations.

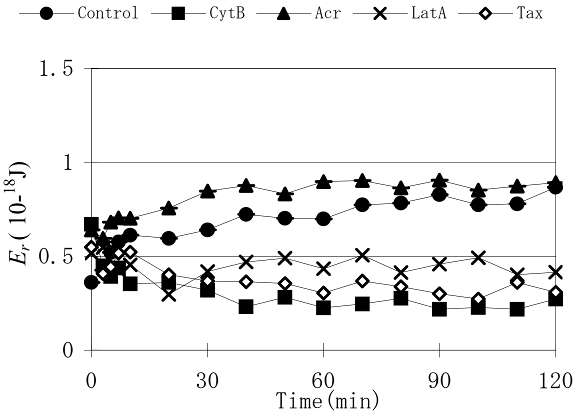

Figure 3. Time course of E_r after treatment with other cytoskeletal drugs.

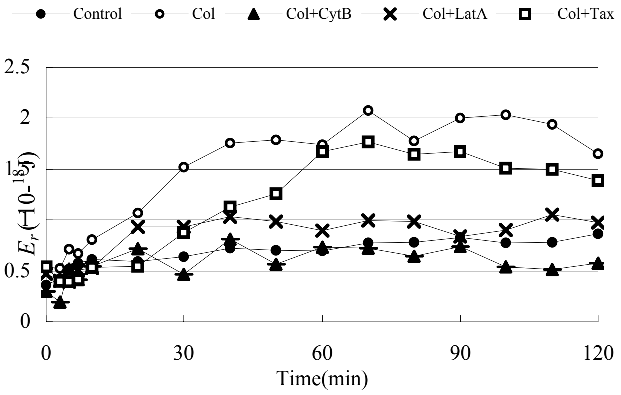

Figure 4. Time course of E_r after simultaneous treatment with colchicine and another drug.

When MT are depolymerized, their inhibitory influence on MF or actomyosin contraction becomes weaker. The depolymerization of MT does not take place uniformly throughout the cell, which results in generating some polarity of the cell. Then the activation of MF or actomyosin contraction occurs where there are less MT, resulting in redistribution of MF and their associated myosin filaments. We suspect that this redistribution of MF accompanied by actomysin contraction results in the increase in E_r. The above results seem to conform with this hypothesis.

REFERENCES

Benink HA, Mandato CA, Bement WM. Analysis of cortical flow models in vivo. Mol Biol Cell 2000:11:2553-63.

Canman JC, W.M.Bement WM. Microtubules suppress actomyosin-based cortical flow in Xenopus oocytes. J Cell Science 1997:110:1907-17.

Mandato CA, Benink HA, Bement WM. Microtubule-actomyosin interactions in cortical flow and cytokinesis. Cell Motil Cytoskel 2000:45:87-92.

Moeller W, Nemoto I, Matsuzaki T, Hofer T, Heyder J. Magnetic phagosome motion in J774A.1 macrophages: Influence of cytoskeletal drugs. Biophys J 2000:79:720-30.

Nemoto I. A model of magnetization and relaxation of ferrimagenttic particles in the lung. IEEE Trans Biomed Eng 1982:29:745-52.

Nemoto I, Ogura K, Toyotama H. Estimation of the energy of cytoplasmic movements by magnetometry: Effects of temperature and intracellular concentration of ATP. IEEE Trans Biomed Eng 1989:36:598-607.

Nemoto I, Moeller W. A viscoelastic model of phagosome motion within cells based on cytomagnetometric measurements. IEEE Trans Biomed Eng 2000:47:170-82.

Valberg PA, Albertini DF. Cytoplasmic motions, rheology, and structure probed by a novel magnetic particle method. J Cell Biol 1985:101:130-40.

Development of a Portable Pneumomagnetic Measurement Device

Y. Zheng[1], M. Kotani[2], Y. Utsukawa[3] and T. Nakadate[4]

[1]School of Information Environment, Tokyo Denki University, Chiba, 270-1382, Japan, [2]Faculty of Engineering, Tokyo Denki University, Tokyo, 101-8457, Japan, [3]College of Science and Engineering, Tokyo Denki University, Saitama, 350-0394, Japan, 4Dept. Hygiene & Prev., School of Med., Showa Univ. Tokyo, 157-8577, Japan

ABSTRACT

In our laboratory there is a substantial device available for measuring the remanent field from magnetic contaminants in the lung. Since the device is huge and quite cumbersome, to carry it to worksites is difficult. Also, it is not convenient and expensive for laborers of small or medium-sized enterprises to come to our campus for taking the examination. Therefore, to develop a portable device is significant. Thus, one can easily carry such a portable device to worksites for the examination by using magnetopneumography (MPG).

This paper reports a portable MPG measurement device developed by our group and the results measured by it. The performance of the portable device is also evaluated by using it to examine the lungs of many labors. It has been proved that the device can obtain more accurate measurements results at worksites, which are beyond our anticipation. The reason is that the background magnetic noise at worksites usually is much less than that at our Kanda campus located in the center of Tokyo, where the level of magnetic noise caused by subways is substantially higher than that at worksites usually located at suburbs or countryside. Therefore, some measurements unable to be down at our campus can be successfully completed at worksites by using this portable device. In addition, it should be noticed that the level of the magnetic noise recorded is greatly depended on the location and the direction of the installation of its fluxgate magnetometer's probe.

KEY WORDS

magnetopneumography, portable, iron oxide particles, inverse problem, elimination method

INTRODUCTION

Siderosis found among arc welders have been considered to be one of benign type of pneumoconiosis. At present, siderosis is mainly diagnosed by using X- rays. However, most small particles which had been long accumulated in the lung can hardly be detected by X- ray diagnosis. The illness cannot be detected until changes in lung tissues come to appear. Furthermore, when siderosis is already discovered, personnel reshuffling at work places will be too late to conduct. Thus the illness advances into a more serious stage due to the accumulation of the particles in the lung further. Therefore, it is necessary to know the amount of particles accumulated in the lung before the illness occurs. An effective method for finding such particles at an earlier stage is presented by Cohen el al [1], i.e. magnetopneumography (MPG), which determines the amount of particles accumulated in the lung based on the characteristics of magnetism [2,3].

DEVELOPMENT OF THE MEASURING DEVICE

The MPG method for measuring particulate deposited in the lung utilizes the magnetic properties of particles drawn by lungs. If an external, DC (constant) magnetic field is applied to the lung, the accumulated particles will be magnetized, producing a residual magnetic field. This field will last about 30 minutes even after the external field is removed. Thus, we can know the amount of particles in the lung by measuring this new magnetic field over the surface of the lung. This is MPG method. It is necessary for measuring accurately the amount of particles accumulated and distribution in the lung to use not only the MPG method but also use the inverse problem analysis**.** In this technique the magnetic properties of the particles and the magnetic fields density of the particles are known beforehand. Based on the lung magnetic field measuring law, the authors of this paper, during the past 20 and more years, have developed various portable prototypes for measuring the lung magnetic field. Labors at different working environments have been examined, and many doubted particles accumulated in the lungs of these workers are measured by using these prototypes. It is seen from these measured results that there are many micro-particles in lungs of workers, and especially, the amount of these micro-particles accumulated within the lung is quite large so that the problem is very serious. But, the conventional device used for lung magnetic field measurement is huge and quite cumbersome, so moving it is almost impossible. Thereupon, in the recent years we have focused on the improvement of the device in order to make it movable easily. The portable lung magnetic field measuring equipment developed by us is a combined device. Each component of the device separate, so is able to be moved alone. Main components are: (1) Magnetization machine (magnetization coil) and its power supply, which are used for magnetizing a part of the lung by the magnetic density of about 50 mT. (2) High sensitivity magnetic fluxgate and its installation stand for measuring the feeble magnetic field. (3) Computer system, including the record of measuring data, the calculation of the amount and distribution of particles within the lung, and a pen recorder for printing out the measured curves. The schematic construction of this device is shown in Figure 1. A picture of the scene, in which a worker is being examined using the device, is shown in fig. 2. The measured results will be reported in the next section.

MEASURING METHOD

A new version of the device has been developed in this year in order to improve further the performance of the version developed in the last year. In this study we use a man lung's model to simulate the examination of a laborer. First, the iron oxide particles （Fe_3O_4) of 10 mg, placed at 2 cm high above the center (R= 0) of a magnetic coil, were magnetized. Then the magnetized particles, i.e. dipole, were filled in the center of the model. When the measure distance from the subject to magnetization coil surface is h = 2 cm, the measured magnetic flux density is about 200 mT. If the distance is 4 cm, the measured magnetic density is about 50 mT. By fixing a magnetization coil and magnetic fluxgate probe to a measurement stand, and keeping other measurement conditions unchanged for each time, we obtain good reproducibility of measurement results. The results tell us the quantity of the particles accumulated in lungs and a magnetic field distribution with sufficient accuracy. Subject stand on a measurement bogie can be moved to right or left with a uniform velocity. A light sensor is attached on the board of the bogie, and black line of 3 mm width is drawn on the lower part of the measurement stand by 25 regular intervals of 2 cm. As measurement stand with these lines moves, the optical sensor in front of it will output a pulse for each black line. Therefore, these pulse signals come from the optical sensor and magnetic flux density curve detected by the probe are spatially one-to-one correspondence, shown in Fig. 3, where magnetic density curve corresponds to the voltage output come from the magnetic probe. The two outputs, come from the magnetic probe and the optical sensor respectively are transmitted to a digital oscilloscope. The digital oscilloscope with memory card is connected to a computer for further analysis. Fig. 3 shows the typical curves corresponding to the two signals. It is seen from fig. 3 that the magnetic flux density curve has a lag of 3 seconds behind the output signal of the optical sensor. The reason is that the output of the probe goes through a low-pass filter, and that the response of the probe is somewhat slower than the optical sensor. In addition, it is also seen from Fig.3 that the baseline of the magnetic curve deflects a little bit from the zero-line, which is caused by city noise. The city noise is sharply changed with time, place, and different directions, unlike geomagnetism, which is comparatively uniform in the Tokyo area. The environmental noise caused by geomagnetism and urban noise (such as close to subway) is removable by using a differential type probe. Therefore, the device has extremely high sensitivity, and is able to detect the magnetic density at the nT order of magnitude. Thus, a very weak pulse signals can be detected even without a shield room. Furthermore, it is significant to keep the probe not moved because the moving of the probe also produces noise. For this reason, we prefer to move the subject to be examined with a uniform velocity.

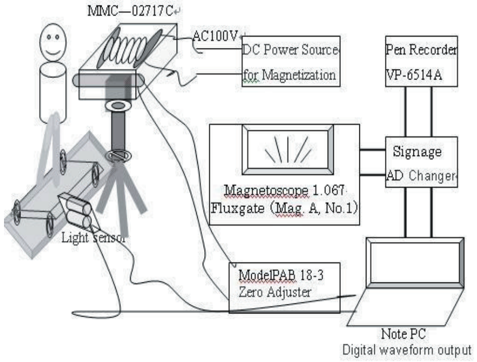

Fig.1. Construction figure of this device.

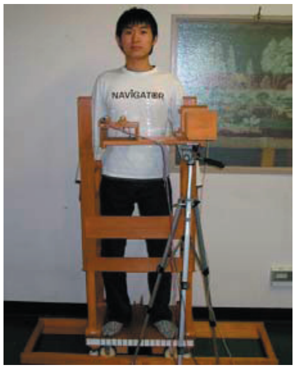

Fig.2. Subject is being measured by the portable lung magnetic field equipment.

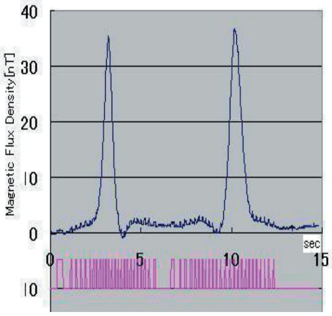

Fig.3. The data is measured a magnetized iron oxide particle dipole.

RESULTS

In this study, we use a examination data of a laborer. The magnitude of the magnetic field at a certain point of the body surface is represented by area of a circle map. Then, according to the inverse problem analysis, we can determine, by using the magnetic noise elimination method [4], the distribution of particulars accumulated in the lung, shown in Fig. 4. Therefore, this is a concise method for diagnosing and evaluating the lung's performance. In order to measure accurately the amount of particles accumulated in the lungs, we need to use not only MPG technique but also use the magnetic noise elimination method for analyzing the inverse problem.

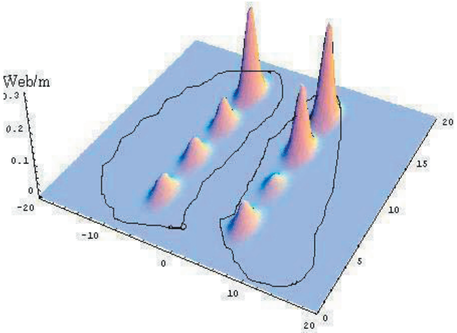

Fig.4. A 3-D distribution graph of particulars accumulated in the lung, determined by using the magnetic noise elimination method.

SUMMARY

The particles accumulated in the lung can be detected by exploiting their magnetic characteristics. Magnetic fields of the lungs are extremely difficult to be measured because the magnetic field of the human body is very weak and affected by the strong magnetic field of earth as well as the urban magnetic noise. Instruments based on the MPG technique had been developed to measure magnetic fields emanating from the lung several years ago. Such instruments are capable of determining the quantity and distribution of particles deposited in the lungs, but these devices are huge and quite cumbersome. Therefore, there is a need to develop a portable pneumomagnetic measurement device. Such a portable device has been developed by us in recent years. It utilizes MPG technique, and possesses more merits, such as, convenience in handling, environmental adaptation for laborers of small or medium-sized enterprises, less background noise, and better accuracy. Furthermore, the distribution of particulars accumulated in the lung is accurately determined by using the magnetic noise elimination method.

Therefore, with the portable pneumomagnetic measurement device and the magnetic noise elimination method Used the device measurement of MPG is not only to, we can not only investigate the lungs of hospital patients but also prevent from pneumoconiosis for those laborers working at the contaminating worksites.

REFERENCES

1. D. Cohen, M. Kotani and N. Cuffin, "Magnetic Fields of the lungs", Report of the Low-Field Group, Magnet. Lab. M. I. T., Feb. 1-268. 1978.
2. S.J.Williamson, L.Kaufman,"Biomagnetism", Journal of Magnetism and Magnetic Materials 22(1981),162-166.
3. The Ministry of Labor work hygiene department, "The Journal of Japan Working Hygiene", Vol.9, 30-35, 1995.
4. Y. Zheng, M. Saito, Y. Uchikawa and M. Kotani, "Research of Laborer's Magnetopneumography", The Journal of the JBBS, Vol.13-1, 86-87, 2000.

Caecal Contraction Activity and Feed Transit Time in Rabbits (Oryctolagus cuniculus), by AC Biosusceptometry (ACB)

U., Andreis[1]; R., Moraes[1]; L.A., Corá[1]; M.F., Américo[2]; O., Baffa[2]; A.J., Spadotto[1]; F.C., Paixão[1]; J.R.A., Miranda[1]
[1] Universidade Estadual Paulista – UNESP, São Paulo, Brazil;[2] Universidade de São Paulo – USP, São Paulo, Brazil

The rabbit presents interest to biophysical and physiological studies of the gastrointestinal tract (GIT), in view of its peculiarities, like slow down motility gastric, caecal great developed and accomplishment of cecotrofagy. Moreover, also presents interest to industry of animal nutrition, a time that techniques able to evaluate motility in rabbits are rare. In the present work the ACB was used to evaluate the behavior of magnetic ration in the rabbit GIT, through of caecal frequency, orocaecal transit time (OCTT) and cecotrofagy time. The AC Biosusceptometry (ACB) is a tool able to analyze with accuracy the GIT motility. The working principle is based on a double magnetic flux transformer with as air nucleus, in which the pair (excitation/detection), located more distant from magnetic material (ferrite), acts as reference. This system is sensitive to distance variations between the detector coil and the magnetic material, thus this technique is very sensitive to movement of the ferrite inside the organ. The ration previously marked with magnetic material, ferrite ($MnFe_2O_3$), was followed using ACB system. Eleven adult females (average weight of 3.5 kg), were positioned in ventral decubitus on a horizontal table and the biomagnetic measurements were made every 2h for 4 days. Results showed a caecal motility frequency of 3 contractions/minute and a gastric residence time was 5±2 (mean±SD) hours. The OCTT was 11±3 (mean±SD) hours and cecotrofagy onset was 18±5 (mean±SD) hours, after the ingestion of the ration and this process occurred for about 12 hours, mainly during night. The values obtained to total transit time with cecotrofagy were 90±11 (mean±SD). The ACB is a non-invasive and radiation-free technique to evaluate diverse parameters of the gastrointestinal motility in rabbits. In summary, the ACB technique is a research tool with applicability in the industry of animal nutrition through new approaches modifying nutritional patterns and contributing to improve physiology knowledge. **Financial Support:** FAPESP.

Biomagnetic measurements of possible transnodal spreading of action potential in green algae *Chara corallina*

F. Baudenbacher[2], L. E. Fong[2], V. Jazbinsek[1], G. Thiel[3], Z. Trontelj[1]
[1]IMFM, U. of Ljubljana, Slovenia; [2]Vanderbilt U., Nashville, USA; [3]Inst. of Botany, TU Darmstadt, BRD

The green alga *Chara corallina* is the plant equivalent to the squid axon in studying ion transport in plants. Extensive experimental work was stimulated by the simple cylindrical geometry of their single internodal cells, which allowed to study the propagation of electrical excitation. Less attention has been devoted to an understanding of the electrical connections between adjacent cells or through the entire plant. These simple plants comprise a linear chain of cells, where the two long internodal cells are connected via a structure of smaller nodal cells. The aim of our research was to study the cellular conduction properties when the action potential (AP) signal reaches the end of internodal cell of a *Chara* internode. In particular, what is the response of the nodal cellular structure and still more, how much of the excitation is transferred to the next neighboring internodal cell.

Electrical excitation was triggered at one end of the internodal cell and spreading of excitation was measured magnetically - using SQUID microscope - at different positions along the first and the second internodal cell as well as in the area of smaller nodal cells connecting the two internodal cells. In parallel electrical measurements, using the technique of potassium ions anesthesia, also the APs were recorded. Several groups of internodal cells consisting of a chain of two or three internodal cells were studied. While we always observed a response from the internodal cell where the electrical excitation started, there was no response in the vicinity of neighboring internodal cell and no response from any of small nodal cells.

The results of this experiment confirm the hypothesis that the long internodal cells of *Chara corallina* need for each cell an independent mechanism of information transfer in different critical situations.

Analysis of Propagation of Gastric Magnetic Fields

L.A. Bradshaw, A.G. Myers, J.G. McDowell, and W.O. Richards
Vanderbilt University, USA

Biomagnetic techniques may be utilized to assess the electrical activity of the stomach noninvasively, but cutaneous electrodes are limited to characterization of the frequency dynamics of gastric slow waves [1]. Gastric diseases such as diabetic gastroparesis may cause alterations in the normally well-coupled gastric syncytium that may not produce noticeable frequency differences but would result in altered propagation of electrical activity. We anesthetized and intubated seven pigs to control respiratory artifact. The animal was placed underneath a multichannel Superconducting QUantum Interference Device (SQUID) magnetometer (Tristan Model 637i, Tristan Technologies, San Diego), and gastric magnetic fields were recorded for 15 minutes with two 60-second periods of suspended respiration. The gastric musculature was then surgically divided to uncouple the stomach and additional recordings obtained for one hour. The data were analyzed by creating false-color maps of the electrical activity at different time instants and examining progressive changes. We calculated the propagation velocity of the gastric magnetic fields by (1) computing the location of the signal maxima and minima and tracking it through successive time frames, and by (2) computing the time lag between signals in different channels by analyzing the cross-correlation. The gastric magnetic field frequency was determined to be 3.15 ± 0.27 cycles-per-minute (cpm) during baseline. Propagating magnetic fields were clearly observed in the false-color map movies during baseline, but mechanical division resulted in a distinct lack of propagation. The propagation velocity before division was 3.5 ± 0.4 mm/s using method 1 and 4.1 ± 0.6 mm/s using method 2, which are consistent with values from the literature and the relative size of the animal model. These results encourage us to continue to evaluate biomagnetic methods as a means of noninvasive characterization of abnormal gastric activity.

[1] Bradshaw LA, et al. The human vector MGG and MENG. *IEEE Trans. BME* 46(8): 959-970, 1999.

Identification of Magnetic Field Injury Currents in Ischemic Small Intestine

L.A. Bradshaw, O.P. Roy, A.G. Myers, J.G. McDowell, J.P. Wikswo and W.O. Richards
Vanderbilt University, USA

Measurement of injury currents is critical in the diagnosis of such pathologies as myocardial infarction and cortical spreading depression, but no reports of injury currents in alimentary tract smooth muscle have appeared, though mesenteric ischemia is known to affect intestinal magnetic fields [1]. We divided fourteen New Zealand rabbits into two groups of seven experimental and control subjects. For all animals, we performed a laparotomy and exteriorized a segment of small bowel. We placed the exteriorized segment on a platform underneath a Superconducting QUantum Interference Device (SQUID) gradiometer. We placed umbilical tape around the mesenteric artery supplying the exteriorized segment that could be easily tied to induce intestinal ischemia. The magnetic field DC baseline was measured by modulating the animal's position to locations near and away from the gradiometer. We recorded pre-ligation data for fifteen minutes. We then ligated the mesenteric artery in the experimental animals and recorded during ischemia or sham ischemia for 60 minutes. The magnetic field baseline was computed as the difference between the baseline in the "in" and "out" positions, and these baseline values were normalized to the pre-ligation values. The normalized magnetic field baseline changed significantly during ischemia by 355 ± 128 pT for the experimental group and 5 ± 10 pT for the control group. Longitudinal and between-groups statistical analysis was performed, and the baseline difference between experimental and control animals during ischemia was 38 ± 4%. The existence of a baseline change during ischemia indicates the presence of injury currents in the alimentary tract smooth muscle. These are the first measurements of injury currents reported in gastrointestinal smooth muscle cells. They suggest the possibility that such measurements may be valuable to future methods for noninvasive diagnosis of gastrointestinal pathology

[1] Seidel SA, et al. Noninvasive detection of ischemic bowel. *J. Vasc. Surg*. 30(2): 309-319, 1999.

An Anatomically Based Model for MGG Simulation

M.L. Buist, L.K. Cheng, R. Yassi, A.J. Pullan
Bioengineeing Institute, The University of Auckland, New Zealand

Through the use of a SQUID gradiometer, the weak magnetic field generated as a result of muscular activity in the wall of the stomach can be measured noninvasively. However, relating these recordings to the underlying electrical state of the stomach remains a challenge. A computational model of the stomach and torso has been created from the visible human data set that is capable of calculating external magnetic fields and field gradients from cellular level electrical activity in the stomach. Through this model the relationship between the experimentally recorded fields and the gastric electrical control activity (ECA) can be elucidated. The stomach was modeled as a large number of coupled cells in a bidomain framework where both smooth muscle cells and interstitial cells of Cajal were included in the model, along with an anatomically based muscle fiber architecture. The electrically passive torso was modeled using a high order boundary element technique. The resulting model was solved for four minutes of simulation time corresponding to 12 gastric slow waves and taking 24 hours of CPU time on eight IBM Power4 processors. The frequency, duration and propagation velocity of the ECA in the stomach were within the range of the experimental data. The magnetic field gradients associated with normal gastric ECA have been simulated and are in quantitative agreement with recordings taken from a normal individual, thus providing a rational basis from which to begin interpreting experimental recordings.

Measurement of Magnetic Fields of Compound Nerve Action Current Using High Resolution SQUID

K. Iramina, H. Tatsuoka*, S. Ueno
Department of Biomedical Engineering, The University of Tokyo
* Research Center for Frontier Medical Engineering, Chiba University

Magnetic Fields produced by the compound nerve action current of the frog sciatic nerve were measured using high resolution SQUID magnetometer. It was possible to observed that the several components of compound action magnetic fields which have different conduction velocities in A fibers.

Wikswo succeeded in estimating equivalent dipole sources of action currents by a transformer technique in which a ferrite toroidal core was introduced. In this study, we succeeded to measure the magnetic fields of compound action potential by high resolution SQUID.

The SQUID system consists of single channel magnetometer which has Ketchen type DC-SQUID. The effective diameter of the pick coil is 300 μm. The typical system noise in the magnetically shielded room is 1.2 pT/ √Hz in the frequency of the white noise region. The distance between the pick up coil and the outside surface of the diameter is 800 μm. The performance of the spatial resolution of this system is about 675 μm.

The dissected sciatic nerve bundle of bullfrog in the moist chamber was located 1.5 mm below the SQUID magnetometer. The nerve bundle was electrically stimulated and the compound action magnetic fields and the compound action potentials were measured. Several components of the magnetic fields derived from action current were observed within 4ms latency. It is difficult to detect these signals using by large size pick up coil.

Influence of ac magnetic fields on MNP-bearing solitary cells

G. Glöckl[1], L. Trahms[2], W. Weitschies[1]
[1]Institute of Pharmacy, University of Greifswald, D-17487 Greifswald, Germany
[2]Physikalisch-Technische Bundesanstalt, D-10487 Berlin, Germany

The aim of the present study is to determine the biological effects of ac magnetic fields on solitary cells that are labeled with superparamagnetic iron oxide nanoparticles (magnetic hyperthermia). Theoretical considerations predict that magnetic heating does not affect solitary cells as a minimal critical tissue volume is required [1]. Materials and methods: Different human tumor cell lines are employed. Biocompatible magnetic nanoparticles as they are used for contrast media in MRI were first fractionated and the specific loss power (SLP) of the fractions was determined, where special attention was drawn to increase the particles SLP by variation of the particle size and the magnetic field parameters. The human tumor cell lines were incubated with the fractions of magnetic nanoparticles. Furthermore, the thermal sensitivity of the cell lines was characterized by water bath hyperthermia. Cell viability was determined by the fluorescent resazurin assay. Results: For the investigated particles the frequency within the tolerable range is of minor influence on the SLP compared to the field amplitude and the particle diameter. The SLP decreases significantly due to immobilisation after cellular uptake. Water bath hyperthermia shows that even a small temperature increase above 37 °C causes considerable decreases in cell viability for most cell lines, however some cell lines tolerate moderately increased temperatures over expanded periods. Exposure of cells labeled with magnetic nanoparticles to alternating magnetic fields (400 kHz, 10 mT) yielded no macroscopically determinable heating. However effects on cell viability were occasionally observed by the stimulation of metabolic activity, even with unlabeled cells after exposure to the ac magnetic field.

The support by the Deutsche Forschungsgemeinschaft (DFG, No. WE 2555/4-1) is gratefully acknowledged.

[1] Rabin, Y. 2002. Int J Hyperthermia 18, 194-202.

Passive room temperature sensor for oral drug tracking and delivery studies

S. Kumar,[1] W.F. Avrin,[2] D. Hecht,[1] S. Bennett[1] and D. Walsh[3]
[1]Quantum Magnetics, San Diego, CA, USA, [2]Insight Magnetics, San Diego, CA, USA, [3]Vista Clara, Mukilteo, WA, USA

There has been recent interest in the study of magnetic methods for understanding of oral delivery including the tracking and location of a magnetically tagged target in the gastrointestinal tract.[1,2] The study techniques have involved the use of a multichannel SQUID sensor for passive magnetic detection, AC susceptometry, and passive magnetic detection using room temperature magnetic sensors. [3] While the SQUID detection can track a small amount of taggant, it requires a cryogenic system in a shielded room. Previous work using room-temperature sensors for passive magnetic tracking has involved a powerful magnetic source, an NdFeB magnet. Existing AC susceptometry techniques, while effective in tracking the passage of the magnetic target do not have the localization capability of the multichannel SQUID system. Moreover AC susceptometry will also be limited in sensitivity by the susceptibility response of the body to the applied AC excitation. We are currently designing a room temperature sensor to locate and track a magnetically tagged capsule or tablet in the gastrointestinal tract from outside the body. While previous work involving tracking with room temperature sensors has used NdFeB magnets, we use modest amount of iron oxide powder that can be mixed in with the drug in the capsule or tablet. Our sensor can track and locate to a precison of 1 cm or better. The sensor is passive, can operate in a magnetically shielded environment, and does not need an external excitation field as long as the target is magnetized. The sensor promises to provide a low-cost alternative to the multichannel SQUID and an alternative to radiological tracking in the gastrointestinal tract, thereby potentially allowing more frequent oral drug delivery studies on patients, pregnant women and children. We will present some preliminary in-vitro results. This project is supported by a grant from the United States National Institutes of Health.

[1] Hartmann V, et al. 2002. Proc. BIOMAG 2002 (VDE, Berlin), 1106. [2] Americo M.F., et al. 2002. Proc. BIOMAG 2002 (VDE, Berlin), 1105.
[3] Innovent Technologieentwicklung Jena, Germany, http://www.innovent-jena.de/inno-eng/mws/MWS_marker-e.htm

In Vivo Magnetic Marker Monitoring of Hydrophilic Gel Matrix Tablets

E. Söderlind[1], W. Weitschies[2], B. Abrahamsson[1], H. Mönnikes[3], K. Fach[3], O. Kosch[4], L. Trahms[4]
[1]Preformulation & Biopharmaceutics, AstraZeneca R&D Mölndal, Sweden. [2]Institute of Pharmacy, Ernst-Moritz-Arndt University, Greifswald, Germany. [3]Universitätsklinikum Charité, Berlin, Germany. [4]Physikalisch-Technische Bundesanstalt, Berlin, Germany.

Hydrophilic gel matrix tablets is a commonly used formulation principles to achieve extended release (ER) of drug from an oral dosage form. For poorly soluble drugs the release rate from such formulations is determined by the tablet erosion rate. The tablet erosion *in vivo* and the GI transit are two important processes influencing the drug concentration in plasma, and consequently, the clinical response. It is therefore of great importance to investigate the tablet erosion at different locations in the GI tract under different conditions in order to optimise design and use of such formulations. The main aim of the present study was to evaluate the usefulness of the magnetic marker monitoring (MMM) technique [1] for such biopharmaceutical studies. Hydrophilic gel matrix tablets containing a model drug were magnetically marked and administered to volunteers in both the fasted and fed state. The tablet localization and the net magnetization were recorded using multi-channel SQUID devices allowing simultaneous monitoring of the GI transit and the *in vivo* tablet erosion. The drug release rate *in vivo* was estimated from magnetization data using *in vitro* drug release profiles. Plasma samples were collected in order to investigate the relation between tablet erosion and drug absorption rate. The usefulness of MMM as a tool to investigate the *in vivo* behaviour of solid ER dosage forms was demonstrated. Physiological parameters such as GI residence times could be determined. Effects of food on the erosion rate and drug plasma profiles were also illustrated.

[1] Weitschies, W., Cordini, D., Karaus, M., Trahms, L., Semmler, W. 1999. Magnetic marker monitoring of esophageal, gastric and duodenal transit of non-disintegrating capsules. Pharmazie, 54, 426.

This page has been intentionally left blank